MINISTRY OF EDUCATION AND SCIENCE UKRAINE
ODESSA I. I. MECHNIKOV NATIONAL UNIVERSITY

ФОТОЭЛЕКТРОНИКА

PHOTOELECTRONICS
INTER-UNIVERSITIES SCIENTIFIC ARTICLES

Founded in 1986

Number 23

ODESSA
2014

UDC 621.315.592:621.383.51:537.221

«PHOTOELECTRONICS»
№ 2 3 – 2 0 1 4

INTER-UNIVERSITIES SCIENTIFIC ARTICLES

Founded in 1986

Certificate of State Registration KB № 15953

«ФОТОЭЛЕКТРОНИКА»
№ 23–2014

МЕЖВЕДОМСТВЕННЫЙ НАУЧНЫЙ СБОРНИК

Основан в 1986 г.

Свидетельство о Государственной регистрации КВ № 15953

The results of theoretical and experimental studies in problems of the semiconductor and microelectronic devices physics, opto- and qantum electronics, quantum optics, spectroscopy and photophysics of nucleus, atoms, molecules and solids are presented in the issue. New directions in the photoelectronics, stimulated by problems of the super intense laser radiation interaction with nuclei, atomic systems and substance, are considered. Scientific articles «Photoelectronics» collection abstracted in ВИНИТИ and «Джерело»

Scientific articles «Photoelectronics» collection abstracted in ВИНИТИ and «ДЖЕРЕЛО»,and are in scientificmetric base INDEX COPERNICUS with ICV 5.19 ..

The issue is introduced to the List of special editions of the Ukrainian Higher Certification Commission in physics-mathematics and technical sciences.

For lecturers, scientists, post-graduates and students.

У збірнику наведено результати теоретичних і експериментальних досліджень з питань фізики напівпровідників та мікроелектронних приладів, опто- та квантової електроніки, квантової оптики, спектроскопії та фотофізики ядра, атомів, молекул та твердих тіл. Розглянуто нові напрямки розвитку фотоелектроніки, пов'язані із задачами взаемодії надінтенсивного лазерного випромінювання з ядром, атомними системами, речовиною.

Збірник включено до Переліку спеціальних видань ВАК України з фізико-математичних та технічних наук. Збірник «Photoelectronics» реферується у ВІНІТІ (Москва) та «Джерело» (Київ) і знаходиться у науковометричній базі INDEX COPERNICUS з ICV 5.19

Для викладачів, наукових працівників, аспіранів, студентів

В сборнике приведены результаты теоретических и экспериментальных исследований по вопросам физики полупроводников и микроэлектронных приборов, опто- и квантовой электроники, квантовой оптики, спектроскопии и фотофизики ядра, атомов, молекул и твердых тел. Рассмотрены новые направления развития фотоэлектроники, связанные с задачами взаимодействия сверхинтенсивного лазерного излучения с ядром, атомными системами, веществом.

Сборник включен в Список специальных изданий ВАК Украины по физико-математическим и техническим наукам. Сборник «Photoelectronics» реферируется в ВИНИТИ (Москва) и «Джерело» (Киев) и находится в наукометричной базе INDEX COPERNICUS с ICV 5.19.

Для преподавателей, научных работников, аспирантов, студентов.

Address of editorial board:

Odessa I. I. Mechnikov National University 42, Pasteur str., Odessa, 65026, Ukraine
e-mail: wadz@mail.ru, tel.: +38-048765 32 16.

Information is on the site: http://onu.edu.ua/en/science/sp/photoelectronics

TABLE OF CONTENTS:

UDC 621.385.221

R. M. Balabai, A. G. Barilka

Kryvyi-Rig National University, Department of Physics
(54, Gagarin Ave., Kryvyi Rig 50085, Ukraine; e-mail: oks_pol@cabletv.dp.ua)

TRIBOLOGICAL CHARACTERISTICS OF THE DIAMOND-LIKE CARBON FILMS COVERED BY HYDROGEN OR FLUORINE*: AB INITIO* CALCULATIONS

Within the methods of electron density functional and ab initio pseudopotential, it were obtained the spatial distributions of density of valence, the total energy, the static friction force for diamond and diamond-like films with uncoated surfaces or covered completely with hydrogen, or with a half coating hydrogen or fluorine. It was found that the half concentration of the broken bonds of carbon atoms on the smooth surfaces of diamond films, which exist in tribological contact, increases the slip resistance by comparison with the films with surface complete covered by hydrogen.

Keywords: the electron density functional method, the pseudopotential method, the diamond-like carbon, adhesion, the static friction force, hydrogen, fluorine.

Introduction and statement of the problem

Tribology is the science of friction, wear and lubrication material - is an important, given its numerous technological applications. Processes of friction, wear and lubrication of new composite materials, which are currently replace protective metal surface coatings, significantly different from the processes characteristic of metals [1], hence, the understanding of tribology of nonmetals is important. Knowledge about tribology at the atomic level can be obtained on a theoretical basis by means of the molecular dynamics and the quantum chemical calculations.

In this paper, we performed the first principles simulation of tribology processes. The essence of this simulation is based on the static energy calculations. Calculation algorithm consisted in the following.

The initial structure of model objects was generated like that; the pair of friction surfaces were aligned in the desired configuration and installed at a short distance of separation D (Fig.1). The energy of such a structure was calculated and stored. Then, the surface atomic layers moved on short distance relatively the deeper atomic layers, in the time of the distance of separation (D) was unchanged, and new energy was calculated.

This procedure repeated again, thereby the energy relief along the trajectory of the shift of atomic layers was generating. Calculated energy relief allows estimating the normal pressure and friction coefficient. The friction coefficient is a measure of the work, which was conducted in the system, is transformed into other less-managed forms of energy. Clearly, there is a significant correlation between the adhesion, the friction and the wear of surfaces, which slide over each other, and the details of the correlations depend on the specifics of their atomic structure.

Diamond-like carbon (DLC) has recently attracted considerable attention as a semiconductor lubricant. The high content of the carbon atoms with diamond bonds in the presence of similar graphite bonds leads to the appearance of the unique characteristics of diamond-like coatings, such as wear resistance, high strength, chemical resistance, low friction, poor abrasion, biocompatibility, transparency in the infrared range of the spectrum and ecological purity [2]. Some factors,

such as surface atoms in the DLC and structure of the film are essential to improve tribological characteristics of DLC [3].

Models and methods of calculation

In these computing experiments, we investigated the influence of the roughness and the dangling bonds of the slipping surfaces on the value of adhesion and friction coefficient using its own software complex [4].

All of our evaluations of the static structural properties through the evolution of energy are based on the following assumptions. (1) The electrons are in the ground state in relation to the instant positions of nucleases (adiabatic approximation of the Born-Oppenheimer). (2) The multiparticle effects are assessed in the framework of the local density functional formalism. (3) There is used approximation of frozen cores that is pseudopotential. Pseudopotential theory gives the possibility to use convenient mathematical Fourier functions. Through a pseudopotential weakness as a basis in expanding the single-particle electron wave functions possible applicants the plane waves. Relying on artificial translational symmetry objects, which we explore the expression for the total energy simply is formulated in the momentum space. The total

$$
\begin{aligned}
E_{tot}/\Omega = & \sum_{k,G,i} \left|\Psi_i(\vec{k}+\vec{G})\right|^2 \frac{\hbar^2}{2m}(\vec{k}+\vec{G})^2 + \\
& + \frac{1}{2}4\pi e^2 \sum_{G}{}' \frac{\left|\rho(\vec{G})\right|^2}{\vec{G}^2} + \sum_{G} \varepsilon_{xc}(\vec{G})\rho^*(\vec{G}) + \\
& + \sum_{G,\tau}{}' S_\tau(\vec{G}) V_\tau^L(\vec{G})\rho^*(\vec{G}) + \\
& \sum_{k,G,G',i,l,\tau}{}' S_\tau(\vec{G}-\vec{G}')\Delta V_{l,\tau}^{NL}(\vec{k}+\vec{G},\vec{k}+\vec{G}') \times \\
& \times \Psi_i(\vec{k}+\vec{G})\Psi^*{}_i(\vec{k}+\vec{G}') + \\
& + \left\{\sum_\tau \alpha_\tau\right\}\left[\Omega^{-1}\sum_\tau Z_\tau\right] + \Omega^{-1}\gamma_{Ewald},
\end{aligned}
\qquad (1)
$$

where $\vec{k}$ is the value from the first Brillouin zone, $\vec{G}$ - vector of the reciprocal lattice, $\Psi_i(\vec{k}+\vec{G})$ - the single-particle electron wave function, *i* - denotes the occupied states for a specific $\vec{k}$, $\rho(\vec{G})$ - coefficient in expanding the valence electrons density, $\sum'$ – primes in the summation exclude $\vec{G}$=0 term, $\vec{\tau}$ - the number of atoms in the unit cell, $S_\tau(\vec{G})$ is a structural factor, V_τ^L is the local (l-independent) spherically symmetric pseudopotential, 1 denotes the orbital quantum number, $\Delta V_{l,\tau}^{NL}$ - a nonlocal (1-dependent) additive V_τ^L, Z_τ - charge of an ion, γ_{Ewald} - it is the energy of Madelung of the point ions in a uniform negative background.

The coefficients of the Fourier transformation of the electron charge density are calculated by the formula:

$$
\rho(\vec{G}) = \sum_i \sum_{\vec{G}',\alpha} \Psi_i(\vec{k}+\vec{G})\Psi^*{}_i(\vec{k}+\alpha\vec{G}'), \qquad (2)
$$

where $\Psi_i(\vec{k}+\vec{G})$ - the coefficients in expending the single-particle electron wave functions over the plane wave are obtained from the zone-structural calculations, α – the operator symmetric transformations from the point group symmetry of the unit cell.

To calculate the electron exchange-correlation energy ε_{xc}, we used the Ceperley-Alder approximation with the Perdew-Zunger parameterization.

The $\vec{k}$ integration was replaced by a discrete summation over the special points the Brillouin zone.

The tribological contact model created from the diamond-like films by each thickness of about 7 Å. In films the percentage of the graphite-like bonds changed from zero (see Fig.1) to 50 (see Fig.2). The percentage part changed the smoothness of surfaces.

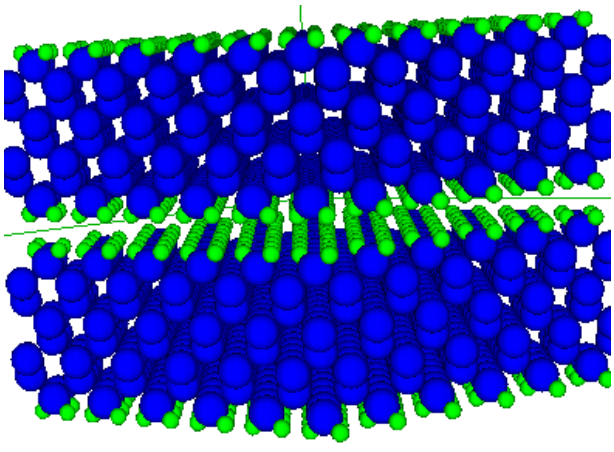

Fig.1. The (100) surface of the diamond-like carbon films with the surface hydrogen atoms and 100% diamond-like bonds in tribological contact.

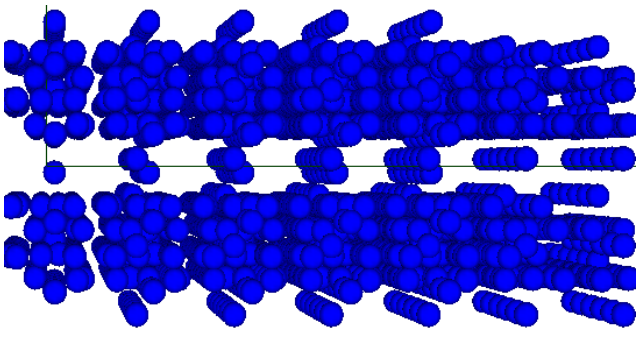

Fig. 2. Two diamond-like carbon films with a mixture of 50% the diamond-like and 50% the graphite-like bonds in tribological contact.

In connection with that, the algorithm of calculation expects presence of translational symmetry in the probed atomic system, the artificial superlattice of orthorhombic type was at first created. The object of study defines the super lattice parameters and the atomic basis. Therefore, the atomic basis of the primitive cell of the artificial super lattice for simulation of two diamond-like carbon films with a mixture of 50% the diamond-like and 50% the graphite-like bonds in tribological contact consisted from 88 the carbon atoms. Translation operations of the described cells resulted to the two infinite films. They were paralleled axis Z and located at a certain distance D from each other (Fig. 2, Fig. 6). We calculated the total energy of objects in tribological contact and theirs spatial distribution of the valence electrons density.

The calculation results and theirs discussion

On Fig.3 and Fig.4 there are changes of the total energy and the rate of the total energy change of two the diamond-like carbon films with a mixture of 50% the diamond-like and 50% the graphite-like bonds versus the change of the separation distance between films D (the value of the derivative dE/dD is considered to be the friction force).

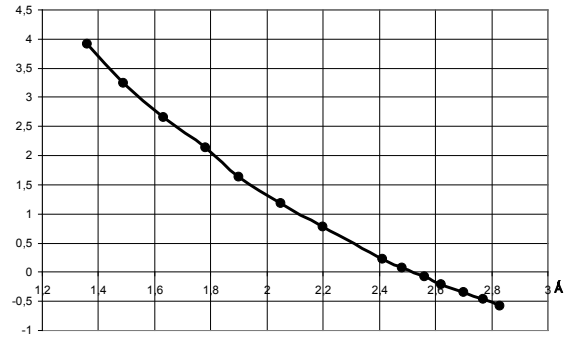

Fig. 3. The changes of the total energy of two diamond-like carbon films with a mixture of 50% the diamond-like and 50% the graphite-like bonds versus the change of the separation distance between films D. Energy is supplied in atomic units per atom, distance - in Å.

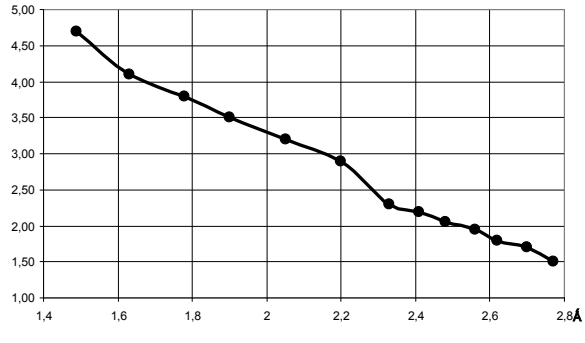

Fig.4. Friction force change (dE/dD) of two the diamond-like carbon films with a mixture of 50% the diamond-like and 50% the graphite-like bonds versus the change of the separation distance between films D.

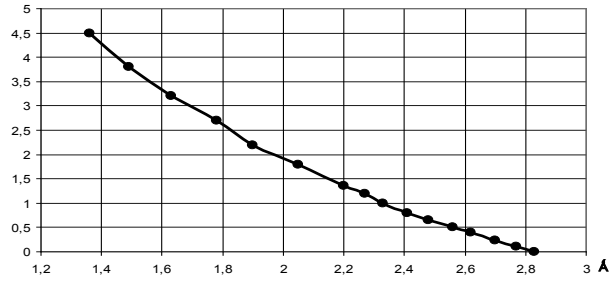

Fig. 5. The adhesion energy change (dE/dD) of two the diamond-like carbon films with a mixture of 50% the diamond-like and 50% the graphite-like bonds versus the change of the separation distance between films D. Energy is supplied in atomic units per atom, distance - in Å.

a

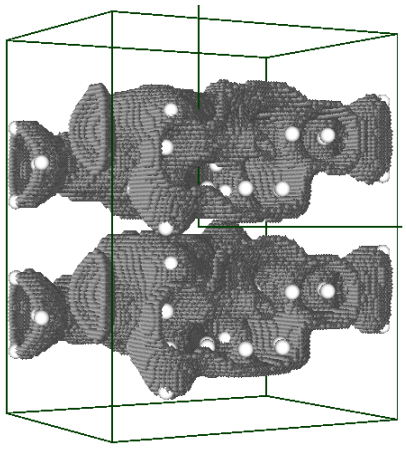

b

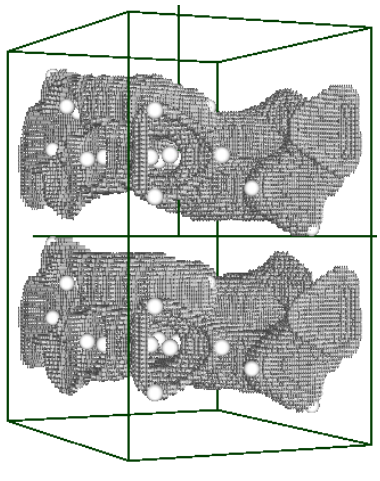

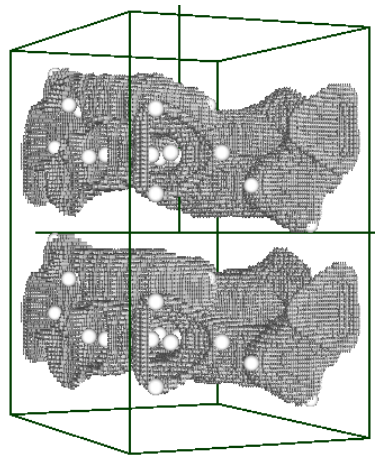

c

Fig. 6. The spatial distribution of the valence electrons density for value 0.1 from the maximum in two the diamond-like carbon tribological contacted films with a mixture 50% the diamond-like and 50% the graphite-like bonds, the separation distance D between the films is: a) 1.36 Å, b) 2.2 Å, c) 2,77 Å.

The graph in Fig.4 shows that for the separation distance (D) in the area of 2.2-2.3 Å on the (dE/dD) curve there is an inflection, which can be associated with changes in the nature of interaction between the films. Comparing this fact with the spatial distribution of the density of the valence electrons for different distances of separation (D) between films, we conclude that the electronic exchange between films disappears at these distances, i.e. the acceptor-donor type of interaction disappears. As to the more long Coulomb interactions between the carbon ions, then they disappear on distances close to 2.83 Å. About this the zero value of adhesion energy between the films in Fig.5 witnesses. The adhesion energy between the films was calculated as a difference between the total energy of the two isolated diamond-like films and the energy of the tribological contacted films.

Further, the atomic basis of the primitive cell of the artificial super lattice for simulation of two the diamond films by thickness of 7.5 Å with a complete coverage of hydrogen consisted of 48 atoms; and for simulation of the 50% coverage of hydrogen or fluorine consisted of 40 atoms. Translation operations of the described cells resulted to the two infinite films. They were paralleled axis Z and located at a certain distance

D from each other. For simulation of the elastic displacements (without destruction of chemical bonds) of the surface layers of the sliding films relatively the deeper layers at a constant distance between the films, the atomic layers of hydrogen and the nearest carbon are moved not more than 7% of the interatomic distances. We calculated the total energy objects in the tribological sliding contact, the static friction force, as a derivative ($\Delta E/\Delta l$), where ΔE is the energy change versus the displacement of the surface atoms on the Δl, and the spatial distribution of density of valence electrons.

On Fig.7 and Fig. 8, it shows the change of the total energy of two the diamond sliding films with a complete coverage of hydrogen and the 50% coverage of hydrogen or fluorine versus a change of the distance of separation D between films.

From Fig. 7 and Fig. 8, it shows that with increasing a separation distance between the diamond films, the total energy of the films with the fully hydrogen passivated surfaces and the 50% coated films by fluorine or hydrogen decrease monotonically. Herewith, on 14% greater energy in the close contact films (the separation distance D between the films was 1.197 Å) the film contacts with the incomplete hydrogen coverage has by comparison with the film contacts with the complete hydrogen coverage. In addition, on 37% greater energy the film contacts with the incomplete fluorine coverage has by comparison with the film contacts with the incomplete hydrogen coverage. When the films with the various surface coverage's are removed one from other to the distance D, equal 2.336 Å, the total energy of these systems had almost the same value.

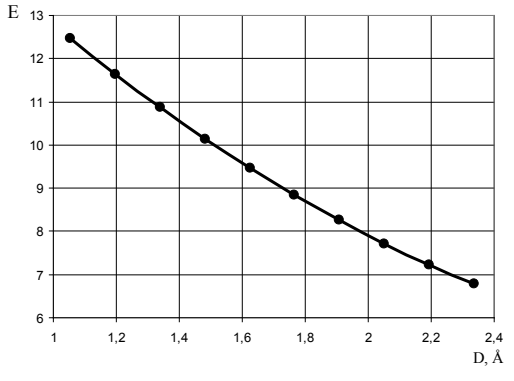

a

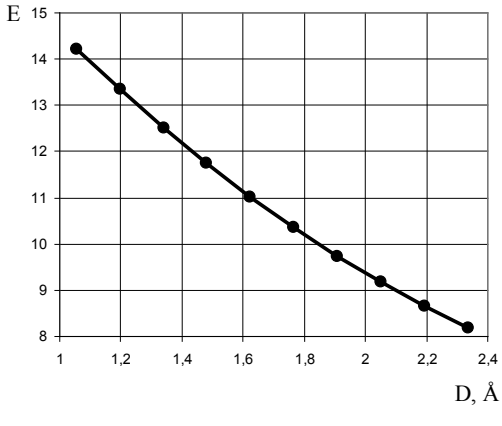

b

Fig. 7. The change of the total energy of two the sliding diamond films with the full hydrogen coverage (a) and the 50% hydrogen coverage (b) at change of the separation distance D between films. Energy is supplied in atomic units per atom, distance - in Å.

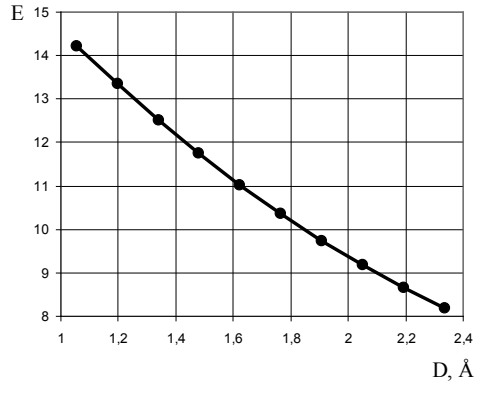

a

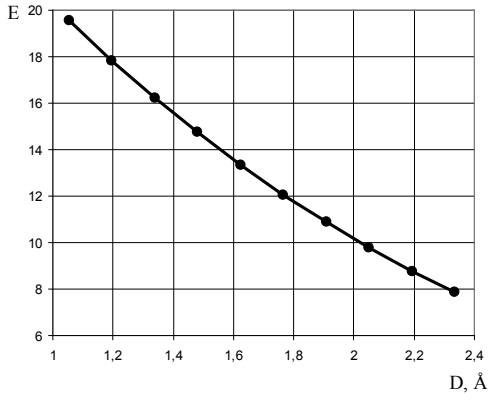

b

Fig. 8. The change of the total energy of two the sliding diamond films with the 50% hydrogen coverage (a) and the 50% fluorine coverage (b) at change of the separation distance D between films. Energy is supplied in atomic units per atom, distance - in Å.

At the fixed separation distances (D) between films (the most close contact, D=1.197 Å, the most remote contact, D=2.336 Å) the static friction forces in tribological contacts of two diamond films coated by 50% fluorine, or 50% hydrogen, or complete hydrogen coverage are examined. The dependencies of the calculated friction forces versus the displacement of the surface atomic layers are shown in Fig. 9, Fig. 10 and Fig. 11.

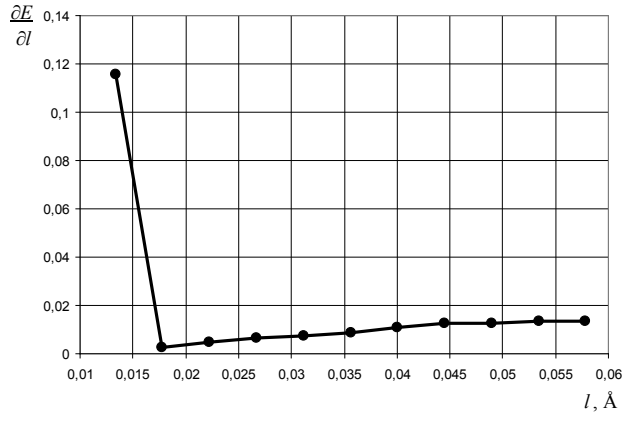

a

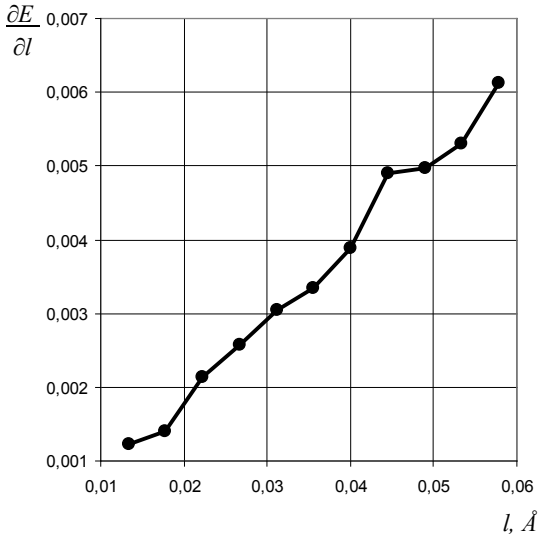

b

Fig. 9. The static friction force of two diamond films with full hydrogen coating, these films slid one comparatively other with the displacement of the surface atoms. The separation distances D between the films were: a) 1.197 Å, b) 2.336 Å.

From Fig. 9b and Fig. 10b it shows that the partial removal of hydrogen atoms from the surface of the film leads to the increase of the static friction force more in comparison with a complete hydrogen coverage of surfaces of diamond films in the most remote tribological contact. Incomplete fluorine covering of the films surfaces increases the coefficient of friction else on order of magnitude in comparison with hydrogen coatings (see Fig. 11).

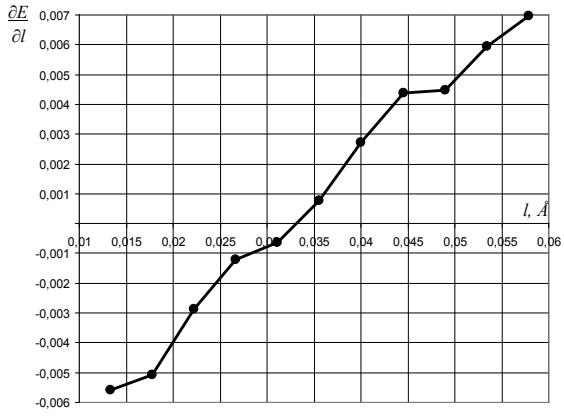

a

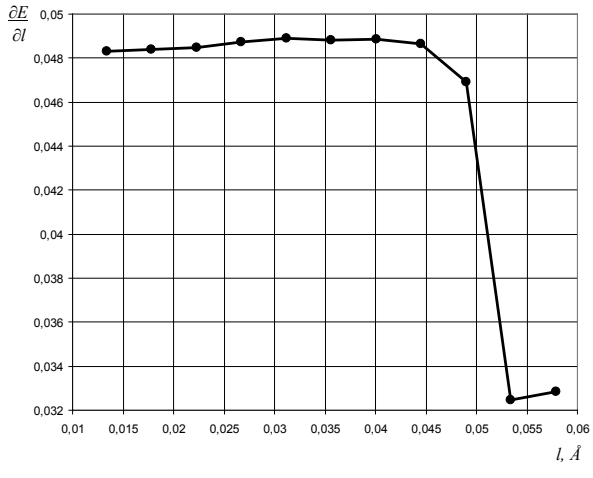

b

Fig. 10. The static friction force of two diamond films with 50% hydrogen coating, these films slid one comparatively other with the displacement of the surface atoms. The separation distances D between the films were: a) 1.197 Å, b) 2.336 Å.

Analyzing the static friction forces of two diamond films, which slid one comparatively other with the displacement of the surface atoms and were covered under different conditions (Fig. 9 - Fig. 11), we observe a non-monotonic fluctuations in the value of the static friction force in

these systems. Almost all above discussed tribological contacts were characterized by increase a friction coefficient when the shift of the surface atomic layers comparatively more deep increase, except the diamond films coated by 50% fluorine, which were in the closest contact (see Fig. 11a).

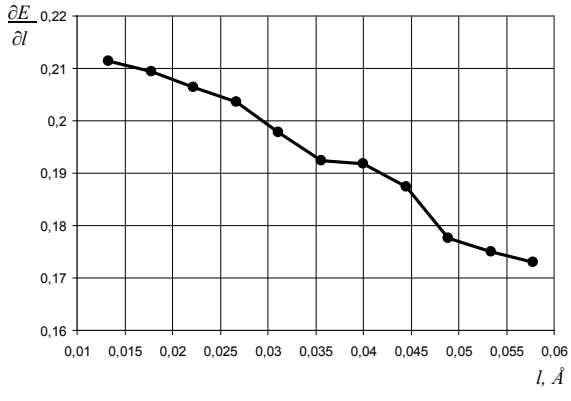

a

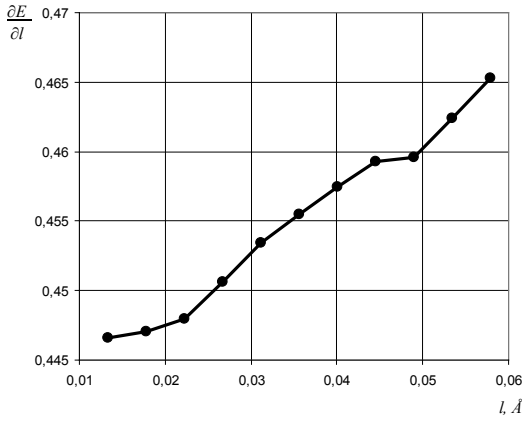

b

Fig. 11. The static friction force of two diamond films with 50% fluorine coating, these films slid one comparatively other with the displacement of the surface atoms. The separation distances D between the films were: a) 1.197 Å, b) 2.336 Å.

Conclusions regarding the increase of the coefficient of friction, were installed and other researchers in considering the properties of carbon materials. Frictional properties of monocrystalline diamond surface (111) were studied in ultra-high vacuum (UHV) with the help of silicon (Si) needle the AFM. On the surface the presence or absence of hydrogen (H) being tracked by diffraction of slow electrons (LEED). Removal of the hydrogen from the surface leads to the increase of average coefficient of friction is more than two orders of magnitude compared with the surface covered with hydrogen. This is a vivid and convincing example of how loose connection can connect border and increase the influence of adhesion to friction, and how passivation those relations that react may significantly weaken these forces [5-10].

In Fig. 12 and Fig. 13 the spatial density distributions of valence electrons within the interval of 0.1–0.2 of the maximum value (this lowest value of density defines the limit of the films and determines their size and shape) in the diamond films with the different coverage of the surface are given. Herewith the separation distances D between the films changed from 1.054 Å to 2.336 Å with step 0.1424 Å. From these drawings it is clear that the type of the surface coating of the diamond film considerably influences upon the restructuring of the distribution of the valence electrons on the surface, and in the field of between films and in the inner layers of the films. As follows at the presence of the incomplete bonds of the surface carbon atoms in the spatial distribution of electrons the extracted from the surface regions are appeared.

In Fig. 14 the spatial density distributions of valence electrons within the interval of 0.3–0.4 of the maximum value in the diamond films with the 50% fluorine coverage of the surface are given. Herewith the separation distances D between the films changed from 1.054 Å to 2.336 Å with step 0.1424 Å.

On drawing Fig. 15 comparison of the spatial distributions of the valence electrons density in the tribological contact of two diamond films coated by 50% hydrogen or 50% fluorine are realized, these films were situated on distance of separation between films 1.197 Å and 2.336 Å.

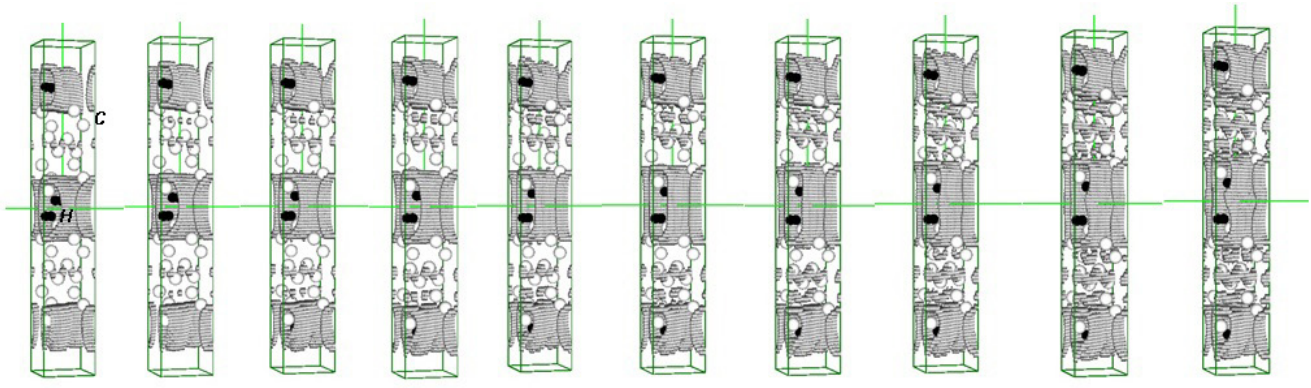

Fig. 12. The spatial distribution of the valence electrons density within the interval of 0.1–0.2 of the maximum value in the tribological contact of two diamond films with the complete hydrogen coverage for the separation distance D between films 1.054 Å, 1.197 Å, 1.339 Å, 1.482 Å, 1.624 Å, 1.766 Å, 1.909 Å, 2.051 Å, 2.194 Å, 2.336 Å (respectively from left to right).

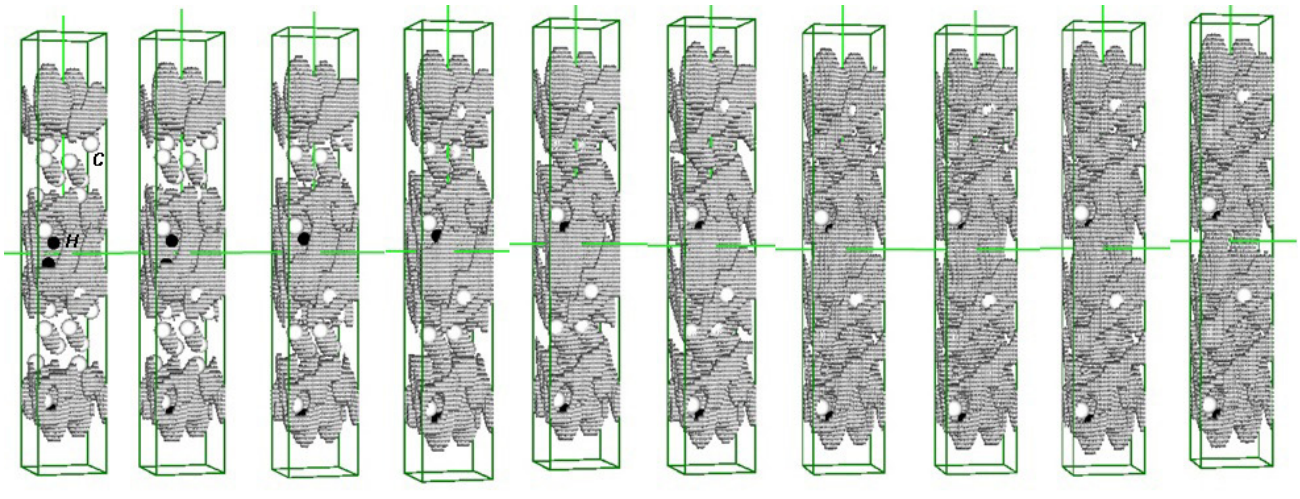

Fig. 13. The spatial distribution of the valence electrons density within the interval of 0.1–0.2 of the maximum value in the tribological contact of two diamond films with the incomplete (50%) hydrogen coverage for the separation distance D between films 1.054 Å, 1.197 Å, 1.339 Å, 1.482 Å, 1.624 Å, 1.766 Å, 1.909 Å , 2.051 Å, 2.194 Å, 2.336 Å (respectively from left to right).

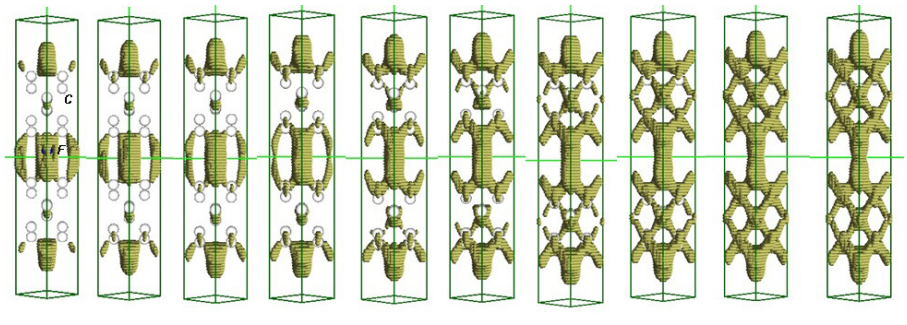

Fig. 14. The spatial distribution of the valence electrons density within the interval of 0.3–0.4 of the maximum value in the tribological contact of two diamond films with the incomplete (50%) fluorine coverage for the separation distance D between films 1.054 Å, 1.197 Å, 1.339 Å, 1.482 Å, 1.624 Å, 1.766 Å, 1.909 Å , 2.051 Å, 2.194 Å, 2.336 Å (respectively from left to right).

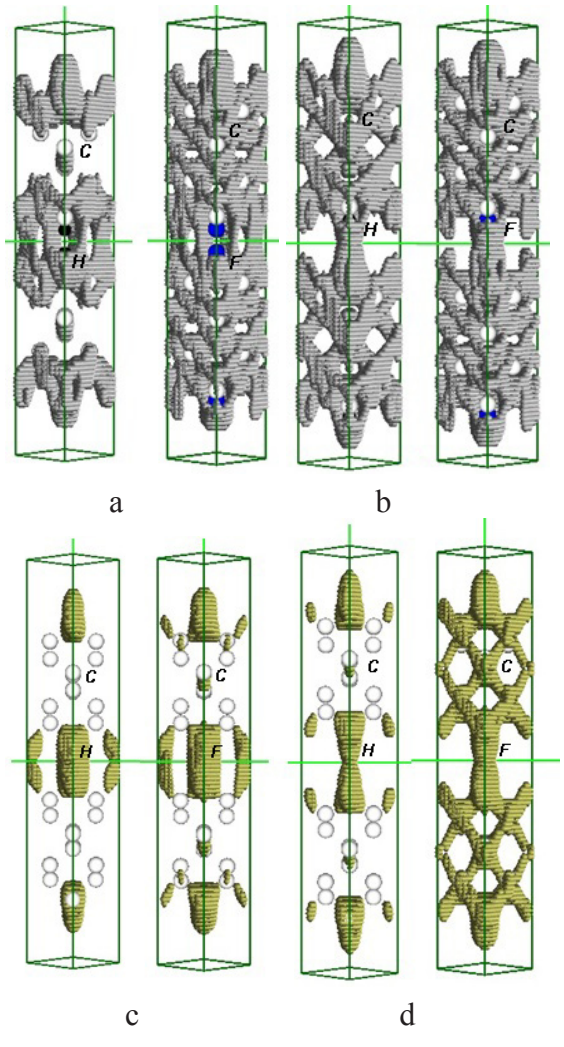

Fig.15. The spatial distribution of the valence electrons density within the interval of 0.1–0.2 of the maximum value and within the interval of 0.3–04 in the tribological contact of two diamond films coated by 50% hydrogen and 50% fluorine, respectively: a), c) the separation distance between the films is 1.197 Å; b), d) the separation distance between the films is 2.336 Å.

Comparing the valence electron density distributions for the two diamond sliding films coated by 50% hydrogen or 50% fluorine (Fig. 13-15), see the localization of electronic charge in the contact area between the films is present. This charge can be interpreted as static charging films that slip. The most brightly seen localization of its kind in tribological contacts of films coated by hydrogen is fixed when the separation distance D between the films is 1.197 Å.

Conclusions

The methods of electron density functional and pseudopotential theories were used to calculate the distributions of valence electron density, the total energy and static friction for diamond or diamond-like films with uncovered surfaces or covered by hydrogen or fluorine.

It is determined that the change in the friction force between two the slip rough diamond-like carbon films with thickness about 7 Å each and with a mixture of 50% diamond-like and 50% graphite-like bonds without coverage is due to the changing nature between atomic interaction from the short donor-acceptor to the long-range Coulomb.

It was found that the half concentration of the broken bonds of carbon atoms on the smooth surfaces of diamond films, which exist in tribological contact, increases the slip resistance by comparison with the films with surface complete covered by hydrogen. This increase occurs on magnitude of one order for the films coated by 50% hydrogen and on two orders for the films coated by 50% fluorine.

For diamond films coated by 50% fluorine or 50% hydrogen, which slithered one comparatively another with a shift of the surface atoms, a nonmonotonic fluctuations in the value of static friction are characterized, i.e. the instability of their tribological properties is revealled.

For two diamond films coated by hydrogen or 50% fluorine, which exist in tribological contact, it is observed the areas of localization of electronic charge at the site of contact between the films, which were treated as static charging of films that slipped.

References

1. K. Holmberg, H. Ronkainen, A. Matthews. Tribology of thin coatings // Ceram. Int. – 2000. – Vol. 26. – P. 787–795.
2. K. Hayashi, K. Tezuka, N. Ozawa, T. Shimazaki, K. Adachi, and M. Kubo. Tribochemical Reaction Dynamics Simulation of Hydrogen on a Diamond-

Like Carbon Surface Based on Tight-Binding Quantum Chemical Molecular Dynamics // J. Phys. Chem. C, 115(46), pp. 22981-22986 (2013).
3. G. T. Gao , Paul T. Mikulski , Judith A. Harrison. Molecular-Scale Tribology of Amorphous Carbon Coatings: Effects of Film Thickness, Adhesion, and Long-Range Interactions // J. Am. Chem. Soc., 124 (24), pp 7202–7209 (2002).
4. R. M. Balabai, Ukrainian Jourmal of Physics 58, 389 (2013).
5. Researchers unstick nanoparticle friction // Nano Today, 2011, Volume 7, Issue 1, P. 2.
6. Raisa Neitola, Tapani A. Pakkanen. Ab Initio Studies on the Atomic-Scale Origin of Friction between Diamond (111) Surfaces // J. Phys. Chem. B, 2001, 105 (7), pp 1338–1343.
7. Guangtu Gao, Rachel J. Cannara , Robert W. Carpick , Judith A. Harrison. Atomic-Scale Friction on Diamond: A Comparison of Different Sliding Directions on (001) and (111) Surfaces Using MD and AFM // Langmuir, 2007, 23 (10), pp 5394–5405.
8. G. Zilibotti, M. C. Righi. Ab Initio Calculation of the Adhesion and Ideal Shear Strength of Planar Diamond Interfaces with Different Atomic Structure and Hydrogen Coverage // Langmuir, 2011, 27 (11), pp 6862–6867.
9. Maria-Isabel De Barros Bouchet, Giovanna Zilibotti, Christine Matta, Maria Clelia Righi, Lionel Vandenbulcke, Beatrice Vacher, Jean-Michel Martin. Friction of Diamond in the Presence of Water Vapor and Hydrogen Gas. Coupling Gas-Phase Lubrication and First-Principles Studies // J. Phys. Chem. C, 2012, 116 (12), pp 6966–6972.
10. Shandan Bai, Tasuku Onodera, Ryo Nagumo, Ryuji Miura, Ai Suzuki, Hideyuki Tsuboi, Nozomu Hatakeyama, Hiromitsu Takaba, Momoji Kubo, Akira Miyamoto. Friction Reduction Mechanism of Hydrogen- and Fluorine-Terminated Diamond-Like Carbon Films Investigated by Molecular Dynamics and Quantum Chemical Calculation // J. Phys. Chem. C, 2012, 116 (23), p. 12559.

This article has been received within 2014

UDC 621.385.221

R. M. Balabai, A. G. Barilka

TRIBOLOGICAL CHARACTERISTICS OF THE DIAMOND-LIKE CARBON FILMS COVERED BY HYDROGEN OR FLUORINE: AB INITIO CALCULATIONS

Abstract

It was found that the half concentration of the broken bonds of carbon atoms on the smooth surfaces of diamond films, which exist in tribological contact, increases the slip resistance by comparison with the films with surface complete covered by hydrogen. This increase occurs on magnitude of one order for the films coated by 50% hydrogen and on two orders for the films coated by 50% fluorine.

For two diamond films coated by hydrogen or 50% fluorine, which exist in tribological contact, it

is observed the areas of localization of electronic charge at the site of contact between the films, which were treated as static charging of films that slipped

Key words: tribological contact, the concentration, the diamond-like carbon, hydrogen, fluorine

УДК 621.385.221

Р. М. Балабай, А. Г. Барилка

ТРИБОЛОГІЧНІ ХАРАКТЕРИСТИКИ АЛМАЗОПОДІБНИХ ВУГЛЕЦЕВИХ ПЛІВОК, ПОКРИТИХ ВОДНЕМ АБО ФТОРОМ: РОЗРАХУНКИ AB INITIO

Резюме

Було встановлено, що половинна концентрація незавершених зв'язків атомів вуглецю на гладких поверхнях алмазних плівок, що у трибологічному контакті, збільшує опір ковзанню у порівнянні з плівками з повністю завершеними воднем поверхнями: на порядок для плівок, покритих на 50% воднем, і на два порядки для плівок, покритих на 50% фтором.

Для двох алмазних плівок з покриттям воднем чи фтором у 50% у трибологічному контакті спостерігалися області локалізації електронного заряду в місці контакту між плівками, котрі трактувалися як статичне зарядження плівок, що ковзали.

Ключові слова: трибологічний контакт, концентрація, алмазоподібні вуглецеві плівки, водень, фтор.

УДК 621.385.221

Балабай Р. М., Барилка А. Г.

ТРИБОЛОГИЧЕСКИЕ ХАРАКТЕРИСТИКИ АЛМАЗОПОДОБНЫХ УГЛЕРОДНЫХ ПЛЕНОК, ПОКРЫТЫХ ВОДОРОДОМ ИЛИ ФТОРОМ: РАСЧЕТЫ AB INITIO

Резюме

Было установлено, что половинная концентрация незавершенных связей атомов углерода на гладких поверхностях алмазных пленок, в трибологическом контакте, увеличивает сопротивление скольжению по сравнению с пленками с полностью завершенными водородом поверхностями: на порядок для пленок, покрытых на 50% водородом, и на два порядка для пленок, покрытых на 50% фтором.

Для двух алмазных пленок с покрытием водородом или фтором в 50% в трибологическом контакте наблюдались области локализации электронного заряда в месте контакта между пленками, которые трактовались как статический заряд пленок, которые скользили.

Ключевые слова: трибологический контакт, концентрация, алмазоподобные углеродные плёнки, водород, фтор.

UDC 621.315.592

A. P. Chebanenko, A. E. Stupak

PHOTOELECTRIC PROPERTIES OF THE STRUCTURE Cr-ZnSe WITH SCHOTTKY BARRIER

I. I. Mechnikova National University of Odessa, Dvoryanska St.,2, Odessa,65026,Ukraine

Explored the structures based on the ZnSe single crystal with a semitransparent layer of chromium. The current-voltage and capacitance-voltage characteristics of the structures indicate that Cr-ZnSe contact is a lock and close in its properties to the Schottky barrier. The calculated equilibrium barrier height is 1.22 eV. In the structures in the reverse biased direction to the detected occurrence of photosensitivity wavelength region of the spectrum up to 230 nm wavelength. This is due to the deterioration of conditions for the recombination of photoexited carriers in fast recombination centers in a strong electric field in the surface region of the reverse bias pin barrier. Calculated from critical frequency of the photocurrent spectrum contact barrier height value of 1.18 eV goes with the results obtained from the C-V characteristics.

1. INTRODUCTION

In recent years, especially acute problem of reception and quantifying ultraviolet (UV) radiation. One of the most promising types of UV photodiode receivers is the Schottky barrier. Surface potential barrier provides effective separation of charge carriers born in this area as a result of absorption of energy quantums significantly larger than band gap. For the manufacture of such detectors wide semiconductor compounds are used mainly [1, 2].

The literature contains information about the photo detectors based on the contact Ni-ZnSe [3, 4], having a sufficiently high sensitivity in the range of 0,25-0,5 microns. Other possible metals suitable for the manufacture of zinc selenide with a Schottky barrier may be an element of the same group of the periodic table - chromium. Optical characteristics of the semitransparent film of chromium in the aforementioned spectral region is not worse than the thin films of nickel. The films show good adhesion of chromium to the surface of the zinc selenide crystal. However, increasing the work function of chromium (4,6 eV) than that of nickel (4,4 eV) allows us to expect that the potential barrier in contact Cr-ZnSe is higher than in contact Ni-ZnSe. This should yield higher intensity of the internal electric field in the surface region of the contact barrier and, finally, lead to increased photosensitivity of photodetector in the near UV - spectrum [5]. In this paper, on the chemically polished surface of low-resistivity single crystals of zinc selenide were deposited translucent chromium films. Purpose of the research was to determine the parameters of the contact barrier Cr-ZnSe, the study of its electrical and spectral characteristics and finding the possibility of using such a structure as a photodetector in the near-UV - spectrum.

2. EXPERIMENT AND DISCUSSION

Figure 1 shows the current-voltage characteristics of the structure of Cr-ZnSe, measured at opposite polarities of bias. As can be seen, the

contact shows rectifying properties (rectification ratio at 0,8 V voltage reaches 10^7). This indicates that in the Cr-ZnSe contact exists a sufficiently high potential barrier. Under reverse bias (Fig. 1, curve 2) current-voltage characteristic obeys to dependency $I \sim V^{1/2}$, which is typical for "thick" Schottky barrier.

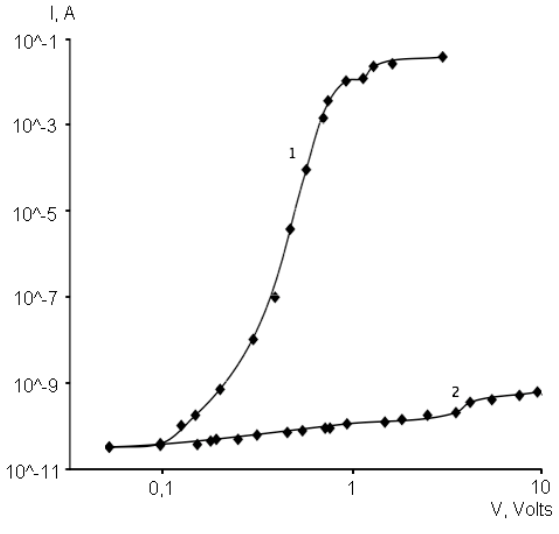

Fig. 1. The current-voltage characteristics of the Cr-ZnSe contact, measured by direct (1) and reverse (2) bias.

With direct polarity of the applied bias (Fig. 1, curve 1) current-voltage characteristic is described by I~exp (e·V/ß·k·T), as evidenced by its straightening in coordinates lnl ÷ V.

ß ideality factor was ß ≈ 1,47. The obtained value of ß, significantly greater than one, allows to conclude that in Cr-ZnSe contact a thin oxide layer is present, as well as a sufficiently high density of surface states.

Figure 2 (curve 1) shows the capacitance-voltage characteristics of the test contact. Curve 2 shows the dependency C-V, built in the coordinates $(S/C)^2$-V, typical for the Schottky barrier [6]. Extrapolation of this dependence on the voltage axis (Fig. 2, curve 2) allows to determine the equilibrium height of φ barrier for electrons from the semiconductor. It is equal to φ ≈ 0,98 eV.

Using the numerical value of the capacitance at zero bias (Fig. 2, curve 1) was estimated the equilibrium barrier thickness (L ≈ 2,8 μm). The numerical value of the slope of the curve 2 (Fig. 2) allowed to calculate the equilibrium of concentration of free electrons in the ZnSe crystal ($n_0 \approx 1{,}2*10^{14}$ cm^{-3}) and the energy separation of the equilibrium of Fermi level from the bottom of the conduction band in the semiconductor (E_f=0,24 eV). In the calculations for zinc selenide were accepted the values of the relative permittivity ε= 9,1 and electron mobility μ_n = 500 $cm^2/V{\cdot}s$.

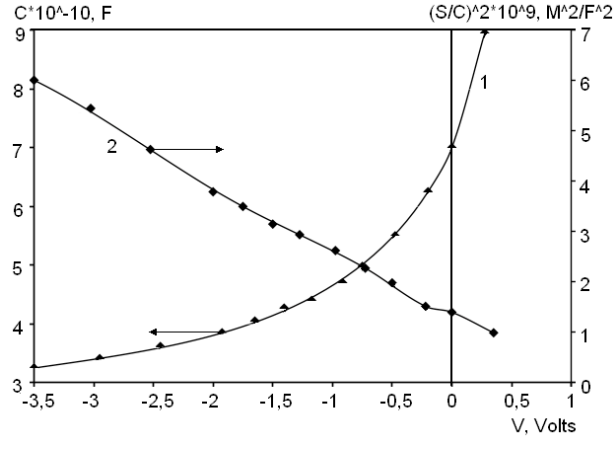

Fig. 2. Capacitance-voltage characteristics of Cr-ZnSe contact.

Point values of E_f and φ allowed us to construct the energy diagram of the Cr-ZnSe test contact, which in the absence of applied bias is shown schematically in Fig. 3.

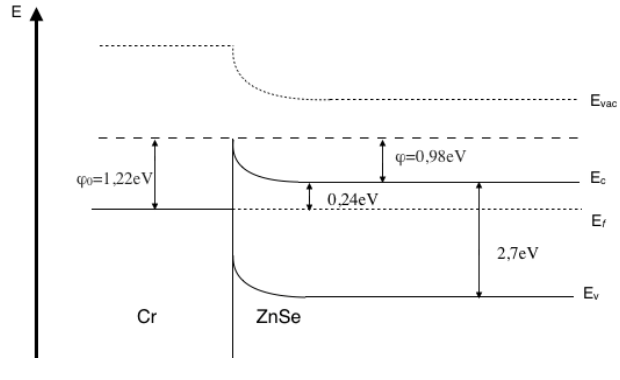

Fig. 3. Energy diagram of the Cr-ZnSe contact balance.

Figure 4 represents the spectral characteristics of photocurrent at different bias conditions of the structure. Curve 1 (Fig. 4) shows the photocurrent spectrum in direct applied voltage V=+l V,

i.e. in an environment where the potential barrier φ is practically "smoothed". Therefore, the curve 1 actually reflects the spectral photosensitivity of the total volume of the ZnSe crystal. Slump photosensitivity in the wavelength region of the spectrum due to the fact that the incident light rays with energies, greater than the band gap, are absorbed in a thin surface layer of the crystal, where is a high density of surface fast recombination centers. Depending on this, apart from its own high photosensitivity (λ_{max} = 460 nm), there are also two bands of impurity photoconductivity. These are a mild band with a maximum at a wavelength at λ_{max} = 530 nm and a broad band with a maximum at λ_{max} = 800 nm. Nature of these bands is known and associated with associative defects ($V_{Zn}Al_{Zn}$).

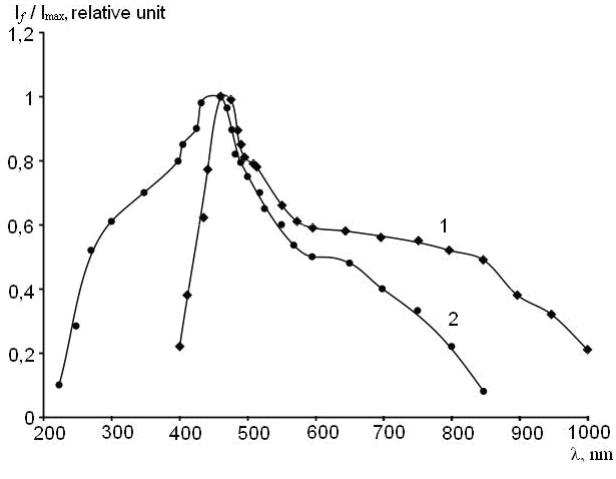

Fig. 4. Spectral dependence of the photocurrent structure of Cr-ZnSe and a forward bias V=+1 V (1) and a reverse bias V=-5 V (2).

Curve 2 (Fig. 4) shows the photocurrent spectrum measured under reverse bias contact V=-5V. A significant increase in photosensitivity short wavelengths up to wavelength λ ≈ 230 nm can be seen. It is due to the fact that the surface in the excited electrons of the semiconductor layer under the influence of the field in the region of the barrier are moved from the illuminated surface into the sample without time to recombine with holes.

Maximum on the graph corresponds to transitions, when the incident photon energy is close to the band gap. Also on the schedule (curve 2) can be seen a lingering long-wavelength tail, which can be explained by the photoemission of electrons from the metal. If the energy of the incident quantum is not less than the height of the barrier, the electrons to overcome barriers contribute to the photocurrent, leading to an increase in the photocurrent. If the quantum energy is less than the height of the potential barrier, the electrons are no longer able to overcome it and the photocurrent decreases, which explains the long-wavelength limit.

According to the Fowler formula [7], a long wavelengths photocurrent under reverse bias can be transformed into coordinates $I_{\phi}^{1/2}$- (hv), in which this dependence should rectify (Fig. 5). By extrapolating the resulting line on the energy axis the height of the barrier from the metal φ_0' can be determined. It proved to be φ_0'= 1,18 eV, which goes well with the results obtained from the energy diagram (Fig. 3) φ_0 = 1,22 eV.

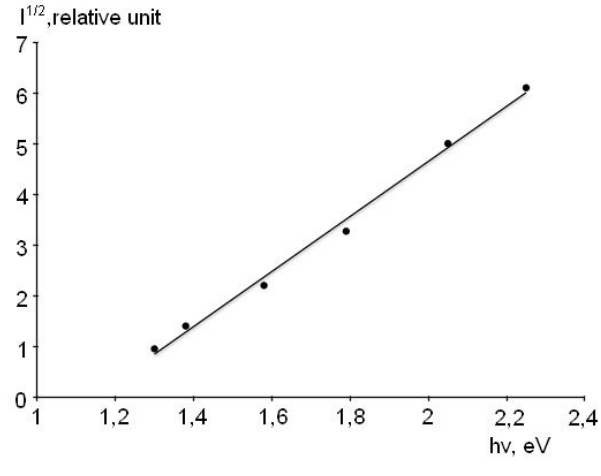

Fig. 5. Long wavelengths photocurrent under reverse bias V =-5 V, built in coordinates $I_f^{1/2}$- (hv).

3. CONCLUSIONS

The results show that the locking contact Cr-ZnSe shows sufficient photosensitivity in spectral region of wavelengths λ≥0,23 microns. It can be used in the development of radiation detectors in the near-UV region of the spectrum.

REFERENCES

1. 1. Blank T.V., Goldberg Yu.A. - Poluprovodnikovyye fotopreobrazovateli dlya UF oblasti spektra. - Fizika i tekhnika poluprovodnikov, 2003, t. 37, vyp. 9, s.1025-1055.
2. 2. Monroy E., Omnes F., Calle F. – Wide-bandgap semiconductor ultraviolet photodetectors. – Semiconductor science and technology. – 2003, vol. 18, p. R33-R55.
3. 3. Ilchuk G. A., Rud V. Yu., Rud Yu. V. i dr. - Fotochuvstvitelnost struktur na osnove monokristallov ZnSe. - Fizika i tekhnika poluprovodnikov, 2000, t. 34, vyp. 7, s. 809-813.
4. 4. Perevertaylo V. L., Dobrovolskiy Yu. G., Popov V. M. i dr. - Fotodiod ultrafioletovogo diapazona na osnove selenida tsinka.- Tekhnologiya i konstruirovaniye v elektronnoy apparature, №2, 2010, s. 17-21.
5. 5. Bouhdada M., Hanzaz F., Vigue I.P., Furie I. – Shottky barier near-ultraviolet photodetectors based on ZnSe. – Active and passive electronic devise. – 2005, vol. 1, p. 79-89.
6. 6. Kosyachenko L. F., Sklyaruk V. M., Maslyanchuk O. L. - Osobennosti elektricheskikh kharakteristik diodov Shottki na osnove CdTe s pochti sobstvennoy provodimostyu. - Zhurnal tekhnicheskoy fiziki, 2006, t. 32, vyp. 24, s. 29-37.
7. 7. Melebayev D., Melebayev G. D., Rud V. Yu., Rud Yu. V. - Fotochuvstvitelnost i opredeleniye vysoty baryera Shottki v strukturakh Au - n - GaAs. - Zhurnal tekhnicheskoy fiziki, 2008, t. 78, vyp. 1, s. 137-141.

This article has been received within 2014

UDC 621.315.592

A. P. Chebanenko, A. E. Stupak

PHOTOELECTRIC PROPERTIES OF THE STRUCTURE Cr-ZnSe WITH SCHOTTKY BARRIER

Abstract

Explored the structures based on the ZnSe single crystal with a semitransparent layer of chromium. The current-voltage and capacitance-voltage characteristics of the structures indicate that Cr-ZnSe contact is a lock and close in its properties to the Schottky barrier. The calculated equilibrium barrier height is 1.22 eV. In the structures in the reverse biased direction to the detected occurrence of photosensitivity wavelength region of the spectrum up to 230 nm wavelength. This is due to the deterioration of conditions for the recombination of photoexited carriers in fast recombination centers in a strong electric field in the surface region of the reverse bias pin barrier. Calculated from critical frequency of the photocurrent spectrum contact barrier height value of 1.18 eV goes with the results obtained from the C-V characteristics.

Key words: Schottky barrier, UV receiver, photosensitivity, fast recombination centers.

UDC 621.315.592

А. П. Чебаненко, О. Е. Ступак

ФОТОЕЛЕКТРИЧНІ ВЛАСТИВОСТІ СТРУКТУР Cr-ZnSe З БАР'ЄРОМ ШОТТКИ

Резюме

Досліджено структури на основі монокристалів ZnSe з напівпрозорим шаром хрому. Вольт-амперні та вольт-фарадні характеристики структур свідчать, що контакт Cr-ZnSe є запірним та близьким за своїми властивостями до бар'єру Шоттки. Розрахована рівноважна висота бар'єру складає 1,22 еВ. В структурах, зміщених у зворотньому напрямку, виявлено виникнення фоточутливості в короткохвильовій області спектру аж до довжини хвилі 230 нм. Це зумовлено погіршенням умов для рекомбінації фотозбуджених носіїв на центрах швидкої рекомбінації в сильному електричному полі у приповерхневому шарі зворотньо зміщеного контактного бар'єру. Розраховане із довгохвильової межі спектру фотоструму значення висоти контактного бар'єру 1,18 еВ добре узгоджується з результатами, отриманими із C-V характеристик.

Ключові слова: бар'єр Шоттки, УФ-приймач, фоточутливість, центри швидкої рекомбінації.

PACS: 73.20.Hb, 73.25.+I; UDC 621.315.592

А. П. Чебаненко, А. Э. Ступак

ФОТОЭЛЕКТРИЧЕСКИЕ СВОЙСТВА СТРУКТУР Cr-ZnSe С БАРЬЕРОМ ШОТТКИ

Резюме

Исследованы структуры нас основе монокристаллов ZnSe с полупрозрачным слоем хрома. Вольт-амперные и вольт-фарадные характеристики структур свидетельствуют, что контакт Cr-ZnSe является запорным и близким по своим свойствам к барьеру Шоттки. Рассчитанная равновесная высота барьера составляет 1,22 эВ. В структурах, смещенных в обратном направлении, обнаружено появление фоточувствительности в коротковолновой области спектра вплоть до длины волны 230 нм. Это связано с ухудшением условий для рекомбинации фотовозбужденных носителей на центрах быстрой рекомбинации в сильном электрическом поле в приповерхностной области обратно смещенного контактного барьера. Рассчитанное из длинноволновой границы спектра фототока значение высоты контактного барьера 1,18 эВ хорошо согласуется с результатами, полученными из C-V характеристик.

Ключевые слова: барьер Шоттки, УФ-приемник, фоточувствительность, центры быстрой рекомбинации.

UDC 539.184

O. Yu. Khetselius

Odessa State Environmental University, 15, Lvovskaya str., Odessa, Ukraine
Odessa National Politechnical University, 1, Shevchenko av., Odessa, Ukraine
e-mail: nuckhet@mail.ru

OPTIMIZED PERTURBATION THEORY TO CALCULATING THE HYPERFINE LINE SHIFT AND BROADENING FOR HEAVY ATOMS IN THE BUFFER GAS

It is presented review of a new consistent relativistic approach to determination of collisional shift and broadening hyperfine lines for heavy atoms in an atmosphere of the buffer inert gas. It is based on the atomic gauge-invariant relativistic perturbation theory and the exchange perturbation theory. As illustration, consistent approach is applied to calculating the interatomic potentials, hyperfine structure line collision shift and broadening for heavy atoms, in particular, atoms of alkali elements – rubidium, caesium, and thallium, ytterbium, in an atmosphere of the buffer inert gas.

1 Introduction

The broadening and shift of atomic spectral lines by collisions with neutral atoms has been studied extensively since the very beginning of atomic physics, physics of collisions etc [1–5]. High precision data on the collisional shift and broadening of the hyperfine structure lines of heavy elements (alkali, alkali-earth, lanthanides, actinides and others) in an atmosphere of the buffer (for example, inert) gases are of a great interest for modern quantum chemistry, atomic and molecular spectroscopy, astrophysics and metrology as well as for studying a role of weak interactions in atomic optics and heavy-elements chemistry [1-10]. As a rule, the cited spectral lines shift and broadening due to a collision of the emitting atoms with the buffer atoms are very sensitive to a kind of the intermolecular interaction. It means that these studies provide insight into the nature of interatomic forces and, hence, they provide an excellent test of theory.

An accurate analysis of the spectral line profiles is a powerful technique for studying atomic and molecular interactions and is often necessary for probing matter in extreme conditions, such as in stellar atmospheres, ultracold traps and Bose–Einstein condensates [3,6]. Besides, calculation of the hyperfine structure line shift and broadening allows to check a quality of the wave functions (orbitals) and study a contribution of the relativistic and correlation effects to the energetic and spectral characteristics of the two-center (multi-center) atomic systems. From the applied point of view, the mentioned physical effects form a basis for creating an atomic quantum measure of frequency [10,12,14]. The corresponding phenomenon for the thallium atom has attracted a special attention because of the possibility to create the thallium quantum frequency measure. Alexandrov et al [10] have realized the optical pumping thallium atoms on the line of 21GHz, which corresponds to transition between the components of hyperfine structure for the Tl ground state. These authors have measured the collisional shift of this hyperfine line in the atmosphere of the He buffer gas.

The detailed non-relativistic theory of collisional shift and broadening the hyperfine structure lines for simple elements (such as light alkali elements etc.) was developed by many authors (see, for example, Refs. [1-14]). However, until now an accuracy of the corresponding available data has not been fully adequate to predict or identify transitions within accuracy as required for many applications. It is obvious that correct taking into account the relativistic and correlation effects is absolutely necessary in order to obtain

sufficiently adequate description of spectroscopy of the heavy atoms in an atmosphere of the buffer gases. This stimulated our current investigation whose goals were to propose a new relativistic perturbation theory approach to calculating the interatomic potentials and hyperfine structure line collision shifts and broadening for the alkali and lanthanide atoms in an atmosphere of the inert gases. The basic expressions for the collision shift and broadening hyperfine structure spectral lines are taken from the kinetic theory of spectral lines [6,7,11,12].

The exchange perturbation theory (the modified version EL-HAV) has been used to calculate the corresponding potentials (see details in [1-5]). Let us note that sufficiently detailed reviews of the different versions of exchange perturbation theory are presented, for example, in Refs.[1-9]. It is worth to remind about the known difficulties of the exchange perturbation theory, associated with complex structure series, which contain the overlap integrals and exchange integrals [1]. Due to the ambiguity of the expansion in the antisymmetric functions it had been built a number of different formalisms of an exchange perturbation theory. Usually one could distinguish two groups in dependence on the zero-order approximation of the Hamiltonian. In the symmetry adapted theories the zeroth-approximation Hamiltonian is an asymmetric, but the zeroth- approximation functions have the correct symmetry. In symmetric formalisms there is constructed a symmetric zeroth-approximation Hamiltonian such as the antisymmetric function is its eigen function. Further formally standard Rayleigh - Schrodinger perturbation theory is applied. However, this approach deals with the serious difficulties in switching to systems with a number of electrons, larger than two. In addition, the bare Hamiltonian is not hermitian.

So the symmetry adapted theories gain more spreading. In particular, speech is about versions as EL-HAV (Eisenschitz-London-Hirschfeledervan der Avoird), MS-MA (Murrel-Shaw-Musher-Amos) and others (see details in Refs. [4,5]). The detailed analysis of advantages and disadvantages of the exchange perturbation theory different versions had been performed by Batygin et al (see, for example, [11,12]) in studying the hyperfine structure line shift of the hydrogen atom in an atmosphere of an inert buffer gas. In our work the modified version of the EL-HAV exchange perturbation theory has been used to calculate the corresponding potentials (see details in [4]). On fact [4] this is the Schrödinger type perturbation theory for intermolecular or interatomic interactions, using the wave operator formalism. To include all exchange effects, wavefunctions are used whose symmetry with respect to permutations of both electronic and nuclear coordinates can be prescribed arbitrarily. The interaction energy is obtained as a series in ascending powers of the interaction operator. Further van der Avoird [4] has proved that every term in this series is real and that the terms of even order are negative definite for perturbation of the ground state. It has been also verified that up to and including third order the results of this theory, if they are restricted to electron exchange only, agree exactly with those of the Eisenschitz-London theory (see other details in Refs. [1-5]).

The next important point is choice of the most reliable version of calculation for multielectron atomic field and generating the basis of atomic orbitals. In Refs. [17-30] a consistent relativistic energy approach combined with the relativistic many-body perturbation theory has been developed and applied to calculation of the energy and spectroscopic characteristics of heavy atoms and multicharged ions. This is the relativistic many-body perturbation theory with the optimized Dirac-Fock (Dirac-Kohn-Sham) zeroth approximation and taking into account the nuclear, radiation, exchange-correlation corrections. It is worth to remind that this approach has been successfully used to calculate the b-decay parameters for a number of allowed (super allowed) transitions and study the chemical bond effect on b-decay parameters [29]. This approach has been used in our work to generate a basis of relativistic orbiltals for heavy atoms. Besides, the correct procedures of accounting for the many-body exchange-correlation effects and relativistic orbital basis optimization (in order to provide a performance of the gauge-invariant principle) as well as accounting for the highly excited and continuum states have been used.

Earlier it was shown [21-30] that an adequate description of the energy and spectral characteristics of the multi-electron atomic systems requires

using the optimized basis of wave functions. In Ref. [31] a new ab initio optimization procedure for construction of the optimized basis had been proposed and based on the principle of minimization of the gauge dependent multielectron contribution $ImdE_{ninv}$ of the lowest QED perturbation theory corrections to the radiation widths of atomic levels. The minimization of the functional $ImdE_{ninv}$ leads to the Dirac-Kohn-Sham-like equations for the electron density that are numerically solved. This procedure has been implemented into our approach. In result, the numerical data on the hyperfine line collision shifts and broadening for some alkali (Rb, Cs), thallium and ytterbium atoms in atmosphere of the inert gas (such as He, Ke, Xe) are presented and compared with available theoretical and experimental data (see, for example, [1-12]). Besides, new data on the van der Waals constavts and other parameters for the studied two-atomic systems are presented too.

2 Optimized atomic perturbation theory and kinetic theory of spectral lines

In order to calculate a collision shift of the hyperfine structure spectral lines one can use the following expression known in the kinetic theory of spectral lines shape (see Refs. [6,7,11,12]):

$$f_p = \frac{D}{p} = \frac{4\pi w_0}{kT}\int_0^\infty [1+g(R)]dw(R)\exp\left(-U(R)/kT\right)R^2 dR \tag{1a}$$

$$g(R) = \begin{cases} \dfrac{2}{3\sqrt{\pi}}\left(-\dfrac{U(R)}{kT}\right)^{3/2}, & U<0, \\ 0, & U>0, \end{cases} \tag{1b}$$

Here $U(R)$ is an effective potential of interatomic interaction, which has the central symmetry in a case of the systems A—B (in our case, for example, A=Rb,Cs; B=He); T is a temperature, w_0 is a frequency of the hyperfine structure transition in an isolated active atom; $dw(R)=Dw(R)/w_0$ is a relative local shift of the hyperfine structure line; $(1+g(R))$ is a temperature form-factor.

The local shift is caused due to the disposition of the active atoms (say, the alkali atom and helium He) at the distance R. In order to calculate an effective potential of the interatomic interaction further we use the exchange perturbation theory formalism (the modified version EL-HAV) [9]).

Since we are interested by the alkali (this atom can be treated as a one-quasiparticle systems, i.e. an atomic system with a single valence electron above a core of the closed shells) and the rare-earth atoms (here speech is about an one-, two- or even three-quasiparticle system), we use the classical model for their consideration. The interaction of alkali (A) atoms with a buffer (B) gas atom is treated in the adiabatic approximation and the approximation of the rigid cores. Here it is worth to remind very successful model potential simulations of the studied systems (see, for example, Refs. [32-41]).

In the hyperfine interaction Hamiltonian one should formally consider as a magnetic dipole interaction of moments of the electron and the nucleus of an active atom as an electric quadrupole interaction (however, let us remind that, as a rule, the moments of nuclei of the most (buffer) inert gas isotopes equal to zero) [6].

The necessity of the strict treating relativistic effects causes using the following expression for a hyperfine interaction operator H_{HF} (see, eg., [1,5]):

$$H_{\mathrm{HF}} = a\sum_{i=1}^{N} I\frac{\alpha_i \times r_i}{r_i^3}, \qquad a = -2\mu\frac{e^2 h}{2m_p c}, \tag{2}$$

where I – the operator of the nuclear spin active atom, a_i – Dirac matrices, m_p – proton mass, μ - moment of the nucleus of the active atom, expressed in the nuclear Bohr magnetons. Of course, the summation in (2) is over all states of the electrons of the system, not belonging to the cores. The introduced model of consideration of the active atoms is important to describe an effective interatomic interaction potential (an active atom – an passive atom), which is centrally symmetric (J_A=1/2) in our case (the interaction of an alkali atom with an inert gas atom).

Let us underline that such an approximation is also acceptable in the case system "thallium atom – an inert gas atom" and some rare-earth atoms, in spite of the presence of p-electrons in the thallium (in the case of rare-earth atoms, the situation is more complicated).

Next, in order to determine a local shift within the consistent theory it should be used the expression obtained in one of versions of the exchange perturbation theory, in particular, EL-HAV version (see [1-5,8,9]). The relative local shift of the hyperfine structure line is defined with up to the second order in the potential V of the Coulomb interaction of the valence electrons and the cores of atoms as follows:

$$\delta\omega\ (R)=\frac{S_0}{1-S_0}+\Omega_1+\Omega_2-\frac{C_6}{R^6}\left(\frac{2}{\overline{E_a}}+\frac{1}{\overline{E_a}+\overline{E}_B}\right),$$
$$\overline{E}_{a,b}=\left(I_{a,\,b}+E_{1a,\,b}\right)/2. \qquad (3)$$

Here S_0 is the overlapping integral; C_6 is the van der Waals coefficient; I is the potential of ionization; $E_{1a,b}$ is the energy of excitation to the first (low-lying) level of the corresponding atom. The values W_1, W_2 in Eq. (3a) are the first order non-exchange and exchange non-perturbation sums correspondingly. These values are defined as follows:

$$\Omega_1=\frac{2}{N(1-S_0)\rho_0}\sum_k{}' \frac{\langle\Phi_0'(1)\left|H_{HF}'\right|\Phi_k'(1)\rangle V_{k0}}{E_0-E_k} \qquad (4a)$$

$$\Omega_2=\frac{2}{N(1-S_0)\rho_0}\sum_k{}' \frac{\langle\Phi_0'(1)\left|H_{HF}'\right|\Phi_k'(1)\rangle U_{k0}}{E_0-E_k} \qquad (4b)$$

where $\acute{I}_{HF}' = \frac{[a\times r_1]_z}{r^3}$ is the transformed operator of the hyperfine interaction; $[a\times r_1]_z$ is Z component of the vector product; Z - quantization axis directed along the axis of the quasimolecule; N is the total number of electrons, which are taken into account in the calculation; E_k, $\Phi_k'(1)=F_{k_a}'(1)\varphi_{k_b}(2...N)$ are an energy and a non-symmetrized wave function of state $k=\{k_a,,k_b\}$ for the isolated atoms A and B.

The non-exchange matrix element of the Coulomb interatomic interaction is as:

$$V_{ko}=<\Phi'_k(1)\ |\ V(1)\ |\ \Phi'_0(1)>. \qquad (5a)$$

Correspondingly the exchange matrix element is as follows:

$$U_{k0}=\sum_{i=2}^{N}\langle\Phi_k'(1)\left|V(i)\right|\Phi_0'(i)\rangle \qquad (5b)$$

The operator $V(i)$ (for example, in a case of the system Rb(a)-He(b)) can be presented as follows:

$$V(i)=U_{SCF}(r_{a3})+U_{SCF}(r_{a4})-2U_{SCF}(R)+\frac{1}{r_b}, \qquad (6)$$

where $U_{SCF}(r)$ is the self-conjunctive field, created by an active atom core.

The useful expressions for approximating the interaction potential and shift are presented in Refs. [11,12]:

$$U_{\text{A-B}}(R)=U^{ex}_{A-B}-C_6/R^6, \qquad (7)$$

$$\delta^{(1)}_{\text{A-B}}(R)=\frac{2}{N\rho_0}(\chi^{1/2}(R)-\chi_0^{1/2})U^{ini}_{\text{A-B}}(R)+(\Omega_1^{3/2}+\Omega_2^{3/2})_{\text{A-B}}\sqrt{\frac{S_{0\text{A-B}}}{S_{0\text{A-B}}}} \qquad (8)$$

where the overlap integrals $S_{0A\text{-}B}$ are determined by the standard expressions, and the potential $U^{ex}_{A\text{-}B}$ is calculated in the framework of the exchange perturbation theory [12]:

$$U^{ex}=(V_{00}-U_{00})/(1-S_0). \qquad (9)$$

It should also be noted that as a rule, in the alternative non-relativistic theories of [6-9] the commutator technique [11] is used when calculating the sums of the type (4). Earlier the reason of using actually approximate non-relativistic methods was the lack of reliable information on the wave functions of the excited states of the complex atoms. Starting approximations in alternative theories [11,12] were rather simple approximations for the electronic wave functions of both active and passive atoms. In particular, in Refs. [11] the electronic wave functions were approximated by simple Slater expression (the approximation of the effective charge = Z-approximation) or simple analytical approximation formulas by Löwdin (L- approximation) and Clementi-Roothaan (C - approximation) [42] in studying the shift and broadening the hyperfine lines for such atoms as He, Rb, Cs etc. In Refs. [12] the wave functions had been determined within the Dirac-Fock approximation, however, these authors had used the approximate non-relativistic expressions to describe the interatomic interaction potential. Besides, determination of the polarizabilities and the van der Waals constants has been performed with using the following London's expressions [6,12]:

$$C_6^I = \frac{3}{2}\alpha_A \alpha_B \frac{I_A I_B}{I_A + I_B}, \qquad (10a)$$

$$C_6^I = \frac{3}{2}\alpha_A \alpha_B \frac{1}{\sqrt{\frac{\alpha_A}{n_A} + \sqrt{\frac{\alpha_B}{n_B}}}}, \qquad (10b)$$

$$C_6^{III} = \frac{3}{2}\alpha_B I_B \sum_k \frac{f_{ko}}{(E_o - E_k)(E_o - E_k + I_B)}. \qquad (10c)$$

where f is the oscillator strength, other notations are the standard. However, sufficiently large error in definition of the van der Waals constants could provide a low accuracy of calculating the interatomic potentials. It is worth to note that the authors of the cited works indicate on the sufficiently large error (~ 50%) in the calculation of the collision shifts.

Let us return to consideration of the van der Waals coefficient C_6 for the interatomic *A-B* interaction. The van der Waals coefficient may be written as [13,43,44]:

$$C_6(L,M) = C_{6,0}(L) - \frac{3M^2 - L(L+1)}{(2L-1)(2L+3)} \cdot C_{6,2}(l), \qquad (10)$$

where $C_{6,0}$ (L) is the isotropic component of the interaction and $C_{6,2}$ (L) is the component corresponding to the $P_2(cosq)$ term in the expansion of the interaction in Legendre polynomials, where the angle specifies the orientation in the space-fixed frame.

The dispersion coefficients $C_{6,0}$ (L) and $C_{6,2}$ (L) may be expressed in terms of the scalar and tensor polarizabilities $\alpha_0(L;iw)$ and $\alpha_2(L;iw)$ evaluated at imaginary frequencies [13]. In particular, one may write in the helium case as follows:

$$C_{6,0}(L) = \frac{3}{\pi} \cdot \int_0^\infty \alpha_0(L;iw)\overline{\alpha}_{He}(iw)dw, \qquad (11)$$

where $\overline{\alpha}_{He}$ is the dynamic polarizability of He. The polarizabilities at imaginary frequencies are defined in atomic units by the following formula:

$$\alpha_{\parallel}(L,M;iw) = 2\sum_{\gamma,M_\gamma} \frac{(E_\gamma - E_L)|< LM|\hat{z}|L_\gamma M_\gamma >|^2}{(E_\gamma - E_L)^2 + w^2} \qquad (12)$$

where E_g is the energy of the electronically excited state $|L_g M_g>$ and the *z* axis lies along the internuclear axis.

Obviously, generally speaking, the calculation of the dynamic polarizability and the resulting van der Waals constants is connected with a summation over infinite number of intermediate states (the states of the discrete spectrum and integrating over the states of the continuous spectrum).

On the other hand, it is known that the space of functions of the atomic states can be stretched over the space of the Sturm orbitals, which is both discrete and countable [6,35,43]. Thus, it allows to eliminate a problem of accounting the continuous spectrum within the formally exact approach.

Naturally, the set of Sturm orbitals should be introduced with specially prescribed asymptotics that is crucial for the convergence of the spectral expansion, including a spectral expansion of the corresponding Green's functions.

3 Relativistic many-body perturbation theory with the Kohn-Sham zeroth approximation and the Dirac-Sturm method

3.1 Relativistic many-body perturbation theory with the Kohn-Sham zeroth approximation

As it is well known (see also Refs. [1,7]), the non-relativistic Hartree-Fock method is mostly used for calculating the corresponding wave functions. More sophisticated approach is based on using the relativistic Dirac-Fock wave functions (first variant) [15,16]. Another variant is using the relativistic wave functions as the solutions of the Dirac equations with the corresponding density functional, i.e within the Dirac-Kohn-Sham theory [45-48]. In fact, the theoretical models involved the use of different consistency level approximations led to results at quite considerable variance.

It is obvious that more sophisticated relativistic many-body methods should be used for correct treating relativistic, exchange-correlation and even nuclear effects in heavy atoms. (including the many-body correlation effects, intershell correlations, possibly the continuum pressure etc [21-30]). In our calculation we have used the relativistic functions, which are generated by the

Dirac-Kohn-Sham Hamiltonian [18,27-30]. In a number of papers it has been rigorously shown that using the optimized basis in calculating the atomic electron density dependent properties has a decisive role. This topic is in details discussed in many Refs. (see, for example, [6,15,28-32,49]).

As usual, a multielectron atom is described by the Dirac relativistic Hamiltonian (the atomic units are used):

$$H = \sum_i h(r_i) + \sum_{i>j} V\left(r_i r_j\right). \tag{13}$$

Here, *h(r)* is one-particle Dirac Hamiltonian for electron in a field of the finite size nucleus and *V* is potential of the inter-electron interaction. In order to take into account the retarding effect and magnetic interaction in the lowest order on parameter a^2 (the fine structure constant) one could write [18]:

$$V\left(r_i r_j\right) = exp\left(i\omega_{ij} r_{ij}\right) \cdot \frac{\left(1 - \alpha_i \alpha_j\right)}{r_{ij}}, \tag{14}$$

where w_{ij} is the transition frequency; a_i ,a_j are the Dirac matrices. The Dirac equation potential includes the electric potential of a nucleus and electron shells and the exchange-correlation potentials. The standard KS exchange potential is as follows [45]:

$$V_X^{KS}(r) = -(1/\pi)[3\pi^2 \rho(r)]^{1/3}. \tag{15}$$

In the local density approximation the relativistic potential is [45]:

$$V_X[\rho(r), r] = \frac{\delta E_X[\rho(r)]}{\delta \rho(r)}, \tag{16}$$

where $E_X[\rho(r)]$ is the exchange energy of the multielectron system corresponding to the homogeneous density $\rho(r)$, The corresponding correlation functional is [6, 28]:

$$V_C[\rho(r), r] = -0.0333 \cdot b \cdot \ln[1 + 18.3768 \cdot \rho(r)^{1/3}], \tag{17}$$

where *b* is the optimization parameter (for details see Refs. [6,31,32]).

As it has been underlined, an adequate description of the multielectron atom characteristics requires using the optimized basis of wave functions. In our work it has been used ab initio optimization procedure for construction of the optimized basis of the relativistic orbitals. It is reduced to minimization of the gauge dependent multielectron contribution $ImdE_{ninv}$ of the lowest QED perturbation theory corrections to the radiation widths of atomic levels.

The minimization of the functional $ImdE_{ninv}$ leads to the Dirac-Kohn Sham-like equations for the electron density that are numerically solved. According to Refs. [31], the gauge dependent multielectron contribution can be expressed as functional, which contains the multi-electron exchange-correlation ones. From the other side, using these functionals within relativistic many-body perturbation theory allows effectively to take into account the second –order atomic perturbation theory (fourth-order QED perturbation theory) corrections. In our work the corresponding functionals of Ref. [34] have been used. As a result one can get the optimal perturbation theory one-electron basis. In concrete calculations it is sufficient to use more simplified procedure, which is reduced to the functional minimization using the variation of the correlation potential parameter *b* in Eq. (16).

The differential equations for the radial functions *F* and *G* (components of the Dirac spinor) are:

$$\frac{\partial F}{\partial r} + \left(1 + \chi\right)\frac{F}{r} - \left(\varepsilon + m - V\right)G = 0,$$

$$\frac{\partial G}{\partial r} + \left(1 - \chi\right)\frac{G}{r} + \left(\varepsilon - m - V\right)F = 0, \tag{18}$$

where *F*, *G* are the large and small components respectively; *c* is the quantum number.

At large c, the functions *F* and *G* vary rapidly at the origin; we have $F(r), G(r) \approx r^{\gamma - 1}$, $\gamma = \sqrt{\chi^2 - \alpha^2 z^2}$. This creates difficulties in numerical integration of the equations in the region $r \to 0$. To prevent the integration step from becoming too small it is usually convenient to turn to new functions isolating the main power dependence: $f = Fr^{1-|\chi|}$, $g = Gr^{1-|\chi|}$. The Dirac equations for *F* and *G* components are transformed as follows [18]:

$$f' = -(\chi + |\chi|)f / r - \alpha Z V g - (\alpha Z E_{n\chi} + 2/\alpha Z)g,$$

$$g' = (\chi - |\chi|)g / r - \alpha Z V f + \alpha Z E_{n\chi} f. \tag{19}$$

Here E_{nc} is one-electron energy without the rest energy. The boundary values are defined by the first terms of the Taylor expansion:

$$g = \left(V(0) - E_{n\chi}\right) r\alpha Z / (2\chi + 1); \quad f = 1 \text{ at } \chi < 0,$$
$$f = \left(V(0) - E_{n\chi} - 2/\alpha^2 Z^2\right)\alpha Z; \quad g = 1 \text{ at } \chi > 0 \qquad (20)$$

The condition $f, g \to 0$ at $r \to \infty$ determines the quantified energies of the state E_{nc}. The system of equations (19) is numerically solved by the Runge-Kutta method. The details can be found in Refs. [21-30].

2.2 The Dirac-Sturm approach

The basic idea of the Dirac-Sturm approach is as follows [6,9,35,43]. In the usual formulation as basis functions used system of eigenfunctions of the generalized eigenvalue problem for the family of operators:

$$(H_0 - \varepsilon)\Phi_\nu = \Lambda_\nu \hat{g}\Phi_\nu, \qquad (21)$$

where H_0 – unperturbed Hamiltonian of a system, $\hat{g}$ is a weighting operator, generally speaking, do not commute with the operator H_0; Λ_ν, Φ_ν - eigenvalues and eigenfunctions of equation (21). A weighting operator in Eq. (21) is usually chosen so that unlike a spectrum of H_0, the spectrum of (21) is a purely discrete. Using the orthogonality and completeness conditions, it is easy to show that the Green operator of the unperturbed problem is diagonal in a representation, defined by a set of functions Φ_ν and the corresponding expansion is as follows:

$$G_0(\varepsilon) = \sum_\nu |\Phi_\nu \rangle\langle \Phi_\nu| / \Lambda_\nu(\varepsilon) \qquad (22)$$

and contains only a single summation over the quantum numbers $\{n\}$. As the operator H_0 we use the Dirac-Kohn-Sham Hamiltonian. The Dirac-Kohn-Sham equation can be written in the next general form [9]:

$$[h_{DKS}(x) - \varepsilon_n]u_n(x) = 0 \qquad (23)$$

Along with discrete spectrum ($e = e_n \le e_F$) there is a continuous spectrum of the eigenvalues ($e > e_F$), corresponding to the Dirac-Kohn-Sham virtual orbitals. In the Sturmian formulation of the problem one should search for the eigen-values and eigen-functions of the equation:

$$[h_{DKS}(x) - \varepsilon]\varphi_\nu = \lambda_\nu \rho(x)\varphi_\nu \qquad (24)$$

where

$$\varepsilon = E - \sum_{k=1}^{N-1} \varepsilon_{n_k} \qquad (25)$$

When $e<0$ equation (24) has a purely discrete spectrum eigenvalues $l_n = l_n(e)$.

As the weight of the operator there are commonly used operators, proportional to a part or even all potential energy in the Hamiltonian H_0. Further, it is easily to understand that the Fourier-image of the one-particle Green's function in the Dirac-Kohn-Sham approximation can be represented as an expansion on the eigenfunctions of (24) [6,9]:

$$G^{(+)} = (x, x'; \varepsilon) = \sum_\nu \frac{\tilde{\varphi}_\nu(x)\tilde{\varphi}_\nu^*(x')}{\lambda_\nu(\varepsilon) - 1}, \qquad (26)$$

where $\tilde{\varphi}_\nu(x)$ is the Sturm designed function:

$$\tilde{\varphi}_\nu(x) = \varphi_\nu(x) - \sum_{k=1}^{N} u_{n_k}(x) < u_{n_k} | \varphi_\nu > \qquad (27)$$

In the case of the single-particle perturbed operator, say,

$$W(x) = \sum_{a=1}^{N} w_a(x) \qquad (28)$$

the second-order correction to an energy of the atom is determined by the standard expression of the following type:

$$\delta E^{(2)} = -\sum_{k=1}^{N} < u_{n_k} | w G^{(+)}(\varepsilon_{n_k}) w | u_{n_k} > =$$
$$= -\sum_{k=1}^{N}\sum_\nu | < \tilde{\varphi}_\nu | w | u_{n_k} > |^2 / [\lambda_\nu(\varepsilon_{n_k}) - 1] \qquad (29)$$

and it actually contains only the summation over the occupied states (core) and virtual orbitals of the Dirac-Kohn-Sham-Sturm type relating to a purely discrete spectrum.

If the operator $w_a(x)$ is an interaction with an external electric field, the expression (29) determines the many-electron atom polarizability. Let

us illustrate the specific numerical implementation of relativistic method of the Sturm expansions on the example of the rubidium atom. Calculation of the static polarizability is actually reduced to two stages. In the first stage one should solve the system of relativistic Dirac-Kohn-Sham equations with respect to the Dirac radial functions and the Lagrange diagonal parameters e^{5s},e^{4p}, e^{4s} etc. In the second stage of the calculation procedure the system of equations equivalent to (24) is solved numerically:

$$(-i\alpha c\nabla + V_N(r) + \delta_i V_C(r) + V_X(r \mid b_i) - \varepsilon_i)\varphi_i = 0 \quad (30)$$

where, as above, V_N is the potential of the electron-nuclear interaction, V_C is a mean-field potential generated by the other electrons; V_X is the Kohn-Sham potential.

Two parameters e_i, d_i correspond to each orbital "i" of a real or Sturmian state. The parameter d_i =1 for orbitals of the real states. It is also important to emphasize that all orbitals of the Sturmian supplement of the Eq. (26) have an exponential asymptotic behavior as $r \to \infty$, which coincides with the asymptotic behavior of the last real state orbitals in the corresponding basis of the real state orbitals. In each case, the functions of the accounted real states represent a reduced spectral expansion of the Green's function G. The residual part decreases as $\exp[-r(-2e)^{1/2}]$ for $r \to \infty$ (e is the eigen energy of the explicitly accounted last real state). All orbitals of the Sturm supplement have absolutely the same asymptotic in the corresponding basis. This fact is very significant in terms of convergence of the method. Number of explicitly accounted real state functions is determined by concrete numerical application of method to computing studied atomic characteristics. Other details can be found in Refs. [6,9,35].

4 Shift and broadening of the hyperfine spectral line for multielectron atoms in an atmosphere of the buffer gas

4.1 Shift and broadening of the thallium and ytterbium hyperfine line in an atmosphere of the inert gas

At first, let us consider the thallium atom in atmosphere of the inert gas. Its studying is of a great interest as this atom a sufficiently heavy. In contrast to more simple alkali atoms (look below) the thallium atom contains p-electrons outside closed shells and has a nuclear charge Z = 81. In Table 1 the theoretical values of the van der Waals constants (in atomic units) respectively, for atom Tl (Tl - He, Kr, Xe) are listed. There are presented our results (*) obtained from our relativistic calculation by the optimized Dirac-Kohn-Sham method combined with the Dirac-Sturm approach, the calculation results by Batygin et al, based on the approximation formulas (10a)-(10c), the Hartree-Fock data by Penkin et al, as well as experimental data (from refs. [8,9,10-13]).

It is noteworthy sufficiently large error for values of the van der Waals constants, obtained during calculating on basis of formula (10), and standard Hartree-Fock method.

Table 1

Theoretical values of the van der Waals constants (in atomic units) respectively, for atom Tl (Tl - He, Kr, Xe); see explanations in the text.

	TI – He	TI – Ar	TI-Kr	TI-Xe
C_6^{I} (10a)	17.5	129	180	291
C_6^{II} (10b)	20.5	148	212	318
C_6^{III} (10c)	20.33	133	193	296
C_6 (Hartree-Fock)	6.59	48	71	111
C_6 (our data [a])*	12.1	106	157	265
C_6 (our data[b])*	14.5	119	173	289
C_6 (experiment)	-	100	150	260

Note:[a] – calculation with optimization*; [b] – calculation without optimization;

The calculation shows the importance of the quality of the atomic wave functions (using an optimization and correct account for the exchange-correlation effects and continuum "pressure" etc.) for an adequate description of the corresponding constants

In Table 2 there are listed the results of our calculation of the interatomic interaction potential $U(R)$ and the values of the local shift $\delta\omega(R)$ (all values are in atomic units) of the thallium hyperfine spectral line for different values of the internuclear distance in the system TI - He. For comparison, similar results of the calculation of

the potential $U(R)$ and the local shift $\delta\omega(R)$ with using the single-configuration Dirac-Fock method [12] are presented too.

Table 2

Local shift and interatomic interaction potential (in atomic units) for the pair TI - He.

R	Dirac-Fock method [12]		Our theory [8,9]	
	$\delta\omega(R)\bullet10^2$	$U(R)\bullet10^3$	$\delta\omega(R)\bullet10^2$	$U(R)\bullet10^3$
5	4.22	7.6	3,92	6.93
6	1.34	2.0	1,21	1.76
7	0.329	0.44	0.27	0.38
8	0.0788	0.099	0.070	0.085
9	0.0032	0.024	0.0025	0.020
10	-0.0145	-0.076	-0.0131	-0.067
11			-0.0119	-0.008

In Table 3 we list the results of our calculation (as all values are given in atomic units) interatomic interaction potential $U(R)$ and the values of the local shift $\delta\omega(R)$ for pairs TI-Kr, TI-Xe.

Table 3

Local shift and interatomic interaction potential (in atomic units) for the pair TI – Kr, Xe (see text)

R	T1-Kr (Our theory)		T1-Xe (Our theory)	
	$\delta\omega(R)\bullet10^2$	$U(R)\bullet10^3$	$\delta\omega(R)\bullet10^2$	$U(R)\bullet10^3$
5	-14.30	13.24	-19,05	18.31
6	-2.88	6.10	-8.22	5.95
7	-1.44	1.72	-2.67	2.04
8	-0.67	0.49	-1.52	0.65
9	-0.48	0.06	-0.74	0.01
10	-0.35	-0.03	-0.48	-0.08
11	-0.24	-0.04	-0.37	-0.09

Further in Table 4 we present our theoretical values (theory C) for the thallium atom hyperfine line collisional shift at the temperature T = 700K for a number of the diatomic systems, in particular, the pairs of TI - He, TI - Kr, Tl-Xe.

Table 4

The collisional shift f_r (in Hz/Torr) of the thallium hyperfine line for pairs TI - He, TI - Kr, Tl-Xe at T = 700°K; Experiment and the qualitative estimate by Choron-Scheps-Galagher (Virginia group); Theory: A- single-configuration Dirac-Fock method; B – the optimized Dirac-Fock method; C- our theory (see text).

System	T1-He	T1-Kr	T1-Xe
Experiment	130 ± 30	-490±20	-1000±80
Qualitative estimate	-	-	-5500
Theory A	155.0	-850.0	-1420.0
Theory B	139.0	-	-
Theory C	137.2	-504	-1052

In Table 5 we present the theoretical data on the collisional shift f_r (in Hz/Torr) the thallium atom hyperfine line at different temperatures (T^0K) for the systems TI - He, TI - Kr, Tl-Xe: Theory A - the single-configuration Dirac-Fock method Batygina DF et al. [12]; C- our theory [8,9].

As can be seen from the presented data, our theory provides a physically reasonable agreement with experimental data on the hyperfine line collisional shifts for the pairs of TI-He, TI-Kr, Tl-Xe.

Table 5

The temperature dependence of the collisional shift f_r (in Hz/Torr) for pairs TI - He, TI - Kr, Tl-Xe; Theory: A- single-configuration Dirac-Fock method; C- our theory;

Pair	T1—He	T1—He	T1—Kr	T1—Xe
T, K	Theory A	Theory C	Theory C	Theory C
700	155	137,2	-504	-1052
750	153.0	135,3	-461	-964
800	151	134,1	-422	-899
850	149	133,3	-391	-841
900	147.5	131,4	-362	-794
950	146	129,1	-330	-751
1000	143	126,2	-308	-713

For comparison, in this table there are also listed the results of calculation on the basis of the single-configuration Dirac-Fock method Batygina DF et al. [12] (theory A), the optimized DF-like method [8] (theory B), as well as experimental data Choron-Scheps-Galagher (the Virginia group) . The qualitative estimate from Ref. [10] has been listed as well. In Table 6 we present our calculated values for adiabatic broadening Γ_a/p (in Hz / Torr) of the thallium atom hyperfine line at different temperatures for the TI – He pair: C - our theory; A theory [12]. In Table 7 we list the similar theoretical data on the Tlatom hyperfine line adiabatic broadening of Γ_a/p (in Hz / Torr) for the pairs TI - Kr, TI-Xe.

Table 6

Adiabatic broadening Γ_a/p (in Hz / Torr) for the TI - He: Theory A- single-configuration Dirac-Fock method; C- our theory.

T, K	TI – He Theory A	TI – He Theory C
700	2.83	2.51
800	2.86	2.54
900	2.90	2.58
1000	2.89	2.56

Table 7

Adiabatic broadening Γ_a/p (in Hz / Torr) for the TI – Kr, Yl-Xe (our theory).

T, K	TI- Kr	TI- Xe
700	6.81	17.3
800	5.89	14.6
900	5.26	12.9
1000	5.24	11.5

It is easily to estimate that the ratio values (Γ_a/p) / f_p ~ 1/50 for the system TI - He, (Γ_a/p) / f_p ~ 1/70 for the system TI - Kr and (Γ_a/p) / f_p ~ 1/60 for the TI-Xe. These estimates (at first it had been noted in Ref.[12]) show that well-known in the theory of optical range spectral line broadening Foley law $\Gamma_a \sim|\Delta|$ (see, for example, [6]) is incorrect for the spectral lines of transitions between components of the hyperfine structure. At least this fact is absolutely obvious for the thallium atom.

In any case we suppose that more detailed experimental studying are to be very actual and important especially a light of availability of the theoretical data on temperature dependences of the thallium hyperfine line collisional shift and broadening. Obviously, this is also very actual from the point of view of the construction the thallium quantum frequency measure, as well as studying a role of the weak interactions in atomic physics and physics of collisions (see, for example, [6,10]).

Now let us consider the pair 'Yb-He". The ground configuration for the ytterbium atom is: [Xe]$4f^{14}6s^2$ (term: ^1S). Further we present our results for the scalar static polarizability a_0 (in units of a_0^3, a_0 is the Bohr radius) and isotropic dispersion coefficient $C_{6,0}$ (in units of $E_H \times a_0^6$, E_H is the Hartree unit of energy). Our data are as follows [9]: $C_{6,0}$= 45.2 and a_0=169.3. For comparison let us present the corresponding data by Dalgarno et al [13]: $C_{6,0}$= 39.4, a_0=157.3 and by Buchachenko et al [44]: $C_{6,0}$= 44.5.

In table 8 we present our calculation results for the observed f_r (in Hz/Torr) shift for the system of Yb-He.

Table 8

The observed f_r (in, Hz/Torr) shift for the system Yb-He (see text)

T, K	f_ρ
700	148.1
750	146.0
800	143.8
850	141.5
900	138.9

It is obvious that the pair Yb-He is more complicated system in comparison with the pair of Tl-He or "alkali atom-He". Until now there are no any experimental or theoretical data for this system. So, we believe that our data may be considered as the first useful reference

4.2 Shift and broadening of the alkali atom hyperfine line in an atmosphere of the inert gas

Here we present the results of our studying hyperfine line collisional shift for alkali atoms (rubidium and caesium) in the atmosphere of the helium gas. In Table 9 we present our data on the van der Waals constants in the interaction potential for alkali Rb, Cs atoms with inert gas atoms Ne, Kr, Xe, and also available in the literature experimental data [10,11]. In Table 10 we list the results of our calculating (in atomic units) interatomic potentials, local shifts $dw(R)$ for the pair Cs-He. Noteworthy is the fact that an accuracy of the experimental data for the van der Waals constants does not exceed 10 % for heavy alkali atoms. Calculation has shown that the optimization of the relativistic orbitals basis and accounting for the exchange-correlation effects seem to be very important for obtaining adequate accuracy of the description of the constants.

Table 9

The van der Waals constants (in atomic units.) for alkali atoms, interacting with inert gas atoms Ne, Kr, Xe (see text).

Pair of atoms	Our theory	Experiment
Rb-He	42	41
Rb –Kr	484	470
Rb –Xe	758	-
Cs-He	52	50
Cs-Kr	582	570
Cs-Xe	905	-

Table 10. **The interatomic potential (10^5) and local δω(R) shift (10^5) for Cs-He pair (in atomic units; see text)**

R	$\delta\omega(R)$	U (R)
8	4280	610
9	2845	336
10	1890	169
11	955	77
12	482	32
13	251	12.8
14	113	4.1
15	59	1.9

In Table 11 and 12 we present our theoretical results for the hyperfine line observed shift f_p (1/Torr) in a case of the Rb-He and Cs-He pairs. The experimental and alternative theoretical results by Batygin et al [11] for f_p are listed too. At present time there are no precise experimental data for a wide interval of temperatures in the literature.

Table 11

The observed f_r (10^{-9} 1/Torr) shifts for the systems of the Cs-He and corresponding theoretical data (see text).

T, K	Experiment	Our theory	Theory [a] [11]	Theory [b] [11]	Theory [c] [11]
223	-	178	164	142	169
323	135	137	126	109	129
423	-	123	111	96	114
523	-	112	100	85	103
623	-	105	94	78	96
723	-	98	-	-	-
823	-	92	-	-	-

Note:[a] –calculation with using the He wave functions in the Clementi-Rothaane approximation; [b] – calculation with using the He wave functions in the Z-approximation;

[c] –calculation with using the He wave functions in the Löwdin approximation;

Table 12

The observed f_r (10^{-9} 1/Torr) shifts for the systems of Rb-He and corresponding theoretical data (see text).

T, K	Experiment	Our theory	Theory [a] [11]	Theory [b] [11]	Theory [c] [11]
223	-	113	79	67	81
323	105	101	73	56	75
423	-	89	62	48	64
523	-	80	55	43	56
623	-	73	50	38	50
723	-	71	47	36	47
823	-	69	-	-	-

Note:[a] –calculation with using the He wave functions in the Clementi-Rothaane approximation; [b] – calculation with using the He wave functions in the Z-approximation;

[c] –calculation with using the He wave functions in the Löwdin approximation;

The theoretical data from Refs. [11] are obtained on the basis of calculation within the exchange perturbation theory with using the He wave functions in the Clementi-Rothaane approximation [42] (column: Theory[a]), and in the Z-approximation (column: Theory[b]), and in the Löwdin approximation (column: Theory[c]).

The important feature of the developed optimized perturbation theory approach is using the optimized relativistic orbitals basis, an accurate accounting for the exchange-correlation and continuum pressure effects with using the effective functionals [18,34].

The difference between the obtained theoretical data and other alternative calculation results can be explained by using different perturbation theory schemes and different approximations for calculating the electron wave functions of heavy atoms. It is obvious that the correct account for the relativistic and exchange-correlation and continuum pressure effects will be necessary for an adequate description of the energetic and spectral properties of the heavy atoms in an atmosphere of the heavy inert gases (for example, such as Xe).

5 Conclusion

In this chapter a brief review of the experimental and theoretical works on the hyperfine structure line collision shifts for heavy atoms in an atmosphere of the buffer inert gases is given. A new, consistent relativistic perturbation theory combined with the exchange perturbation theory, is presented and applied to calculating the interatomic potentials, van der Waals constants, hyperfine line collision shift and broadening for some heavy atoms in an atmosphere of the buffer inert gases. It should be noted that the presented approach can be naturally generalized in order to describe the energy and spectral characteristics of other atomic systems and buffer mediums.

The calculation results on the hyperfine line collision shift and broadening for the alkali (Rb, Cs), thallium, and ytterbium atoms in an atmosphere of the inert gas (He, Kr, Xe) are listed and compared with available alternative theoretical and experimental results. The obtained data for the $(\Gamma_a/p) / f_p$ ratio allowed to confirm that the well-known Foley law $\Gamma_a \sim f_p$ in the theory of optical range spectral line broadening is incorrect for the spectral lines of transitions between components of the hyperfine structure of the heavy multielectron atoms.

The studying hyperfine structure line collision shifts and widths for different heavy atomic systems in the buffer gases opens new prospects in the bridging of quantum chemistry and atomic and molecular spectroscopy and physics of collisions. These possibilities are significantly strengthened by a modern experimental laser and other technologies [10,50-56]. Really, new experimental technologies in physics of collisions may provide a measurement of the atomic and molecular collision spectral parameters with very high accuracy.

References

1. I.G. Kaplan, *Theory of intermolecular interactions* (Nauka, Moscow, 1995), p.1-380; I.G. Kaplan and O.B. Rodimova, Phys.-Uspekhi. **126**, 403 (1997).
2. E.E. Nikitin, *Semiempirical methods of calculation of interatomic interaction potentials*. Series: Structure of molecules and chemical bond, vol. **4**, ed. by E.E.Nikitin and S.Ya. Umansky (VINITI, Moscow, 1990), p.1-220; A.L. Devdariani, Chemistry of plasma, vol. **15**, ed. by B.M. Smirnov, A.L.Devdariani and A.L. Zagrebin (Nauka, Moscow, 1989), p.44.
3. I.M. Torrens, *Interatomic potentials* (Academic Press, , N-Y., 1992), p.1-390; A.J. Freeman and R.H. Frankel, *Hyperfine interactions* (Plenum, N.-Y., 1997), p.1-360; J. Weiner, V.S. Bagnato, S. Zilio, and P.S. Julienne, Rev. Mod. Phys. **71**, 1 (1999).
4. R.Eisenschitz and F. London, Zs.Phys. 60, 491 (1930); J.O.Hirschfelder, Chem. Phys. Lett. 1,325, 363 (1997);

Ad van der Avoird, J.Chem.Phys. 47, 3649 (1997);
5. J.N. Murrel, G. Shaw, J. Chem. Phys. 46, 1768 (1967); J.I.Musher and A.T. Amos, Phys. Rev. 164, 31 (1997).
6. I.I. Sobel'man, *Introduction to theory of atomic spectra* (Nauka, Moscow, 1997), p.1-380; A.V. Glushkov, *Relativistic and correlation effects in theory of atomic spectra* (Astroprint, Odessa, 2006), p.1-450.
7. G. Grim, *Broadening spectral lines in plasmas* (Acad. N.-Y., 1994), p.1-480; E. Oks, Int. Journ. of Spectr. **10,** 852581 (2010); A. Unsöld, *The New Cosmos* (Springer-Verlag, Berlin, 1977), p.169.
8. O.Yu.Khetselius, A.V. Glushkov, A.V. Loboda, E.Gurnitskaya, E. Mischenko, T.A.Florko, D.E. Sukharev, Spectral Line Shapes. **15**, 231 (2008); A.V. Glushkov, O.Yu.Khetselius, A.V. Loboda, E.Gurnitskaya, E.Mischenko, Theory and Applications of Computational Chemistry (AIP) **1113**, 131 (2009);
9. S.V.Malinovskaya, A.V. Glushkov, O.Yu. Khetselius, A.A. Svinarenko, E.V. Mischenko and T.A. Florko, Int. Journ. of Quant.Chem. **109**, 3325 (2009); O.Yu. Khetselius, T.A. Florko, A.A. Svinarenko and T.B.Tkach, Phys. Scripta. **T153**, 014037 (2013);
10. B. Cheron, R. Scheps and A. Gallagher, J. Chem. Phys. **65**, 326 (1976); *Photonic, Electronic, Atomic Collisions*. Ed by F.Aumar and H. Winter (World Scientific, Singapore:, 1997), 630p; D. Turner, C. Baker, A.Baker and C.Brunrile, Molecular Photoelectron Spectroscopy (Wiley, N.-Y., 1997), p.1-540;
11. V.V. Batygin, Yu.V.Guzhva, B.Matisov and I.N.Toptygin, JETP. 47, 2414 (1997); V. Batygin, M.B. Gorny, A.N.Ivanov and B.G.Matisov, J.Techn. Phys. **47**, 2414 (1977); V.V. Batygin, M.B. Gorny and B.M. Gurevich, J.Techn.Phys. **48**, 1097 (1998).
12. V.V. Batygin and B.G.Matisov, J.Techn. Phys. **46**, 221 (1996); E.B. Alexandrov, V.I. Popov, N.N. Yakobson, Opt. Spectr. **46**, 404 (1999); V.V. Batygin, I.M. Sokolov, Opt. Spectr. **55**, 30 (1993).
13. N.P.Penkin, V.P.Ruzov and L.N.Shabanova, Opt. Spectr. **35,** 601 (1993); **X**. Chi, A. Dalgarno, G.C. Groenenborn, Phys. Rev. A. **75**, 032723 (2007); M.J. Jamieson, G.W.F.Drake and A.Dalgarno, Phys.Rev. A. 51, 3358 (1995);
14. A.V. Glushkov, *Relativistic quantum theory. Quantum mechanics of atomic systems* (Astroprint, Odessa, 2008), 700p.; O.Yu. Khetselius, *Hyperfine structure of atomic spectra: New methods and applications* (Astroprint, Odessa, 2008), 240p.
15. I.P. Grant, *Relativistic Quantum Theory of Atoms and Molecules, Theory and Computation*, Springer Series on Atomic, Optical, and Plasma Physics, vol. **40** (Springer, Berlin, 2007), p.1-587; I.P. Grant and H.M. Quiney, Int. J. Quant. Chem. **80**, 283 (2000).
16. S. Wilson, *Recent Advances in Theoretical Physics and Chemistry Systems*, Series: Progress in Theoretical Chemistry and Physics, vol. **16**, ed. by J. Maruani, S. Lahmar, S.Wilson, and G. Delgado-Barrio (Springer, Berlin, 2007), p. 11.
17. A.V. Glushkov, S.V. Ambrosov, O.Yu. Khetselius, A.V. Loboda, E.P. Gurnitskaya, in *Recent Advances in the Theory of Chemical and Physical Systems* Series: Progress in Theoretical Chemistry and Physics, vol. **15**, ed. By J.-P. Julien et al, (Springer, Berlin, 2006), p. 285.
18. A.V. Glushkov, O.Yu. Khetselius, E.P. Gurnitskaya, A.V. Loboda, T.A. Florko, D.E. Sukharev, L. Lovett, in *Frontiers in Quantum Systems in Chemistry and Physics* Series: Progress in Theoretical Chemistry and Physics, vol. **18**, ed. by S.Wilson, P.J.Grout, J. Maruani, G. Delgado-Barrio, P. Piecuch (Springer, Berlin, 2008), p. 505.
19. A.V. Glushkov, S.V. Malinovskaya, A.A. Svinarenko, and Yu.G. Chernyakova,

Int. Journ. Quant. Chem. **99**, 889 (2004).
20. A.V. Glushkov, S.V. Ambrosov, A.V. Loboda, E.P. Gurnitskaya and G.P. Prepelitsa, **104**, 562 (2005).
21. A.V. Glushkov, S.V. Ambrosov, O.Yu. Khetselius, A.V. Loboda, Yu.G. Chernyakova, A.A. Svinarenko, Nucl. Phys.A.**734S,** 21 (2004); A.V.Glushkov, O.Yu. Khetselius, L. Lovett, E.P.Gurnitskaya, Yu.V. Dubrovskaya and A.V. Loboda, Int.J. Mod.Phys. A: Particles and Fields, Nucl.Phys. **24**, 611 (2009).
22. O.Yu. Khetselius, Int.J.Quant.Chem. **109**, 3330 (2009); O.Yu. Khetselius, Phys.Scripta. T**135**, 014023 (2009).
23. O.Yu. Khetselius, J. of Physics: C Ser. 397, 012012 (2012).
24. A.V. Glushkov, S.Ambrosov, A.Loboda, G. Prepelitsa, E. Gurnitskaya, Int. Journ. Quant.Chem. **104**,562 (2005);
25. A.V.Glushkov, S.V.Malinovskaya, O.Yu.Khetselius, Yu.V. Dubrovskaya, E.P. Gurnitskaya, J. Phys.CS. **35**, 425 (2006);
26. S.V. Malinovskaya, A.V.Glushkov, O.Yu. Khetselius, A.A.Svinarenko, A.V.Loboda, Yu.M. Lopatkin, L.V.Nikola, Int. Journ. of Quant.Chem. **111**, 288 (2011).
27. A.V. Glushkov, O.Yu. Khetselius and S.V. Malinovskaya, in *Frontiers in Quantum Systems in Chemistry and Physics*, Series: Progress in Theoretical Chemistry and Physics, vol. **18**, ed. by S.Wilson, P.J.Grout, J. Maruani, G. Delgado-Barrio, P. Piecuch (Springer, Berlin, 2008), p. 523; Europ.Phys. Journ. ST **160**, 195 (2008); Molec. Phys. **106**, 1257 (2008).
28. A.V. Glushkov, O.Yu. Khetselius, A.V. Loboda, A.A. Svinarenko, in *Frontiers in Quantum Systems in Chemistry and Physics*, *Progress in Theoretical Chemistry and Physics*, vol. **18**, ed. by S. Wilson, P.J. Grout., J. Maruani, G. Delgado-Barrio, P. Piecuch (Springer, Berlin, 2008), p. 541; A.V. Glushkov, A.V. Loboda, E.P. Gurnitskaya, A.A. Svinarenko, Phys. Scripta T **135**, 014022 (2009).
29. A.V. Glushkov, O.Yu. Khetselius, L. Lovett, L., in: *Advances in the Theory of Atomic and Molecular Systems Dynamics, Spectroscopy, Clusters, and Nanostructures*. Series: Progress in Theoretical Chemistry and Physics, vol. **20**, ed. by P.Piecuch, J. Maruani, G. Delgado-Barrio, S. Wilson (Springer, Berlin, 2009), p.125-172.
30. A.V. Glushkov, O.Yu. Khetselius, A.A. Svinarenko, in: *Advances in the Theory of Quantum Systems in Chemistry and Physics.* Series: Progress in Theoretical Chemistry and Physics, vol. **22**, ed. by P.Hoggan, E.Brändas, G. Delgado-Barrio, P.Piecuch (Springer, Berlin, 2012), p.51-70.
31. A.V. Glushkov, L.N. Ivanov and E.P Ivanova, *Autoionization Phenomena in Atoms*, (Moscow University Press, Moscow, 1996), p.58; A.V. Glushkov and L.N. Ivanov, Phys. Lett. A. **170**, 33 (1992).
32. A.V. Glushkov, JETP Lett. **55**, 97 (1992); Opt. Spectr. **84**, 670 (1998); Russian Journ. of Struct. Chem. **39**, 220 (1998); A. Glushkov, S.V.Malinovskaya, Russian Journ. of Phys. Chem. **62**, 100 (1988).
33. L.N. Ivanov and E.P. Ivanova, Atom. Data Nucl .Data Tabl. **24**, 95 (1979).
34. E.P. Ivanova, L.N. Ivanov, A.V. Glushkov, A. Kramida, Phys. Scripta **32**, 512 (1985); A.Glushkov, E.Ivanova, J. Quant. Spectr. Rad. Transfer. **36**, 127 (1986).
35. L.N. Ivanov, E.P. Ivanova, L. Knight, Phys. Rev. A **48,** 4365 (1993); E.P. Ivanova, L.N. Ivanov, E.V. Aglitsky, Phys. Rep. **166**, 315 (1988); E.P. Ivanova, L.N. Ivanov, JETP **83**, 258 (1996); E.P. Ivanova, I.P. Grant, J. Phys. B **31**, 2871 (1998).
36. L.N. Ivanov, V.S. Letokhov, Com. Mod. Phys. D **4**, 169 (1985); A.V.Glushkov, L.N.Ivanov, V.S. Letokhov, Preprint of Inst. for Spectroscopy of USSR Acad. of Sci. (ISAN), AS-5 (Moscow, 1991).

37. E. Vidolova-Angelova, L.N. Ivanov, and D.A. Angelov, J.Phys.B: At. Mol. Opt. Phys. **21**, 3877 (1998); E. Vidolova-Angelova, E.P. Ivanova, and L.N. Ivanov, Opt. Spectr. **50**, 243 (1981); G.I. Bekov, E. Vidolova-Angelova, L.N. Ivanov, V.S. Letokhov, and V.I. Mishin, Soviet-JETP. **80**, 866 (1991).
38. A. Nemukhin and N.Stepanov, Herald of Moscow State Univ. Ser. Chem. **18**, 282 (1984); D. Kupriyanov and S.Sokolov, Sov. Chem.Phys. **5**, 1160 (1986);
39. M. Aubert , M.Bessis and G.Bessis, Phys.Rev.A. 10, 51 (1974); 10, 61 (1994); L. Bellomonte, P. Cavaliere and G. Ferrante, J.Chem.Phys. 61, 3225 (1994);
40. J. Aguilar and H. Nakamura, Chem. Phys. 32, 115 (1976); F. Masnou, N. Philips, P. Valiron, Phys.Chem.Lett. 41, 395 (1978).
41. W.-T. Luh and J.T. Bahns, J.Chem. Phys. **88,** 2235 (1988); M. Frauss and W.J. Stevens, J.Chem.Phys. **93**, 4236 (1990);
42. E. Clementi and C.C.J. Roothaan and M. Yoshimine, Phys.Rev. **127**, 1618 (1992); P.O. Löwdin, Phys. Rev. **30**, 120 (1993).
43. P.F.Gruzdev, S.Solov'eva, A.Sherstyuk, Russian Phys. Journ. **29** (N1), 73 (1988); A.Glushkov, A.Kivganov, V.Polischuk, V.Khokhlov, T.Buyadzhi, L.Vitavetskaya G.Borovskaya, Russian Phys. Journ. **41** (N3), 36 (1998);
44. A.A. Buchachenko, M.M. Szczesniak, and G. Chalazinski, J.Chem.Phys. **124**, 114301 (2006); M.J. Jamieson, A. Dalgarno, M. Aymar and J. Tharamel, J. Phys. B: At. Mol. Opt. Phys. **42**, 095203 (2009);
45. W. Kohn, L.J. Sham, Phys. Rev. A **140**, 1133 (1964); P. Hohenberg, W. Kohn, Phys. Rev. B **136**, 864 (1994);
46. X. Chu and Shin-I Chu, Phys.Rev.A. **63,** 013414 (2000); **63,** 023411 (2001);
47. E.G. Gross, W. Kohn, *Exchange-Correlation Functionals in Density Functional Theory* (Plenum, New York, 2005).
48. *The Fundamentals of Electron Density, Density Matrix and Density Functional Theory in Atoms, Molecules and the Solid State*, Series: Progress in Theoretical Chemistry and Physics , vol. 14, eds. N. Gidopoulos and S. Wilson (Springer, Berlin, 2004), p.1.
49. M.D. Krunisz, Acta Phys. Pol. **A62**, 285 (1982);
50. A.Glushkov, O.Khetselius, A. Svinarenko Phys.Scr. **T153**, 014029 (2013).
51. V. Horvatic, D. Veza, M.Movre, K. Niemax, C.Vadla, Spectroch.Acta.Part B. **63**, 652 (2008).
52. M. Kötteritzsch, W. Gries and A.Hese, J. Phys. B: At. Mol. Opt.. **25,** 913 (1992).
53. E.Ehrlacher, J. Huennekens, Phys. Rev.A. **46**, 2642 (1992);
54. K.Singer, M.Reetz-Lamour, T. Amthor, L.Marcassa and M. Weidemuller, Phys. Rev. Lett. **93**, 163001 (2004).
55. C.Hancox, S.Doret, M.Hummon, L.Luo, J. Doyle, Nature (London). **431,** 281 (2004); C.Hancox, S.Doret, M. Hummon, R.Krems, J. Doyle, Phys. Rev.Lett. **94,** 013201 (2005).
56. O.Yu. Khetselius, in: *Quantum Systems in Chemistry and Physics: Progress in Methods and Applications*. Series: Progress in Theoretical Chemistry and Physics, vol. **26**, ed. by K.Nishikawa et al (Springer, 2012), p.217-230.

This article has been received within 2014

UDC 539.184

O. Yu. Khetselius

OPTIMIZED PERTURBATION THEORY TO CALCULATING THE HYPERFINE LINE SHIFT AND BROADENING FOR HEAVY ATOMS IN THE BUFFER GAS

Abstract

It is presented review of a new consistent relativistic approach to determination of collisional shift and broadening hyperfine lines for heavy atoms in an atmosphere of the buffer inert gas. It is based on the atomic gauge-invariant relativistic perturbation theory and the exchange perturbation theory. As illustration, consistent approach is applied to calculating the interatomic potentials, hyperfine structure line collision shift and broadening for heavy atoms, in particular, atoms of alkali elements – rubidium, caesium, and thallium, ytterbium, in an atmosphere of the buffer inert gas.

Key words: Relativistic many-body perturbation theory, hyperfine line collision shift

УДК 539.184

О. Ю. Хецелиус

ОПТИМИЗИРОВАННЯ ТЕОРИЯ ВОЗМУЩЕНИЙ ДЛЯ ОПРЕДЕЛЕНИЯ СДВИГА И УШИРЕНИЯ ЛИНИЙ СВЕРХТОНКОЙ СТРУКТУРЫ В ТЯЖЕЛЫХ АТОМАХ В БУФЕРНЫХ ГАЗАХ

Резюме

Представлен обзор нового последовательного релятивистского подхода к определению столкновительного сдвига и уширения линии сверхтонкой структуры тяжелых атомов в атмосфере буферных инертных газов. Метод основан на атомной калибровочно-инвариантной теории возмущений и обменной теории возмущений. В качестве иллюстрации приведен пример расчета межатомных потенциалов, столкновительного сдвига и уширения сверхтонких линий для тяжелых атомов, в частности, атомов щелочных элементов, таллия, иттербия в атмосфере буферных инертных газов.

Ключевые слова: релятивистская теория возмущений, столкновительный сдвиг линий сверхтонкой структуры

УДК 539.184

О. Ю. Хецеліус

ОПТИМІЗОВАНА ТЕОРІЯ ЗБУРЕНЬ ДЛЯ ВИЗНАЧЕННЯ ЗСУВУ ТА УШИРЕННЯ ЛІНІЙ НАДТОНКОЇ СТРУКТУРИ У ВАЖКИХ АТОМАХ В БУФЕРНИХ ГАЗАХ

Резюме

Представлено огляд нового послідовного релятивістського підходу до визначення зсуву та уширення лінії надтонкої структури важкого атома в атмосфері буферних інертних газів. Метод базується на атомній калібрувально-інваріантній теорії збурень та обмінній теорії збурень. Як ілюстрація наведено приклад розрахунку міжатомних потенціалів, зсуву та уширення за рахунок зіткнень надтонких ліній для важких атомів, зокрема, атомів лужних елементів, таллія, іттербія в атмосфері буферних інертних газів.

Ключові слова: релятивістська теорія збурень, зсув за рахунок зіткнень ліній надтонкої структури

UDC 539.182

V. V. Buyadzhi, A. V. Glushkov, L. Lovett

Odessa State Environmental University, L'vovskaya str.15, Odessa-16, 65016, Ukraine
E-mail: dirac13@mail.ru
UK National Academy of Sciences and Bookdata Co., London, SW1Y 5AG, United Kingdom
E-mail: qclovett@gmail.com

SPECTROSCOPY OF ATOM AND NUCLEUS IN A STRONG LASER FIELD: STARK EFFECT AND MULTIPHOTON RESONANCES

The consistent relativistic energy approach to atom in a strong realistic laser field, based on the Gell-Mann and Low S-matrix formalism, is applied to studying the resonant multiphoton ionization of krypton by intense uv laser radiation and calculating the multiphoton resonances shift and width in krypton. An approach to treating the multiphoton resonances in nuclei is outlined on example of the ^{57}Fe nucleus.

1. Introduction

At the present time a physics of multiphoton phenomena in atoms, molecules ets has a great progress that is stimulated by development of new laser technologies (see Refs. [1-10]). The appearance of the powerful laser sources allowing to obtain the radiation field amplitude of the order of atomic field in the wide range of wavelengths results to systematic investigations of the nonlinear interaction of radiation with atomic and molecular systems [1-14]. At the same time a direct laser-nucleus interactions traditionally have been dismissed because of the well known effect of small interaction matrix elements [9-11]. Some exceptions such as an interaction of x-ray laser fields with nuclei in relation to alpha, beta-decay and x-ray-driven gamma emission of nuclei have been earlier considered. With the advent of new coherent x-ray laser sources in the near future, however, these conclusions have to be reconsidered. From the design report (look table II in Ref. [10]) for SASE 1 at TESLA XFEL and parameters for current and future ion beam sources, the signal rate due to spontaneous emission after real excitations of the nuclei can be estimated. For nuclei accelerated with an energy resolution of 0.1% such that 12.4 keV photons produced by SASE 1 become resonant with the $E1$ transition in a whole number of nuclei (for example, ^{153}Sm, ^{181}Ta, ^{223}Ra, ^{225}Ac , ^{227}Th etc). It means that the resonance condition (w~De, where De is a typical level spacing, w is a laser frequency) is fulfilled [10]. The coherence of the laser light expected from new sources (TESLA XFEL at DESY) may allow to access the extended coherence or interference phenomena. In particular, in conjunction with moderate acceleration of the target nuclei it allows principally to achieve realization of multiphoton phenomena, nuclear Rabi oscillations or more advanced quantum optical schemes in nuclei.

The interaction of atoms with the external alternating fields, in particular, laser fields, has been the subject of intensive experimental and theoretical studied (see, for example, Refs. [1-8, 12-24]). A definition of the k-photon emission and absorption probabilities and atomic levels shifts, study of dynamical stabilization and field ionization etc are the most actual problems to be solved. At present time, a progress is achieved in the description of the processes of interaction atoms with the harmonic emission field [1,12-14]. But in the realistic laser field the according processes are in significant degree differ from ones in the harmonic field. It has been proved a significant role of the photon-correlation effects and influence of the laser pulse multi-modity. Surely,

a number of different theoretical approached has been developed in order to give a adequate description of the atoms in a strong laser field. Here one could mention such approaches as the standard perturbation theory (surely for low laser filed intensities), Green function method, the density-matrix formalism, time-dependent density functional formalism, direct numerical solution of the Schrödinger (Dirac) equation, multi-body multi-photon approach, the time-independent Floquet formalism etc (see [1-8,12-24] and Refs. therein). The effects of the different laser line shape on the intensity and spectrum of resonance fluorescence from a two-level atom are studied in Refs. [1-5,15-17,19-23]. Earlier the relativistic energy approach to studying the interaction of atom with a realistic strong laser field, based on the Gell-Mann and Low S-matrix formalism, has been developed. Originally, Ivanov has proposed an idea to describe quantitatively a behaviour of an atom in a realistic laser field by means studying the radiation emission and absorption lines and further the theory of interaction of an atom with the Lorenz laser pulse and calculating the corresponding lines moments has been in details developed in Ref. [19-25]. It has been checked in numerical simulation of the multiphoton resonances shifts and widths in the hydrogen and caesium. Theory of interaction of an atom with the Gauss and soliton-like laser pulses and calculating the corresponding lines moments has been in details presented in Refs. [23,26,27]. Here we apply this approach to studying the resonant multiphoton ionization of krypton by intense uv laser radiation and calculating the multiphoton resonances shift and width. Besides, at first we also outline the corresponding scheme to treating the multiphoton resonances in nuclei on example of ^{57}Fe nucleus.

2. Relativistic energy approach to atom in a strong laser field: Multiphoton resonances

The relativistic energy approach in the different realizations and the radiation lines moments technique is in details presented in Refs. [19-30]. So, here we are limited only by presenting the master elements. In the theory of the non-relativistic atom a convenient field procedure is known for calculating the energy shifts dE of degenerate states. This procedure is connected with the secular matrix M diagonalization. In constructing M, the Gell-Mann and Low adiabatic formula for dE is used [20-23,31]. In relativistic theory, the Gell-Mann and Low formula dE is connected with electrodynamical scattering matrice, which includes interaction with as a laser field as a photon vacuum field. A case of interaction with photon vacuum is corresponding to standard theory of radiative decay of excited atomic states. Surely, in relativistic theory the secular matrix elements are already complex in the second perturbation theory (PT) order. Their imaginary parts are connected with radiation decay possibility. The total energy shift is usually presented in the form [23]:

$$\delta E = \mathrm{Re}\delta E + \mathrm{i}\ \mathrm{Im}\delta E\ ,\ \ \mathrm{Im}\ \delta E = -\mathrm{P}/2 \qquad (1)$$

where P is the level width (decay possibility). Spectroscopy of an atom in a laser field is fully defined by position and shape of the radiation emission and absorption lines. The lines moments m_n are strongly dependent upon the laser pulse quality: intensity and mode constitution [15-23]. Let us describe the interaction "atom-laser field" by the Ivanov potential [21,23]:

$$V(r,t)=V(r)\int d\omega f(\omega-\omega_0)\sum_{n=-\infty}^{\infty}\cos[\omega_0 t+\omega_0 n\tau] \qquad (2)$$

Here w_0 is the central laser radiation frequency, n is the whole number. The potential V represents the infinite duration of laser pulses with known frequency t. The function f(w) is a Fourier component of the laser pulse. The condition $\int d\mathrm{w} f^2(\mathrm{w})=1$ normalizes potential $V(rt)$ on the definite energy in the pulse. Let us consider the pulses with Lorentz shape (coherent 1-mode pulse): $f(\mathrm{w}) = b/(\mathrm{w}^2+\mathrm{D}^2)$, Gaussian one (multi-mode chaotic pulse): $f(\mathrm{w}) = b\exp[\ln 2(\mathrm{w}^2/\mathrm{D}^2)]$ and the soliton-like pulse: $f(\mathrm{t}) = b\ ch^{-1}[t/D]$ (b -normalizing multiplier). A case of the Lorentz shape has been earlier studied [20-23]. A case of the Gauss and soliton-like shape is considered in Refs.[23,26,27]. The master program results in the calculating an imaginary part of energy shift $\mathrm{Im}dE_a(w_0)$ for any atomic level as the function of the central laser frequency w_0. An according function has the shape of the resonance,

which is connected with the transition a-p (a, p-discrete levels) with absorption (or emission) of the "k" number of photons. For the resonance we calculate the following values [20-23]:

$$\delta\omega(p\alpha|k)=\int' d\omega \ \mathrm{Im}\ \delta E_\alpha(\omega)(\omega - \omega_{p\alpha}/k)/N, \quad (3)$$

$$\mu_m = \int' d\omega \ \mathrm{Im}\ \delta E_\alpha(\omega)\ (\varpi - \omega_{p\alpha}/k)^m / N$$

where $\grave{o}\ \not{c}d\mathrm{w}\mathrm{Im}E_a$ is the normalizing multiplier; w_{pa} is position of the non-shifted line for transition a-p, $\mathrm{dw}(pa|k)$ is the line shift under k-photon absorption; $v_{pa}=w_{pa}+ k\times\mathrm{dw}(pa|k)$. The first moments m_1, m_2 and m_3 determine the atomic line centre shift, its dispersion and the asymmetry. To find m_m, we need to get an expansion of E_a to PT series: $E_a = \mathring{a}\ E_a^{(2k)}\ (w_0)$. One may use here the Gell-Mann and Low adiabatic formula for dE_a :

$$\delta E_\alpha = \lim_{\gamma\to 0} i\gamma g \ln\langle\Phi_\alpha|S_\gamma(0,-\infty|g)|\Phi_\alpha\rangle|_{g=1} \quad (4)$$

The representation of the S- matrix in the form of the PT series induces the expansion for dE_a:

$$\delta E_\alpha(\omega_0) = \lim_{\gamma\to 0}\ \gamma \sum_{k_1 k_2 \ldots k_n} a(k_1, k_2,\ldots,k_n), \quad (5)$$

$$I_\gamma(k_1, k_2,\ldots,k_n) = \prod_{j=1} S_\gamma^{(kj)}, \quad (6)$$

$$S_\gamma^{(m)}=(-1)^m \int_{-\infty}^{0} d\ t_1 \ldots \int_{-\infty}^{t_m-1} d\ t_m \langle\Phi_\alpha|V_1 V_2 \ldots V_m|\Phi_\alpha\rangle \quad (7)$$

$$V_j = \exp(iH_0 t_j)\ V(rt_j)\exp(-iH_0 t_j)\exp(\gamma t_j). \quad (8)$$

Here H is the atomic hamiltonian, $a(k_1, k_2,\ldots,k_n)$ are the numerical coefficients. The structure of matrix elements $S_g^{(m)}$ is in details described in [19-23]. Here we only note that one may to simplify a consideration by account of the k-photon absorption contribution in the first two PT orders. Besides, summation on laser pulse is exchanged by integration. The corresponding (l+2k+1)-times integral on (l+2k) temporal variables and r (l=0,2) (integral I_g) are calculated [19-23]. Finally, after some cumbersome transformations one can get the expressions for the line moments. The corresponding expressions for the Gaussian laser pulse are as follows:

$$\delta\omega(p\alpha \mid k) = \{\pi\Delta/(k+1)k\}[E(p,\omega_{p\alpha}/k)-E(\alpha,\omega_{p\alpha}/k)], \quad (9)$$

$$\mu_2 = \Delta^2/k$$

$$\mu_3=\{4\pi\Delta^3/[k(k+1)]\}[E(p,\omega_{p\alpha}/k)-E(\alpha,\omega_{p\alpha}/k)],$$

where

$$E(j,\omega_{p\alpha}/k)=0{,}5\sum_{p_i} V_{jpi}\, V_{pij}\left[\frac{1}{\omega_{jp_i}+\omega_{p\alpha}/k} + \frac{1}{\omega_{jp_i}-\omega_{p\alpha}/k}\right] \quad (10)$$

The summation in (10) is over all atomic states. Let us note that these formulas for the Gaussian pulse differ of the Lorenz shape laser pulse expressions [21-23]. For the soliton-like pulse it is necessary to carry out the numerical calculation or use some approximations to simplify the expressions [27]. In order to calculate (10), we use an effective Ivanov-Ivanova technique [28,29] of calculating sums of the QED PT second order, which has been earlier applied by us in calculations of some atomic and mesoatomic parameters [26,27,30-32]. Finally the computational procedure results in a solution of the ordinary differential equations system for above described functions and integrals. In concrete numerical calculations the PC "Superatom-ISAN" package is used. The construction of the operator wave functions basises within the QED PT, the technique of calculating the matrix elements in Egs. (9,10) and other details is are presented in Refs. [19-30]. The special features of treating the multiphoton resonances in a nucleus within the outlined approach are obviously connected with estimating the corresponding matrix elements on the basis of the nuclear wave functions and some other details. In a modern theory of a nucleus there is sufficiently great number of the different models for generating the proton and neutron wave functions basis's. At present time it is accepted that quite adequate description of the nuclear density is provided by the relativistic mean-field (RMF) and other models of the nucleus [32-36]. As alternative approach one could use the advanced RMF or shell models based on the effective Dirac-Wood-Saxon type Hamiltonian [32].

3. Results and conclusions

Further we present the results of the numerical simulation for the three-photon resonant, four-photon ionization profile of atomic krypton (the 4p ® 5d[1/2]$_1$ and 4p ® 4d[3/2]$_1$ three photon Kr resonances are considered). In Ref. [18] it has been performed the experimental studying the resonant multiphoton ionization of krypton by intense uv (285-310 nm) laser radiation for the intensity range $3´10^{12}$-10^{14} W/cm^2 . The experiment consisted of the measurement of the number of singly charged Kr and Xe ions produced under collisionless conditions as a function of laser frequency and intensity. The output of a dye-laser system operating at 2.5 Hz is frequency doubled in a 1-cm potassium dihydrogen phosphate (KDP) crystal to give a 0.5-mJ, 1.3-ps, transform-limited 0.1-nm-bandwidth beam tunable between 285 and 310 nm. There have been determined the corresponding parameters of the 4p ® 5d[1/2]$_1$ (i) and 4p ® 4d[3/2]$_1$ (ii) three photon Kr resonances. The resonance shift is proportional to intensity with a width dominated by lifetime broadening of the excited state. The corresponding shift and width have been found as follows: (i) the shift $dw_0(pa|3)=aI$, a_{exp}=3.9 meV/(Tw×cm^{-2}); width b_{exp}= 1.4 meV/(Tw×cm^{-2}); (ii) shift $dw_0(pa|3)=aI$, a_{exp}=8.0 meV/(Tw×cm^{-2}); width b_{exp}=4 meV/(Tw×cm^{-2}). The authors [18] have used quite simple model of an effective two-level atom with the assumption of a rate limiting three-photon excitation step followed by rapid one-photon ionization from the excited state. As expected, the three-photon resonances broaden and shift further as the laser pulse intensity is increases. The important feature of the corresponding profiles is linked with available asymmetry [18]. Naturally, it is easy to understand that the asymmetric profile is typical of realistic laser pulses with the spatially and temporally varying intensity. Besides, the authors of Ref. [18] have noticed that while all resonances are "blue" shifted, ac Stark shift calculations, which are difficult to perform for excited states lead to both "blue" and " red" shifts. Our numerical simulation results for the 4p ® 5d[1/2]$_1$ (i) and 4p ® 4d[3/2]$_1$ (ii) three photon Kr resonances are as follows: (i) the shift $dw_0(pa|3)=aI$, a_{exp}=3.95 meV/(Tw×cm^{-2}) and width b_{exp}= 1.5 meV/(Tw×cm^{-2}); (ii) shift $dw_0(pa|3)=aI$, a_{exp}=8.1 meV/(Tw×cm^{-2}) and width b_{exp}=4.2 meV/(Tw×cm^{-2}). One could conclude that there is a physically reasonable agreement of the theoretical and experimental data.. Analysis shows that the shift and width of the multi-photon resonance line for the interaction "atom- multimode laser pulse" is greater than the corresponding shift and width for a case of the "atom- single-mode pulse" (the Lorenz pulse model) interaction. From the physical point of view it is obviously provided by action of the photon-correlation effects and influence of the laser pulse multi-modity. A great interest represents the possibility of the quantitative construction of the corresponding resonances profiles with explanation of the asymmetric nature by means calculating sufficiently "large" number of the multiphoton transition line moments. It is interesting to note that such an approach easily explains the qualitative features of the multiphoton resonances lines in the ^{57}Fe nucleus. According to Ref. [34], the nuclear multiphoton transitions are taking a place in ^{57}Fe nucleus subjected to radio-frequency electromagnetic field w_0=30MHz. This picture was experimentally observed in the Mössbauer spectra of ^{57}Fe nuclei in Permalloy by Tittonen et al [35]. Really, the eight transitions are possible between the four hyperfine substates of the 14.4 keV excited level e and the two substates of the ground state g in the radio-frequency magnetic field [34]. If the static magnetic hyperfine splitting of the ground and excited states are respectively $w_g>0$ and $w_e>0$, the transition frequencies corresponding to forbidden g-ray transitions are $(E_e-E_g)/h\pm 3w_g/2\pm w_g/2$, where E_e, E_g are respectively the energies of the 14.4-keV and ground states of the ^{57}Fe nucleus in an absence of any external field.

References

1. Batani D, Joachain C J, eds. 2006 *Matter in super-intense laser fields*, AIP Serie, N.-Y.
2. Ivanova E P 2011 *Phys.Rev.A* 84 043829
3. Jaron-Becker A, Becker A, Faisal F H M 2004 *Phys.Rev.A* 69 023410

4. Plummer M, Noble C J 2003 *J.Phys. B: At. Mol. Opt. Phys*. 36 L219
5. van der Hart H W, Lysaght M A, Burke P G 2007 *Phys.Rev.*A 76 043405
6. Mercouris T, Nikolaides C A 2003 *Phys. Rev. A* 67 063403
7. Brandas E, Floelich P 1997 *Phys. Rev. A* 16 2207
8. Kwanghsi Wangt, Tak-San Hot, Shih-I Chu 1985 *J.Phys. B: At. Mol. Opt. Phys*. 18 4539; 2006 *Phys.Rev.A* 73 023403
9. Glushkov A V, Ivanov L N, Letokhov V S Nuclear quantum optics *1991 Preprint of Institute for Spectroscopy, USSR Academy of Sciences*, Troitsk-N7
10. Bürvenich T J, Evers J, Keitel C H 2006 *Phys.Rev.Lett.* 96 142501; 2006 Phys. *Rev.C* 74 044601
11. Shahbaz A, Müller C, Staudt A, Bürvenich T J, Keitel C H 2007 *Phys.Rev. Lett.* 98 263901
12. Fedorov M V 1999 *Physics-Uspekhi* 169 66
13. Delone N B, Kraynov V P 1998 *Physics-Uspekhi* 168 531
14. Belyaev V S, Kraynov V P, Lisitsa V S, Matafonov A P *Physics-Uspekhi* 178 823
15. Zoller P. 1982 *J.Phys. B: At. Mol. Opt. Phys*. 15 2911
16. Lompre L-A, Mainfrau G, Manus C, Marinier J P 1991 *J.Phys. B: At. Mol. Opt. Phys*.14 4307
17. Khetselius OYu, 2012 *J. of Phys.: Conf. Ser.*. 397 012012; 2009 *Phys.Scr.* T.135 014023.
18. Landen O L, Perry M D, Campbell E M 1997 *Phys.Rev.Lett*. 59 2558
19. Ivanov L N, Letokhov V S 1975 *JETP* 68 1748; 1985 *Com. Mod. Phys.* D4 169
20. Ivanov L N, Ivanova E P, Aglitsky E V 1998 *Phys. Rep.* 166 315
21. Glushkov A V, Ivanov L N, *1995 Preprint of ISAN, USSR Academy of Sci.*, Troitsk, N3.
22. Glushkov A V, Ivanov L N, Ivanova E P, 1986 *Autoionization Phenomena in Atoms*, Moscow Univ. Press, Moscow, p 58
23. Glushkov A V, Ivanov L N 1992 *Phys. Lett. A* 170 33.
24. Glushkov A V, Ivanov L N 1992 *Proc. of 3rd Seminar on Atomic Spectroscopy* (Chernogolovka, Moscow reg.) p 113
25. Glushkov A, Ivanov L N 1993 *J.Phys. B: At. Mol. Opt. Phys*. 26 L179.
26. Glushkov A V, Loboda A, Gurnitskaya E, Svinarenko A 2009 *Phys. Scripta* T135 014022
27. Glushkov A V, Khetselius O Yu, Loboda A V, Svinarenko A A 2008 *Frontiers in Quantum Systems in Chem. and Phys., Ser. Progress in Theoretical Chemistry and Physics*, vol. 18. ed. S Wilson, P J Grout, J Maruani, G; Delgado-Barrio, P Piecuch (Berlin: Springer) p 543
28. Ivanov L N, Ivanova E P 1974 *Theor. Math.Phys.* 20 282
29. Ivanova E P, Ivanov L N, Glushkov A V, Kramida A E 1995 *Phys. Scripta* 32 512
30. Glushkov A V 2012 *Advances in the Theory of Quantum Systems in Chemistry and Physics. Ser. Progress in Theoretical Chemistry and Physics*, vol. 28, ed. by K Nishikawa, J Maruani, E Brandas, G Delgado-Barrio, P Piecuch (Berlin: Springer) p 131
31. Glushkov A V, Khetselius O Yu, Malinovskaya S V 2008 *Europ. Phys. Journ ST* 160 195.
32. Glushkov A V, 2012 *J. of Phys.: Conf. Ser.*. 397 012011
33. Serot B, Walecka J 1996 *Adv.Nucl.Phys.* 16 1
34. Olariu S, Sinor T W, Collins C B 1994 *Phys.Rev.B* 50 616
35. Tittonen I, Lippmaa M, Ikonen E, Linden J, Katila T 1992 *Phys.Rev.Lett.* 69 2815
36. Khetselius O Yu, 2009 *Int. Journ. Quant. Chem*. 109 3330

This article has been received within 2014

UDC 539.182

V. V. Buyadzhi, A. V. Glushkov, L. Lovett

SPECTROSCOPY OF ATOM AND NUCLEUS IN A STRONG LASER FIELD: STARK EFFECT AND MULTIPHOTON RESONANCES

Abstract

The consistent relativistic energy approach to atom in a strong realistic laser field, based on the Gell-Mann and Low S-matrix formalism, is applied to studying the resonant multiphoton ionization of krypton by intense uv laser radiation and calculating the multiphoton resonances shift and width in krypton. An approach to treating the multiphoton resonances in nuclei is outlined on example of the ^{57}Fe nucleus.

Key words: electromagnetic and strong interactions, laser field, multiphoton resonances

УДК 539.182

В. В. Буяджи, А. В. Глушков, Л. Ловетт

СПЕКТРОСКОПИЯ АТОМА И АТОМНОГО ЯДРА В СИЛЬНОМ ЛАЗЕРНОМ ПОЛЕ: ЭФФЕКТ ШТАРКА И МНОГОФОТОННЫЕ РЕЗОНАНСЫ

Резюме

Последовательный релятивистский энергетический подход к атому в сильном реалистичном лазерном поле, основанный на S-матричном формализме Гелл-Манна и Лоу, применяется для изучения резонансной многофотонной ионизации криптона интенсивным ультрафиолетовым лазерным излучением и вычисление многофотонных резонансных смещений и ширины в криптоне. Подход к рассмотрению многофотонных резонансов в ядрах изложен на примере ядра 57Fe.

Ключевые слова: электромагнитное и сильное взаимодействия, лазерное поле, многофотонные резонансы.

УДК 539.182

В. В. Буяджи, О. В. Глушков, Л. Ловетт

СПЕКТРОСКОПІЯ АТОМА І АТОМНОГО ЯДРА В СИЛЬНОМУ ЛАЗЕРНОМУ ПОЛІ: ЕФЕКТ ШТАРКА І БАГАТОФОТОННІ РЕЗОНАНСИ

Резюме

Послідовний релятивістський енергетичний підхід до атома в сильному реалістичному лазерному полі, оснований на S-матричному формалізмі Гелл-Манна і Лоу, застосовується для вивчення резонансної багатофотонної іонізації криптона інтенсивним ультрафіолетовим лазерним випромінюванням і обчислення багатофотонних резонансних зміщень і ширини в криптоні. Підхід до розгляду багатофотонних резонансів у ядрах викладений на прикладі ядра 57Fe.

Ключові слова: електромагнітна і сильна взаємодія, лазерне поле, багатофотонні резонанси.

UDC 621.794: 546.48: 539.51

Iatsunskyi I. R.,[a,b] *Nowaczyk G,*[b] *Pavlenko M. M.,*[a] *Fedorenko V. V.,*[a] *Smyntyna V. A.*[a]

[a]Odessa I. I. Mechnikov National University, Department of Experimental Physics, str. Pastera 42, Odessa, Ukraine, 65023, yatsunskiy@gmail.com
[b]Nanobiomedical Center, Adam Mickiewicz University in Poznan, ul. Umultowska 85, Poznań, Poland, PL 61614 cnbmadm@amu.edu.pl

ONE AND TWO-PHONON RAMAN SCATTERING FROM NANOSTRUCTURED SILICON

Raman scattering from highly/low resistive nanostructured silicon films prepared by metal-assisted chemical etching was investigated. Raman spectrum of obtained silicon nanostructures was measured. Interpretation of observed one and two-phonon Raman peaks are presented. First-order Raman peak has a redshift and broadening. This phenomenon is analyzed in the framework of the phonon confinement model taking into account mechanical stress effects. Second-order Raman peaks were found to be shifted and broadened in comparison to those in the bulk silicon. The peak shift and broadening of two-phonon Raman scattering relates to phonon confinement and disorder. A broad Raman peak between 900-1100 cm^{-1} corresponds to superposition of three transverse optical phonons ~2TO (X), 2TO (W) and 2TO (L). Influence of *e*xcitation wavelength on intensity redistribution of two-phonon Raman scattering components (2TO) is demonstrated and preliminary theoretical explanation of this observation is presented.

1. Introduction

Nanostructured silicon is presently of widespread interest because Si is an extremely promising material not only for electronics but optoelectronics, solar cells, sensors etc. Advanced nanosilicon technologies require a detailed study of obtained structures. Therefore, new methods and approaches should be performed for nanosilicon study.

Raman scattering has become a standard tool to study the silicon and nanostructured silicon for many years [1-15]. Raman-scattering studies of nanomaterials give us information about energy dispersion, structure, bonding and disorder. The analysis of nanostructures is mainly based on the phonon confinement model in which the finite crystallite size is taken into account by weighting the phonon-scattering efficiency [3-8]. Confinement effects in nanostructures lead to modifications of the electronic, optical and vibrational properties. Unfortunately, if a first-order Raman spectrum of nanocrystalline silicon has been studied extensively, the second-order Raman scattering is investigated marginally [1-3].

In the second-order Raman scattering process, two phonons of equal and opposite momentum participate and produce either line or broad continuous spectrum. Zone edge phonons, which appear only in higher-order Raman scattering, correspond to large wave vectors and are sensitive to short-range disorder. The nature of a material, such as crystalline or amorphous, can therefore be ascertained by analyzing the higher-order phonons as well. Study of second-order Raman scattering, in addition to first-order spectra, provides important information on the vibrational modes, energy structure, and morphology of nanostructured materials. Besides, second-order Raman scattering exhibits a higher sensitivity to nanoparticles size than first-order scattering [3-5].

In this paper we present the one- and two-phonon Raman spectra of nanostructured silicon fab-

ricated by metal-assisted chemical etching. We have measured the Raman frequency shifts and line shapes at room temperature. We focused on the changes in the second-order Raman scattering. New effect dealing with second-order Raman scattering was found.

2 Experimental procedure

2.1 Nanostructured silicon fabrication

The nanostructured silicon samples were fabricated using a metal-assisted chemical etching process (MACE) [16-18]. The MACE exhibits good process controllability to generate various nanostructured silicon surface morphologies. Similar to electrochemical etching to create porous silicon, MACE acts as a localized electrochemical etching process in which local electrodeless etching occurs at the metal/silicon interface, each nanometer-sized metal particle acts as a local cathode and the silicon surface acts as an anode. The metal particles are critical in the process to promote H_2O_2 decomposition and cause electron–hole injection into the silicon surface; silicon is dissolved by HF to create pits or other nanostructures on the surface.

Monocrystalline p-type Si samples with resistivity of 0.005 Ohm cm (*samples A, B*) and with resistivity of 80 Ohm cm (*samples C, D*), after standard RCA cleaning, were cleaned with acetone and deionized water via ultrasonic cleaning. A thin oxide layer was formed, and the surface became hydrophilic. This oxide layer was removed by dipping the samples into a dilute HF solution. The silver particles, which act as catalysts to assist the etching of silicon, were deposited on Si samples by immersion in 0.23 M HF and 10^{-3} M $AgNO_3$ metallization aqueous solutions. The time of immersion was varied – 40 s. for samples A and sample C; and 200 s. for sample B and sample D. After the electroless metallization, the wafers were etched in aqueous solutions containing HF (40%), H_2O_2 (30%), and ultrapure H_2O at ratio concentration - $H_2O_2/H_2O/HF$=10/80/40, for 30 minutes. After etching, the samples were etched in HNO_3 solution to remove silver particles and then were cleaned with deionized water and blown dry with nitrogen. The etching and immersion procedures were performed at room temperature.

2.2 Surface morphology characterization

Structural properties of porous silicon prepared by metal-assisted chemical etching have been investigated by Scanning Electron Microscopy (SEM) - Jeol 7001TTLS and Atomic Force Microscope (Bruker company) BioScope Catalyst. AFM measurements were carried out in contact mode. Using AFM and SEM, we could characterize the shape and sizes of nanostructures, their distribution and other parameters of morphology. In order to determine mechanical stresses of obtained structures we used X-ray diffraction analysis. . X-ray diffraction (XRD) data were collected using an Empyrean diffractometer using a copper X-ray source operating at 30 mA and 40 kV providing K_α radiation at a wavelength of 1.5408 Å. XRD data were collected in the range 20° to 80° 2θ with a step size of 0.013°.

2.3 Raman measurement

Raman scattering measurements were performed using a Renishaw micro-Raman spectrometer equipped with a confocal microscope (Leica). The samples were measured in backscattering geometry with a spectral resolution better than 1.0 cm^{-1}. The incident light was not polarized; also the detection setup contained no polarization filters. The Raman scattering spectra were excited by 488 nm, 514 nm and 633 nm. The beam was focused on the samples with a 50 x microscope objective with a numerical aperture of 0.4. The incident optical power was changed by using neutral density filters in the beam path. The minimum power for which a signal could be measured was limited by the signal to noise resolution of the detector in the spectrometer. All measurements were performed at room temperature in ambient atmosphere.

3 Results and Discussions

3.1 Morphology study of nanostructured silicon

Figs. 1 (A)–(D) are the images of scanning electron microscopy, which show the surface morphology of nanostructured silicon samples fabricated by MACE. Samples A and B have mostly the porous structure. This morphology

shown in images indicates pores of different sizes depending on the chemical procedures. On the other hand, AFM studies of that samples show the presence of nanometer-sized pyramids (hillocks) between the macropores. These hillocks apparently correspond to Si nanocrystallites, whereas the hollows between them correspond to the narrow (nanometer) pores on the surface. The lateral dimensions of the hillocks, which were determined from AFM images as their largest linear dimensions at a base, are in the range of 15–20 nm. The sizes of hillocks increase down to the bottom of pores. It should be noted that the actual lateral dimensions of the elements of the structure are smaller than the dimensions of the AFM images by approximately the doubled radius of the probe tip.

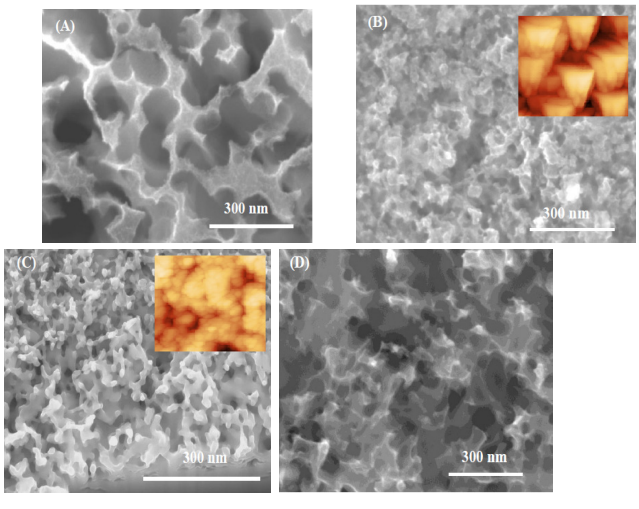

Fig. 1 SEM images of nanostructured silicon (insets are AFM images): Ag particles were deposited on Si samples by immersion in 0.23 M HF and 10^{-3} M $AgNO_3$ metallization aqueous solutions. The time of immersion was varied – 40 s. for samples (A) and sample (C); and 200 s. for sample (B) and sample (D). Etching solution contained HF (40%), H_2O_2 (30%), and ultrapure H_2O at ratio concentration - H_2O_2/ H_2O/HF=10/80/40, for 30 minutes.

Samples C and D have mostly the "coral-like" structure similar to nanowires with different orientation. Wires have approximate dimensions lying in the range of 10–25 nm. AFM shows mostly the cauliflower-like structure. This morphology shown in 2D images indicates several particles (granules) embedded in each grain (Fig.1(c) inset). However, the shapes, as well as arrangement of the grains, were found to be different.

All these results confirm that different morphologies can be produced by varying either the dopant level and, of course, the type of etchant and deposition solution.

1.2 Raman scattering investigations of nanostructured silicon

Under normal conditions (standard pressure and temperature), silicon crystallizes in a diamond lattice structure, which belongs to the O_n^7 space group. The diamond structure of silicon allows only one first-order Raman active phonon of symmetry Γ_{25} located at the Brillouin zone (BZ) centre corresponding to a phonon wave vector 520.0 ± 1.0 cm^{-1} with the full width at half maximum (FWHM) – 3.5 cm^{-1}. In order to interpret other Raman peaks, the Table .1 shows more important phonon frequencies of silicon [1-15].

Table 1

Silicon Phonon Frequencies

Physical property	Phonon frequencies (cm^{-1})
LTO (Γ)	517-519
TA (X3)	149-151
LAO (X1)	410-411
TO (X4)	460-464
TA (L3)	113-115
TA (Σ)	230
LA (L2)	377-379
LO (L1)	420
TO (L3)	490
TO (W)	470

Raman scattering spectra of samples 1-4 are shown in Fig.2, for an incident laser power of 10 mW. For all samples one can notice the quite similar Raman spectrum. High peak at 518-519 cm with the FWHM of 8.5-15 cm^{-1} can be seen in the Raman spectrum of nanostructured Si. The intensity of the first-order scattering which is due

to the optical phonons (TO, LO) at the center Γ point of the BZ, as was mentioned above, is much stronger in comparison with that from the initial Si wafer. In comparison with the first-order optical phonon peak of *c*-Si, the corresponding Raman peak of nano-Si has very small frequency down-shifted, its linewidth broadened and its line shape becomes asymmetric with a little tail on the low-energy side extending to 470-480 cm^{-1} for all samples what indicate on partial amorphous-like structure. The first-order spectrum from bulk Si single crystal represents scattering by optical phonons with quasimomentum **q**=0 because of its conservation in an infinite lattice. Studies of the morphology and structure of nano - Si by SEM/AFM has revealed the presence of nanostructures with dimensions on a nanometer scale (Fig. 1). The limitation of the translation symmetry leads to relaxation of this selection rule, and phonons with quasimomentum out of the region around the Γ point determined by the size of the crystallite can contribute to the scattering. Due to the decrease in the frequency of optical phonons with **q** in the vicinity of the BZ center, the Raman line of a spectrum from nanocrystalline material is shifted to lower energies and broadened. But comparing our experimental data with references one should conclude that there are additional reasons of the red-shifting and broadening. It is well known that effects of sample heating caused by laser radiation, compressive stress and defects give rise to a frequency shift of the Raman peak [2, 5, 9]. Therefore, it is necessary to take into account the relative contributions of different mechanisms to the Raman shift and broadening if one need to obtain more precise results for peak line shape.

Khorasaninejad et al. showed that the main reason of red-shifting, but not the peak broadening, is heating effect [22]. They also showed that if confinement effects take place the red-shifting would be approximately 1-2 cm^{-1} which corresponds to our case. Regarding the impact of compressive stress and defects we can estimate it taking into account the following equations [3]

$$\frac{\delta\omega}{\omega} = -3\gamma\frac{a_{PS}-a_0}{a_0}, \quad (1)$$

where $\delta\omega\,\delta$ is the peak width, a_{PS} a_B is the lattice constant of porous silicon (PS) nanostructures, and $\gamma\,\gamma \approx 1.0$ is the Gruneisen constant. The derived values of strain $\frac{a_{PS}-a_0}{a_0}\frac{a_B-a_0}{a_0}$ can be estimated from X-Ray diffraction analysis. We have obtained this value and it turned out to be an order of 10^{-3} for different samples.

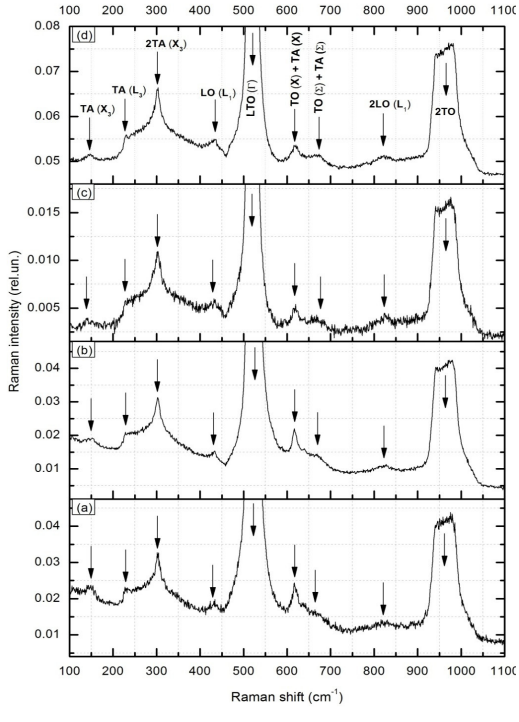

Fig. 2 Normalized Raman spectrum of Si nanostructures taken with a 514 nm laser. (A) – (D) – sample, respectively.

Campbell and Fauchet [23] developed a quantitative model that calculates the Raman spectrum of PS as depending on the size *L* and on the shape of the porous silicon crystallites. If PS is modeled as an assembly of quantum wires, the phonon confinement is assumed to be two dimensional, while if the PS is modeled as an assembly of quantum dots, the confinement is three dimensional. The Raman spectrum is given by:

$$I(\omega) \cong \int_{BZ} \frac{d^3q\,|C(0,q)|^2}{(\omega-\omega(q))^2-(\frac{\Gamma_0}{2})^2}, \quad (2)$$

where

$$|C(0,q)|^2 = \exp(-\frac{q^2L^2}{16\pi^2}). \quad (3)$$

The first-order Raman spectrum $I(\omega)$ is thus given by:

$$I(\omega) \cong \int_{BZ} \frac{4\pi q^2 \exp(-\frac{q^2L^2}{16\pi^2})d^3q}{(\omega-\omega(q))^2-(\frac{\Gamma_0}{2})^2}, \quad (4)$$

where Γ_0 is the natural linewidth for c-Si at room temperature but we should add to this value linewidth corresponding to compressive stress $\boldsymbol{\delta\omega}$ and $\omega(q)$ is the dispersion relation for optical phonons in c-Si. This expression can be taken as [23]:

$$\omega = \omega_0 - 120\,(\frac{q}{q_0})^2. \quad (5)$$

Here, ω_0 is the position of the c-Si Raman peak. By specifying the size of the silicon nanocrystallites, from eqs. (4) and (5) the relation between the peak shift and the linewidth in the framework of the phonon confinement model can be determined. Taking into account the impact of compressive stress and confinement effects we reconstructed the Raman spectrum. The results of calculations are presented in Fig. 3. It can be noticed that values of nanocrystallites sizes obtained from calculations are smaller than from SEM. That can be explained by the limited resolution of the electron microscope.

In contrast to c-Si, one can see the first-order scattering from acoustical phonons at 150 cm^{-1} and optical phonon at 430 cm^{-1}. These peaks correspond to TA phonon at *X* critical points – TA (X) and to LO phonon at L critical points –LO (L), respectively (Table 1). The last peak suggests that nanostructured silicon in some extent is in amorphous form [7, 15].

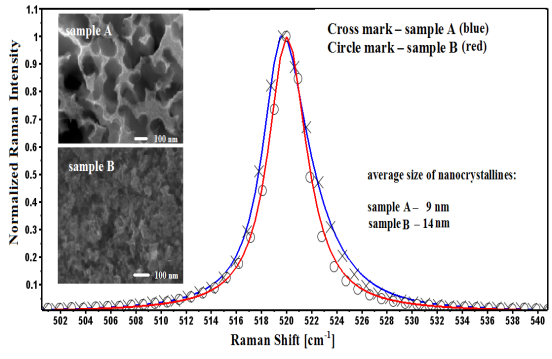

Fig. 3 Experimental and calculated curves of nanostructured silicon surface (sample A, B).

A strong enhancement of multiphonon features occurs for nanostructured silicon. The second order spectrum is much weaker than the first-order peak LTO (Γ) with features ranging from 100–1100 cm^{-1}. The second-order spectrum of transverse 2TA acoustical phonons is clearly observed near 300 cm^{-1}. Some authors suggest this peak is corresponding to LA modes [11, 13] but there is not accurately confirmation of this fact. Probably we observe the superposition of transverse and longitudinal acoustic modes. Comparing the peak position with the values in the Table 1, we can assume that this peak corresponds to TA overtones at *X* critical points – 2TA (X). We can also observed few little two-phonon peaks - 2TA (L) at 230 cm^{-1} and 2LO (L) at 830 cm^{-1}. Some authors explain the 2LO (L) by some kind of disorder but it still is open question. In addition, we also found two obvious peaks of Si nanocrystallines at 630 and 670 cm^{-1} which can be ascribed to the quantum confinement effect of Si. These peaks are composed of contributions from combinations and also from overtones of transverse optical and acoustical modes of different critical points. The peak at 630 cm^{-1} probably corresponds to the combination TO (X) +TA (X) modes and weaker peak corresponds to TO (Σ) +TA (Σ) [5, 9]. Probably, longitudinal modes are also taking part in these combinations as indicated in some publications [4, 11]. And finally, there is a broad peak between 900-1100 cm^{-1} which is from the scattering of few transverse optical phonons ~2TO phonons. A more detailed discussion of this peak will be further.

Since fundamental phonon modes are shifted and broadened, the second-order modes of nanostructured silicon are also shifted and broadened. In addition to the peaks which can be attributed to the scattering from crystalline material, all spectra of our nanostructured silicon samples, although to different extents, exhibit broadband.

1.3 Wavelengths effect of two-phonon Raman scattering

For second-order scattering, the two phonons involved must have equal but opposite wave vector in order to fulfill momentum conservation. Therefore, the strongest scattered signal is due to phonons where the density of states (DOS) is highest [19]. The intensity of the second order Raman signal strongly depends on the scattering geometry due to symmetry reasons. Our results for second-order Raman scattering are shown in Fig.4. One can see the Raman spectrum of sample A. The laser power for different wavelengths had approximately the same values less than 10 mW to prevent heating effects. We can see a broad peak between 900-1100 cm^{-1} which is from the scattering of few transverse optical phonons ~2TO phonons for different wavelength of the excitation light. To date, there is no consensus about the origin of the broad peak. Some authors argue that this peak is formed by the superposition of two or more optical modes [1-5, 19-21]. It can be seen that shape line has a kind of complexity. The Raman peak was split onto separate peaks. The peaks, located at 930-940, 950-960 and 980-985 cm^{-1} have been found. As discussed above, the scattering in second-order reflects the phonon DOS. For bulk silicon, the DOS features few strong singularities due to TO phonon at the X-point, the W-point and the L-point. The shoulder at 930-940 cm^{-1}, which is identified as two-TO-phonon overtone at zone-edge point X, emerges at 930 cm^{-1} – 2TO (X). The peak at 945-955 cm^{-1}, which is identified as two-TO-phonon overtone at zone-edge point W, emerges at 940 cm^{-1} – 2TO (W). Furthermore, the peak at 980 cm^{-1} corresponding to 2TO-phonon overtone scattering from the critical point L, appears at 980 cm^{-1} – 2TO (L). It was noticed that the 2TO peaks narrow as the size of the nanostructures become larger. It is clear from these results that the 2TO band is affected by confinement effects and shifts towards lower frequency and becomes broader as the dimension of the nanocrystals decreases.

Exploring the patterns of change in this peak, depending on the wavelength of the excitation light (λ_{exc}) we found an interesting effect. Changing the λ_{exc} leads to an intensity redistribution of Raman scattering components. One can notice that for λ_{exc}=488 nm and λ_{exc}=514 nm the peaks of 2TO (L) and 2TO (W) prevail over the 2TO (X) mode. For the λ_{exc}=633 nm 2TO (X) phonon overtone comes maximum and the left shoulder of the broad peak becomes much higher than right shoulder. We compared this result with other publications [1-5, 9-10, 13, 15-16]. Indeed, in other publication one can notice, although to different extents, the same effect. Unfortunately, no one paid attention to this experimental observation.

In order to explain this effect we considered following assumptions: increasing in the intensity of the second-order Raman scattering depends on Raman tensor and effective Raman scattering cross-section. On the other hand, the Raman tensor depends on the probability of interband optical transitions [20-21]. Photons with energies corresponding to the absorption edge for a certain zone-edge point of BZ should have a higher probability of optical transitions and thereby the intensity of Raman peak for certain zone-edge point would increase or decrease its value.

The intensity of second-order spectra, $I_2(\omega)$, is related to that of first-order scattering, $I_1(\omega)$, through [21]

$$I_2(\omega) \approx I_1(\omega) f(\frac{\hbar\omega_i}{\hbar\omega_g}), \qquad (6)$$

where $\hbar\omega_i$ energy of laser photon, $\hbar\omega_g$ energy equal to band gap width in material. The function $f(\frac{\hbar\omega_i}{\hbar\omega_g})$ depends in a fairly complex way on the ratio $(\frac{\hbar\omega_i}{\hbar\omega_g})$. If $\hbar ù_i$ is close to $\hbar\omega_g$, the intensity of second-order Raman scattering becomes

resonantly enhanced. The function describing the dependence of the second-order Raman scattering intensity on the ratio of laser beam energy to band gap width can be written as [21]

$$f(\frac{\hbar\omega_i}{\hbar\omega_g}) \approx \left[(1 - f(\frac{\hbar\omega_i}{\hbar\omega_g})^{-1.5} + const \right]^2 . \qquad (7)$$

It is well known, that the band gap energy increasing with the decreasing of nanostructures size and it results in a growth of $f(\frac{\hbar\omega_i}{\hbar\omega_g})$ function.

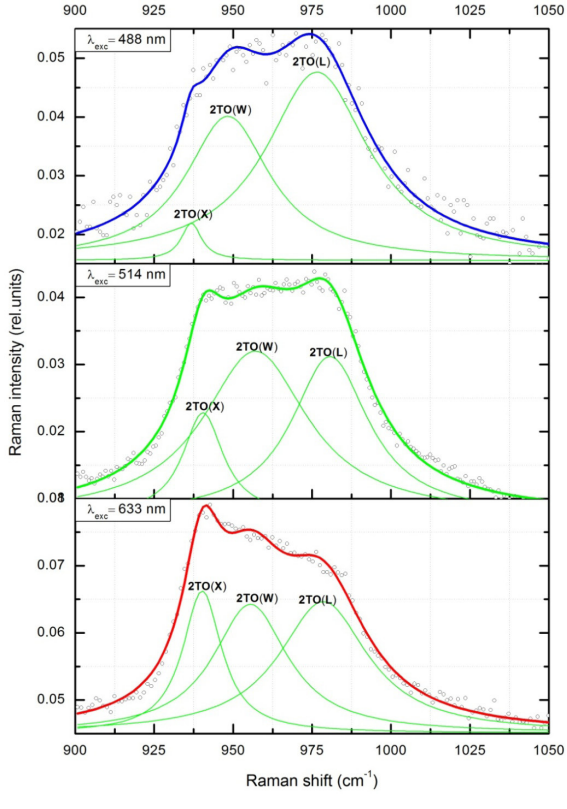

Fig. 4 Normalized Raman two-phonon scattering for three different laser wavelengths for sample A. The calculated separate second-order modes are indicated by solid green line curve and the experimental data are plotted as colored bold line.

Thus, calculation of second-order Raman spectra intensity allows one to estimate the optical energy gap. As far as the intensity of 2TO is concerned, estimated calculations shows that if we use red laser instead of blue one the intensity of 2TO (X) peak should increase the intensity approximately in 2.5 times. On the other hand, for peaks (2TO (L) and 2TO (W)), their intensities should increase approximately in 1.3-1.5 times, that we observed in the experiment. However, the present explanations are tentative, and require further theoretical proof.

Conclusions

One- and two-phonon Raman scattering characteristics of nanostructured silicon fabricated by metal-assisted chemical etching were investigated and the results are summarized. First-order Raman peak has a small redshift and broadening compared with bulk silicon as predicted by the phenomenological phonon confinement effect for nanostructures. In addition to the fundamental phonon modes, overtone and combinations of modes were also observed and analyzed. Second-order Raman peaks were found to be shifted and broadened in comparison to those in the bulk silicon. A broad peak between 900-1100 cm^{-1} corresponds to superposition of three transverse optical phonons ~2TO (X), 2TO (W) and 2TO (L). It was observed the anomalous behavior of the 2TO peaks depending on the wavelength of the excitation light. Our findings are important for characterizing of nanostructures by Raman scattering.

References

1. Rong-ping Wang, Guang-wen Zhou, Yu-long Liu, Shao-hua Pan, Hong-zhou Zhang, Da-peng Yu, and Ze Zhang, “Raman spectral study of silicon nanowires: High-order scattering and phonon confinement effects”, *Phys. Rev. B* **61**(24), 16827-16832 (2000).
2. Puspashree Mishra, and K. P. Jain, “First- and second-order Raman scattering in nanocrystalline silicon”, *Phys. Rev. B* **64**(7), 073304-073308 (2001).
3. S. Piscanec, M. Cantoro, A. C. Ferrari, J. A. Zapien, Y. Lifshitz, S. T. Lee, S. Hofmann, and J. Robertson, “Raman Spectrum of silicon nanowires”, *Phys.*

Rev. B **68**(24), 241312-241316 (2003).
4. N. Korsunska, B. Bulakh, B. Jumayev, L. Khomenkova,V. Yukhymchuk, and T. Torchynska, "Raman scattering characterization of macro- and nanoporous silicon", *Applied Surface Science* **243**, 30–35 (2005).
5. Cedrik Meiera, Stephan Lu, Vasyl G. Kravets, Hermann Nienhaus, Axel Lorke,and Hartmut Wiggers, "Raman properties of silicon nanoparticles", *Physica E* **32**, 155–158 (2006).
6. S.K. Mohanta, R.K. Soni, S. Tripathy, C.B. Soh, S.J. Chua, and D. Kanjilal, "Raman scattering from nanopatterned silicon surface prepared by low-energy $Ar^{+}Ar^{+}$-ion irradiation", *Physica E* **35**, 42–47 (2006).
7. Wensheng Wei, "One- and two-phonon Raman scattering from hydrogenated nanocrystalline silicon films", *Vacuum* **81**, 857–865 (2007).
8. Wensheng Wei, Gangyi Xu, Jinliang Wang, and Tianmin Wang, "Raman spectra of intrinsic and doped hydrogenated nanocrystalline silicon films", *Vacuum* **81**, 656–662 (2007).
9. Chil-Chyuan Kuo, "Micro-Raman spectroscopy characterization of polycrystalline silicon films fabricated by excimer laser crystallization", *Optics and Lasers in Engineering* **47**, 612–616 (2009).
10. Dorra Abidi, Bernard Jusserand, and Jean-Louis Fave, "Raman scattering studies of heavily doped microcrystalline porous silicon and porous silicon free-standing membranes", *Phys. Rev. B* **82**(7), 075210-075221 (2010).
11. Y. Duan, J. F. Kong, and W. Z. Shen, "Raman investigation of silicon nanocrystals: quantum confinement and laser-induced thermal effects", *J. Raman Spectrosc.* **43**(6), 756-760 (2012).
12. M. Khorasaninejad, J Walia, and S Saini, "Enhanced first-order Raman scattering from arrays of vertical silicon nanowires", *Nanotechnology* **23**, 275706- 275713 (2012).
13. Suk-Kyu Ryu, Qiu Zhao, Michael Hecker, Ho-Young Son, and Kwang-Yoo Byun, "Micro-Raman spectroscopy and analysis of near-surface stresses in silicon around through-silicon vias for three-dimensional interconnects", *J. Appl. Phys.* **111**, 063513-063521 (2012).
14. M. Khorasaninejad, M. M. Adachi, J. Walia, K. S. Karim, and S. Saini, "Raman spectroscopy of core/shell silicon nanowires grown on different substrates", *Phys. Status Solidi A* **210**(2), 373–377 (2013).
15. Narasimha Rao Mavilla, Chetan Singh Solanki,and Juzer Vasi, "Raman spectroscopy of silicon-nanocrystals fabricated by inductively coupled plasma chemical vapor deposition" *Physica E* **52**, 59–64 (2013).
16. Z. Huang, N. Geyer, P. Werner, J. De Boor, and U.Gosele, "Metal-assisted chemical etching of silicon: A review", *Advanced Materials* **23**(2), 285–308 (2011).
17. W. K. Kolasinski, "Silicon nanostructures from electroless electrochemical etching", *Current Opinion in Solid State &Materials Science* **9**, 73–83 (2005).
18. C. Chartier, S. Bastide, and C. Levy, "Metal-assisted chemical etching of silicon in HF-H_2O_2", *Electrochimica Acta* **53**(17), 5509–5516 (2008).
19. A Valentin, J Sée, S Galdin-Retailleau, and P Dollfus, "Phonon dispersion in silicon nanocrystals", *Journal of Physics: Conference Series* **92**, 012048-012052 (2007).
20. M. Aouissi, I. Hamdi, and N. Meskini, "Phonon spectra of diamond, Si, Ge, and α-Sn: Calculations with real-space interatomic force constants", *Phys. Rev. B* **74**(5), 054302-054312 (2006).
21. R. Loudon, "The Raman effect in crystals", *Adv. Phys.* **50**(7), 813-864 (2001).

This article has been received within 2014

UDC 621.794: 546.48: 539.51

I. R. Iatsunskyi, G. Nowaczyk, M. M. Pavlenko, V. V. Fedorenko, V. A. Smyntyna

ONE AND TWO-PHONON RAMAN SCATTERING FROM NANOSTRUCTURED SILICON

Abstract

Raman scattering from highly/low resistive nanostructured silicon films prepared by metal-assisted chemical etching was investigated. Raman spectrum of obtained silicon nanostructures was measured. Interpretation of observed one and two-phonon Raman peaks are presented. First-order Raman peak has a redshift and broadening. This phenomenon is analyzed in the framework of the phonon confinement model taking into account mechanical stress effects. Second-order Raman peaks were found to be shifted and broadened in comparison to those in the bulk silicon. The peak shift and broadening of two-phonon Raman scattering relates to phonon confinement and disorder. A broad Raman peak between 900-1100 cm^{-1} corresponds to superposition of three transverse optical phonons ~2TO (X), 2TO (W) and 2TO (L). Influence of e*xcitation wavelength* on intensity redistribution of two-phonon Raman scattering components (2TO) is demonstrated and preliminary theoretical explanation of this observation is presented.

Key words: porous silicon, Raman scattering, metal-assisted chemical etching.

УДК 621.794: 546.48: 539.51

И. Р. Яцунский, Г. Новачик, Н. Н. Павленко, В. В. Федоренко, В. А. Смынтына

ОДНО И ДВУХФОНОННОЕ РАМАНОВСКОЕ РАССЕЯНИЕ НАНОСТРУКТУРИРОВАННОГО КРЕМНИЯ

Резюме

В работе представлено исследование комбинационного рассеяния (КРС) наноструктурированного кремния полученного методом химического неэлектролитического травления. Представлена интерпретация наблюдаемых одно и двухфононных пиков КРС. Было выявлено, что пики КРС первого и второго порядка смещаются и уширяются относительно пика объемного кремния. Данное явление анализируется в рамках фононного конфайнмента с учетом механических напряжений. Широкий пик КРС второго порядка в области 900-1100 $см^{-1}$ соответствует суперпозиции трех поперечных оптических фононов ~ 2TO (X), 2TO (W) и 2TO (L).

Ключевые слова: пористый кремний, Рамановское рассеяние, неэлектролитическое травление.

УДК 621.794: 546.48: 539.51

І. Р Яцунський, Г. Новачик, М. М. Павленко, В. В. Федоренко, В. А. Сминтина

ОДНО ТА ДФОХФОНОНЕ РАМАНІВСЬКЕ РОЗСІЯННЯ НАНОСТРУКТУРОВАНОГО КРЕМНІЮ

Резюме

У роботі представлено дослідження комбінаційного розсіяння (КРС) наноструктурованого кремнію отриманого методом хімічного неелектролітическіх травлення. Представлена інтерпретація спостережуваних одне і двухфононних піків КРС. Було виявлено, що піки КРС першого і другого порядку зміщуються і розширюються щодо піка об'ємного кремнію. Дане явище аналізується в рамках фононного конфайнмента з урахуванням механічних напружень. Широкий пік ВРХ другого порядку в області 900-1100 см-1 відповідає суперпозиції трьох поперечних оптичних фононів ~ 2TO (X), 2TO (W) і 2TO (L).

Ключові слова: поруватий кремній, Раманівське розсіяння, неелектролітичне травлення.

UDC 539.186

A. V. Glushkov

Odessa State Environmental University, L'vovskaya str.15, Odessa-16, 65016, Ukraine
e-mail: dirac13@mail.ru

THE GREEN'S FUNCTIONS AND DENSITY FUNCTIONAL APPROACH TO VIBRATIONAL STRUCTURE IN THE PHOTOELECTRON SPECTRA OF MOLECULES: REVIEW OF METHOD

We present the basis's of the new combined theoretical approach to vibrational structure in photoelectron spectra of molecules. The approach is based on the Green's function method, which generalizes the Cederbaum-Domske formalism, and quasiparticle density functional theory. It generalizes the known Green's function approach by It is presented a new procedure for determination of the density of states, which describe the vibrational structure in molecular photoelectron spectra

I. Introduction

A number of phenomena, provided by interaction of electrons with vibrations of the atomic nuclei in molecules or solids under availability of of the electron states degeneration is usually called as the Jahn-Teller effect. This interaction may lead to local deformations, which are the reason of the structural phase transitions in the solids (statical Jahn-Teller effect)or appearance of the connected electron-vibrational states (a dynamical Jahn-Teller effect) [1-4]. Indeed, the physics of the interaction of electrons with vibrations of the atomic nuclei in molecules or solids is more richer (c.f.[1-111]). One could mention here a great field of the resonant collisions of electrons with molecules, which are one of the most efficient pathways for the transfer of energy from electronic to nuclear motion. While the corresponding theory has been refined over the years with sophisticated and elaborate non-local treatments of the reaction dynamics, such studies have for the most part treated the nuclear dynamics in one dimension. This situation has resulted from the fact that, as the field of electron-molecule scattering developed, both experimentally and theoretically, the phenomena of vibrational excitation and dissociative attachment were first understood for diatomics, and it seemed natural to extend that understanding to polyatomic molecules using 1-D or single-mode models of nuclear motion. However a series of experimental measurements of these phenomena in small polyatomic molecules have proven to be uninterpretable in terms of atomic motion with single degree of freedom. Reader can find more details about this topic in the recent paper by Rescigno et al [4].

In last several decades quantum chemistry methods has been refined with a sophisticated and comprehensive approaches of the correct interelectron correlations and electron-nuclear dynamics treatments [9-49]. Very interesting quote has been indicated by Bartlett and Musiał and earlier by Wilson: "*Ab initio quantum chemistry is an emerging computational area that is fifty years ahead of lattice gauge theory and a rich source of new ideas and new approaches to the computation of many fermion systems"* [26]. Following to ref. [26] we repeat that *d*riving these developments are the types of problems addressed by quantum chemists, as shown in Fig. 1. Primary among these are potential-energy surfaces (PES) which describe the behavior of the electronic energy with respect to the locations of the nuclei, subject to the underlying Born-Oppenheimer or clamped nuclei approximation. From the ground- and excited-state wave functions one could in principle obtain all properties that arise from a solution to vibrational Schrödinger equation that gives the frequencies and with derivatives of the dipole moment, the

infrared intensities [26-39]. Electronic excited states are also accessible along with electronic and photo-electron spectra. The properties that arise from the one-particle density matrix, such as dipole moments, hyperfine coupling constants, and electric-field gradients, are readily available.

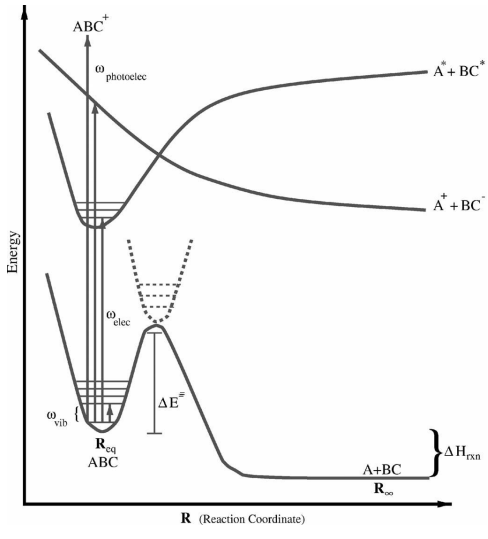

Figure 1. The nature of quantum chemical problems (from ref. [26]).

From even higher-order electric-field derivatives, one obtains hyperpolarizabilities, which determine nonlinear optical behavior. From derivatives relative to atomic displacements in molecules, one obtains anharmonic effects on vibrational-rotational spectra. In result , one could mention that a main objective is an accurate solution of the Schrödinger equation for molecules composed of comparatively light elements.

As it is often takes a place, the old multi-body quantum theoretical approaches, which have been primarily developed in a theory of superfluity and superconductivity, and generally speaking in a theory of solids, became by the powerful tools for developing new conceptions in molecular calculations [50-65]. Many of them offers a synthesis of cluster expansions, Brueckner's summation of ladder diagrams, the summation of ring diagrams Gell-Mann and an infinite-order generalization of many-body perturbation theory MBPT (Kelly, 1969; Bartlett and Silver, 1974a, 1976. Using quantum-field methods in molecular theory allowed to obtain a very powerful approach for correlation in many-electron systems. Only with this property are applications to polymers, solids, or the electron gas possible, and, even for small molecules, its effects are numerically quite significant. Configuration interaction methods, long the focus of the correlation problem in quantum chemistry Shavitt, 1998, do not, in general, have this property which is responsible for the emphasis on the coupled cluster theory and its multi-body perturbation theory approximations (Kelly, 1969; Bartlett and Silver, 1974a, 1974b; Pople *et al.*, 1976) in chemistry. For more details, the history of coupled cluster theory is best told from the viewpoint of some of its principal developers (look review [26]).

The Green's method is very well known in a quantum theory of field, quantum electrodynamics , quantum theory of solids (c.f.[61-63]). Naturally, an attractive idea was to use it in the molecular calculations. Returning to problem of description of the vibrational structure in photoelectron spectra of molecules, it is easily understand that this approach has great perspective as it was shown by Cederbaum et al (c.f.[65-68]). One could note that the experimental photoelectron (PE) spectra usually show a pronounced vibrational structure. Many papers have been devoted to treatment of the vibrational spectra by construction of potential curves for the reference molecule (the molecule which is to be ionized) and the molecular ion. Usually the electronic Green's function is defined for fixed position of the nuclei. As result, only vertical ionization potentials (V.I.P.'s) can be calculated [65]. The cited method, however, requires as input data the geometries, frequencies, and potential functions of the initial and final states. Since in most cases at least a part of these data are unavailable, the calculations have been carried out with the objective of determining the missing data by comparison with experiment. Naturally, the Franck-Condon factors are functions of the derivatives of the difference between the potential curves of the initial and final states with respect to the normal coordinates. One could agree here that highly accurate calculations are necessary to obtain good results with the above methods. To avoid this difficulty and to gain additional information about the ionization process, Cederbaum et al [65-

68] extended the Green's functions approach to include the vibrational effects and showed that the Green's functions method allowed the *ab initio* calculation of the intensity distribution of the vibrational lines, of the vibrational frequencies of the reference molecule and its ions, and of geometry shifts due to ionization and particle attachment. Besides, a great advancement here is connected with a possibility of the quite exact calculation of ionization potentials (I.P.'s) for molecules. According to ref.[65], starting from Hartree-Fock (HF) calculation [71,72] the electronic Green's functions have been calculated applying a many-body perturbation expansion. In this method the Koopmans' defect, i.e., the difference between the I.P. and the value derived from the Koopmans' theorem, is calculated directly, avoiding the usual subtraction of large numbers of roughly equal magnitude.

Further let us remember that for larger molecules and solids, far more approximate but more easily applied methods such as density-functional theory (DFT) [40-42] or from the wave-function world the simplest correlated model MBPT are preferred. Indeed, in the last decades DFT theory became by a great, quickly developing field of the modern quantum computational chemistry of atoms, molecules, solids. Naturally, this approach does not allow to reach a spectroscopic accuracy in description of the different molecular properties, nevertheless, the key idea is very attractive and can be used in new combined theoretical approaches.

Here we present the basis's of the new combined theoretical approach to vibrational structure in photoelectron spectra of molecules. The approach is based on the Green's function method and Fermi-liquid DFT formalism [80-86]. It generalizes the known Green's function approach by Cederbaum-Domcke (we use this version as a starting basis). The density of states, which describe the vibrational structure in molecular photoelectron spectra, is calculated with the help of combined DFT-Green's-functions approach. In addition to exact solution of one-bode problem different approaches to calculate reorganization and many-body effects are presented. In all cases no data about the molecular ion are needed and all transitions except those between linear and bent configurations are included. The density of states is well approximated by using only the first order coupling constants in the one-particle approximation. It is important that the calculational procedure is significantly simplified with using the quasiparticle DFT formalism Thus quite simple calculation becomes a powerful tool in interpreting the vibrational structure of photoelectron spectra for different molecular systems.

2. The combined Green's functions and density functional approach

2.1 The Hamiltonian of the system. The density of states in one –body solution

According to [65], the quantity which contains the information about the ionization potentials and the molecular vibrational structure due to quick ionization is the density of occupied states[9]:

$$N_k(\epsilon) = (1/2\pi\hbar)\int dt e^{i\hbar^{-1}\epsilon t}\langle\psi_0|a_k^t(0)a_k(t)|\psi_0\rangle, \quad (1)$$

where $|\Psi_0\rangle$ is the exact ground state wavefunction of the reference molecule and $a_k(t)$ is an electron destruction operator, both in the Heisenberg picture. For particle attachment the quantity of interest is the density of unoccupied states:

$$N_k(\epsilon) = (1/2\pi\hbar)\int dt e^{i\hbar^{-1}\epsilon t}\langle\psi_0|a_k(t)a_k^t(0)|\psi_0\rangle \quad (2)$$

Usually in order to calculate the value (1) states for photon absorption one should express the Hamiltonian of the molecule in the second quantization formalism. The corresponding Hamiltonian is as follows:

$$H = T_E(\partial/\partial x) + T_N(\partial/\partial X) + U(x,X), \quad (3)$$

where T_E is the kinetic energy operator for the electrons, T_N is the kinetic energy operator for the nuclei, and U represents the interaction

$$U(x,X) = U_{EE}(x) + U_{NN}(X) + U_{EN}(x,X), \quad (4)$$

where x denotes electron coordinates, X denotes nuclear coordinates, U_{EE} represents the Coulomb interaction between electrons, etc.Below we fol-

low to original version of the Cederbaum-Domske approach to vibrational structure of the molecular spectra. Further the following field operator is usually introduced:

$$\Psi(R,\theta,x)=\sum_i \phi_i(x,R,\theta)a_i(R,\theta) \qquad (5)$$

where the ϕ_i are Hartre-Forck (HF) one–particle functions and the a_i are destruction operators for a HF particle in the state described by the subscript *i*. Fixing $\theta(\theta=\theta_0)$, the Hamiltonian in the occupation number representation is given by [65]

$$H=H_{\mathrm{EN}}(R,\theta_0)+U_{\mathrm{N\,N}}(R,\theta_0)+T_{\mathrm{N}}(\partial/\partial R), \qquad (6)$$

$$H_{EN}=\sum_i \epsilon_i(R)a_i^t a_i+\frac{1}{2}\sum V_{ijkl}(R)a_i^t a_j^t a_l a_k - \sum_{ij}\sum_{k\in f}[V_{ikkj}(R)]a_i^t a_j, \qquad (7)$$

$$V_{ijkl}=\langle ij\left|e^2\right|r-r'\left|^{-1}\right|kl\rangle$$

The $\epsilon_i(R)$ are the one-particle HF energies and f denotes the set of orbitals occupied in the HF ground state. As usually in the adiabatic approximation one could write the eigenfunctions to H as products $|x,R,\theta_0\rangle_E\times|R\rangle_N$,and further expand $\epsilon_i(R)$, $V_{ijkl}(R)$, and $U_N(R,\theta)$ about R_0 leaving the operators a_i and a_i^t unchanged:

$$H=\sum_i {}^{o}{}_i(R_0)a_i^t a_i+\frac{1}{2}\sum V_{ijkl}(R_0)a_i^t a_j^t a_l a_k - \sum_j\sum_{k\in f}[V_{ikjk}(R_0)-V_{ikkj}(R_0)]a_i^t a_j + +\sum_i\left[\sum_{s=1}^{M}\left(\frac{\partial \epsilon_1}{\partial R_s}\right)_0(R-R_0)+ +\frac{1}{2}\sum_i\sum_{s,s'=1}^{M}\left(\frac{\partial^2 \epsilon_i}{\partial R_s\partial R_{s'}}\right)_0(R_s-R_{s0})(R_{s'}-R_{s'0})\right]a_i^t a_i+\ldots+U_N(R_0,\theta_0)+\ldots+T_N\left(\frac{\partial}{\partial R}\right) \qquad (8)$$

where M is the number of normal coordinates.

Choosing R_0 as the equilibrium geometry on the HF level and introducing dimensionless normal coordinates Q_s one can write the following Hamiltonian (the subscript 0 stands for R_0):

$$H=H_E+H_N+H_{EN}^{(1)}+H_{EN}^{(2)},$$

$$H_E=\sum_i \epsilon_i(R_0)a_i^t a_i+\frac{1}{2}\sum V_{ijkl}(R_0)a_i^t a_j^t a_l a_k - -\sum_{i,j}\sum_{k\in f}[V_{ikjk}(R_0)-V_{ikkj}(R_0)]a_i^t a_j,$$

$$H_N=\hbar\sum_{s=1}^{M}\omega_s(b_s^t b_s+\frac{1}{2}),$$

$$H_{EN}^{(1)}=2^{-1/2}\sum_{s=1}^{M}\left(\frac{\partial \epsilon_i}{\partial Q_s}\right)_0(b_s+b_s^t)[a_i^t a_i-n_i]+ +\frac{1}{4}\sum_i\sum_{s,s'=1}^{M}\left(\frac{\partial^2 \epsilon_i}{\partial Q_s\partial Q_{s'}}\right)_0(b_s+b_s^t)(b_{s'}+b_{s'}^t)[a_i^t a_i-n_i],$$

$$H_{EN}^{(2)}=2^{-3/2}\sum\sum_{s=1}^{M}\left(\frac{\partial V_{ijkl}}{\partial Q_s}\right)_0(b_s+b_s^t)[\delta v_1 a_i^t a_j^t a_k+ +\delta v_2 a_l a_k a_i^t a_j^t+2\delta v_3 a_j^t a_k a_l a_i^t] \qquad (9)$$

$$\frac{1}{8}\sum\sum_{s,s'=1}^{M}\left(\frac{\partial^2 V_{ijkl}}{\partial Q_s\partial Q_{s''}}\right)_0(b_s+b_s^t)(b_{s'}+ +b_{s'}^t[\delta v_1 a_i^t a_j^t a_k+\delta v_2 a_l a_k a_i^t a_j^t+2\delta v_3 a_j^t a_k a_l a_i^t]$$

where the index set v_1 means that at least ϕ_k and ϕ_l or ϕ_i and ϕ_j are unoccupied, v_2 that at most one of the orbitals is unoccupied, and v_3 that ϕ_k and ϕ_j or ϕ_l and ϕ_j are unoccupied. Besides, here for simplicity all terms leading to anharmonicities are neglected. The ω_s are the HF frequencies and the b_s and b_s^t are destruction and creation operators for vibrational quanta defined by

$$Q_s=(1/\sqrt{2})(b_s+b_s^t),$$

$$\partial/\partial Q_s=(1/\sqrt{2})(b_s-b_s^t) \qquad (10)$$

The interpretation of the above Hamiltonian is given in ref. [3]. The first term H_E describes the electronic motion for nuclei fixed at the HF ground state geometry. The second term H_N describes the motion of the nuclei in the harmonic HF potential (the extension to anharmonic terms can easily be done). $H_{EN}^{(1)}$ represents the coupling of the HF particles with the nuclear motion. The coupling constants are the normal coordinate derivatives of the HF one-particle energies. The first

sum in the expression for $H_{\mathrm{I\!N}}^{(1)}$ is responsible for the geometry shifts and the second one for the charge of frequencies due to electronions. There is also a modification of the interaction between electrons through the coupling to the nuclear motion. The term $H_{\mathrm{I\!N}}^{(2)}$, which describes this modification, is due to its nature less important than $H_{\mathrm{I\!N}}^{(1)}$. The exact solution of the one-body HF problem has been given in ref.[65] too. The HF-single-particle component H_0 of the Hamiltonian (9) is as follows:

$$H_0 = \sum_i \epsilon_i(R_0) a_i^t a_i + \sum_{s=1}^{M} \hbar\omega_s (b_s^t b_s + \frac{1}{2}) + \\ + \sum_{s=1}^{M} \sum_i 2^{-1/2} \left(\frac{\partial \epsilon_i}{\partial Q_s} \right) [a_i^t a_i - n_i](b_s + b_s^t)_0 + \\ + \sum_{s,s'=1} \sum_i \frac{1}{4} \left(\frac{\partial^2 \epsilon_1}{\partial Q_s \partial Q_{s'}} \right)_0 [a_i^t a_i - n_i](b_s + b_s^t)(b_{s'} + b_{s'}^t) \tag{11}$$

Correspondingly in the one-particle picture the density of occupied states is given by

$$N_k^0(\omega) = \frac{1}{2\pi\hbar} \int_{-\infty}^{\infty} dt e^{i\hbar^{-1}\omega t} \langle \Phi_0 | \; a_k^t(0) a_k(t) | \; \Phi_0 \rangle, \quad k \in f, \tag{12}$$

and the density of unoccupied states by

$$N_k^0(\omega) = \frac{1}{2\pi\hbar} \int_{-\infty}^{\infty} dt e^{i\hbar^{-1}\omega t} \langle \Phi_0 | \; a_k(t) a_k^t(0) | \; \Phi_0 \rangle, \\ k \notin f \tag{13}$$

with $$a_k(t) = e^{i\hbar^{-1} H_{0'} t} a_k e^{-i\hbar^{-1} H_0 t}. \tag{14}$$

Here $|\Phi_0\rangle$ is the product of the electronic and vibrational ground states, i.e., $|\Phi_0\rangle = | \; \Phi_0 \rangle | \; 0 \rangle$, where $|\Phi_0\rangle$ is the ground state to the HF operator $\sum \omega_i(R_0) a_i^t a_i$ and $| \; 0 \rangle$ is the state containing no vibrational quantum, i.e., $b_s | \; 0 \rangle = 0$ for all s. From Definitions (12) and (13) it follows immediately that

$$N_k^0(\omega) = \frac{1}{2\pi\hbar} \int_{-\infty}^{\infty} dt e^{i\hbar^{-1}(\omega - \omega_k)t} \langle 0 | \; e^{\pm i\hbar^{-1} \tilde{H}_{0'} t} | 0 \rangle, \tag{15}$$

with

$$\tilde{H}_0 = \sum_{s=1}^{M} \hbar\omega_s b_s^t b_s + \sum_{s=1}^{M} g_s^k (b_s + b_s^t) \\ + \sum_{s,s'=1}^{M} \gamma_{ss'}^k (b_s + b_s^t)(b_{s'} + b_{s'}^t) \tag{16}$$

where

$$g_s^i = \pm \frac{1}{\sqrt{2}} \left(\frac{\partial \omega_i}{\partial Q_s} \right)_0, \quad \gamma_{ss'}^i = \pm \frac{1}{4} \left(\frac{\partial^2 \omega_i}{\partial Q_s \partial Q_{s'}} \right)_0. \tag{17), (18}$$

As a first step in the evaluation of Eg. (15) new operators

$$c_s = \sum_{l=1}^{M} (\lambda_1^s b_l + \lambda_2^s b_l^t) \tag{19}$$

with real coefficients λ_1^s, λ_2^s were introduced in ref. [65]. The coefficients λ_1^s, λ_2^s are now determined in such a way that $\tilde{H}_0$, expressed in the new operators, takes the form

$$\tilde{H}_0 = \sum_{s=1}^{M} \hbar\hat{\omega}_s c_s^t c_s + \sum_{s=1}^{M} \hat{g}_s (c_s + c_s^t) + k. \tag{20}$$

Inserting the inverse transformation

$$b_s = \sum_{l=1}^{M} \lambda_1^s c_l - \lambda_2^s c_l^t) \tag{21}$$

in Eg. (16) and comparing with Eg. (21) we obtain the equations

$$\sum_l \hbar\omega_l (\lambda_1^s \lambda_1^{s'l} + \lambda_2^s \lambda_2^{s'l}) + \\ 2 \sum_{ll'} \gamma_{ll'} (\lambda_1^s - \lambda_2^s)(\lambda_1^{s'l'} - \lambda_2^{s'l'}) = 0 \quad (s \neq s') \tag{22}$$

$$\sum_l \hbar\omega_l(\lambda_1^{s'l}\lambda_2^{sl} + \lambda_1^{sl}\lambda_2^{s'l}) -$$

$$-2\sum_{ll'} \gamma_{ll'}(\lambda_1^{sl} - \lambda_2^{sl})(\lambda_1^{s'l'} - \lambda_2^{s'l'}) = 0 \quad (23)$$

$$\hbar\hat{\omega}_s = \sum_l \hbar\omega_l(\lambda_1^{sl} + \lambda_2^{sl})^2, \quad (24)$$

$$\hat{g}_s = \sum_l g_l(\lambda_1^{sl} + \lambda_2^{sl}), \quad (25)$$

$$k = \sum_l \frac{1}{2}(\hbar\hat{\omega}_l - \hbar\omega_l). \quad (26)$$

Equation (22) and (23) together with Egs. (18) and (19) constitute a system of $2M^2$ independent equations for the $2M^2$ unknown coefficients λ_1^{sl}, λ_2^{sl}. Solution of this system yields the change in normal coordinates in terms of the coupling constants $\gamma_{ss'}$. Equations (24)-(26) determine the vibrational frequencies $\hat{\omega}_s$ of tion, the new coupling parameters $\hat{g}_s$ and the constant k.

The nexy unitary operator $U = \prod_{l=1}^{M} \exp[f_l(c_l - c_l^t)]$ diagonalizes $\tilde{H}_0$ if is chosen: $f_l = \hat{g}_l / \hbar\hat{\omega}$

$$U\tilde{H}_0U^t = \sum_s \hbar\hat{\omega}_s c_s^t c_s + \Delta^o \quad (28)$$

with $\Delta^o = k - \sum_s \hat{g}_s^2 / \hbar\hat{\omega}_s$. Then the equation (14) can be rewritten as follows [13]:

$$N_k^0(\epsilon) = \frac{1}{2\pi\hbar}\int dt \exp[i\hbar^{-1}(\epsilon - \epsilon_k \pm \Delta\epsilon_k)t]$$
$$\langle 0|\, U^t \exp\left(\pm i\sum_s \hat{\omega}_s c_s^t c_s t\right) U|\, 0\rangle \quad (30)$$

or using the symbol $|\, \hat{n}\rangle$ for states belonging to operators c_s, i.e., $c_s^t c_s|\, \hat{n}\rangle = n_s|\, \hat{n}\rangle$, the density of states takes the form

$$N_k^0(^o) = \sum_{n_1\cdots n_M} |\, \langle \hat{n}\, |U\, |0\rangle\, |^2 \delta(^o - {}^o{}_k \pm \Delta^o{}_k \pm n\cdot\hbar\hat{\omega}) \quad (31)$$

Further naturally the δ function in Eg. (31) contains the information about the adiabatic ionization potential and the spacing of the vibrational peaks, whereas the squared matrix element $|\, \langle \hat{n}\, |U\, |0\rangle\, |^2$ is the well-known Franck-Condon factor, which gives the intensity distribution of the vibrational spectrum. Following to ref. [65] one can decompose the matrix element $\langle \hat{n}\, |U\, |0\rangle$ as

$$\langle \hat{n}\, |U\, |0\rangle = \sum_{m_1\cdots m_M} \langle \hat{n}|\, U|\, \hat{m}\rangle\langle \hat{m}|\, 0\rangle. \quad (32)$$

where $\langle \hat{m}|\, 0\rangle$ is the overlap of unshifted wave functions of different frequency and $\langle \hat{n}|\, U|\, \hat{m}\rangle$ is the overlap integral between shifted oscillator wave functions of the same frequency, which is calculated:

$$\langle \hat{n}|\, U|\, \hat{m}\rangle = \prod_{l=1}^{M} e^{-(1/2)f_l^2}\left(\frac{m_l!}{n_l!}\right)^{1/2}(-f_l)^{n_l-m_l} L_{m_l}^{n_l-m_l}(f_l^2) \quad (33)$$

Here L_m^k is the generalized Laguerre polynominal and $f_l = \hat{g}_l / \hbar\hat{\omega}_l$. A procedure for calculating the overlap integrals $\langle \hat{m}|\, 0\rangle$ wis described in ref. [65]. In order to reveal explicitly the connection between the quantities $f_l, \lambda_1^{sl}, \lambda_2^{sl}$ and the geometry shifts and frequency changes it is written as

$$\breve{\hat{Q}} = JQ + \hat{K}', \quad (35)$$

where the vector Q denotes the normal coordinates in the ground state of the reference molecule and $\hat{Q}$ denotes the normal coordinates of the ion, both on the one-particle level. If L and $\hat{\mathrm{L}}$ are the transformation matrices from internal to normal coordinates in the initial and final states, respectively, R is the change in equilibrium position

and Γ, Ã are the diagonal matrices of frequencies $\omega_s/\hbar$, $\hat{\omega}_s/\hbar$, then

$$\mathrm{J} = \hat{\Gamma}^{1/2}\hat{\mathrm{L}}^{\dagger}\,\mathrm{L}\Gamma^{-1/2},$$
$$\hat{\mathrm{K}} = \hat{\Gamma}^{1/2}\hat{\mathrm{L}}^{\dagger}\,\mathrm{R}. \qquad (36)$$

The connection between transformation matrix J, λ's is given by $\lambda_1^{\dagger} + \lambda_2^{\dagger} = J_{\dagger}$, $\lambda_1^{\dagger} - \lambda_2^{\dagger} = J_{\dagger}^{-1}$; normal coordinate shift $\hat{\mathrm{K}}$ is related to f_l by $f_l = \mp 2^{-1/2}\hat{K}_l$. The simplification of method is possible in case of diagonality of matrix $\gamma_{ss'}$ of coupling constants.

2.2 The Cederbaum-Domske approach to the many-body problem

Below we give the Cederbaum-Domske perturbation theory approach to *ab initio* calculation of frequencies, geometry shifts, and Franck-Condon factors starting from the one-particle picture discussed above. In a diagrammatic method in order to obtain the function $N_k(\omega)$ one should calculate the Green's function $G_{kk'}(\omega)$ first:

$$G_{kk'}(\epsilon) = -i\hbar^{-1}\int_{-\infty}^{\infty} dt e^{i\hbar^{-1}\epsilon t}\,\langle\psi_0|\; T\{\; a_k(t)a_{k'}^{\dagger}(0)\;\}\;|\psi_0\rangle \qquad (41)$$

where T is Wick's time ordering operator and the function $N_k(\omega)$ then follows from relation

$$\pi N_k(\epsilon) = a\,\mathrm{Im}\,G_{kk}(\epsilon - ai\eta), \qquad (42)$$

$a = -sign\,\omega_k$, where η is a positive infinitesimal. Choosing the unperturbed Hamiltonian H_0 to be

$$H_0 = \sum \omega_i a_i^{\dagger} a_i + H_N \qquad (43)$$

one finds for the corresponding Green's functions

$$G_{kk'}^0(\epsilon) = \delta_{kk'}/(\epsilon - \epsilon_k - ai\eta) \qquad (44)$$

The Dyson equation

$$G_{kk'} = G_{kk'}^0 + \sum_{k''} G_{kk}^0 \Sigma_{kk''} G_{k''k'} \qquad (45)$$

relates the Green's functions to the free ones introducing a new function $\Sigma_{kk''}(\omega)$ called the (proper) self-energy part. In in order to calculate $\Sigma_{kk'}$, a well-known diagrammatic method is used. It is useful to remind that the sum of Feynman diagrams leading to the self-energy part is shown in Fig. 1. All notations are standard.

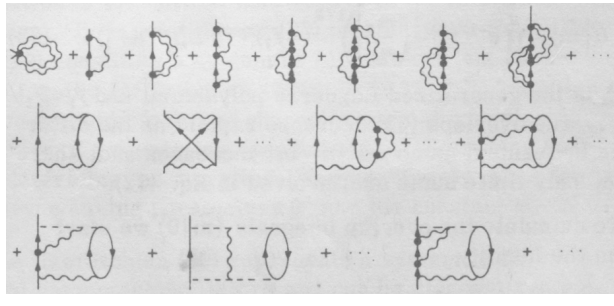

Fig. 1. The sum of diagrams contributing to the self-energy part.

The one-body problem treated above results in the exact solution of the Dyson equation with the self-energy part given by the infinite number of diagrams shown in the first row of Fig. 1 and the corresponding Green's function is as follows [65]:

$$G_{kk'}^{OB}(t) = \pm\delta_{kk'} i\exp\left[-in^{-1}(\varepsilon_k \mp \Delta\varepsilon)t\right] \times \sum_n \left|\langle \hat{n}_k|U_k|0\rangle\right|^2 \exp\left(\pm in_k\cdot\hat{\omega}_k t\right) \qquad (47)$$

The corresponding Dyson-like equation is as follows:

$$G_{kk'}(\epsilon) = G_{kk'}^{OB}(\epsilon) + \sum_{kk'} G_{kk}^{OB}(\epsilon)\hat{O}_{kk''}G_{k''k'}(\epsilon) \qquad (48)$$

where $\hat{O}_{kk'}$, is equal to $\Sigma_{kk'}$, less the diagrams of the first row in Fig.1. The perturbation expansion of Φ is shown in Fig. 2 where $G_{kk'}^{\Phi}$, is symbolized by a double solid line.

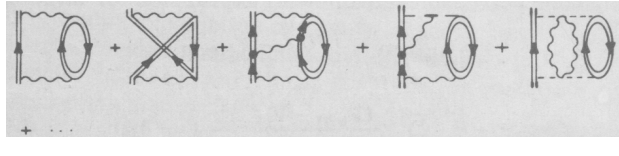

Fig. 2. Perturbation expansion of $\Phi_{kk'}$.

The expression for the sum of the first two diagrams appearing in Fig. 2 are written by a standard way:

$$\Phi_{kk'}(\in)=\sum_{\substack{i,j\in F\\ l\notin F}}\sum_{n_i,n_j,n_l}\frac{(V_{klij}-V_{klij})V_{k'lij}U_{n_i i}U_{n_j j}U_{n_l l}}{\in+E_l-E_i-E_j}+$$

$$+\sum_{\substack{i,j\in F\\ l\notin F}}\sum_{n_i,n_j,n_l}\frac{(V_{klij}-V_{klij})V_{k'lij}U_{n_i i}U_{n_j j}U_{n_l l}}{\in+E_l-E_i-E_j}$$

$$U_{n_i i=}\left|\left\langle\hat{n}_i\middle|U_i\middle|0\right\rangle\right|^2 \text{ and } E_i=\in_i\mp\Delta\in_i\mp h\hat{n}_i\cdot\hat{\omega}_i \tag{49}$$

The direct method for calculation of $N_k(\in)$ as the imaginary part of the corresponding Green's function implicitly includes the determination of the V. I. P. s of the reference molecule and then of $N_k(\in)$. The zeros of the functions

$$D_k(\in)=\in-\left[\in^{op}+\Sigma(\in)\right]_k, \tag{50}$$

where $\left(\in^{op}+\Sigma\right)_k$ denotes the kth eigenvalue of the diagonal matrix of the one-particle energies added to the matrix of the self-energy part, are the negative V. I. P. 's for a given geometry. Further it is easily to write:

$$(V.I.P.)_k=-(\in_k+F_k),$$

$$F_k=\Sigma_{\boldsymbol{k}}\left(-(V.I.P.)_k\right)\approx\frac{1}{1-\partial\Sigma_{\boldsymbol{k}}(\in_k)/\partial_\in}\Sigma_{\boldsymbol{k}}(\in_k). \tag{51}$$

Expanding the ionic energy E_k^{N-1} about the equilibrium geometry of the reference molecule in a power series of the normal coordinates of this molecule:

$$E_k^{N-1}=E_k^{N-1}(0)-\sum_{s=1}^{M}\left(\frac{\partial(\in_k+F_k)}{\partial Q_s}\right)_0 Q_s-$$

$$-\frac{1}{2!}\sum_{s,s'=1}^{M}\left(\frac{\partial^2(\in_k+F_k-E_0^N)}{\partial Q_s\partial Q_{s'}}\right)_0 Q_sQ_{s'} \tag{52}$$

leads to a set of linear equations in the unknown normal coordinate shifts δQ_S,

$$-\left(\frac{\partial(\in_k+F_k)}{\partial Q_s}\right)_0=\sum_{s'\neq s}\left(\frac{\partial^2(\in_k+F_k)}{\partial Q_s\partial Q_{s'}}\right)_0\delta Q_{s'},$$

$$+\left[\left(\frac{\partial^2(\in_k+F_k)}{\partial Q_3^2}\right)_0-h\omega_s\right]\delta Q_s, s=1...M, \tag{53}$$

where ω_s are frequencies of the reference molecule. The new coupling constants are then:

$$g_1=\pm\left(1/\sqrt{2}\right)\left[\partial(\in_k+F_k)/\partial Q_l\right]_0 \tag{54}$$

$$\gamma_{ll'}=\pm\left(\frac{1}{4}\right)\left[\partial^2(\in_k+F_k)/\partial Q_l/\partial Q_{l'}\right]_0$$

Further it can be shown [65-67] that the coupling constants g_l and $y_{ll'}$ are calculated by the well-known perturbation expansion of the self-energy part using the Hamiltonian H_{EN} of Eq. (6). In second order one obtains:

$$\sum\nolimits_{lk}^{(2)}(\in)=\sum_{\substack{i,j\\ s\notin F}}\frac{(V_{ksij}-V_{ksji})V_{ksij}}{\in+\in_s-\in_i-\in_j}+\sum_{\substack{i,j\\ s\notin F}}\frac{(V_{ksij}-V_{ksji})V_{ksij}}{\in+\in_s-\in_i-\in_j} \tag{58}$$

and the coupling constant g_l, can be written as

$$g_l\approx\pm\frac{1}{\sqrt{2}}\frac{\partial\in_k}{\partial Q_l}\frac{1+q_k(\partial/\partial\in)\sum_{\boldsymbol{k}}\left[-(V.I.P.)_k\right]}{1-(\partial/\partial\in)\sum_{\boldsymbol{k}}\left[-(V.I.P.)_k\right]}, \tag{59}$$

where

$$q_k=\frac{\sum\frac{(V_{ksij}-V_{ksji})^2}{\left[-(V.I.P.)_k+\in_s-\in_i-\in_j\right]^2}\left[\frac{\partial\in_s}{\partial Q_l}-\frac{\partial\in_i}{\partial Q_l}-\frac{\partial\in_j}{\partial Q_l}\right]}{\frac{\partial\in_k}{\partial Q_l}\sum\frac{(V_{ksij}-V_{ksji})^2}{\left[-(V.I.P.)_k+\in_s-\in_i-\in_j\right]^2}} \tag{60}$$

It is suitable to use further the pole strength of the corresponding Green's function

$$\rho_k=\left\{1-\frac{\partial}{\partial\in}\sum_{\boldsymbol{k}}\left[-(V.I.P)_k\right]\right\}^{-1};1\geq\rho_k\geq0, \tag{61}$$

$$g_l\approx g_l^0\left[\rho_k+q_k(\rho_k-1)\right],\quad g_l^0=\pm2^{-1/2}\partial\in_k/\partial Q_l \tag{62}$$

Below we firstly give the DFT definition of the pole strength corresponding to V. I. P.'s and confirm earlier data [65]: $p_k\approx0,8$-0,95. The closeness of p_k to 1 in fact means that a role of the multibody correlation effects is small ($g_l\approx g_l^0$).

The above presented results can be usefully treated in the terms of the correlation and reor-

ganization effects. Usually it is introduced the following expression for an I.P.:

$$(I.P.)_k = -\epsilon_k - \sum_{j\notin F, i\in F} \frac{(V_{kikj} - V_{kijk})}{\epsilon_j - \epsilon_i} - \frac{1}{2}\sum_{\substack{i\in F \\ j,l\notin F}} \frac{(V_{kijl} - V_{kilj})}{\epsilon_k + \epsilon_i - \epsilon_j - \epsilon_l}(1-\delta_{kl}) - \frac{1}{2}\sum_{\substack{p,q\in F \\ j\notin F}} \frac{(V_{kjpq} - V_{kjqp})^2}{\epsilon_k + \epsilon_i - \epsilon_p - \epsilon_q}(1-\delta_{jp})(1-\delta_{iq}) \quad (64)$$

The first correction term is due to reorganization, the remaining correction terms are due to correlation effects. Then the coupling constant g_l, can be written as

$$g_l \approx g_l^0\left\{1 + \sum_{j\notin F}\frac{(V_{kkkj})^2}{(\epsilon_j - \epsilon_k)^2} - \frac{1}{2}\left[\sum_{\substack{i\in F \\ j,l\notin F}} \frac{(V_{kijl} - V_{kilj})^2}{(\epsilon_k + \epsilon_i - \epsilon_j - \epsilon_l)^2}(1-\delta_{kl}) + \sum_{\substack{p,q\in F \\ j,\notin F}} \frac{(V_{kjpq} - V_{kjqp})^2}{(\epsilon_k + \epsilon_i - \epsilon_p - \epsilon_q)^2}(1-\delta_{jp})(1-\delta_{iq})\right]\right\} \quad (65)$$

The second coupling constant can be written

$$\gamma_{ll} = \gamma_l^0\left(\frac{g_l}{g_l^0}\right) + \frac{1}{4}\sqrt{2}g_l^0\frac{\partial}{\partial Q_l}\left(\frac{g_l}{g_l^0}\right) \quad (66)$$

γ_{ll}^0, is defined analogously g_l^0.

3. Quasiparticle Fermi-liquid DFT

In this chapter we present the quasiparticle Fermi-liquid version of the DFT theory, starting from the problem of searching for the optimal one-electron representation and following to refs. [60-68,111]. Two decades ago Davidson had pointed the principal disadvantages of the traditional representation based on the self-consistent field approach and suggested the optimal "natural orbitals" representation [22,23]. Nevertheless there remain insurmountable calculational difficulties in the realization of the Davidson program. One of the simplified recipes represents, for example, the Kohn-Sham DFT theory [40-42]. In ref. [111] the QED DFT version, based on the formally exact QED perturbation theory (PT), has been developed and a new approach to construction of the optimized one-quasiparticle representation has been proposed. In fact this approach is based on the energy approach, which is well known in the theory of radiative and non-radiative decay of the quasi-stationary states for multielectron systems. The energy approach uses the adiabatic Gell-Mann and Low formula [59] for the energy shift dE with electrodynamic scattering matrices. In a modern theory of molecules there is a number of tasks, where an accurate account for the complex exchange-correlation effects, including the continuum pressure, energy dependence of a mass operator etc., is critically important. It includes also the calculation of the vibration structure for the molecular systems. In this case it can be very useful the quasiparticle DFT [60]. In order to get the master equations and construct an optimal basis of the one-particle wave functions φ_λ one could use the Green's function method. Let us define the one-particle Hamiltonian for functions φ_λ so that the Greens' function pole part in the (φ_λ) representation is diagonal on λ. Starting equation is the Dyson equation for multi-electron (for example atom or molecule):

$$(\varepsilon - p^2/2 + \sum Z_\alpha / r_\alpha)\cdot G(x,x',\varepsilon) - \int \Sigma(x,x'',\varepsilon)\cdot G(x'',x',\varepsilon)dx'' = \delta(x-x') \quad (67)$$

where $x = (r,s)$ are the spatial and spin variables, Σ is the mass operator; Z , as usually, a charge of a nucleus (nuclei) «α», G is the Green's function. In the representation of auxiliary functions φ_λ' the equation (67) has the following form:

$$(\varepsilon - \varepsilon_{\lambda_1})G_{\lambda_1\lambda'} - \sum_{\lambda_1}[\frac{p^2}{2} - \sum\frac{Z_\alpha}{r_\alpha} + \sum(x,x',\varepsilon)]_{\lambda\lambda_1}G_{\lambda_1\lambda'} = \delta_{\lambda\lambda'} \quad (68)$$

where λ_1 is an index of summation. It is natural to choose φ_λ so that the following expression will be diagonal:

$$[p^2/2 - \sum_\alpha Z_\alpha / r_\alpha + \sum(x,x',\varepsilon)]_{\lambda\lambda_1} = E_\lambda(\varepsilon)\cdot\delta_{\lambda\lambda_1} \quad (69)$$

$$G_{\lambda\lambda'} = G_\lambda\cdot\delta_{\lambda\lambda'}, G_\lambda = 1/[\varepsilon - E_\lambda(\varepsilon)] \quad (70)$$

and the functions $\varphi_\lambda^{/}$, which diagonalizes G , satisfy to equation as follows: :

$$(p^2/2-\sum_\alpha Z_\alpha/r_\alpha)\varphi_\lambda^{/}(x,\varepsilon)+ \\ +\int\sum(x,x^{/},\varepsilon)\varphi_\lambda^{/}(x_1,\varepsilon)dx_1-E_\lambda(\varepsilon)\varphi_\lambda^{/}(x,\varepsilon) \quad (71)$$

One could introduce the mixed representation for a mass operator as follows:

$$\sum(x,p,\varepsilon)=\int\sum(x,x_1,\varepsilon)\exp[i(r-r_1)p]dr_1 \quad (72)$$

Then equation (71) with account for of the expression (72) can be written as follows:

$$[p^2/2-\sum_\alpha Z_\alpha/r_\alpha+\sum(x,p,\varepsilon)]\varphi_\lambda^{/}(x,\varepsilon)= \\ =E_\lambda(\varepsilon)\varphi_\lambda^{/}(x,\varepsilon) \quad (73)$$

It can be shown that an operator $p=i\nabla$ in (67) acts on functions which are on the right of $\sum(x,p,\varepsilon)$. So, in order to find the one-particle energies, defined by the pole part of the Green's function G, it is sufficient to know the functions $\varphi_\lambda^{/}$ under $\varepsilon=\varepsilon_\lambda$. The Greens' function pole part is as follows:

$$G_{\lambda\lambda^{/}}=a^\lambda\delta_{\lambda\lambda^{/}}/(\varepsilon-\varepsilon_\lambda+i\gamma_\lambda) \quad (74)$$

where

$$a^\lambda=1/(1-\partial E_\lambda/\delta\varepsilon)|_{\varepsilon=\varepsilon_\lambda},(\partial E/\partial\varepsilon)|_{\varepsilon=\varepsilon_\lambda}=(\partial E/\partial\varepsilon)|_{\lambda\lambda^{/}}$$

$$\varepsilon_\lambda=E_\lambda(\varepsilon)=\{p^2/2-\sum_\alpha Z_\alpha/r_\alpha+\sum(x,p,\varepsilon)\}|_{\lambda\lambda} \quad (75)$$

The functions $\varphi_\lambda^{/}(x)=\varphi_\lambda^{/}(x,\varepsilon_\lambda)$ are satisfying to following equation:

$$[p^2/2-\sum_\alpha Z_\alpha/r_\alpha+\sum(x,p,\varepsilon_\lambda)]\varphi_\lambda=\varepsilon_\lambda\varphi_\lambda(x) \quad (76)$$

Introducing an expansion for self-energy part $\sum$ into set on degrees $x,\varepsilon-\varepsilon_F,p^2-p_F^2$ (here ε_F and p_F are the Fermi energy and pulse correspondingly):

$$\sum(x,p,\varepsilon)=\sum{}_0(x)+(\partial\sum/\partial p^2)(p^2-p_F^2)+ \\ +(\partial\sum/\partial\varepsilon)(\varepsilon-\varepsilon_F)+...$$

then equation (76) is rewritten as follows:

$$[p^2/2-\sum_\alpha Z_\alpha/r_\alpha+\sum{}_0(x)+p(\partial\sum/\partial p^2)p]\Phi_\lambda(x)= \\ =(1-\partial\sum/\partial\varepsilon)\varepsilon_\lambda\Phi_\lambda(x) \quad (77)$$

The functions Φ_λ in (77) are orthogonal with a weight $r_k^{-1}=a^{-1}=[1-\partial\sum/\partial\varepsilon]$. Now one can introduce the wave functions of the quasiparticles $\varphi_\lambda=a^{-1/2}\Phi_\lambda$, which are, as usually, orthogonal with weight 1. For complete definition of $\{\varphi_\lambda\}$ it should be determined the values $\sum{}_0,\partial\sum/\partial p^2,\partial\sum/\partial\varepsilon$. Naturally, the equations (77) can be obtained on the basis of the variational principle, if we start from a Lagrangian of a system L_q (density functional). It should be defined as a functional of the following quasiparticle densities:

$$\nu_0(r)=\sum_\lambda n_\lambda|\Phi_\lambda(r)|^2, \\ \nu_1(r)=\sum_\lambda n_\lambda|\nabla\Phi_\lambda(r)|^2, \\ \nu_2(r)=\sum_\lambda n_\lambda[\Phi_\lambda^*\Phi_\lambda-\Phi_\lambda^*\Phi_\lambda]. \quad (78)$$

The densities ν_0 and ν_1 are similar to the HF electron density ρ ($\rho=\nu\cdot a$) and kinetical energy density correspondingly; the density ν_2 has no an analog in the HFock or standard Kohn-Sham theory and appears as result of account for the energy dependence of the mass operator $\sum$. Lagrangian L_q can be written as sum of a free Lagrangian and Lagrangian of interaction:

$$L_q=L_q^0+L_q^{\text{int}},$$

where a free Lagrangian L_q^0 has a standard form:

$$L_q^0 = \int dr \sum_\lambda n_\lambda \Phi_\lambda^* (i\partial / \partial t - \varepsilon_p)\Phi_\lambda, \quad (79)$$

And an interaction Lagrangian is defined in the form, which is characteristic for a standard (Kohn-Sham) density functional theory (as a sum of the Coulomb and exchange-correlation terms), however, it takes into account for the energy dependence of a mass operator $\sum$:

$$L_q^{\text{int}} = L_K - \frac{1}{2}\sum_{i,k=0}^{2} \int \beta_{ik} F(r_1, r_2)\nu_i(r_1)\nu_k(r_2)dr_1 dr_2 \quad (80)$$

where β_{ik} are some constants (look below), F is an effective potential of the exchange-correlation interaction. Let us explain here the essence of the introduced constants. Indeed, in some degree they have the same essence as similar constants in well-known Landau Fermi liquid theory and Migdal finite Fermi-systems theory. The Coulomb interaction part L_K looks as follows:

$$L_K = -\frac{1}{2}\int [1 - \sum\nolimits_2(r_1)]\nu_0(r_1)[1 - \\ - \sum\nolimits_2(r_2)]\nu_0(r_2) / |r_1 - r_2| dr_1 dr_2 \quad (81)$$

where $\sum_2 = \partial \sum / \partial \varepsilon$. Regarding the exchange-correlation potential *F*, it should be noted the there are many possible approximations (directly in the DFT and its modern generalizations). Earlier in our atomic and molecular theories we use the following form:

$$F(r_1, r_2) = X(\int dr \rho_c^{(0)1/3}(r) / |r - r_1||r - r_2| - \\ - (\int dr' \rho_c^{(0)1/3}(r') / |r_1 - r'| \cdot \\ \cdot \int dr'' \rho_c^{(0)1/3}(r'') / |r'' - r_2|) / < \rho_c^{(0)1/3} > \\ < \rho_c^{(0)1/3} > = \int dr \rho_c^{(0)1/3}(r) \quad (82)$$

where X is the numerical coefficient. It has been obtained in the refs. [74-76] on the basis of calculating the Rayleigh-Schrödinger perturbation theory Feynman diagrams of the second and higher order (so called polarization diagrams) in the Thomas-Fermi approximation. The corresponding relativistic generalization of the potential (82) looks as follows [76]:

$$F_{pol}^d(r_1 r_2) = X(\int dr' \rho_c^{(0)1/3}(r')\theta(r') / |r_1 - r'||r' - r_2| - \\ - (\int dr' \rho_c^{(0)1/3}(r')\theta(r') / |r_1 - r'| \int dr'' \rho_c^{(0)1/3}(r'')\theta(r'') / \\ / |r'' - r_2|) / < \rho_c^{(0)1/3} >); \\ < \rho_c^{(0)1/3} > = \int dr \rho_c^{(0)1/3}(r)\theta(r) \quad (83)$$

where , c is the light velocity.

Another alternative expression has been introduced by Victor- Laughlin-Taylor (c.f. refs. [24,25]):

$$F(\vec{r_1}, \vec{r_2}) = \frac{1}{r_{12}} - \frac{\alpha_d}{r_1^2 r_2^2} p_1(\cos\theta_{12}) w_3(r_2 / r_0) w_3(r_2 / r_0) - \\ - \frac{\alpha_d'}{r_1^3 r_2^3} p_2(\cos\theta_{12}) w_4(r_1 / r_0) w_4(r_2 / r_0) \quad (84)$$

where p_1 are the Legander polynomials, $\cos\theta_{12} = \vec{r_1}\vec{r_2}(r_1 r_2)$. In the local density approximation in the density functional the potential *F* can be expressed through the exchange-correlation pseudo-potential V_{XC} as follows [41,42]:

$$F(r_1, r_2) = \delta V_{XC} / \delta \nu_0 \cdot \delta(r_1 - r_2). \quad (85)$$

Further, one can get the following expressions for $\sum_i = -\delta L_q^{\text{int}} / \delta \nu_i$:

$$\sum\nolimits_0 = (1 - \sum\nolimits_e) V_K + \sum\nolimits_0^{ex} + \\ + \frac{1}{2}\beta_{00}\delta^2 V_{XC} / \delta \nu^2 \cdot \nu_0^2 + \beta_{00}\delta V_{XC} / \delta \nu_0 \cdot \nu_0 + \\ + \beta_{01}\delta V_{XC} / \delta \nu_0 \cdot \nu_1 + \beta_{01}\delta^2 V_{XC} / \delta \nu_0^2 \cdot \nu_0 \nu_1 + \\ + \beta_{02}\delta^2 V_{XC} / \delta \nu_0^2 \cdot \nu_0 \nu_2 + \beta_{02}\delta V_{XC} / \delta \nu_0 \cdot \nu_2 \\ \sum\nolimits_1 = \beta_{01}\delta V_{XC} / \delta \nu_0 \cdot \nu_0 + \beta_{12}\delta V_{XC} / \delta \nu_0 \cdot \nu_2 + \\ + \beta_{11}\delta V_{XC} / \delta \nu_0 \cdot \nu_1; \\ \sum\nolimits_2 = \beta_{02}\delta V_{XC} / \delta \nu_0 \cdot \nu_0 + \beta_{12}\delta V_{XC} / \delta \nu_0 \cdot \nu_1 + \\ + \beta_{22}\delta V_{XC} / \delta \nu_0 \cdot \nu_2; \quad (86)$$

Here V_K is the Coulomb term (look above), $\sum_0^{ex}$ is the exchange term. Using the known canonical relationship:

$$H_q = \Phi_\lambda^* \delta L_q / \delta \Phi_\lambda^* + \Phi_\lambda \delta L_q / \delta \Phi_\lambda - L_q$$

after some transformations one can receive the expression for the quasiparticle Hamiltonian, which is corresponding to a Lagrangian L_q:

$$H_q = H_q^0 + H_q^{\text{int}} = H_q^0 - L_K + \\ + \frac{1}{2}\beta_{00}\delta V_{XC}/\delta\nu_0 \cdot \nu_0^2 + \\ + \beta_{01}\delta V_{XC}/\delta\nu_0 \cdot \nu_0 \cdot \nu_1 + \frac{1}{2}\beta_{11}\delta V_{XC}/\delta\nu_0 \cdot \nu_1^2 - \\ - \frac{1}{2}\beta_{22}\delta V_{XC}/\delta\nu_0 \cdot \nu_2^2 \tag{87}$$

Further let us give the corresponding comments regarding the constants b_{ik}. First of all, it is obvious that the terms with constants $\beta_{01}, \beta_{11}, \beta_{12}, \beta_{22}$ give omitted contribution to the energy functional (at least in the zeroth approximation in comparison with others), so they can be equal to zero. The value for a constant β_{00} in some degree is dependent upon the definition of the potential V_{xc}. If as V_{xc} it is use one of the correct exchange-correlation potentials from the standard density functional theory, then without losing a community of statement, the constant β_{00} can be equal to 1. The constant β_{02} can be in principle calculated by analytical way, but it is very useful to remember its connection with a spectroscopic factor F_{sp} of atomic or molecular system (it is usually defined from the ionization cross-sections) [60]:

$$F_{sp} = \left\{1 - \frac{\partial}{\partial \in}\sum\nolimits_{kk}\left[-(V.I.P.)_k\right]\right\} \tag{88}$$

The term $\partial\sum/\partial\varepsilon$ is defined above. It is easily to understand the this definition is in fact corresponding to the pole strength of the corresponding Green's function [62].

In further calculation as potential V_{XC} we use the exchange-correlation pseudo-potential which contains the correlation (Gunnarsson-Lundqvist) potential and relativistic exchanger Kohn-Sham one [40-42]:

$$V_{XC}(r) = f(\theta)V_X(r) - 0{,}0333 \cdot \ln[1 + 18{,}376 \cdot \rho^{1/3}(r)] \tag{89}$$

where $V_X = -(1/\pi)[3\pi^2 \cdot \rho(r)]^{1/3}$

is the Kohn-Sham exchange potential, $\theta = [3\pi^2\rho]^{1/3}/c$, and function $f(\theta)$ is as follows:

$$f(\theta) = 3\ln[\theta + (\theta^2+1)^{1/2}]/[2\theta(\theta^2+1)^{1/2}] - 1/2 \tag{90}$$

Using the above written formula, one can simply define values (61), (88). As example in table 1 we present our calculational data for spectroscopic factors of some atoms together with available experimental data and results, obtained in the Hartree-Fock theory plus random phase approximation.

Further, let us give a short comment regarding an universality of the constants b_{ik}. From the point of view of the analogous universality of the constants in the well-known Landau Fermi-liquid theory and Migdal finite Fermi-systems theory [62]. Indeed, as we know now, the entire universality of the constants in the last theories is absent, though a range of its changing is quite little. Without a detailed explanation, we note here that the corresponding constants in our theory possess the same universality as ones in the Landau Fermi-liquid theory and Migdal finite Fermi-systems theory. More detailed explanation requires a careful check. Further it is obvious that omitting the energy dependence of the mass operator (i.e. supposing $\beta_{01} = 0$) the quasiparticle density functional theory can be resulted in the standard Kohn-Sham theory.

Note: F^*_{exp} - experimental value of spectroscopic factor; $\widetilde{F}_{RPA}$ is the value, obtained in the random phase approximation with exchange.

In this essence the presented approach to definition of the functions basis $\{\Phi_\lambda\}$ of a Hamiltonian H_q can be treated as an improved in comparison

Table 1

Spectroscopic factors of the external ns^2 shells of some atoms and ions

Atom, ion	Терм	N	F_{sp}	$F^*_{\exp}$ $\widetilde{F}_{RPA}$
Ar	1_S	3	0,60	0,56 0,70
TI (IV)	1_S	3	0,50	0,34 0,60
Xe	1_S	5	0,36	
TI	2_P	6	0,36	
Pb^+	2_P	6	0,33	
Pb	3_P	6	0,34	
Pb	1_D	6	0,34	
Pb	1_S	6	0,34	
Bi^+	3_P	6	0,32	
Bi	4_S	6	0,33	
Bi	2_D	6	0,33	
Bi	2_P	6	0,33	
Po^+	4_S	6	0,31	
Po	3_P	6	0,31	
Po	1_D	6	0,31	
Po	S 1	6	0,31	
As^+	3_P	6	0,30	
As	2_P	6	0,30	
As^-	1_S	6	0,31	
Rn^+	2_P	6	0,29	
Rn	1_S	6	0,29	
Fr^+	1_S	6	0,28	
Fr	2_S	6	0,28	
Ra	1_S	7	0,43	
Ac	2_D	7	0,41	
Ac	2_F	7	0,42	
Th	3_H	7	0,41	
Th	3_F	7	0,42	
Pa	4_I	7	0,42	
U	5_L	7	0,42	

with similar basises of other 1-particle representations (HF, Hatree-Fock-Slater, Kohn-Sham etc.). Naturally, this advancement can be manifested during studying those properties of the multi-electron systems, when accurate account for complex exchange-correlation effects, including continuum pressure, energy dependence of mass operator etc., is critically important.

4. The application of the combined Green's function method and quasiparticle DFT approach to diatomics

We choose the diatomic molecules of N_2, CO (and some others) for application of the combined Green's function method and quasiparticle DFT approach. In ref. [65] it has been shown that the diatomics spectra can be in principle reproduced by applying a one-particle theory with account of the correlation and reorganization effects. The corresponding coupling constants depend on the balance of these effects. The nitrogen molecule has been naturally discussed in many papers. The valence V. I. P. 's of N_2 have been calculated [61,62,65] by the method of Green's functions and therefore the pole strengths p_k are known and the mean values q_k *can* be estimated.

In should be reminded that the N_2 molecule is the classical example where the known Koopmans' theorem even fails in reproducing the sequence of the V. I. P. 's in the PE spectrum. From the calculation of Cade *et al.*[71,72] one finds that including reorganization the V. I. P. 's assigned by σ_g and σ_u improve while for the π V. I. P. the good agreement between the Koopmans value and the experimental one is lost, leading to the same sequence as given by Koopmans' theorem. The above-mentioned Green's functions calculation which takes account of reorganization and correlation effects leads to the experimental sequence of V. I. P.'s. In Table 2 the experimental V. I. P. 's (a), the one-particle HF energies (b), the V. I. P. 's calculated by Koopmans' theorem plus the contribution of reorganization (c), the V. I. P. 's calculated with Green's functions method (d), the combined Green's functions and DFT approach (e) and corresponding pole strengths (d,e) are listed.

Table 2

The experimental and calculated V. I. P.'s (in eV) of N_2. R_k is the contribution of reorganization; p_k stands for pole strength.

Orbital	Exp VIP a	$-\epsilon_k^b$	$-(\epsilon_k+R_k)^c$	Calc[d] V.I.P.s	ρ_k^d	Calc[e] V.I.P.s	ρ_k^e
3 σ_g	15,6	17,4	16,0	15,5	0,9	15,5	0,9
1 π_u	16,9	17,1	15,7	16,8	0,9	16,8	0,9
2 σ_u	18,8	20,9	19,9	18,6	0,9	18,6	0,8

Therefore, the results, obtained within the Green functions approach and combined method are very much close. Taking into account a simplification of the calculational procedure within the DFT approach, the generalized Cederbaum et al theory looks more attractive else. As it's known, of the three bands in the experimental low-energy spectrum of N_2 molecule (Fig. 3), only the $1\pi_u$ band exhibits a strong vibrational structure.

When a change of frequency due to ionization is small, the density of states can be well approximated using only one parameter *g:*

$$N_k(\epsilon)=\sum_{n=0}^{\infty} e^{-s}\frac{S^n}{n!}\delta(\epsilon-\epsilon_k+\Delta\epsilon_k+n\cdot\hbar\hat{\omega}),$$
$$S=g^2(\hbar\omega)^{-2} \qquad (70)$$

In case the frequencies change considerably, the intensity distribution of the most intensive lines can analogously be well approximated by an effective parameter *S.* In fig.3 the experimental and calculated photoelectron spectra for the N_2.molecule are presented. The uppermost spectrum is calculated with S^0 (i.e. the constant S calculated with g^0) and Eq. (70) [13]. The middle spectrum is calculated with values of S from Eq. (62).

It is important to note that the original Green's functions and combined Green functions +DFT approach coincide in the scale of the figure. In a whole the agreement between the calculated spectrum (corrected *g*) and the experimental one is improved. As another example, the molecule CO can be considered.

The experimental and calculated photoelectron spectra for CO molecule are listed in Fig.4. One can see quite physically reasonable agreement between experiment and theory. The original Green's functions [13] and combined Green's functions +DFT approach practically coincide. On inclusion of the anharmonicites it should be mentioned that a theory can be generalized by means a standard normal coordinate expansion of Hamiltonian to third and higher orders and correspondingly the theory of the density of states functions N_k developed above can easily be generalized too.

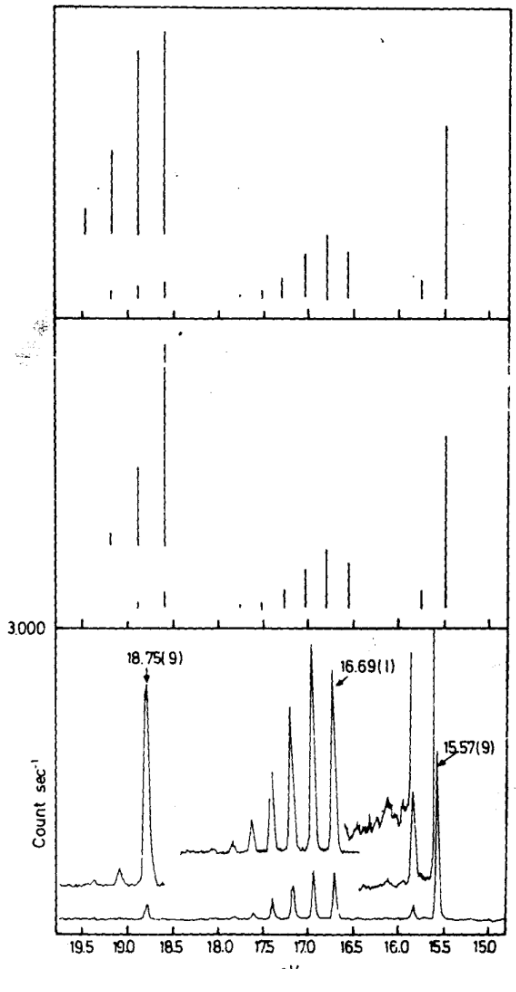

Figure 3. Experimental [65]and calculated PE spectra N_2; Uppermost spectrum is calculated with S^0 and Eq. (70). The middle spectrum is calculated with S values from (62) (see text).

5. Summary

We present a new combined theoretical approach to vibrational structure in photo-electron spectra of molecules, which is based on the Green's function method and DFT.

In fact approach presented generalizes the standard Green's function approach [65-68]. The density of states, which describe the vibrational structure in molecular photoelectron spectra, is calculated with the help of combined DFT-Green's-functions approach. It is important that the calculational procedure is significantly simplified with using the quasiparticle DFT formalism.

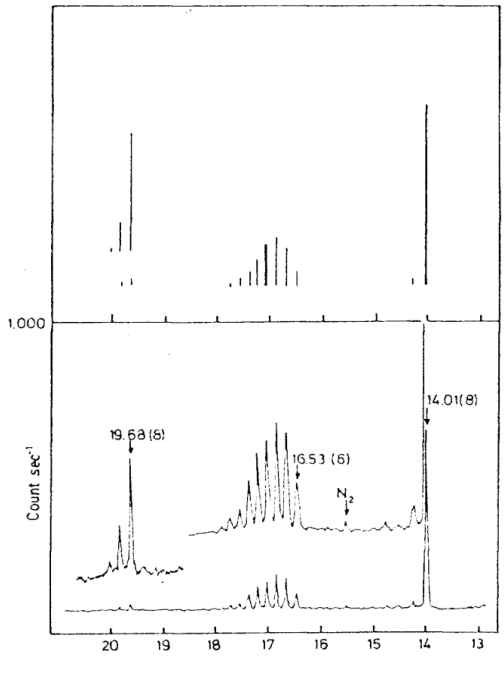

Figure 4. The experimental [65] and calculated photoelectron spectra of CO. The upper spectrum is calculated with S^0 and Eq. (70) (see text).

References

1. W. Domcke, D. R. Yarkony, H. Köppel (Eds.), Conical Intersections: Electronic Structure, Dynamics and Spectroscopy (World Scientific, Singapore, 2004).
2. H. Köppel, W. Domcke, L. S. Cederbaum, Adv. Chem. Phys. **57**, 59-132 (1984).
3. S. Wilson, Ed., in Handbook on Molecular Physics and Quantum Chem. (Wiley, 2003)
4. T.Rescigno, C.McCurdy, D.Haxton, C. Trevisan, A.Orel, J. Phys.:CS. 88, 012027 (2007)
5. S.Wilson, in Recent Advances in Theor. Phys.and Chem. Systems, ed. by J. Maruani et al, Progr.in Theor. Chem. and Phys., vol 16, (2007) p. 11
6. The Fundamentals of Electron Density, Density Matrix and Density Functional Theory in Atoms, Molecules and the Solid State, Eds. Gidopoulos N.I. and Wilson S.-Amsterdam: Springer, 2004.-Vol.14, 244P.
7. A. Glushkov, Atomic systems in an electromagnetic field,Kiev, KNT (2005), 400p.
8. T. Venkatesan, S. Mahapatra, H. Köppel L. Cederbaum, J. Mol. Struct. **838**, 100 (2007)
9. E.Gindensperger, H. Köppel, L. Cederbaum, J. Chem. Phys., **126**, 034106 (2007).
10. I.P. Grant, in Relativistic Quantum Theory of Atoms and Molecules Theory and Computation, Springer Series on Atomic, Opt., Plasma Physics, vol 40, (2007) p. 587-626
11. I.P. Grant, H.M. Quiney, Int. J. Quant. Chem. 80, 283–297 (2000)
12. K.L. Bell, K.A. Berrington, D.S.F. Crothers, A. Hibbert, K.T. Taylor, Bertha: 4-Component Relativistic Molecular Quantum Mechanics, in Supercomputing, Collision Proc. and Application, Ser.: Phys. of Atoms and Molecules, Springer, (2002) p. 213–224
13. M. Reiher, B. Hess, in Modern Methods and Algorithms of Quantum Chemistry, ed. by J. Grotendorst, John von Neumann Institute for Computing, Julich, NIC Series, vol 3, (2000) p. 479–505
14. H.M. Quiney, in Relativistic Quantum Mechanics of Atoms and Molecules. New Trends in Quantum Systems in Chemistry and Physics, Series: Progress in Theoretical Chemistry and Physics, vol 6,(2002) p. 135–173
15. A. Glushkov, Relativistic and Correlation Effects in Spectra of Atomic Systems, Nauka, Moscow-Odessa (2006), 700p.
16. S. Wilson, Journ. of Mol. Str.: Theochem. 547, 279–291 (2001)

17. J.R.Sabin J.R., Adv.Quantum Chem.27, 107-124 (1997).
18. G.A.Aucar, J.Oddershede, J.R.Sabin, Phys. Rev.A. 52, 1054-1065 (1995).
19. G.H.F.Diercksen, J.Oddershede, I.Paidarova, J.R.Sabin, Int.Journ.Quant. Chem. 39, 755-766 (1991).
20. R.Cabrera-Trujillo, J.R.Sabin, Y.Ohrn, E.Deumens, Phys. Rev. A. 71, 012901 (2005).
21. I.Theophilou, S.Thanos, and A. K. Theophilou, J.Chem.Phys. 127, 234103 (2007).
22. E.R. Davidson, Rev. Mod. Phys. 44, 451-460 (1972).
23. E.R. Davidson, D. Feller, J. Chem. Phys. 74, 3977-3988 (1981).
24. A.Hibbert, Adv. in Atom. and Molec. Phys. 18, 309-340 (1982).
25. C.Laughlin, G.A.Victor, Adv. in Atom. Molec. Phys. 25, 163-194 (1988).
26. R.J.Bartlett, M.N.Musiał, Rev. Mod. Phys. 79, 291-328 (2007).
27. R.J.Bartlett, R. J., S. A. Kucharski, and J. Noga, 1989, Chem. Phys. Lett. 155, 133.
28. A.Viel, W.Eisfeld, S. Neumann, W. Domkke, U.Manthe, J. Chem. Phys. **124**, 214306 (2006)
29. S. Faraji, H. Köppel, W. Eisfeld, and S. Mahapatra, Chem. Phys. **347**, 110-120 (2008).
30. Köppel, M. Döscher, I. Bâldea, H.Meyer, P.Szalay, J. Chem. Phys. 117, 2657-2682 (2002).
31. O.Christiansen, H. Koch, P. Jörgensen, and J. Olsen, Chem. Phys. Lett. 256, 185-189 (1996).
32. J.Cížek, Adv. Chem. Phys. 14, 35-82 (1969).
33. F.Coester, H. Kümmel, Nucl. Phys. 17, 477-488 (1990).
34. H. J. Wörner and F. Merkt, J. Chem. Phys. **126**, 144305 and 154304 (2007)
35. T.D.Crawford, H. F. Schaefer, III, in Reviews of Computational Chemistry, eds. K. B. Lipkowitz and D.B. Boyd, Wiley, New York, 14, 33–136 (2000).
36. A. Dalgarno, A. L. Stewart, 958, Proc. R. Soc. London, Ser. A 247, 245-264 (1958).
37. E.R. Davidson, A. A. Jarzecki, Chem. Phys. Lett. 285, 155-160 (1998).
38. 38. T.H.Dunning, Jr., J. Chem. Phys. 90, 1007-1020 (1989)..
39. T.H.Dunning, V. McKoy, J. Chem. Phys. 47, 1735-1744 (1997).
40. P. Hohenberg, W.Kohn, Phys. Rev. B 136, 864-882 (1964).
41. W. Kohn, L.J. Sham, Phys. Rev. A 140, 1133-1146 (1995).
42. E.G.Gross, W. Kohn, Exchange-correlation functionals in density functional theory.-N-Y: Plenum, 2005.-380P.
43. G. Onida, L. Reining, and A. Rubio, Rev. Mod. Phys. 74, 601-670 (2002).
44. M. S. Hybertsen, S. G. Louie, Phys. Rev. B 34, 5390-5402 (1986).
45. E. Runge, E. K. U. Gross, Phys. Rev. Lett. 52, 997-1002 (1984).
46. R. van Leeuwen, Phys. Rev. Lett. 82, 3863-3868 (1999).
47. K.Kowalski, D. J. Dean, M. Hjorth-Jensen, T. Papenbrock, and P. Piecuch, Phys. Rev. Lett. 92, 132501 (2004).
48. P.-O.Löwdin, 1999, Adv. Chem. Phys. 2, 207-262 (1999)..
49. P.-O. Löwdin, Int. J. Quantum Chem. 2, 867-876 (1998).
50. I.Lindgren, M. Morrison, Atomic Many-Body Theory, 2nd ed. _Springer, Berlin (1986).
51. I. Lindgren, S. Salomonsen, Int. J. Quantum Chem. 90, 294-302 (2002).
52. H. Nakatsuji, Chem. Phys. Lett. 59, 362-366 (1998).
53. J.Noga, R. J. Bartlett, M. Urban, Chem. Phys. Lett. 134, 126-130 (1987).
54. J.Noga, W. Kutzelnigg, J. Chem. Phys. 101, 7738-7748 (1994).
55. H.P. Kelly, Adv. Chem. Phys. 14, 129-180 (1969).
56. N.N. Bogoliubov, D. V. Shirkov, Introduction to the Theory of Quantized Fields _Wiley, New York (1959).
57. J. Goldstone, Proc. R. Soc. London, Ser. A 239, 267-286 (1997).
58. M. Gell-Mann, K. A. Brueckner, Phys. Rev. 106, 364-374 (1997).

59. M. Gell-Mann, F.Low, Phys. Rev. 84, 350-358 (1951).
60. T.E.Harris, H. J. Monkhorst, D. L. Freeman, Algebraic and Diagrammatic Methods in Many-Fermion Theory, Oxford University, New York (1992).
61. D. J. Thouless, Quantum Medianics of Many-Body Systems, Academic, New York (1961).
62. A.Abrikosov, L.Gorkov, E.Dzyaloshinskii, Quantum Field Theoretical Methods in Statistical Physics, Pergamon, Oxford (1995).
63. R. Mattuck, Feyman Diagrams in the Many-Body Problem, McGraw-Hill, London (1967).
64. D. W. Turner, C. Baker, A. D. Baker, and C. R. Brunrile, Molecular Photoelectran Spectroscopy, Wiley, New York (1990).
65. L.S. Cederbaum, W. Domcke, J.Chem. Phys. 60, 2878-2896 (1974).
66. L. S. Cederbaum, G. Hohlneicher, Chem. Phys. Lett. 18, 503-508 (1993).
67. L. S. Cederbaum, Theor. Chim. Acta 31, 239-248 (1993).
68. L S. Peverimhoff, W. von Niessen, L. S. Cederbaum, G. Hohlneicher, and W. von Niessen, Mol. Phys. 26, 1405-1418 (1993).
69. J. M. Doll and W. P. Reinhardt, J. Chem. Phys. 57, 1169-1182 (1992).
70. W.P. Reinhardt, J.B. Smith, J. Chem. Phys. 58, 2143-2154 (1973).
71. P. E. Cade, K. D. Sales, and A. C. Wahl, J. Chem. Phys. 44, 1973-1986 .
72. P. E. Cade, W. M. Huo, J. Chem. Phys. 47, 649-660 (1997).
73. L.N. Ivanov, E.P. Ivanova, E.V. Aglitsky, Phys. Rep. 164, 315-386 (1988).
74. E.P. Ivanova, A.V. Glushkov, J. Quant. Spectr. Rad. Transfer 36, 127-145 (1986).
75. E.P. Ivanova, L.N. Ivanov, A.V. Glushkov and A.E. Kramida, Phys. Scr. 32, 513-524 (1995).
76. A.V.Glushkov, Russian Phys. Journal.34, 71-77 (1990).
77. I. Theophilou, S. Thanos, A. Theophilou, J. Chem. Phys. 127, 234103 (2007)
78. A.V. Glushkov, L.N. Ivanov, J. Phys. B: At.Mol.Opt.Phys. 24, L379–386 (1993)
79. A. Glushkov, JETP Lett. 55, 95–98 (1992)
80. A.Glushkov, Optics and Spectr. 66, 31-36 (1989).
81. A. Glushkov, Russian J. Struct. Chem. 31, 9-15 (1990).
82. A. Glushkov, Russian J. Struct. Chem. 32, 11-16 (1992).
83. A. Glushkov, Russian J. Struct. Chem. 34 3-10 (1993).
84. A.Glushkov, Russian Journ. Struct. Chem. 34, 11-20 (1993).
85. A.V. Glushkov, Rus. J. Phys. Chem. 66, 589-596 (1992).
86. A.V. Glushkov, Rus. J. Phys. Chem. 66, 1259-1276 (1992).
87. A.V. Glushkov, Relativistic quantum theory. Quantum mechanics of atomic systems, Odessa, Astroprint (2008).
88. A.V. Glushkov, S. Ambrosov, V. Ignatenko, D. Korchevsky, Int. J. Quant. Chem. 99, 936–939 (2004)
89. A.V. Glushkov, S.V. Ambrosov, A.V. Loboda, Yu.G. Chernyakova, O.Yu. Khetselius, A.V. Svinarenko,Nucl. Phys. A 734, 21–28 (2004)
90. A.V. Glushkov, S.V. Ambrosov, A.V. Loboda, E.P. Gurnitskaya, O.Yu. Khetselius, in Recent Advances in Theoretical Physics and Chemistry Systems, ed. by J.-P. Julien et al, , Ser: Progr. in Theoretical Chem. and Phys. (Springer), vol 15,(2006) 285–300
91. A.V. Glushkov, S.V. Malinovskaya, Yu.V. Dubrovskaya, L.A. Vitavetskaya, in Recent Advances in Theoretical Physics and Chemistry Systems, ed. by J.-P. Julien, J. Maruani, D. Mayou, S. Wilson, G. Delgado-Barrio, series: Progress in Theoretical Chemistry and Physics (Springer), vol 15, (2006) p. 301–308
92. A.V. Glushkov, S.V. Ambrosov, A.V. Loboda, E.P. Gurnitskaya, G.P. Prepelitsa, Int. J. Quant. Chem. 104, 562–569 (2005)
93. A.V. Glushkov, S.V. Malinovskaya, in New Projects and New Lines of Research in Nuclear Physics, ed. by G. Fazio, F. Hanappe (World Scient., Singapore, 2003) p. 242–264
94. A.V. Glushkov, S.V. Malinovskaya, Yu.G.

Chernyakova, A.A. Svinarenko, Int. J. Quant. Chem. 99, 889–896 (2004)
95. A.V. Glushkov, S.V. Malinovskaya, A.V. Loboda, E.P. Gurnitskaya, D.A. Korchevsky, J. Phys. CS 11, 188–198 (2004)
96. A.Glushkov, S. Ambrosov, V. Ignatenko, D. Korchevsky, Int. J. Quant. Chem. 99, 936–940 (2004)
97. A. Glushkov, S.V. Malinovskaya, G. Prepelitsa, V. Ignatenko, J. Phys. CS 11, 199–208 (2004)
98. A.V.Glushkov, in Low Energy Antiproton Physics. Eds. Grzonka D., Czyzykiewicz R., Oelert Walter, Rozek T., Winter P., AIP, 796, 206-210 (1995).
99. A.Glushkov, O.Khetselius, A. Loboda, A.A.Svinarenko, in Frontiers in Quantum Systems in Chemistry and Physics, Eds. Wilson S., Grout P.J., Maruani J. et al series: Progress in Theoretical Chemistry and Physics (Springer), vol 18, (2008) 541-558.
100. A.Glushkov, O.Yu.Khetselius, A.Loboda, T.Florko, D.Sukharev,.L. Lovett, in Frontiers in Quantum Systems in Chemistry and Physics, Eds. Wilson S., Grout P.J., Maruani J. et al series: Progress in Theor. Chem. and Phys. (Springer), vol 18, (2008) 505-522.
101. A.V. Glushkov, O.Yu. Khetselius and S.V. Malinovskaya, in Frontiers in Quantum Systems in Chemistry and Physics, Eds. Wilson S., Grout P.J., Maruani J. et al series: Progress in Theoretical Chemistry and Physics (Springer), vol 18, (2008) 523-540.
102. A.V. Glushkov, O.Yu. Khetselius and S.V. Malinovskaya, Europ.Phys.Journ.ST. 160, 195-204 (2008).
103. A.V. Glushkov, O.Yu. Khetselius and S.V. Malinovskaya,, Mol. Phys.(UK). 106, 1257-1260 (2008).
104. V.Gedasimov, A.Zelenkov, V.Kulakov, V.Pchelin, M.V.Sokolovskaya, A.Soldatov, L.Chistyakov, JETP-Sov.Phys. 94, 1169-1178 (1984); A.Soldatov, Preprint of I.V.Kurchatov Institute for Atomic Energy, Moscow, IAE-3916 (1983).
105. V.S.Letokhov,Laser Spectroscopy, N.-Y.: Acad.(1977); Phys. Lett.A 46, 257-260 (1994)
106. V.S.Letokhov, V.G.Minogin, JETP-Sov. Phys. 69, 1568-1578 (1995).
107. A.V.Glushkov, L.N.Ivanov, E.P.Ivanova, Autoionization Phenomena in Atoms, Moscow: Moscow Univ. Press (1986).
108. V.I.Goldansky, V.S.Letokhov, JETP-Sov. Phys. 67, 513-516 (1994).
109. L.N.Ivanov, V.S.Letokhov, JETP-Sov. Phys. 68, 748-758 (1995).
110. G.G.Baldwin, J.C.Salem, V.I.Goldansky, Rev.Mod.Phys. 53, 687-742 (1991).
111. A.V. Glushkov, L.N. Ivanov, Phys. Lett. A 170, 33–38 (1992)

This article has been received within 2014

UDC 539.186

A. V. Glushkov

THE GREEN'S FUNCTIONS AND DENSITY FUNCTIONAL APPROACH TO VIBRATIONAL STRUCTURE IN THE PHOTOELECTRON SPECTRA OF MOLECULES: REVIEW OF METHOD

Abstract. We present the basis's of the new combined theoretical approach to vibrational structure in photoelectron spectra of molecules. The approach is based on the Green's function method, which generalizes the Cederbaum-Domske formalism, and quasiparticle density functional theory. It generalizes the known Green's function approach by It is presented a new procedure for determination of the density of states, which describe the vibrational structure in molecular photoelectron spectra.

Key words: density functional theory, Green's function method, photoelectron spectra

УДК 539.186

А. В. Глушков

МЕТОД ФУНКЦИЙ ГРИНА И ТЕОРИЯ ФУНКЦИОНАЛА ПЛОТНОСТИ ДЛЯ ОПРЕДЕЛЕНИЯ КОЛЕБАТЕЛЬНОЙ СТРУКТУРЫ В ФОТОЭЛЕКТРОННЫХ СПЕКТРОВ МОЛЕКУЛ: ОБЗОР МЕТОДА

Резюме

Изложены основы нового комбинированного теоретического подхода к определению колебательной структуры в фотоэлектронных спектрах молекул. Подход основан на квазичастичном методе функций Грина, обобщающем формализм Цедербаума-Домске, и квазичастичной теории функционала плотности. Приведена процедура вычисления плотности состояний, описывающей колебательную структуру в молекулярных фотоэлектронных спектрах.

Ключевые слова: теория функционала плотности, метод функций Грина, фотоэлектронные спектры.

УДК 539.182

О. В. Глушков

МЕТОД ФУНКЦІЙ ГРІНА І ТЕОРІЯ ФУНКЦІОНАЛА ГУСТИНИ ДЛЯ ВИЗНАЧЕННЯ КОЛИВАЛЬНОЇ СТРУКТУРИ У ФОТОЕЛЕКТРОННИХ СПЕКТРАХ МОЛЕКУЛ: ОГЛЯД МЕТОДУ

Резюме

Викладені основи нового комбінованого теоретичного підходу до визначення коливальної структури в фотоелектронних спектрах молекул. Підхід заснований на квазічастинковом методі функцій Гріна, що узагальнює формалізм Цедербаума-Домске, і квазічастинковій теорії функціонала густини. Наведена процедура обчислення густини станів, яка описує коливальну структуру в молекулярних фотоелектронних спектрах.

Ключові слова: теорія функціонала густини, метод функцій Гріна, фотоелектронні спектри

UDC 539.186

T. N. Sakun

National Aviation University, 1, Komarov Ave, 03680 Kiev, Ukraine
E-mail: nucsukh@mail.ru

PHOTOCONDUCTIVITY OF POLIMERIC LAYERS WITH DIAZONY SALTS

It has been performed the experimental and theoretical (with using the quantum-chemical calculation methods: methods MNDO/d and AM1) studying the photoelectric properties of the polymeric layers with diazony salts (SD). In particular, it is studied the hole photoconductivity in the matrix, the photocurrent kinetics for different concentrations of the studied diazony salts in the polymer matrix, other photoelectric properties.

1. Introduction

To present time there are carried out numerous experimental and theoretical works data showing that the excitation relaxation processes in polymeric materials with different complex salts do not prevent leakage of important science and practice processes in the highly excited states such as generation of carriers, photochemical and radiation-chemical processes. For example, studying a photoconductivity of the polyacene linear crystals (anthracene, tetracene, pentatsen) [2] showed that its high quantum efficiency is observed only under irradiation of the highly excited molecules when there is possible a birth of holes and free electrons. During the process of relaxation from the highly excited state a molecule can stay at an intermediate state corresponding to electron transfer between the molecule and the crystal. Let us remind that the processes of charge separation in the non-equilibrium relaxation of highly excited state are theoretically considered already in the works by Onsager [3].

We have earlier found that light-sensitive components are able to provide the reaction phototransfer electron of these components in the matrix and vice versa. Only diazonium salts (SD) (photosensitive components of diazonium type materials) provide only one-way process - from the matrix to the diazonium cation [2-6].

The second reason for the use of diazonium salts is the fact that they have CN^- bond, which is characteristic of type Xe-O. As result, the SD has a high photochemical activity. This type of bond is present in the excited molecules of resazurin (NO- bond), on which it was found photochemical activityin the rezazuryne.

In this paper we present the results of experimental and theoretical studying the photoelectric properties of a system “polymer – SD”. As binding polymer we have taken the polyvinyl alcohol (PVA) (I), polyvinyl-pyrrolidone (PVP) (II), poliviniletylal (PVE) (III) and polyvinyl acetate (PVA) (IV). Diazo-components were choosen as the tetrafluoroboraties of the para-dietylamino-fenildiazonium (DEAFD) and para-metoksy-fenildiazonium (MFD). Device for measuring photovoltaic properties of polymer layers described in Refs. [2-4]. It is worth mentioning that in the manufacture of plastic layers from solution on a horizontal quartz surface they are heterogeneous in thickness: about denser layers of the substrate and on the free surface loosened. Therefore, we can find only the average parameters describing photoconductivity of polymer layers.

2. Quantum-chemical studying

For the theoretical description of the experimental data we used methods of formal kinetics of photoprocesses in layers and known quantum-chemical methods of research (the method of mo-

lecular dynamics MM +, based on the method MM2 [2] and semi-empirical methods such as MNDO/d and AM1 [6-15].

For elucidation of the mechanism of electron transfer in the system matrix, we performed the MD calculations of energy in such a system without electron transfer, with transfer from the matrix to SD and vice versa, calculations of the energy structure of the SD in the undissociated and dissociated states, an electron phototransfer excitation spectrum.

Besides, we studied the opportunities of the electron dark transfer electrons in the system "matrix – photoproducts", formed by dissociation diazonium cation. The calculation results are presented in Tables.1 and 2.

Table 1.

Ionization potential (IG) and energy affinity (EA) to electron matrix molecules and SD (in brackets - in the ground state).

Molecule	I_G eB	E_A eB
PVE	10,44	-3,03
PVP	8,72	-3,54
PVA	10,93	-0,61
PVS	10,67	-2,59
MFD·BF_4	10,48	3,15
DEAFD·BF_4	9,30	2,88
MFD	12,97	6,65 (10,61)
DEAFD	12,04	6,26 (9,52)

In table 2 we list the data on the energy required for charge transfer. These data do not take into account the Coulomb interaction between the charges after the charge transfer process. After the charge transfer, the geometric structure of the system turns non-optimized. Optimization significantly reduces the energy system. It should be emphasized that this reduction exceeds the energy of the Coulomb interaction between the charges after charge transfer. Thus, the geometric optimization of molecular system influences on the distance of the holes and an appearance of photocurrent (photovoltage). As a result, we will see hole photoconductivity in the matrix. The positions of the wavelength absorption band in the MFD - 3.96 eV, and DEAFD - 3.26 eV.

According to Table .. V.2 in PvE is generation at E> 4,19 eV (MFA) and E> 4,43 eV (DEAFD). Similarly, in PVA - 4.35 and 4.60 eV, in PVP - 3.96 and 4.20 eV.

Table 2.

The energy required for electron transfer (T) from the matrix (M) on SD and from the SD on the matrix.

T on SD	T on M	Condition	E_{opt}	Content
7,30	13,51	nopt		PVE + MFD·BF_4
4,19	10,85	opt	3,11	
7,55	12,32	nopt		PVE + DEAFD ·BF_4
4,43	9,81	opt	3,12	
5,73	13,99	nopt		PVP + MFD ·BF_4
3,97	10,22	opt	1,76	
5,32	12,84	nopt		PVP + DEAFD ·BF_4
4,24	9,22	opt	1,77	
7,78	11,09	nopt		PVA + MFD ·BF_4
4,35	9,95	opt	3,44	
8,04	9,91	nopt		PVA + DEAFD ·BF_4
4,60	8,92	opt	3,45	

Note: nopt – is corresponding to the electron transfer without changing the geometry of molecules (Kramers-Kronih process), opt - after optimizing the geometry.

Thus, the use of the MFD provide a photoconductivity in the PVP during excitation in the long-wavelength absorption band. In a case of the other polymers or using DEAFD it would be necessary excitation into higher states.

The SD photolysis leads to the formation of the aryl cation. It is important to know whether processes involving these cations may cause the phenomenon of photoconductivity. We calculated the energy balance for different transformations of the aryl cation. It turned out that the metoksyfenil cations in the dark conditions can capture an electron from the matrix, leading to hole conductivity.

At the same time the dietylaminofenil cations can not capture electrons (threshold value within 1,2 ÷ 1,6 eV).

Calculation has showed that both types of aryl cations can drag the hydrogen atom from the macromolecule. In addition, both aryl cations readily react with the anion, resulting in formation of two neutral molecules. Thus, this reaction does not give a contribution to photoconductivity. However, it appears that in the presence of water vapor it is possible formation of the phenols and acid in the presence of water vapor

$$(H_2O + H^+BF_4^- \rightarrow H_3O^+ + BF_4^-))$$

and it can give a contribution to the slow component of photoconductivity.

3. Experimental results and discussion

In Figure 1 we present the photocurrent kinetics for different concentrations of the studied SD in the PVA matrix during the excitation switching on and off. From the figure it is clear that the current increasing stops in over time *t*. So we can assume that all carriers have reached the opposite electrode and there is a dynamic equilibrium. In this case current increasing stops.

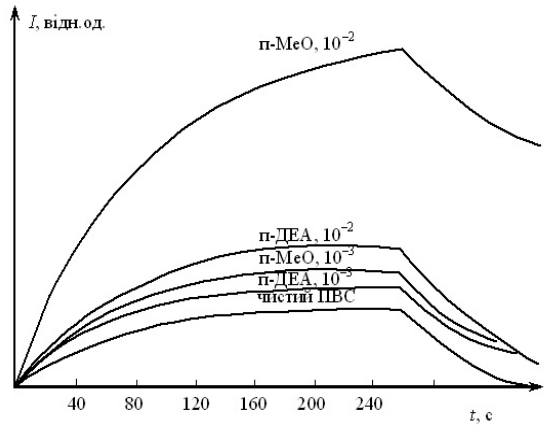

Figure 1. The photocurrent kinetics for different concentrations of the studied SD in the PVA matrix during the excitation switching on and off.

Using data on photoconductivity of polymer layers, we calculated the average values of the concentration of the charge carriers (generated by light) n upon the concentration of the molecules SD (Fig. 2). These values show that the introduction of SD into the PVA and PVP increases concentration of n, however introduction of the SD into the PVE reduces it. As for the PVA matrix, its reaction to the introduction of the MFD and DEAFD diametrically opposite. Really, the DEAFD increases value n and MDF decreases its value.

The defective or uncontrolled impurities can be by reson of the above said fact. In fact, they provide adequate electrical conductivity. When one adds the low concentrations of the SD it is possible removing the defects and consequently reducing the photocurrent.

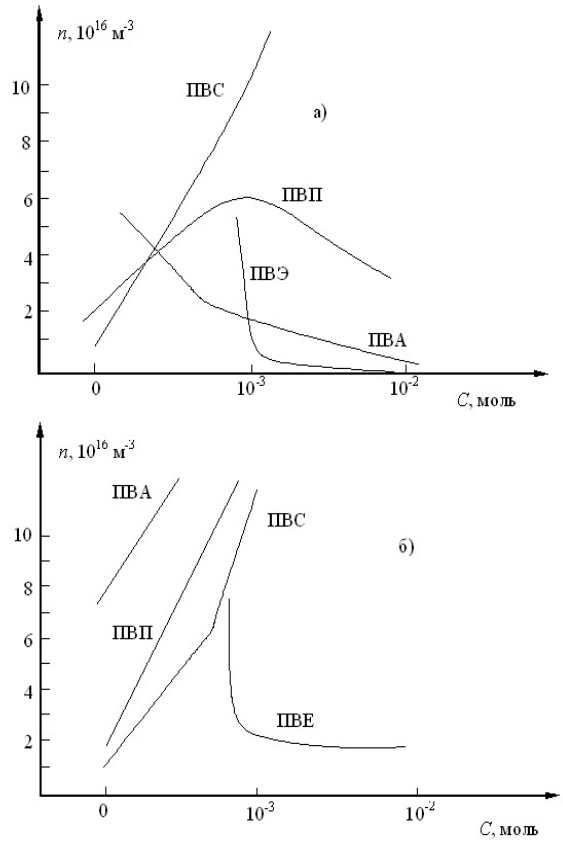

Figure 2. The dependence of the carrier concentration upon the concentration of SD in layers: a - MFD; b- DEAFD.

It is also understandable that the concentration of the photogenerated charge carriers for layers with MFD is more than for layers with DEAFD in all polymer matrices, with the exception of PVA. This picture is explainable when one compares the energy structure of SD (look Table 1) and polymer matrices used in the experiment.

From the data of the EPR spectroscopy at low temperatures (77 K) [5] and the results of photochemical studies at the room temperature [5,62] it is known that the quantum phototransfer yield of an electron on the MFD is more than on the DEAFD, i.e. its energy levels are lying lower than in DEAFD. Thus, the electron is much easier to go from the matrix on the MFD in comparison with the DEAFD. This conclusion is confirmed by the results of quantum-chemical calculations are presented in Table1.

Availability phototransfer electron in the system "SD-matrix" according to the reaction:

$$SD + M \xrightarrow{h\nu} SD^- + M^+$$

can be determined by evaluating the heat of reaction:

$$Q = I_M - E_A^{СД} - h\nu - E_C .$$

If this value is less than zero, the electron transfer reaction proceeds exothermically. Otherwise it is endothermic.

Since the SD is dissociated into ions in polymer matrix, then the SD affinity energy to electron is reduced by more than 3 eV. Substituting the data of Table 1 in the formula for calculating the value of Q, we find that DEAFD •BF_4^- in the lower excited state may take one electron from the PVP (Q = -0,1 eV).

For other matrices, this value is greater than 1 eV. Thus, electron transfer is possible only when excited into higher energy states or from impurities in the polymer matrix.

In the case of the MFD•BF_4 electron transfer is possible from all matrices on SD. The value of Q is -1.05 eV in PVP and does not exceed 0.3 eV in other matrices (heat and electric field are able to overcome such barriers) .Thus, the largest energy barrier exists between the lower free energy state of the excited cation DEAFD and top employed state of the PVS and PVA matrices. The value of the photocurrent in these cases should be minimal, that is observed experimentally. However, the integral absorption of MFD is less than DEAFD. This leads to the fact that value of the photocurrent in the PVA with the MFD is almost two times lower than with DEAFD.

Author would like to thank Professor P.A. Kondratenko for useful advises and discussion.

References

1. Kondratenko P.A., Photochemical action of light./ (Tutorial).- Kiev: Publishing center "Kyiv University".-2005.– 401P.
2. Turro N., Molecular Photochemistry.- M.:Mir, 1997-328P.
3. Kondratenko P.A., Lopatkin Yu.M, Sakun T.N., Relaxation Processes in Highly Excited Molecules of Resazurin // Physics and Chemistry of Solids -2007.-Vol.8,№1.-P.100-108
4. Kondratenko P.A.,.Lopatkin Yu.M, Sakun T.N., Spectroscopic properties of the resazurin in liquid and solid solutions// Physics and Chemistry of Solids.-2006.-Vol.7,N4. – P.695-700
5. Becker H.G.O., Hoffman G. Israel G. Ionische und radikalische Dediazonierungen von Aryldiazonium-salzen ein Beispiel für wellenlan-genab-hängige Photoreaktionen // J. Prakt. Chem. – 1997. – Vol.319, N6. – P.1021-1030.
6. Kondratenko NP, PA Kondratenko .. Sensitization sensitivity diazonium salts // Scientific Notes of the Dragomanov's NPU. Ser. Phys.-Math.- 2001. - C. 83-88.
7. Kondratenko P.A., Lopatkin Yu.M., Kondratenko N.P. // Molecules with a Xe-O type interfragmentary bond. Diazonium salts and azides. // Functional Materials. – 2002. –Vol.9, N4.- P.713-720
8. Siliņš EA. The electronic states of organic molecular crystals. – Riga: Zinatne.-1998.- 344p.
9. Onsager L., Initial recombination of ions // Physical Reviews. - 1998. - Vol.54. - P.554-557.
10. Kondratenko P.A., Lopatkin Yu.M., Single and double quantum processes in solid solutions of dyes//Physics and Chemistry of Solids.-2004.-Vol.5, № 3.-P.474-480.
11. Kondratenko P.A., Maksimyuk V.A., Tantsyura L.Y., Two-photon processes in the methylene blue in photo-thermoplastic environment//Chemical Physics.- 1993.- N7.-P.955-962.

12. Dewar M., Zoebisch E., Healy E., Stewart J., AM1: New general quantum mechanical molecular model// J.Amer. Chem. Soc.-1985.-Vol.107.-P.3902-3909
13. Dewar M.J.S., Thiel W., Ground states of molecules. 38. The MNDO method. Applications and parameters // J. Amer. Chem. Soc.-1997.-Vol.99,N15.-P.4899 - 4907.
14. Glushkov A.V., Kondratenko P.A., Lepikh Ya.I. , Fedchuk A.P., Svinarenko A.A., Lovett L., Electrodynamical and quantum - chemical approaches to modelling the electrochemical and catalytic processes on metals, metal alloys and semiconductors//Int. Journ. of Quantum Chem.-2009.-Vol.109,N14.-P.3473-3481.
15. Glushkov A.V., Fedchuk A.P., Kondratenko P.A., Lepikh Ya.I., Lopatkin Yu.M., Svinarenko A.A., The Green's functions and density functional approach to vibrational structure in the photoelectron spectra: Molecules of CH, HF// Photoelectronics.-2011.-Vol.20.-P.58-62.

This article has been received within 2014

UDC 539.186

T. N. Sakun

PHOTOCONDUCTIVITY OF POLIMERIC LAYERS WITH DIAZONY SALTS

Abstract

It has been performed the experimental and theoretical (with using the quantum-chemical calculation methods: methods MNDO/d and AM1) studying the photoelectric properties of the polymeric layers with diazony salts. In particular, it is studied the hole photoconductivity in the matrix, the photocurrent kinetics for different concentrations of the studied diazony salts in the polymer matrix, other photoelectric properties.

Key words: polymer layers with diazonium salts, photoelectric properties

УДК 539.186

Т. Н. С акун

ФОТОПРОВОДИМОСТЬ ПОЛИМЕРНЫХ СЛОЕВ С СОЛЯМИ ДИАЗОНИЯ

Резюме

Проведено экспериментальное и теоретическое (с помощью квантово-химических методов расчета типа методов MNDO/d, AM1) изучение фотоэлектрических свойств полимерных слоев с солями диазония. В частности, изучена дырочная фотопроводимость в матрице, кинетика фототока для различных концентраций рассмотренных солей диазония в полимерной матрице, другие фотоэлектрические свойства.

Ключевые слова: полимерные слои с солями диазония, фотоэлектрические свойства

УДК 539.186

Т. М. Сакун

ФОТОПРОВІДНІСТЬ ПОЛІМЕРНИХ ШАРІВ З СОЛЯМИ ДІАЗОНІЮ

Резюме

Проведене експериментальне і теоретичне (за допомогою квантово-хімічних методів розрахунку: типу методів MNDO/d , AM1) вивчення фотоелектричних властивостей полімерних шарів з солями діазонію. Зокрема, вивчена дирочна фотопроводимість в матриці, кінетика фотоструму для різних концентрацій розглянутих солей діазонію в полімерній матриці, інші фотоелектричні властивості.

Ключові слова: полімерних шарів з солями діазонію, фотоелектричні властивості

UDC 621.315.592

Yu. F. Vaksman, Yu. A. Nitsuk

I. I. Mechnikov Odessa National University
e-mail: nitsuk@onu.edu.ua

PHOTOLUMINESCENCE AND PHOTOCONDUCTIVITY OF ZnS:Ti SINGLE CRYSTALS

The photoconductivity and photoluminescence of ZnS:Ti crystals in the visible spectra region are studied. The scheme of optical transitions within Ti^{2+} impurity centers is established. It is shown that the high-temperature photoconductivity of ZnS:Ti crystals is controlled by optical transitions of electrons from the $^3A_2(F)$ ground state to the higher levels of excited states of Ti^{2+} ions, with subsequent thermal activation of the electrons to the conduction band. Efficient excitation of intracenter luminescence of ZnS:Ti crystals is attained with light corresponding to the region of intrinsic absorption in Ti^{2+} ions.

INTRODUCTION

The zinc sulphide single crystals, doped with transitional metals ions are promising materials for use as laser media. At present lasing in such crystals in the mid-infrared (IR) region is being extensively studied. On the basis of ZnS:Cr crystals, lasers tunable in the wavelength range of 2.35 mkm have already been fabricated [1]. in the spectral region were fabricated based on the ZnS:Cr crystals [1]. In [2] it was reported about creation of impulsive laser based on ZnS:Fe crystal with continuous tuning of the laser wavelength within the range of 3.49-4.65 mkm. At the same time, essentially nothing is known about possibility of infrared laser radiation realization using ZnS:Ti crystals.

The transition elements, among them titanium, are thought to form centers that suppress luminescence in the visible spectral region. For this reason, the number of studies concerned with the effect of titanium ions on the optical properties of ZnS in the visible region is rather limited. At the same time, the calculation of energy states of titanium impurity centers in ZnS [3] suggests that radiative transitions with the photon energy close to the band gap of the semiconductor can really occur. In this context, the study of optical properties of ZnS:Ti crystals in the visible spectral region presents a topical problem. In previous studies of optical absorption in the range 0.4–3.6 eV [4], we detected absorption bands defined by intracenter transitions in Ti^{2+} ions.

In this study, we analyze and identify the structure of the photoconductivity and photoluminescence (PL) spectra of ZnS:Ti crystals in the visible and IR spectral region. The photoconductivity and PL bands associated with transitions within titanium ions are observed.

The purpose of this study is to identify the photoconductivity and PL spectra in ZnS:Ti crystals.

EXPERIMENTAL

The samples to be studied were fabricated by diffusion doping of initially pure ZnS crystals with the Ti impurity. The undoped crystals were obtained by the technique of free growth on single-crystal ZnS substrate oriented in the (111) plane. The advantage of diffusion doping is that it is possible to vary the impurity concentration and profile. The procedure of doping and the studies of optical absorption in the crystals are described in detail elsewhere [4]. The titanium content in the crystals was determined from the change in the band gap as a function of the dopant concentration.

The photoconductivity spectra were recorded with the use of an MUM-2 monochromator. For the source of excitation light, we used a halogen lamp. The power of the light flux was kept constant by controlling the filament current of the lamp. For the photoconductivity measurements, ohmic indium contacts were deposited onto the crystals. The indium contacts were fired-in at the temperature 600 K. This was done with the use of a VUP-4 vacuum setup.

The PL spectra were recorded with the use of an ISP-51 prism spectrograph. The emission signal was detected with an FEU-100 photoelectric multiplier.

The PL signal was excited with light-emitting diodes (LEDs), Edison Opto Corp., the emission peaks of which corresponded to the wavelengths 400, 460, and 500 nm, and with an ILGI-503 nitrogen pulse laser emitting at the wavelength 337 nm.

ANALYSIS OF PHOTOCONDUCTIVITY SPECTRA

Figure 1 shows the photoconductivity spectra of the ZnS:Ti crystals with different Ti concentrations.

The photoconductivity spectrum of the undoped crystal is shown in Fig. 1 for comparison. The undoped crystals exhibit a single photoconductivity band with a peak at 3.64 eV at 300 K (Fig. 1, curve 1). This band is due to interband optical transitions. On doping of the crystals with titanium, the band shifts to lower energies. As the Ti concentration is increased, the shift increases and corresponds to the change in the band gap determined from the optical absorption spectra in [4].

Doping with titanium brings about the appearance of extra photoconductivity bands in the range of photon energies from 1.8 to 3.4 eV (Fig. 1, curves 2, 3). As the Ti concentration is increased, the intensity of these bands increases. We observe well defined bands at 2.0, 2.13, 2.38, 2.52, 2.74, 2.85, and 3.15 eV. The 3.15 eV photoconductivity band changes its position as the Ti concentration is changed. The positions of other bands do not vary with increasing degree of doping.

At the temperature T = 77 K, only one interband photoconductivity band is observed in all of the crystals under study (Fig. 2, curve 1). As the temperature is elevated from 77 to 350 K, the impurity photoconductivity makes a weightier contribution to the spectrum (Fig. 2). We observed a similar effect previously in studying the photoconductivity of ZnSe crystals doped with Fe and Ni [5,6].

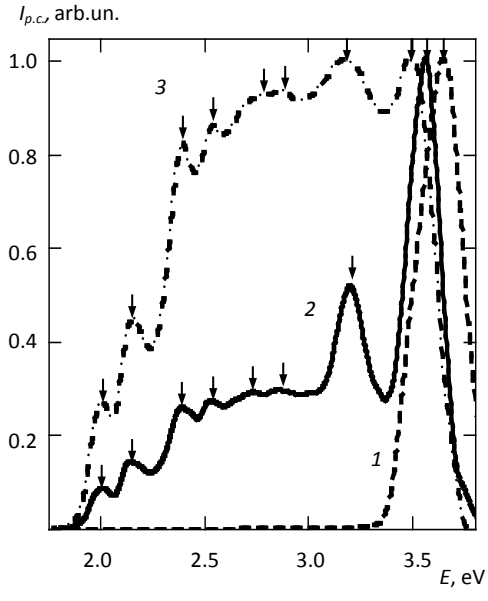

Fig. 1. Photoconductivity spectra of (1) ZnS and (2,3) ZnS:Ti crystals. The Ti dopant concentrations are [Ti] = (2) 2×10^{19} and (3) 5×10^{19} cm^{-3}.

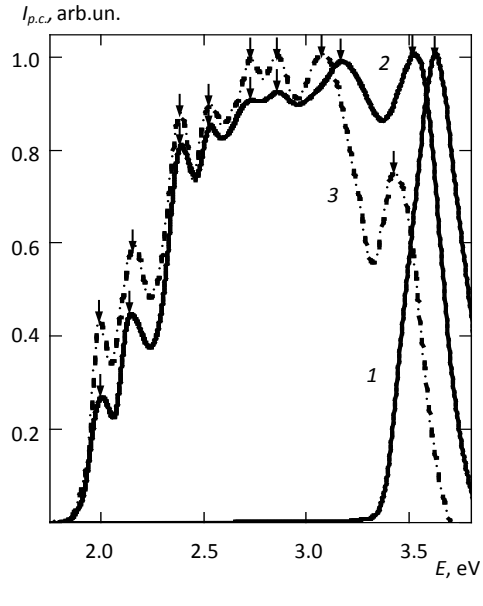

Fig. 2. Photoconductivity spectra of ZnS:Ti crystals at the temperatures (1) 77, (2) 300, and (3) 400 K. [Ti] = 5×10^{19} cm^{-3}.

Table

Energies of optical transitions in ZnS:Ti crystals

Line number	Absorption		Photoconductivity	Luminescence	Stokes shift
	E, eV[4]	transition	*E*, eV	*E*, eV	*E*, meV
1	3.15	$^3A_2(F)+h\nu \rightarrow {}^2E(D)+e^-_{c.b.}$	3.15	---	---
2	2.85	$^3A_2(F) \rightarrow {}^1T_2(G)$	2.87	---	---
3	2.75	$^3A_2(F) \rightarrow {}^1E(G)$	2.76	2.72	40
4	2.52	$^3A_2(F) \rightarrow {}^1T_1(G)$	2.55	2.50	50
5	2.37	$^3A_2(F) \rightarrow {}^1A_1(G)$	2.39	2.34	50
6	2.13	$^3A_2(F) \rightarrow {}^3T_1(P)$	2.10	2.07	30
7	2.0	$^3A_2(F) \rightarrow {}^1T_2(D)$	1.98	1.98	20
8	0.78	$^3A_2(F) \rightarrow {}^3T_1(F)$	---	0.72	60

As the temperature is elevated from 300 to 400 K (Fig. 2, curves 2, 3), the 3.15 eV photoconductivity band shifts to lower photon energies by 80 meV. Such a shift corresponds to the temperature change in the band gap of ZnS. Other impurity photoconductivity bands do not change their position with temperature, suggesting that the corresponding transitions are of intracenter character. In addition, the position of the above-mentioned bands agrees well with the position of optical absorption bands detected for these crystals previously. In [4] these absorption bands were attributed to intracenter optical transitions that occur within the Ti^{2+} ions. The above result suggests that these photoconductivity bands are due to the same optical transitions as those involved in optical absorption. The energies and identification of optical transitions are given in the table. The table summarizes the data obtained in studies of optical absorption [4], photoconductivity, and luminescence and in the calculations of energy states of the Ti^{2+} ions in ZnS [4].

The photoconductivity process in the crystals under study occurs in the manner briefly described below. The 3.15 eV photoconductivity band is associated with optical transitions from the $^3A_2(F)$ ground state of the Ti^{2+} ion into the conduction band. Comparison of the photon energy corresponding to the peak of this photoconductivity band with the energy position of the intrinsic photoconductivity peak for the crystals with the Ti concentration [Ti] = 5×10^{19} cm^{-3} (3.15 eV) allows us to believe that the level of the ground state of the Ti^{2+} ion is 360 meV above the top of the valence band.

The other photoconductivity bands are formed in a two-stage process. Initially, the intracenter optical transitions of electrons from the $^3A_2(F)$ ground state to the higher excited states of the Ti^{2+} ions (table) occur; then thermally activated transitions of these electrons to the conduction band are observed. As a result the local centers transit to the Ti^{3+} charged state. Later the Ti^{3+} centers trap electrons and the centers transit to their initial Ti^{2+} state.

It should be noted that the results of studies of the thermoelectric power are indicative of the electron photoconductivity of the ZnS:Ti crystals.

ANALYSIS OF LUMINESCENCE PROPERTIES OF ZnS:Ti CRYSTALS

The PL spectra were studied in the temperature range from 77 to 300 K. The PL spectra of undoped crystals do not exhibit emission bands in the visible and IR spectral region.

Doping of the crystals with titanium brings about a series of visible emission lines with peaks at 1.98, 2.06, 2.34, 2.50 and 2.72 eV (Fig. 3, curve 1). As the Ti concentration is increased, the intensity of these emission lines increases, whereas their position remains unchanged.

As the temperature is elevated from 77 to 300 K, the intensity of all emission lines decreases, while

the positions of the peaks remain unchanged (Fig. 3, curve 2). Similar temperature behavior was observed for the corresponding absorption lines. This suggests that the absorption and luminescence lines under study are due to intracenter optical transitions that occur within titanium ions.

Figure 3 (curve 3) shows the absorption spectrum of the ZnS:Ti crystals at T = 77 K. The spectrum involves lines that correlate with the emission lines observed in this study. As can be seen from the table, the Stokes shifts of the PL lines with respect to the corresponding absorption lines are in the range 20–60 meV. The inset in Fig. 3 shows the 0.72 eV IR-emission band.

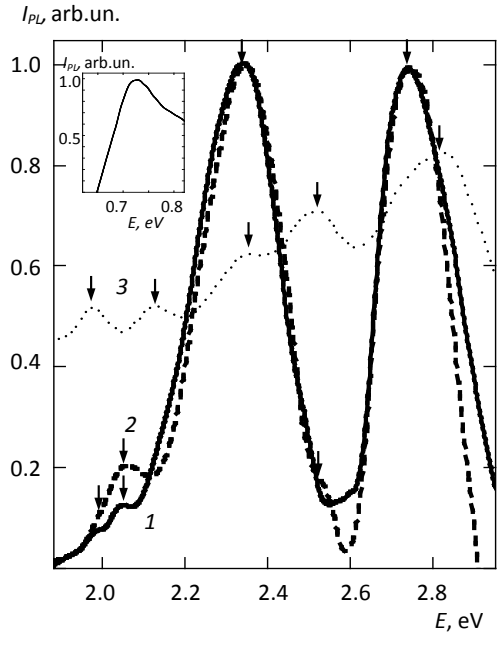

Fig. 3. (1, 2) Photoluminescence and (3) absorption spectra of ZnS:Ti crystals. Inset: IR-emission band.

It is established that the relative luminescence intensity of the ZnS:Ti crystals heavily depends on the photon energy of excitation light.

Emission with the lowest intensity is excited with a nitrogen laser with the photon energy 3.68 eV. The highest emission intensity is attained on excitation with LEDs with the photon energy in the emission peak 3.1 and 2.69 eV. This suggests that the band-to-band excitation of long-wavelength luminescence of the ZnS:Ti crystals is inefficient. At the same time, under changes in the excitation photon energy, the position of emission peaks remains unchanged. It is also established that, as the excitation photon energy is lowered, the contribution of low energy bands to the luminescence spectrum increases. This effect is typical of intracenter luminescence.

CONCLUSIONS

The study allows a number of conclusions. These are as follows:

1. It is shown that the high-temperature long-wavelength photoconductivity of the ZnS:Ti crystals is controlled by intracenter optical transitions within the Ti^{2+} ions and by subsequent thermally induced transitions of electrons from the levels of the excited Ti^{2+} states into the conduction band.

2. It is established that doping with iron gives rise to a series of emission lines in the visible spectral region. The luminescence bands detected for the ZnS:Ti crystals are attributed to intracenter transitions in the Ti^{2+} ions.

3. Efficient excitation in impurity related luminescence of the ZnS:Ti crystals is attained with light corresponding to the region of intrinsic absorption in the Ti^{2+} ions.

REFERENCES

1. Sorokina I.T., Sorokin E., Mirov S., et. al. Broadly tunable compact continuous-wave Cr^{2+}:ZnS laser //Optics letters – 2002. – V. 27, N.12. – P. 1040-1042.
2. Kozlovskii V.I., Korostelin Yu.V., Landman A .I., et. al. Pulsed Fe^{2+}:ZnS laser continuously tunable in the wavelength range of 3.49 — 4.65 μm// Quantum Electronics.–2011.- V.41. - P.1 -3.
3. Li H.F., Wang H.Q., Kuang X. Y. Optical and magnetic properties of transition-metal ions in tetrahedral and octahedral compounds//Sci. China – 2011. - V.54, N.10. - P. 1796–1800.
4. Vaksman Yu. F., Nitsuk Yu. A., Purtov Yu. N., Nasibov A.S., Shapkin P.V. Obtaining and optical properties of ZnS:Ti

crystals // Photoelectronics. 2013. - №22. – P. 78-83.
5. Ваксман Ю.Ф. Ницук Ю.А, Яцун В.В. Влияние примеси железа на люминесценцию и фотопроводимость кристаллов ZnSe в видимой области спектра // ФТП. – 2011. – Т. 45, В. 9. – С. 1171-1174.
6. Ницук Ю.А, Ваксман Ю.Ф., Яцун В.В. Исследование примесной фотопроводимости и люминесценции в кристаллах ZnSe:Ni в видимой области спектра// ФТП. – 2012. – Т. 46, В. 10. – С. 1288-1292.

This article has been received within 2014

UDC 621.315.592

Yu. F. Vaksman, Yu. A. Nitsuk

PHOTOLUMINESCENCE AND PHOTOCONDUCTIVITY OF ZnS:Ti SINGLE CRYSTALS

Abstract

The photoconductivity and photoluminescence of ZnS:Ti crystals in the visible spectra region are studied. The scheme of optical transitions within Ti^{2+} impurity centers is established. It is shown that the high-temperature photoconductivity of ZnS:Ti crystals is controlled by optical transitions of electrons from the $^3A_2(F)$ ground state to the higher levels of excited states of Ti^{2+} ions, with subsequent thermal activation of the electrons to the conduction band. Efficient excitation of intracenter luminescence of ZnS:Ti crystals is attained with light corresponding to the region of intrinsic absorption in Ti^{2+} ions.

Key words: zinc sulfide, titanium impurity, photoconductivity, photoluminescence

УДК 621.315.592

Ю. Ф. Ваксман, Ю. А. Ницук

ФОТОЛЮМИНЕСЦЕНЦИЯ И ФОТОПРОВОДИМОСТЬ МОНОКРИСТАЛЛОВ ZnS:Ti

Резюме

Исследована фотопроводимость и фотолюминесценция кристаллов ZnS:Ti в видимой области спектра. Установлена схема оптических переходов, происходящих в пределах примесных центров Ti^{2+}. Показано, что высокотемпературная фотопроводимость кристаллов ZnSe:Fe обусловлена оптическими переходами электронов из основного состояния $^3A_2(F)$ на более высокие возбужденные энергетические уровни иона Ti^{2+} с их последующей термической активацией в зону проводимости. Эффективное возбуждение внутрицентровой люминесценции кристаллов ZnS:Ti осуществляется светом из области собственного поглощения ионов Ti^{2+}.

Ключевые слова: сульфид цинка, примесь титана, фотолюминесценция, фотопроводимость.

УДК 621.315.592

Ю. Ф. Ваксман, Ю. А. Ніцук

ФОТОЛЮМІНЕСЦЕНЦІЯ І ФОТОПРОВІДНІСТЬ МОНОКРИСТАЛІВ ZnS:Ti

Резюме

Досліджено фотопровідність і фотолюмінесценцію кристалів ZnS:Ti в видимій області спектру. Встановлено схему оптичних переходів, що протікають в межах домішкових центрів Ti^{2+}. Показано, що високотемпературна фотопровідність кристалів ZnS:Ti обумовлена оптичними переходами електронів з основного стану $^3A_2(F)$ на більш високі збуджені енергетичні рівні іону Ti^{2+} з їх подальшою термічною активацією в зону провідності. Ефективне збудження внутришньоцентрової люмінесценції кристалів ZnS:Ti здійснюється світлом з області власного поглинання іонів Ti^{2+}.

Ключові слова: сульфід цинку, домішка титану, фотолюмінесценція, фотопровідність.

UDC 539.182

A. A. Svinarenko

Odessa State Environmental University, 15, Lvovskaya str., Odessa, Ukraine
Odessa National Polytechnical University, 1, Shevchenko av., Odessa, Ukraine
e-mail: quantsvi@mail.ru

SPECTROSCOPY OF AUTOIONIZATION RESONANCES IN SPECTRA OF BARIUM: NEW SPECTRAL DATA

We applied a generalized energy approach (Gell-Mann and Low S-matrix formalism) combined with the relativistic multi-quasiparticle (QP) perturbation theory (PT) with the Dirac-Kohn-Sham zeroth approximation to studying autoionization resonances (AR) in complex atoms and ions, in particular, energies for the Rydberg barium with accounting for the exchange-correlation, relativistic

1. Introduction

Here we continue our investigations of studying the autoionization state and AR in spectra of complex atoms and ions. Let us note [1] that traditionally an investigation of spectra, spectral, radiative and autoionization characteristics for heavy and superheavy elements atoms and multicharged ions is of a great interest for further development atomic and nuclear theories and different applications in the plasma chemistry, astrophysics, laser physics, etc. (look Refs. [1–10]). Theoretical methods of calculation of the spectroscopic characteristics for heavy atoms and ions may be divided into a few main groups [1-6]. First, the well known, classical multi-configuration Hartree-Fock method (as a rule, the relativistic effects are taken into account in the Pauli approximation or Breit hamiltonian etc.) allowed to get a great number of the useful spectral information about light and not heavy atomic systems, but in fact it provides only qualitative description of spectra of the heavy and superheavy ions. Second, the multi-configuration Dirac-Fock (MCDF) method is the most reliable version of calculation for multielectron systems with a large nuclear charge. In these calculations the one- and two-particle relativistic effects are taken into account practically precisely. In this essence it should be given special attention to two very general and important computer systems for relativistic and QED calculations of atomic and molecular properties developed in the Oxford group and known as GRASP ("GRASP", "Dirac"; "BERTHA", "QED") (look [1-5] and refs. therein). In particular, the BERTHA program embodies a new formulation of relativistic molecular structure theory within the framework of relativistic QED. This leads to a simple and transparent formulation of Dirac-Hartree-Fock-Breit (DHFB) self-consistent field equations along with algorithms for molecular properties, electron correlation, and higher order QED effects. The DHFB equations are solved by a direct method based on a relativistic generalization of the McMurchie-Davidson algorithm [4].

In this paper we applied a new relativistic approach [11-15] to relativistic studying the autoionization characteristics of the barium atom. Let us note that new approach in optics and spectroscopy of heavy atomic systems is the combined the generalized energy approach and the gauge-invariant QED many-QP PT with the Dirac-Kohn-Sham (DKS) "0" approximation (optimized 1QP representation) and an accurate accounting for relativistic, correlation, nuclear, radiative effects. In refs. [11-15, 17-20]. It has been in etails presented, so here we give only the fundamental aspects. The generalized gauge-invariant version of the energy approach has been further developed in Refs. [12,13].

2. Relativistic approach in autoionization spectroscopy of heavy atoms

In relativistic case the Gell-Mann and Low formula expressed an energy shift DE through the QED scattering matrix including the interaction with as the photon vacuum field as the laser field. The first case is corresponding to definition of the traditional radiative and autoionization characteristics of multielectron atom. The wave function zeroth basis is found from the Dirac-Kohn-Sham equation with a potential, which includes the ab initio (the optimized model potential or DF potentials, electric and polarization potentials of a nucleus; the Gaussian or Fermi forms of the charge distribution in a nucleus are usually used) [5]. Generally speaking, the majority of complex atomic systems possess a dense energy spectrum of interacting states with essentially relativistic properties. Further one should realize a field procedure for calculating the energy shifts DE of degenerate states, which is connected with the secular matrix *M* diagonalization [8-12]. The secular matrix elements are already complex in the second order of the PT. Their imaginary parts are connected with a decay possibility. A total energy shift of the state is presented in the standard form:

$$\Delta \mathrm{E} = \mathrm{Re}\,\Delta E + i\,\mathrm{Im}\,\Delta E \qquad \mathrm{Im}\,\Delta E = -\Gamma/2\,, \quad (1)$$

where Γ is interpreted as the level width, and the decay possibility $\mathrm{P} = \Gamma$. The whole calculation of the energies and decay probabilities of a non-degenerate excited state is reduced to the calculation and diagonalization of the *M*. The *jj*-coupling scheme is usually used. The complex secular matrix *M* is represented in the form [9,10]:

$$M = M^{(0)} + M^{(1)} + M^{(2)} + M^{(3)}. \quad (2)$$

where $M^{(0)}$ is the contribution of the vacuum diagrams of all order of PT, and $M^{(1)}$, $M^{(2)}$, $M^{(3)}$ those of the one-, two- and three-QP diagrams respectively. $M^{(0)}$ is a real matrix, proportional to the unit matrix. It determines only the general level shift. We have assumed $M^{(0)} = 0$. The diagonal matrix $M^{(1)}$ can be presented as a sum of the independent 1QP contributions. For simple systems (such as alkali atoms and ions) the 1QP energies can be taken from the experiment. Substituting these quantities into (2) one could have summarized all the contributions of the 1QP diagrams of all orders of the formally exact QED PT. However, the necessary experimental quantities are not often available. So, the optimized 1-QP representation is the best one to determine the zeroth approximation. The correlation corrections of the PT high orders are taken into account within the Green functions method (with the use of the Feynman diagram's technique). All correlation corrections of the second order and dominated classes of the higher orders diagrams (electrons screening, polarization, particle-hole interaction, mass operator iterations) are taken into account [10-14]. In the second order, there are two important kinds of diagrams: polarization and ladder ones. Some of the ladder diagram contributions as well as some of the 3QP diagram contributions in all PT orders have the same angular symmetry as the 2QP diagram contributions of the first order [10-12]. These contributions have been summarized by a modification of the central potential, which must now include the screening (anti-screening) of the core potential of each particle by two others. The additional potential modifies the 1QP orbitals and energies. Then the secular matrix is : $M \simeq \tilde{M}^{(1)} + \tilde{M}^{(2)}$, where $\tilde{M}^{(1)}$ is the modified 1QP matrix (diagonal), and $\tilde{M}^{(2)}$ the modified 2QP one. $\tilde{M}^{(1)}$ is calculated by substituting the modified 1QP energies), and $\tilde{M}^{(2)}$ by means of the first PT order formulae for $M^{(2)}$, putting the modified radial functions of the 1QP states in the interaction radial integrals. Let us remind that in the QED theory, the photon propagator D(12) plays the role of this interaction. Naturally, an analytical form of D depends on the gauge, in which the electrodynamic potentials are written. In general, the results of all approximate calculations depended on the gauge. Naturally the correct result must be gauge invariant. The gauge dependence of the amplitudes of the photoprocesses in the approximate calculations is

a well known fact and is in details investigated by Grant, Armstrong, Aymar-Luc-Koenig, Glushkov-Ivanov [1,2,5,9]. Grant has investigated the gauge connection with the limiting non-relativistic form of the transition operator and has formulated the conditions for approximate functions of the states, in which the amplitudes are gauge invariant. These results remain true in an energy approach as the final formulae for the probabilities coincide in both approaches. In ref. [16] it has been developed a new version of the approach to conserve gauge invariance. Here we applied it to get the gauge-invariant procedure for generating the relativistic DKS orbital bases (abbreviator of our method: GIRPT). The autoionization width is defined by the square of interaction matrix element [9]:

$$V^{\omega}_{1234} = [(j_1)(j_2)(j_3)(j_4)]^{1/2} \sum_{\lambda\mu} (-1)^{\mu} \begin{pmatrix} j_1 & j_3 & \lambda \\ m_1 & -m_3 & \mu \end{pmatrix} \times \mathrm{Re}\, Q_{\lambda}(1234) \tag{3}$$

The real part of the interaction matrix element can be expanded in terms of Bessel functions [5,8]:

$$\frac{\cos|\omega|r_{12}}{r_{12}} = \frac{\pi}{2\sqrt{r_1 r_2}} \sum_{\lambda=0} (\lambda) J_{\lambda+1/2}(|\omega| r_<) J_{-\lambda-1/2}(|\omega| r_>) P_{\lambda}(\cos \mathbf{r}_1 \mathbf{r}_2) \tag{4}$$

The Coulomb part $Q^{\mathrm{Qul}}_{\lambda}$ is expressed in the radial integrals R_1, angular coefficients S_1 as follows:

$$\begin{aligned} \mathrm{Re}\, Q^{\mathrm{Qul}}_{\lambda} \sim \mathrm{Re}\{ & R_l(1243) S_{\lambda}(1243) + R_{\lambda}(\tilde{1}24\tilde{3}) S_{\lambda}(\tilde{1}24\tilde{3}) \\ & + R_{\lambda}(1\tilde{2}\tilde{4}3) S_{\lambda}(1\tilde{2}\tilde{4}3) + R_{\lambda}(\tilde{1}\tilde{2}\tilde{4}\tilde{3}) S_{\lambda}(\tilde{1}\tilde{2}\tilde{4}\tilde{3}) \} \end{aligned} \tag{5}$$

where $\mathrm{Re}Q_1(1243)$ is as follows:

$$\mathbf{Re}\, R_{\lambda}(1243) = \iint dr_1 r_1^2 r_2^2 f_1(r_1) f_3(r_1) f_2(r_2) f_4(r_2) Z^{(1)}_{\lambda}(r_<) Z^{(1)}_{\lambda}(r_>) \tag{6}$$

where f is the large component of radial part of the 1QP state Dirac function and function Z is :

$$Z^{(1)}_{\lambda} = [2/|\omega_3|\alpha Z]^{\lambda+1/2} J_{\lambda+1/2}(\alpha|\omega_3|r) [r^{\lambda} \Gamma(\lambda + 3/2)]. \tag{7}$$

The angular coefficient is defined by standard way as above [3]. The calculation of radial integrals $\mathbf{Re}R_1(1243)$ is reduced to the solution of a system of differential equations:

$$\left.\begin{aligned} y_1' &= f_1 f_3 Z^{(1)}_{\lambda}(\alpha|\omega|r) r^{2+\lambda}, \\ y_2' &= f_2 f_4 Z^{(1)}_{\lambda}(\alpha|\omega|r) r^{2+\lambda}, \\ y_3' &= [y_1 f_2 f_4 + y_2 f_1 f_3] Z^{(2)}_{\lambda}(\alpha|\omega|r) r^{1-\lambda}. \end{aligned}\right\} \tag{8}$$

In addition, $y_3(\infty)=\mathbf{Re}R_1(1243)$, $y_1(\infty)=X_1(13)$. The system of differential equations includes also equations for functions $f/r^{|æ|-1}$, $g/r^{|æ|-1}$, $Z^{(1)}_{\lambda}$, $Z^{(2)}_{\lambda}$. The formulas for the autoionization (Auger) decay probability include the radial integrals $R_a(akgb)$, where one of the functions describes electron in the continuum state. When calculating this integral, the correct normalization of the function Y_k is a problem. The correctly normalized function should have the following asymptotic at $r \to 0$:

$$\left.\begin{matrix} f \\ g \end{matrix}\right\} \to (\lambda\omega)^{-1/2} \begin{cases} [\omega + (\alpha Z)^{-2}]^{-1/2} \sin(kr + \delta), \\ [\omega - (\alpha Z)^{-2}]^{-1/2} \cos(kr + \delta). \end{cases} \tag{9}$$

When integrating the master system, the function is calculated simultaneously:

$$N(r) = \{\pi\omega_k [f_k^2 [\omega_k + (\alpha Z)^{-2}] + g_k^2 [\omega_k + (\alpha Z^{-2})]]\}^{-1/2} \tag{10}$$

It can be shown that at $r \to \infty$, $N(r) \to N_k$, where N_k is the normalization of functions f_k, g_k of continuous spectrum satisfying the condition (9). Other details can be found in refs.[10-13,16-20].

3. Results and conclusions

In table 1 we present the data for energies (cm^{-1}) of the barium autoionization resonances 4fnf, n = 15 (averaged over the fine structure) measured experimentally and calculated on the basis of our theory and multichannel quantum defect method (MCQD) with the empirical fit (de Graaf et al) [2]. An analysis shows quite physically reasonable agreement between the theoretical and experimental results. But some difference, in our opinion, can be explained by different accuracy of estimates of the radial integrals, using the different type basises (gauge invariance conservation or a degree of accounting for the exchange-correlation effects) and some other additional calculation approximations. In our theory there are used more optimized basises of the orbitals in comparison with the MCQD).

In ref. [14] (see also [5,12]) it has been predicted a new spectroscopy effect of the giant changing of the AS ROD width in a sufficiently weak electric field (for two pairs of the Tm, Gd AR).

Following to [5], let us remind that any two states of different parity can be mixed by the external electric field. The mixing leads to redistribution of the autoionization widths. In the case of degenerate or near-degenerate resonances this effect becomes observable even at a moderately weak field.

Table 1.

Energies (cm^{-1}) of autoionization resonances 4fnf, n = 15 (averaged over the fine structure) measured experimentally and calculated on the basis of our theory and multichannel quantum defect method (MCQD) with the empirical fit (de Graaf et al)

AC	J	Exp.	MCQD	Our work
$4f_{5/2}15f_{7/2}$	6	89 758.4±0.5	89759.1	89758.8
$4f_{7/2}15f_{5/2}$	6	89 993.6±0.5	89992.4	89993.6
$4f_{7/2}15f_{7/2}$	6	89 926.6±5.0	89937.1	89926.8
$4f_{5/2}15f_{7/2}$	5	89 726.3±1.0	89718.7	89726.9
$4f_{5/2}15f_{5/2}$	5	89 749.2±0.5	89748.6	89749.7
$4f_{7/2}15f_{7/2}$	5	89 951.0±0.5	89952.9	89951.6
$4f_{7/2}15f_{5/2}$	5	-	-	89942.3
$4f_{5/2}15f_{5/2}$	4	89 705.6±0.5	89706.8	89705.4
$4f_{5/2}15f_{7/2}$	4	-	-	89718.5
$4f_{7/2}15f_{5/2}$	4	89 937.8±2.0	89937.2	89937.6
$4f_{7/2}15f_{7/2}$	4	89 951.0±2.0	89951.8	89951.5
$4f_{5/2}15f_{5/2}$	3	-	-	89728.5
$4f_{5/2}15f_{7/2}$	3	89 741.5±2.0	89738.0	89740.9
$4f_{7/2}15f_{7/2}$	3	89 969.3±2.0	89972.0	89969.8
$4f_{7/2}15f_{5/2}$	3	-	-	89953.4
$4f_{5/2}15f_{7/2}$	2	89 766.5±5.0	89774.7	89767.8

In the Tm one could deal with ROD *nd* and *nf* series, converging to the same ionization limit, i.e. they are nearly degenerate states of different parity. Among them one can find some pairs of *nd* and *nf* states with widths Γ, differing by several orders. So, we could suggest that the phenomenological effect of giant broadening of the Rydberg AS could take a place in the barium atom too, however, the corresponding detailed investigation is required.

References

1. Grant I.P., Relativistic Quantum Theory of Atoms and Molecules.-Oxford, 2008.-650P.
2. Luc Koenig E., Aymar M., Van Leeuwen R., Ubachs W., Hogervorst W.//Phys. Rev.A.-1995.-Vol.52.-P.208-215.
3. Quiney H., Relativistic Quantum Mechanics of Atoms and Molecules//New Trends in Quantum Systems in Chemistry and Physics (Springer).-2002.-Vol.6.-P.135–173.
4. Bell K.L., Berrington K., Crothers D., Hibbert A., Taylor K.T., BERTHA: 4-Component Relativistic Molecular Quantum Mechanics// Supercomputing, Collision Processes, and Application, Series: Physics of Atoms and Molecules (Springer).-2002.-P.213–224.
5. Glushkov A.V., Relativistic Quantum Theory. Quantum, mechanics of Atomic Systems.-Odessa: Astroprint, 2008.-900P.
6. Safronova U.I., Safronova M.S., Third-order relativistic many-body calculations of energies, transition rates, hyperfine constants, and blackbody radiation shift in $^{171}Yb^{+}$//Phys. Rev. A.-2009.-Vol.79.-P.022512.
7. Bieron J, Froese-Fischer C., Fritzsche S., Pachucki K., Lifetime and hyperfine structure of $^{3}D_{2}$ state of radium//J. Phys.B:At.Mol.Opt.Phys.-2004.-Vol.37.-P.L305-311.
8. Ivanov L.N.,Ivanova E.P., Extrapolation of atomic ion energies by model potential method: Na-like spectra/ // Atom.Data Nucl .Data Tab.-1979.-Vol.24.-P.95-121.
9. Bekov G.I., Vidolova-Angelova E., Ivanov L.N.,Letokhov V.S., Mishin V.I., Laser spectroscopy of low excited autoionization states of the ytterbium atom// JETP.-1991.-Vol.80.-P.866-878.
10. Vidolova-Angelova E., Ivanov L.N., Autoionizing Rydberg states of thulium. Re-orientation decay due to monopole interaction// J.Phys.B:At.Mol.Opt. Phys.-1991.-Vol.24.-P.4147-4158
11. Ivanov L.N., Letokhov V.S. Spectroscopy of autoionization resonances in heavy elements atoms// Com.Mod.

Phys.D.:At.Mol.Phys.-1985.-Vol.4.-P.169-184.
12. Glushkov A.V., Ivanov L.N., Ivanova E.P., Radiation decay of atomic states. Generalized energy approach// Autoionization Phenomena in Atoms.- M.: Moscow State Univ.-1996.
13. Glushkov A.V., Ivanov L.N. Radiation decay of atomic states: atomic residue and gauge non-invariant contributions // Phys. Lett.A.-1999.-Vol.170.-P.33-38.
14. Glushkov A.V., Ivanov L.N. DC Strong-Field Stark-Effect: consistent quantum-mechanical approach// J.Phys.B: At. Mol. Opt. Phys.-1993.-Vol.26.- P.L379-386.
15. Glushkov A.V., Khetselius O.Yu., Svinarenko A.A., Relativistic theory of cooperative muon-gamma-nuclear processes: Negative muon capture and metastable nucleus discharge// Advances in the Theory of Quantum Systems in Chemistry and Physics (Springer).-2012.-Vol.22.-P.51-70.
16. Glushkov A.V., Khetselius O.Yu., Loboda A.V., Svinarenko A.A., QED approach to atoms in a laser field: Multiphoton resonances and above threshold ionization//Frontiers in Quantum Systems in Chemistry and Physics (Springer).-2008.-Vol.18.-P.541-558.
17. Glushkov A.V., Svinarenko A.A., Ignatenko A.V., Spectroscopy of autoionization resonances in spectra of the lanthanides atoms//Photoelectronics.-2011.-Vol.20.-P.90-94.
18. Svinarenko A.A., Nikola L.V., Prepelitsa G.P., Tkach T., Mischenko E., The Auger (autoionization) decay of excited states in spectra of multicharged ions: Relativistic theory//Spectral Lines Shape.-2010.-Vol.16.-P.94-98
19. Malinovskaya S.V., Glushkov A.V., Khetselius O.Yu., Svinarenko A., Bakunina E., Florko T., Optimized perturbation theory scheme for calculating interatomic potentials and hyperfine lines shift for heavy atoms in buffer inert gas//International Journal of Quantum Chemistry.-2009.-Vol.109.-P.3325-3329.
20. Svinarenko A.A., Mischenko E.V., Loboda A.V., Dubrovskaya Yu.V., Quantum measure of frequency and sensing the collisional shift of the ytterbium hyperfine lines in medium of helium gas// Sensor Electronics and Microsystem Techn.-2009.-N1.-P.25-29.

This article has been received within 2014

UDC 539.183

A. A. Svinarenko

SPECTROSCOPY OF AUTOIONIZATION RESONANCES IN SPECTRA OF HE-LIKE IONS AND ALKALI-EARTH ATOMS: NEW SPECTRAL DATA AND CHAOS EFFECT

Abstract

We applied a generalized energy approach (Gell-Mann and Low S-matrix formalism) combined with the relativistic multi-quasiparticle (QP) perturbation theory (PT) with the Dirac-Kohn-Sham zeroth approximation to studying autoionization resonances (AR) in complex atoms and ions, in particular, energies for the Rydberg barium with accounting for the exchange-correlation, relativistic corrections.

Key words: spectroscopy of autoionization resonances, relativistic energy approach

УДК 539.183

А. А. Свинаренко

СПЕКТРОСКОПИЯ АВТОИОНИЗАЦИОННЫХ РЕЗОНАНСОВ В СПЕКТРАХ БАРИЯ: НОВЫЕ СПЕКТРАЛЬНЫЕ ДАННЫЕ

Резюме

Обобщенный энергетический подход (S-матричный формализм Гелл-Мана и Лоу) и релятивистская теория возмущений с дирак-кон-шэмовским нулевым приближением применены к изучению автоионизационных резонансов в сложных атомах, в частности, энергий автоионизационных резонансов в ридберговом барии с учетом обменно-корреляционных и релятивистских поправок.

Ключевые слова: спектроскопия автоионизационных резонансов, релятивистский энергетический подход

УДК 539.183

А. А. Свинаренко

СПЕКТРОСКОПІЯ АВТОІОНІЗАЦІЙНИХ РЕЗОНАНСІВ В СПЕКТРАХ БАРІЯ: НОВІ СПЕКТРАЛЬНІ ДАНІ

Резюме

Узагальнений енергетичний підхід (S-матричний формалізм Гелл-Мана та Лоу) и релятивістська теорія збурень з дірак-кон-шемівським нульовим наближенням застосовані до вивчення автоіонізаційних резонансів у складних атомах, зокрема, енергій автоіонізаційних резонансів у в рідберговому барії з урахуванням обмінно-кореляційних і релятивістських поправок.

Ключові слова: спектроскопія автоіонізаційних резонансів, релятивістський енергетичний підхід

UDC 539.182

T. A. Florko, A. V. Ignatenko, A. A. Svinarenko, V. B. Ternovsky, T. B. Tkach

Odessa State Environmental University, L'vovskaya str.15, Odessa-16, 65016, Ukraine
e-mail: quantsvi@mail.ru

ADVANCED RELATIVISTIC MODEL POTENTIAL APPROACH TO CALCULATION OF RADIATION TRANSITION PARAMETERS IN SPECTRA OF MULTICHARGED IONS

The combined relativistic energy approach and relativistic many-body perturbation theory with the zeroth order optimized one-particle approximation are used for calculation of the Li-like ions (Z=11-42,69,70) energies and oscillator strengths of radiative transitions from the ground state to the low-excited and Rydberg states, in particular, $2s_{1/2} - np_{1/2,3/2}$, $np_{1/2,3/2}$-$nd_{3/2,5/2}$ (n=2-12). The comparison of the calculated oscillator strengths with available theoretical and experimental (compillated) data is performed.

1. Introduction

The research on the spectroscopic and structural properties of highly ionized atoms has a fundamental importance in many fields of atomic physics (spectroscopy, spectral lines theory), astrophysics, plasma physics, laser physics and so on. It should be mentioned that the correct data about radiative decay widths, probabilities and oscillator strengths of atomic transitions are needed in astrophysics and laboratory, thermonuclear plasma diagnostics and in fusion research. In this light, an special interest attracts studying the spectral characteristics of the He-, Li etc like ions. There have been sufficiently many reports of calculations and compilation of energies and oscillator strengths for the Li-like ions and other alkali-like ions (see, for example, [1–16]). Particularly, Martin and Wiese have undertaken a critical evaluation and compilation of the spectral parameters for Li-like ions (Z=3-28) [1,2]. The results of the high-precision non-relativistic calculations of the energies and oscillator strengths of $1s22s_j1s22p$ for Li-like systems up to $Z = 50$ are presented in Refs. [9-14]. The Hylleraas-type variational method and the $1/Z$ expansion method have been used. Chen Chao and Wang Zhi-Wen [14] have listed the nonrelativistic dipole-length, -velocity and -acceleration absorption oscillator strengths for the 1s22s–1s22p transitions of the LiI isoelectronic sequence on the basis of calculation within a full core plus correlation method with using multiconfiguration interaction wave functions. Fully variational nonrelativistic Hartree-Fock wavefunctions have been used by Biémont in calculation of the 1s2n2L (n <8 =s, p, d or f; 3 < Z<22) states of the LiI isoelectronic sequence [16]. In many papers the Dirac-Fock method, model potential approach, quantum defect approximation in the different realizations have been used for calculating the energies and oscillator strengths of the Li-like ions (see Refs. [1-17]). The consistent QED calculations of the energies, ionization potentials, hyperfine structure constants for the Li-like ions are performed in Refs. [18-21]. However, it should be stated that for Li-like ions with higher Z, particularly for their high-excited (Rydberg) states, there is not enough precise information available in literatures. In our paper the combined relativistic energy approach [22-26] and relativistic many-body perturbation theory with the zeroth order optimized one-particle representation [26] are used for calculation the Li-like ions (Z=11-42,69,70) energies and oscillator strengths of radiative transitions from ground state to low-excited and Ry-

dberg states.. The comparison of the calculated oscillator strengths with available theoretical and experimental (compillated) data is performed.

2. The theoretical method

In the relativistic energy approach [4,5,22-25] the imaginary part of electron energy shift of an atom is directly connected with the radiation decay possibility (transition probability). An approach, using the Gell-Mann and Low formula with the QED scattering matrix, is used in treating the relativistic atom. The total energy shift of the state is usually presented in the form:

$$DE = ReDE + i\ G/2 \qquad (1)$$

where G is interpreted as the level width, and the decay possibility P = G. The imaginary part of electron energy of the system, which is defined in the lowest order of perturbation theory as [4]:

$$\mathrm{Im}\Delta E(B) = -\frac{e^2}{4\pi} \sum_{\substack{\alpha>n>f \\ [\alpha<n\le f]}} V^{|\omega_{\alpha n}|}_{\alpha n \alpha n}, \qquad (2)$$

where (a>n>f) for electron and (a<n<f) for vacancy. The matrix element is determined as follows:

$$V^{|\omega|}_{ijkl} = \iint dr_1 dr_2 \Psi^*_i(r_1)\Psi^*_j(r_2)\frac{\sin|\omega|r_{12}}{r_{12}}(1 - \alpha_1\alpha_2)\Psi^*_k(r_2)\Psi^*_l(r_1) \qquad (3)$$

The separated terms of the sum in (3) represent the contributions of different channels and a probability of the dipole transition is:

$$\Gamma_{\alpha_n} = \frac{1}{4\pi}\cdot V^{|\omega_{\alpha_n}|}_{\alpha_n\alpha_n} \qquad (4)$$

The corresponding oscillator strength : $gf = \lambda^2_g \cdot \Gamma_{\alpha_n} / 6.67\cdot 10^{15}$, where g is the degeneracy degree, l is a wavelength in angstrems (Å). Under calculating the matrix elements (3) one should use the angle symmetry of the task and write the expansion for potential sin|w|r12/r12 on spherical functions as follows [2]:

$$\frac{\sin|\omega|r_{12}}{r_{12}} = \frac{\pi}{2\sqrt{r_1 r_2}}\sum_{\lambda=0}^{\infty}(\lambda) J_{\lambda+1/2}(|\omega|r_1)\cdot J_{\lambda+1/2}(|\omega|r_1) J_{\lambda+1/2}(|\omega|r_2) P_\lambda(\cos \boldsymbol{r}_1\boldsymbol{r}_2) \qquad (5)$$

where J is the Bessel function of first kind and (l)= 2l + 1. This expansion is corresponding to usual multipole one for probability of radiative decay. Substitution of the expansion (5) to matrix element of interaction gives as follows [20]:

$$V^{\omega}_{1234} = [(j_1)(j_2)(j_3)(j_4)]^{1/2}\sum_{\lambda\mu}(-1)^{\mu}\begin{pmatrix} j_1 j_3 & \lambda \\ m_1 - m_3 & \mu \end{pmatrix}\times \mathrm{Im}Q_\lambda(1234)$$

$$Q_\lambda = Q^{\mathrm{Qul}}_\lambda + Q^{\mathrm{Br}}_\lambda, \qquad (6)$$

where j_i is the total single electron momentums, m_i – the projections; Q^{Qul} is the Coulomb part of interaction, Q^{Br} - the Breit part. Their detailed definitions are presented in Refs. [4,20]. The relativistic wave functions are calculated by solution of the Dirac equation with the potential, which includes the "outer electron- ionic core" potential and polarization potential [29]. In order to describe interaction of the outer electron with the He-like core the Ivanova-Ivanov model potential [4] has been used. The calibration of the single model potential parameter has been performed on the basis of the special ab initio procedure within relativistic energy approach [24] (see also [5]).

In Ref.[18] the lowest order multielectron effects, in particular, the gauge dependent radiative contribution Im dE_{ninv} for the certain class of the photon propagator calibration is treated. This value is considered to be the typical representative of the electron correlation effects, whose minimization is a reasonable criterion in the searching for the optimal one-electron basis of the relativistic many-body perturbation theory. The minimization of the density functional Im dE_{ninv} leads to the integral-differential equation that can be solved using one of the standard numerical codes. Therefore, it provides the construction of the op-

timized one-particle representation. All calculations are performed on the basis of the numeral code Superatom-ISAN (version 93).

3. Results

We applied the above described approach to calculating the energies and oscillator strengths of transitions in spectra of the Li-like ions (Z=11-42,69,70). There are considered the radiative transitions from ground state to the low-excited and Rydberg states, particularly, $2s_{1/2} - np_{1/2,3/2}$, $np_{1/2,3/2}$-$nd_{3/2,5/2}$ (n=2-12). To test the obtained results, we compare our calculation data on the oscillator strengths values for some Li-like ions with the known theoretical and compillated results [1,2,8].

As an example, in table 1 we present the oscillator strengths values for the 2s1/2 – 2p1/2,3/2 transitions in Li-like ions S^{13+}, Ca^{17+}, Fe^{23+}, Zn^{27+}, Zr^{37+}, Mo^{39+}, Sn^{47+}, Tm^{66+}, Yb^{67+}. The DF calculation data by Zilitis [6] and the "best" compillated (experimental) data [1,2] for the low-Z Li-like ions are listed in table 1 for comparison too.

Table 1

Oscillator strengths of the $2s_{1/2} - 2p_{1/2,3/2}$ transitions in Li-like ions

Method	DF [6]	DF[6]	[2]	[2]	Our	Our
Ion	$2s_{1/2}$– $2p_{1/2}$	$2s_{1/2}$– $2p_{3/2}$	$2s_{1/2}$– $2p_{1/2}$	$2s_{1/2}$– $2p_{3/2}$	$2s_{1/2}$– $2p_{1/2}$	$2s_{1/2}$– $2p_{3/2}$
S^{13+}	0.0299	0.0643	0.030	0.064	0.0301	0.0641
Ca^{17+}	0.0234	0.0542	0.024	0.054	0.0236	0.0541
Fe^{23+}	0.0177	0.0482	0.018	0.048	0.0179	0.0481
Zn^{27+}	0.0153	0.0477	–	–	0.0156	0.0475
Zr^{37+}	0.0114	0.0543	–	–	0.0118	0.0540
Mo^{39+}	–	–	0.011	0.056	0.0107	0.0556
Sn^{47+}	0.0092	0.0686	–	–	0.0095	0.0684
Tm^{66+}	–	–	–	–	0.0071	01140
Yb^{67+}	0.0067	0.1170	–	–	0.0069	0.1167

It should be reminded that the experimental data on the oscillator strengths for many (especially, high-Z) Li-like ions are absent. In a whole, there is a physically reasonable agreement between the listed data. The important features of the approach used are using the optimized one-particle representation and account for the polarization effect. it should be noted that an estimate of the gauge-non-invariant contributions (the difference between the oscillator strengths values calculated with using the transition operator in the form of "length" and "velocity") is about 0.3%, i.e. the results, obtained with using the different photon propagator gauges (Coulomb, Babushkon, Landau) are practically equal.

In table 2 we present the oscillator strengths values for the $2s_{1/2} - np_j$ (n=3-18, j=1/2) transitions in spectrum of the Li-like ion Zr^{37+}. The quantum defect approximation (QDA) [6,27], the DF oscillator strengths calculation results by Zilitis [6] and some compillated (experimental) data by Martin-Weiss [1] are listed too.

It is self-understood that the QDA oscillator strengths data become more exact with the growth of the principal quantum number. At the same time the accuracy of the DF data may be decreased. The agreement between the Martin-Weiss data and our is sufficiently good.

Table 2

Oscillator strengths of the $2s_{1/2} - np_{1/2}$ transitions in Zr^{37+}.

Transition	QDA [6]	DF [6]	Our data
$2s_{1/2}$–$3p_{1/2}$	13.7	13.3	13.684
$-4p_{1/2}$	-	3.22	3.232
$-6p_{1/2}$	-	-	0.682
$-8p_{1/2}$	0.258	0.257	0.260
$-10p_{1/2}$	0.126	0.124	0.125
$-16p_{1/2}$	0.0291	0.0285	0.0287
$-18p_{1/2}$	-	-	0.0216

References

1. Martin G.A., Wiese W.L., Phys. Rev. A.-1976.-Vol.13.-P.699764; J.Phys. Chem. Ref. Dat.-1976.-Vol.5.-P.538-598.
2. Schweizer W., Faßbinder P., Gonzalez-Ferez R., Atom.Data.Nucl.Data.

Tabl.-1999.-Vol.72.-P.33-124.
3. Ivanova E. P., Ivanov L.N., Atom. Data. Nucl.Data.Tabl.-1999.-Vol. 24.-P.95-109.
4. Ivanov L.N., Ivanova E.P., Aglitsky E.V., Phys. Rep.-1998.-Vol.166.-P.315 -380.
5. Glushkov A.V., Ivanov L.N., Ivanova E. P., Autoionization Phenomena in Atoms, (Moscow: Moscow Univ. Press).-1996.-P.58 -160.
6. Zilitis V.A., Opt. Spectr.-1993.-Vol. 55.-P.215-220.
7. Khetselius O.Yu., J. of Phys.: Conf. Ser.-2012.-Vol.397.-P.012012 .
8. Glushkov A.V., J. of Phys.: Conf. Ser.-2012.-Vol.397.-P.012011 .
9. Zong-Chao Yan, Drake G. W. F., Phys. Rev.A.-1995.-Vol. 52.-P.R4316 -4384.
10. Lianhua Qu, Zhiwen Wang, Baiwen Li, J.Phys.B.-1998.-Vol.31.-P.3601-3608.
11. Yan Z. C., Tambasco M., Drake G. W.F., Phys.Rev.A.-1998.-Vol.57.-P.1652-1674.
12. Xiaoxu Guan, Baiwen Li, Phys. Rev.A.-2001.-Vol.63.-P.043413..
13. Khetselius O.Yu., Phys.Scripta.-2009.-Vol.T135.-P.014023.
14. Chen Chao, Wang Zhi-Wen, Commun. Theor. Phys.-2005.-Vol.43.-P.305-312.
15. Hu Mu-Hong, Wang Zhi –Wen, Chinese Phys.B.-2009.-Vol.18.-P.2244-2258.
16. Bièmont E., Astr. & Astrophys. Suppl. Ser.-1977.-Vol.27.-P.489-497.
17. Zhi-WenWang, Ye Li, J. At. Mol. Sci.-2010.-Vol.1.-P.62-82.
18. Glushkov A.V., Ivanov L.N., Phys. Lett. A.-1999.-Vol.170.-P.33-38.
19. Yerokhin V.A., Artemyev A.N., Shabaev V.M., Phys.Rev.A.-2007.-Vol.75.-P. 062501 .
20. Glushkov A.V., Ambrosov S. V., Khetselius O. Yu., Loboda A.V., Gurnitskaya E.P., Recent Advances in the Theory of Chem. and Phys. Systems, Ser. Progress in Theor.Chem. and Phys., ed. by J P Julien, J Maruani, D Mayou, S Wilson, G Delgado-Barrio, (Amsterdam: Springer).-2006.-Vol.15.-P. 285-300.
21. Ivanova E.P., Glushkov A.V., J.Quant. Spectr. Rad.Transf.-1996.-Vol.36.-P.127-145.
22. Glushkov A.V., Khetselius O. Yu., Loboda A. V., Svinarenko A. A., Phys. Scr.-2009.-Vol.T135.-P.014029 .
23. Ivanov L.N., Ivanova E.P., Knight L., Phys. Rev. A.-1999.-Vol.48.-P.4365-4378.
24. Glushkov A.V., Advances in the Theory of Quantum Systems in Chemistry and Physics. Ser. Progress in Theor. Chem. and Phys., ed. by K Nishikawa, J Maruani, E Brandas, G Delgado-Barrio, P Piecuch (Berlin: Springer) .-2012.-Vol.28.-P.31 -72.
25. Khetselius O.Yu., Int. Journ. Quant. Chem.-2009.-Vol.109.-P.3330-3336.
26. Glushkov A.V., Journ.Appl. Spectr.-1999.-Vol.56.-P.1322.
27. Seaton M.J., Rep. Prog. Phys.-1983.-Vol. 46.-P.1983-1998.

This article has been received within 2014

UDC 539.182

T. A. Florko, A. A. Svinarenko, A. V. Ignatenko, V. B. Ternovsky, T. B. Tkach

ADVANCED RELATIVISTIC MODEL POTENTIAL APPROACH TO CALCULATION OF RADIATION TRANSITION PARAMETERS IN SPECTRA OF MULTICHARGED IONS

Abstract

The combined relativistic energy approach and relativistic many-body perturbation theory with the zeroth order optimized one-particle approximation are used for calculation of the Li-like ions (Z=11-42,69,70) energies and oscillator strengths of radiative transitions from the ground state to the low-excited and Rydberg states, in particular, $2s_{1/2} - np_{1/2,3/2}$, $np_{1/2,3/2}$-$nd_{3/2,5/2}$ (n=2-12). The comparison of the calculated oscillator strengths with available theoretical and experimental (compillated) data is performed.

Key words: relativistic theory, oscillator strengths, radiative transitions

УДК 539.182

Т. А. Флорко, А. А. Свинаренко, А. В. Игнатенко, В. Б. Терновский, Т. Б. Ткач

РАСШИРЕННАЯ РЕЛЯТИВИСТСКАЯ МОДЕЛЬ ПОТЕНЦИАЛЬНОГО ПОДХОД К РАСЧЕТУ ПЕРЕХОДНЫХ ПАРАМЕТРОВ ИЗЛУЧЕНИЯ В СПЕКТРАХ МНОГОЗАРЯДНЫХ ИОНОВ

Резюме

Комбинированный релятивистский энергитический подход и релятивистская теория возмущений многих тел с оптимизированным одночастичным приближением нулевого порядка используются для расчета Li-подобных ионов (Z = 11-42,69,70) энергии и силы осцилляторов радиационных переходов из основного состояния в низкие возбужденные и ридберговские состояния, в частности, $2s_{1/2} - np_{1/2,3/2}$, $np_{1/2,3/2}$-$nd_{3/2,5/2}$ (n=2-12). Сравнение расчетных сил осцилляторов с имеющимися теоретическими и экспериментальными данными выполнено.

Ключевые слова: релятивистская теория, силы осцилляторов, радиационные переходы.

УДК 539.182

Т. А. Флорко, А. А. Свинаренко, А. В. Ігнатенко, В. Б. Терновський, Т. Б. Ткач

РОЗШИРЕНА РЕЛЯТИВІСТСЬКА МОДЕЛЬ ПОТЕНЦІАЛЬНОГО ПІДХОДУ ДО РОЗРАХУНКУ ПЕРЕХІДНИХ ПАРАМЕТРІВ ВИПРОМІНЮВАННЯ В СПЕКТРАХ БАГАТОЗАРЯДНИХ ІОНОВ

Резюме

Комбінований релятивістський енергетичний підхід і релятивістська теорія збурень багатьох тіл з оптимізованим одночастковим наближенням нульового порядку використовується для розрахунку Li-подібних іонів (Z = 11-42,69,70) енергії і сили осциляторів радіаційних переходів із основного стану в низькі збуджені та рідбергівські стани, зокрема, $2s_{1/2} - np_{1/2,3/2}$, $np_{1/2,3/2}$-$nd_{3/2,5/2}$ (n=2-12). Порівняння розрахованих сил осциляторів з наявними теоретичними та експериментальними даними виконане.

Ключові слова: релятивістська теорія, сили осциляторів, радіаційнні переходи.

UDC 539.182

G. P. Prepelitsa

Odessa State Environmental University, 15, Lvovskaya str., Odessa, Ukraine
Odessa National Polytechnical University, 1, Shevchenko av., Odessa, Ukraine
e-mail: quantpre@mail.ru

NONLINEAR DYNAMICS OF QUANTUM AND LASER SYSTEMS WITH ELEMENTS OF A CHAOS

Nonlinear chaotic dynamics of the quantum and laser systems is studied with using advanced techniques such as a wavelet analysis, multi-fractal formalism, mutual information approach, correlation integral analysis, false nearest neighbour algorithm, the Lyapunov exponent's (LE) analysis, and surrogate data method. The detailed analysis of the oscillations in a grid of two autogenerators and single-mode laser with the nonlinear absorption cell shows that the systems exhibit a nonlinear behaviour with elements of a low-dimensional chaos.

1. Introduction

Every science purposes predicting a future state of system under consideration. Consequently, the main problem of science can be defined as: "Is it possible to predict a future behaviour of process using its past states?" Conventional approach applied to resolve this problem consists in building an explanatory model using an initial data and parameterizing sources and interactions between process properties. Unfortunately, that kind of approach is realized with difficulties, and its outcomes are insufficiently correct; moreover, sources and/or interactions of process cannot always be exactly defined. According to modern theory of prediction, time series is considered as random realization, when the randomness is caused by a complicated motion with many independent degrees of freedom. Chaos is alternative of randomness and occurs in very simple deterministic systems. Although chaos theory places fundamental limitations for long-rage prediction (see e.g. [1-9]), it can be used for short-range prediction since ex facte random data can contain simple deterministic relationships with only a few degrees of freedom. The systematic study of chaos is of recent date, originating in the 1960s. One important reason for this is that linear techniques, so long dominant within applied mathematics and the natural sciences, are inadequate when considering chaotic phenomena since the amazingly irregular behaviour of some non-linear deterministic systems was not appreciated and when such behaviour was manifest in observations, it was typically explained as stochastic. Starting from the meteorologist Edward Lorenz, who observed extreme sensitivity to changes to initial conditions of a simple non-linear model simulating atmospheric convection (Lorenz, 1963), the experimental approach relies heavily on the computational study of chaotic systems and includes methods for investigating potential chaotic behaviour in observational time series (see e.g. [1-6]). During the last two decades, many studies in various fields of physics, chemistry, biology, geosciences etc have appeared, in which chaos theory was applied to a great number of dynamical systems, including those are originated from nature. Chaos theory establishes that apparently complex irregular behaviour could be the outcome of a simple deterministic system with a few dominant nonlinear interdependent variables. The past decade has witnessed a large number of studies employing the ideas gained from the science of chaos to characterize, model, and predict the dynamics of various systems phenomena (see e.g. [1-13]).

The outcomes of such studies are very encouraging, as they not only revealed that the dynamics of the apparently irregular phenomena could be understood from a chaotic deterministic point of view but also reported very good predictions using such an approach for different systems.

In a case of quantum systems, using of chaos constructions may seem self-contradictory in many respects (see e.g. [6,7]). To begin with, it associates chaos, a purely classical notion, with quantum physics. Furthermore it implies that this association, which as we will see refers traditionally to the study of low-D non-interacting quantum systems, will be considered in the context of many-body physics [6]. In any case quantum chaos now mainly refers to the study of the consequences, for a quantum system, of the more or less chaotic nature of the dynamics of its classical analogue. It has followed two main avenues. The first one is based on semiclassical techniques - specifically the use of semiclassical Green's functions in the spirit of Gutzwiller's trace formulae, hich provides a link between a quantum system and its $h \to 0$ limit, the second is associated with the Bohigas-Giannoni-Schmit conjecture or related approaches Peres, which states that the spectral fluctuations of classically chaotic systems can be described using the proper ensembles of random matrices [6]. Some of the beauty of quantum chaos is that it has developed a set of tools which have found applications in a large variety of different physical contexts, ranging from atomic, molecular and nuclear physics (see e.g. [1-7]). In a modern quantum electronics and laser physics etc there are many systems and devices (such as multi-element semiconductors and gas lasers etc), dynamics of which can exhibit chaotic behaviour. These systems can be considered in the first approximation as a grid of autogenerators (quantum generators), coupled by different way [2,14,15]. In this chapter we will study a non-linear chaotic dynamics of some quantum generator and laser systems with using advanced generalized techniques such as the non-linear analysis methods to dynamics, such as the wavelet analysis, multifractal formalism, mutual information approach, correlation integral analysis, false nearest neighbour algorithm, Lyapunov exponent's (LE) analysis, and surrogate data method etc (see details in Refs. [8-17]).

2. Methods of a chaos theory in studying dynamics of the complex systems

2.1 Introducing remarks

Let us formally consider scalar measurements $s(n) = s(t_0 + n\mathrm{D}t) = s(n)$, where t_0 is the start time, $\mathrm{D}t$ is the time step, and is n the number of the measurements. In a general case, $s(n)$ is any time series, particularly the amplitude level. Since processes resulting in the chaotic behaviour are fundamentally multivariate, it is necessary to reconstruct phase space using as well as possible information contained in the $s(n)$.

Such a reconstruction results in a certain set of d-dimensional vectors $\mathbf{y}(n)$ replacing the scalar measurements. Packard et al. [18] introduced the method of using time-delay coordinates to reconstruct the phase space of an observed dynamical system. The direct use of the lagged variables $s(n + \mathrm{t})$, where t is some integer to be determined, results in a coordinate system in which the structure of orbits in phase space can be captured. Then using a collection of time lags to create a vector in d dimensions,

$$\mathbf{y}(n) = [s(n), s(n + \tau), s(n + 2\tau, \ldots, s(n + (d\text{-}1)\tau], \quad (1)$$

the required coordinates are provided. In a nonlinear system, the $s(n + j\mathrm{t})$ are some unknown nonlinear combination of the actual physical variables that comprise the source of the measurements. The dimension d is called the embedding dimension, d_E. Example of the Lorenz attractor given by Abarbanel et al. [1,19] is a good choice to illustrate the efficiency of the method.

2.2 Choosing time lag

According to Mañé and Takens [20,21], any time lag will be acceptable is not terribly useful for extracting physics from data. If t is chosen too small, then the coordinates s(n + jt) and s(n + (j + 1)t) are so close to each other in numerical value that they cannot be distinguished from each other. Similarly, if t is too large, then

s(n + jt) and s(n + (j + 1)t) are completely independent of each other in a statistical sense. Also, if t is too small or too large, then the correlation dimension of attractor can be under- or overestimated respectively [7]. It is therefore necessary to choose some intermediate (and more appropriate) position between above cases. First approach is to compute the linear autocorrelation function

$$C_L(\delta) = \frac{\frac{1}{N}\sum_{m=1}^{N}[s(m+\delta)-\bar{s}][\,s(m)-\bar{s}]}{\frac{1}{N}\sum_{m=1}^{N}[s(m)-\bar{s}]^2}, \tag{2}$$

where

$$\bar{s} = \frac{1}{N}\sum_{m=1}^{N} s(m)$$

and to look for that time lag where C_L(d) first passes through zero. This gives a good hint of choice for t at that $s(n + j\mathrm{t})$ and $s(n + (j + 1)\mathrm{t})$ are linearly independent. However, a linear independence of two variables does not mean that these variables are nonlinearly independent since a nonlinear relationship can differs from linear one. It is therefore preferably to utilize approach with a nonlinear concept of independence, e.g. the average mutual information. Briefly, the concept of mutual information can be described as follows [5,7,13]. Let there are two systems, A and B, with measurements a_i and b_k. The amount one learns in bits about a measurement of a_i from measurement of b_k is given by arguments of information theory [5]

$$I_{AB}(a_i,b_k) = \log_2\left(\frac{P_{AB}(a_i,b_k)}{P_A(a_i)P_B(b_k)}\right), \tag{3}$$

where the probability of observing a out of the set of all A is $P_A(a_i)$, and the probability of finding b in a measurement B is $P_B(b_i)$, and the joint probability of the measurement of a and b is $P_{AB}(a_i, b_k)$. The mutual information I of two measurements a_i and b_k is symmetric and non-negative, and equals to zero if only the systems are independent. The average mutual information between any value a_i from system A and b_k from B is the average over all possible measurements of $I_{AB}(a_i, b_k)$,

$$I_{AB}(\tau) = \sum_{a_i,b_k} P_{AB}(a_i,b_k) I_{AB}(a_i,b_k) \tag{4}$$

To place this definition to a context of observations from a certain physical system, let us think of the sets of measurements $s(n)$ as the A and of the measurements a time lag t later, $s(n + \mathrm{t})$, as B set. The average mutual information between observations at n and $n + \mathrm{t}$ is then

$$I_{AB}(\tau) = \sum_{a_i,b_k} P_{AB}(a_i,b_k) I_{AB}(a_i,b_k) \tag{5}$$

Now we have to decide what property of I(t) we should select, in order to establish which among the various values of t we should use in making the data vectors $\mathbf{y}(n)$. In ref. [13] it has been suggested, as a prescription, that it is necessary to choose that t where the first minimum of I(t) occurs. On the other hand, the autocorrelation coefficient failed to achieve zero, i.e. the autocorrelation function analysis not provides us with any value of t. Such an analysis can be certainly extended to values exceeding 1000, but it is known that an attractor cannot be adequately reconstructed for very large values of t. The mutual information function usually [5] exhibits an initial rapid decay (up to a lag time of about 10) followed more slow decrease before attaining near-saturation at the first minimum.

One could remind that the autocorrelation function and average mutual information can be considered as analogues of the linear redundancy and general redundancy, respectively, which was applied in the test for nonlinearity. If a time series under consideration have an n-dimensional Gaussian distribution, these statistics are theoretically equivalent as it is shown in Ref. [22]. The general redundancies detect all dependences in the time series, while the linear redundancies are sensitive only to linear structures. Further, a possible nonlinear nature of process resulting in the vibrations amplitude level variations can be concluded.

2.3 Choosing embedding dimension. Correlation integral

The goal of the embedding dimension determination is to reconstruct a Euclidean space R^d large enough so that the set of points d_A can be unfolded without ambiguity. In accordance with the embedding theorem, the embedding dimension, d_E, must be greater, or at least equal, than a dimension of attractor, d_A, i.e. $d_E > d_A$. In other words, we can choose a fortiori large dimension d_E, e.g. 10 or 15, since the previous analysis provides us prospects that the dynamics of our system is probably chaotic. However, two problems arise with working in dimensions larger than really required by the data and time-delay embedding [1,7,13,19]. First, many of computations for extracting interesting properties from the data require searches and other operations in R^d whose computational cost rises exponentially with d. Second, but more significant from the physical point of view, in the presence of noise or other high dimensional contamination of the observations, the extra dimensions are not populated by dynamics, already captured by a smaller dimension, but entirely by the contaminating signal. In too large an embedding space one is unnecessarily spending time working around aspects of a bad representation of the observations which are solely filled with noise. It is therefore necessary to determine the dimension d_A.

There are several standard approaches to reconstruct the attractor dimension (see, e.g., [1,7,23]), but let us consider in this study two methods only. The correlation integral analysis is one of the widely used techniques to investigate the signatures of chaos in a time series. The analysis uses the correlation integral, $C(r)$, to distinguish between chaotic and stochastic systems. To compute the correlation integral, the algorithm of Grassberger and Procaccia [23] is the most commonly used approach. According to this algorithm, the correlation integral is

$$C(r) = \lim_{N\to\infty} \frac{2}{N(n-1)} \sum_{\substack{i,j \\ (1\le i<j\le N)}} H\left(r - \| \mathbf{y}_i - \mathbf{y}_j \|\right) \qquad (6)$$

where H is the Heaviside step function with $H(u) = 1$ for $u > 0$ and $H(u) = 0$ for $u \le 0$, r is the radius of sphere centered on $\mathbf{y}_i$ or $\mathbf{y}_j$, and N is the number of data measurements. If the time series is characterized by an attractor, then the integral $C(r)$ is related to the radius r given by

$$d = \lim_{\substack{r\to 0 \\ N\to\infty}} \frac{\log C(r)}{\log r}, \qquad (7)$$

where d is correlation exponent that can be determined as the slop of line in the coordinates log $C(r)$ versus log r by a least-squares fit of a straight line over a certain range of r, called the scaling region.

If the correlation exponent attains saturation with an increase in the embedding dimension, then the system is generally considered to exhibit chaotic dynamics. The saturation value of the correlation exponent is defined as the correlation dimension (d_2) of the attractor. The nearest integer above the saturation value provides the minimum or optimum embedding dimension for reconstructing the phase-space or the number of variables necessary to model the dynamics of the system. On the other hand, if the correlation exponent increases without bound with increase in the embedding dimension, the system under investigation is generally considered stochastic. There are certain important limitations in the use of the correlation integral analysis in the search for chaos. For instance, the selection of inappropriate values for the parameters involved in the method may result in an underestimation (or overestimation) of the attractor dimension [24]. Consequently, finite and low correlation dimensions could be observed even for a stochastic process. To verify the results obtained by the correlation integral analysis, we use surrogate data method.

The method of surrogate data [1,7,19] is an approach that makes use of the substitute data generated in accordance to the probabilistic structure underlying the original data. This means that the surrogate data possess some of the properties, such as the mean, the standard deviation, the cumulative distribution function, the power spectrum, etc., but are otherwise postulated as random, generated according to a specific null hypothesis. Here, the null hypothesis consists of a

candidate linear process, and the goal is to reject the hypothesis that the original data have come from a linear stochastic process. One reasonable statistics suggested by Theiler et al. [24] is obtained as follows. If we denote Q_{orig} as the statistic computed for the original time series and Q_{si} for ith surrogate series generated under the null hypothesis and let m_s and s_s denote, respectively, the mean and standard deviation of the distribution of Q_s, then the measure of significance S is given by

$$S = \frac{|Q_{orig} - \mu_s|}{\sigma_s}. \tag{8}$$

An S value of ~2 cannot be considered very significant, whereas an S value of ~10 is highly significant. To detect nonlinearity in the amplitude level data, the one hundred realizations of surrogate data sets were generated according to a null hypothesis in accordance to the probabilistic structure underlying the original data. Often, a significant difference in the estimates of the correlation exponents, between the original and surrogate data sets, can be observed. In the case of the original data, a saturation of the correlation exponent is observed after a certain embedding dimension value (i.e., 6), whereas the correlation exponents computed for the surrogate data sets continue increasing with the increasing embedding dimension. The high significance values of the statistic indicate that the null hypothesis (the data arise from a linear stochastic process) can be rejected and hence the original data might have come from a nonlinear process. It is worth consider another method for determining d_E that comes from asking the basic question addressed in the embedding theorem: when has one eliminated false crossing of the orbit with itself which arose by virtue of having projected the attractor into a too low dimensional space? By examining this question in dimension one, then dimension two, etc. until there are no incorrect or false neighbours remaining, one should be able to establish, from geometrical consideration alone, a value for the necessary embedding dimension. Such an approach was originally described by Kennel et al. [6]. Advanced version is presented in Ref. [16]

2.4 Lyapunov exponents

The LE are the dynamical invariants of the nonlinear system. In a general case, the orbits of chaotic attractors are unpredictable, but there is the limited predictability of chaotic physical system, which is defined by the global and local LE [7,25-29]. A negative exponent indicates a local average rate of contraction while a positive value indicates a local average rate of expansion. In the chaos theory, the spectrum of LE is considered a measure of the effect of perturbing the initial conditions of a dynamical system. Note that both positive and negative LE can coexist in a dissipative system, which is then chaotic. Since the LE are defined as asymptotic average rates, they are independent of the initial conditions, and therefore they do comprise an invariant measure of attractor. In fact, if one manages to derive the whole spectrum of the LE, other invariants of the system, i.e. Kolmogorov entropy and attractor's dimension can be found. The Kolmogorov entropy, K, measures the average rate at which information about the state is lost with time. An estimate of this measure is the sum of the positive LE. The inverse of the Kolmogorov entropy is equal to an average predictability. Estimate of dimension of the attractor is provided by the Kaplan and Yorke conjecture:

$$d_L = j + \frac{\sum_{\alpha=1}^{j} \lambda_\alpha}{|\lambda_{j+1}|}, \tag{9}$$

where j is such that $\sum_{\alpha=1}^{j} \lambda_\alpha > 0$ and $\sum_{\alpha=1}^{j+1} \lambda_\alpha < 0$, and the LE λ_a are taken in descending order. There are a few approaches to computing the LE. One of them computes the whole spectrum and is based on the Jacobi matrix of system [27]. In the case where only observations are given and the system function is unknown, the matrix has to be estimated from the data. In this case, all the suggested methods approximate the matrix by fitting a local map to a sufficient number of nearby points. In our work we use the method with the linear fitted map proposed by Sano and Sawada [27], although the maps with higher order polynomials can be also used. To calculate the spectrum of the

LE from the amplitude level data, one could determine the time delay t and embed the data in the four-dimensional space. In this point it is very important to determine the Kaplan-Yorke dimension and compare it with the correlation dimension, defined by the Grassberger-Procaccia algorithm. The estimations of the Kolmogorov entropy and average predictability can further show a limit, up to which the amplitude level data can be on average predicted.

3. Chaotic elements in dynamics of quantum and laser systems: Some illustrations

3.1. Non-linear analysis of chaotic oscillations in a grid of quantum generators

As the first illustration we present results of non-linear analysis of the chaotic oscillations in a grid o two autogenerators. Its regular and chaotic dynamics has been in details studied in many papers (see e.g. [2,14,31]. In Ref.[2] the time series for the characteristic vibration amplitude are presented in a case of two semiconductors lasers connected through general resonator. We use these data as input ones in the non-linear analysis of chaotic oscillations. Figure 1 presents the variations of the autocorrelation coefficient for the amplitude level. Autocorrelation function exhibits some kind of exponential decay up to a lag time of about 100 time units (sec).

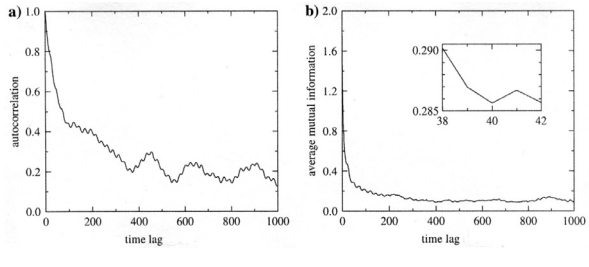

Figure 1. (a) Autocorrelation function and (b) average mutual information

Such an exponential decay can be an indication of the presence of chaotic dynamics in the process of the level variations. The autocorrelation coefficient failed to achieve 0, i.e. autocorrelation function analysis not provides with any value of t. Such an analysis can be certainly extended to values exceeding 1000, but it is known that an attractor cannot be adequately reconstructed for very large values of t. Figure 2 shows the relationship between the correlation exponent values and the embedding dimension values for original data set and mean values of the surrogate data sets as well as for one surrogate realization. Saturation value of the correlation exponent, i.e. correlation dimension of attractor, for the amplitude level series is about 3.5 and occurs at the embedding dimension value of 6. The low, non-integer correlation dimension value indicates the existence of low-dimensional chaos in the vibrations dynamics of the autogenerators. The dimension of the embedding phase-space is equal to the number of variables present in the evolution of the system dynamics. Our study indicate that to model the dynamics of process resulting in the amplitude level variations the minimum number of variables essential is equal to 4 and the number of variables sufficient is equal to 6.. To verify the results obtained by the correlation integral analysis, we use surrogate data method. It is method that makes using substitute data generated in accordance to probabilistic structure underlying the original data.

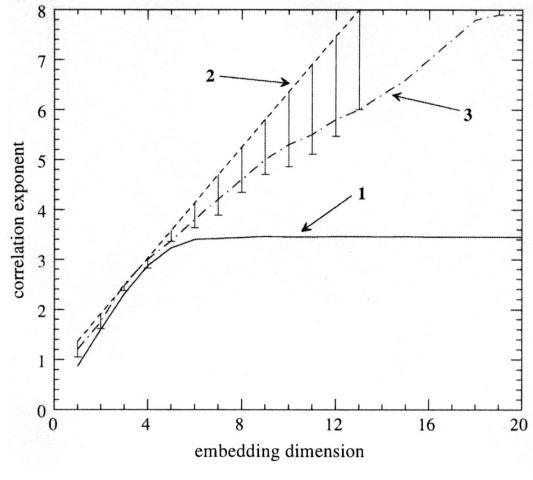

Figure 2. Relationship between correlation exponent and embedding dimension for vibrations amplitude level data for original time series (line 1), mean values of surrogate data sets (line 2), and one surrogate realization (line 3). Error bars indicate minimal values of correlation exponent among all realizations of surrogate data.

The surrogate data possess some of the properties, such as the mean, the standard deviation, the cumulative distribution function, the power spectrum, etc., but are otherwise postulated as random, generated according to a specific null hypothesis. The significance values (*S*) of correlation exponent are computed for each embedding dimension. The high significance values of the statistic indicate that the null hypothesis (the data arise from a linear stochastic process) can be rejected and hence the original data might have come from a nonlinear process. Figure 3 displays the percentage of false nearest neighbours that was determined for the amplitude level series, for phase-spaces reconstructed with embedding D from 1 to 20.

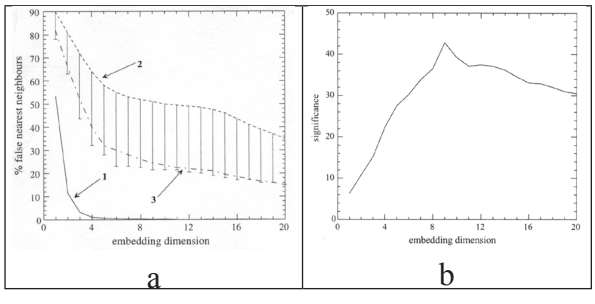

Figure 3. (a) Relationship between significance values of correlation dimension and embedding dimension; (b) Embedding dimension estimation by false nearest neighbour method for amplitude level data for original t series (line 1), mean values of surrogate data sets (2), one surrogate realization (3). Error bars show min % of false nearest neighbour among all realizations of surrogate data.

The percentage drops to almost zero at 4 or 5. This indicates that a 4- or 5-D phase-space is necessary to represent the dynamics (or unfold the attractor) of the amplitude level series. The mean percentage of false nearest neighbours computed for the surrogate data sets decreases steadily but at 20 is about 35%. Such a result seems to be in close agreement with that was obtained from the correlation integral analysis, providing further support to the observation made.

3.2. Non-linear analysis of chaotic self-oscillations in a laser system with absorbing cell

Here we consider a chaotic dynamics of a single-mode laser with the nonlinear absorption cell. This system can be used for the experimental observation of dynamic chaos. We consider a theoretical model of a single-mode laser resonator in which the reinforcement is placed along with a nonlinear absorbing medium. Each of the environments consists of identical two-level atoms. The gain and absorption lines are uniformly broadened and their centers align and coincide with one of the frequencies of the cavity. Such a model can describe the real system of five differential equations [31]:

$$\begin{aligned} de/d\tau &= -e + p_1 + p_2, \\ dp_1/d\tau &= -\delta_1(p_1 + em_1), \\ dp_2/d\tau &= -\delta_2(p_2 + em_2), \\ dm_1/d\tau &= -\rho_1(m_1 - m_{01} - ep_1), \\ dm_2/d\tau &= -\rho_2(m_2 - m_{02} - \beta ep_2). \end{aligned} \qquad (10)$$

Here, the index 1 refers to intensify, and the index of 2 - to an absorbing medium; e, p_1, p_2, m_1, m_2 are the dimensionless variables, e is an amplitude of the laser of the field, p_k is a polarization in the environment, m_k is the difference between the populations of the working levels; p_k and d_k are, respectively, the longitudinal and transverse relaxation rate, related to the half-width of the resonator $dw_p/2$, k=1,2; m_{0k} is the difference between the populations of the working levels in the absence of generation ($m_{01}<0$, $m_{02}>0$), b -the ratio of the coefficients of saturation of the absorbing and amplifying media; $t=tdw_p/2$ is the dimensionless time. Attractor of the system can be as invariant with respect to this change (let's call this attractor "symmetrical") and non-invariant ("asymmetric"). In the latter case certainly, there are two attractor into each other after this change. In fig. 4 we present the results of the numerical simulation for the system (10) [31].

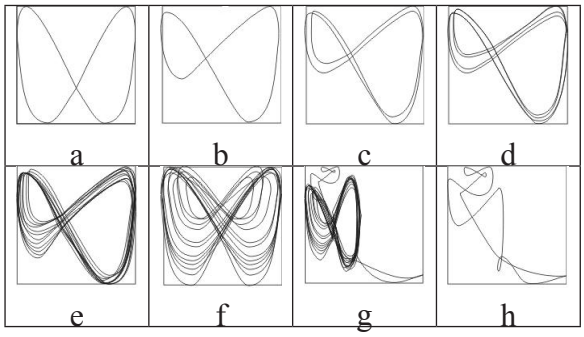

Figure 4. Projections of the phase trajectories for different values of the parameter h: a - 1.7000, b - 1.8200, c - 1.8350, d - 1.8385, e - 1.8500, f - 1.8800, g - 1.9000, h – 1.9500

Strange attractors occur as a result of the sequence of bifurcations of solutions of (10), the first of which is the Hopf bifurcation of stationary solutions with zero intensity of the laser field. This bifurcation occurs when $\eta = \delta_2[1 + (\delta_2)(1 + \delta_1 + m_{02})/\delta_1(1 + \delta_1)]$, if $h<m_{02}$. Our analysis shows that the Hopf bifurcation occurs at moderate values h, if the relative width of the absorption line d_2 is quite small, and the relative width of the gain line d_1 is quite large. The numerical calculation shows that in order to get the chaotic lasing it is necessary the following: to saturate the absorber should be saturated stronger than the amplifier (b>1). At low b the limit cycles generated from the stationary solutions with the zeroth intensity is stable up to very large values of h. In table 1 we present the computed values of the LE l_1-l_6 in the descending order and the Kolmogorov entropy (K). Another important illustration is non-linear analysis of the chaotic self-ocsillations in the backward wave tube (device for generating electromagnetic vibrations of the HF range.)

In Refs.[2] there have been presented the temporal dependences of the output signal amplitude, phase portraits, statistical quantifiers for a weak chaos arising via period-doubling cascade of self-modulation and for developed chaos at large values of the dimensionless length parameter.

Table 1

Numerical parameters of the chaotic regimes in a 1-mode laser with absorbing cell: l_1-l_6 are the Lyapunov exponents in descending order, K – Kolmogorov entropy (our data)

Regime	λ_1	λ_2	λ_3
Weak chaos	0.175	-0.0001	–0.0003
Strong chaos	0.542	0.203	-0.0001
Regime	λ_4	λ_5	λ_6
Weak chaos	–0.244	–	–
Strong chaos	–0.0004	–0.067	–0.188

4. Conclusions

Here we present the results of computing nonlinear chaotic dynamics of some quantum and laser systems with using advanced techniques [8-17,30]. The correlation dimension method provided a low fractal-dimensional attractor thus suggesting a possibility of the existence of chaotic behaviour. The method of surrogate data, for detecting nonlinearity, provided significant differences in the correlation exponents between the original data series and the surrogate data sets. This finding indicates that the null hypothesis (linear stochastic process) can be rejected. It has been shown that the systems exhibit a nonlinear behaviour with elements of a low-dimensional chaos. The LE analysis does support this conclusion.

In conclusion the author would like to thank Prof. A. Glushkov for very helpful discussions and advices.

References

1. H.Abarbanel, R.Brown, J.Sidorowich and L.Tsimring, Rev.Mod.Phys. (1993) 5, 1331.
2. A.Vedenov, A.Ezhov and E. Levchenko,

in Non-linear waves. Structure and bifurcations, ed. by A. Gaponov-Grekhov and M. Rabinovich, (Nauka, Moscow, 1997), pp.53-69.
3. M. Gutzwiller, Chaos in Classical and Quantum Mechanics (N.-Y., Springer, 1999), 720 p.
4. E. Ott, Chaos in dynamical systems, (Cambridge: Cambridge Univ.Press, 2002), 490p.
5. R. Gallager, Information theory and reliable communication (N.-Y.,Wiley, 1986).
6. D. Ullmo, Rep. Prog. Phys. 71, 026001 (2008).
7. A.V. Glushkov, Modern theory of a chaos, (Odessa, Astroprint, 2008), 450p.
8. A. Glushkov, O. Khetselius, S. Brusentseva, P. Zaichko and V. Ternovsky, in Adv. in Neural Networks, Fuzzy Systems and Artificial Intelligence, Series: Recent Adv. in Computer Engineering, vol. 21, ed. by J.Balicki (WSEAS, Gdansk, 2014), pp.69-75.
9. A. Glushkov, A. Svinarenko, V. Buyadzhi, P. Zaichko and V. Ternovsky, in: Adv.in Neural Networks, Fuzzy Systems and Artificial Intelligence, Series: Recent Adv. in Computer Engineering, vol.21, ed. by J.Balicki (WSEAS, Gdansk, 2014), pp.143-150.
10. A.V. Glushkov, O.Yu. Khetselius, A.A. Svinarenko, G.P. Prepelitsa, Energy approach to atoms in a Laser Field and Quantum Dynamics with Laser Pulses of Different Shape, In: Coherence and Ultrashort Pulsed Emission, ed. by F.J. Duarte (Intech, Vienna, 2011), 101-130.
11. A.V. Glushkov, V.N. Khokhlov, I.A. Tsenenko, Atmospheric teleconnection patterns: wavelet analysis, Nonlin. Proc.in Geophys. 11, 285 (2004).
12. A.V. Glushkov, V.N. Khokhlov, N.S. Loboda, N.G. Serbov, K. Zhurbenko, Stoch. Environ. Res. Risk Assess. (Springer) 22, 777 (2008).
13. A.V. Glushkov, V.N. Khokhlov, N.S. Loboda, Yu.Ya. Bunyakova, Atm. Environment (Elsevier) 42, 7284 (2008).
14. A. Glushkov, Y. Bunyakova, A. Fedchuk, N. Serbov, A. Svinarenko and I. Tsenenko, Sensor Electr. and Microsyst. Techn. 3(1), 14 (2007).
15. A.V. Glushkov, V. Kuzakon, V. Ternovsky and V. Buyadzhi, in: Dynamical Systems Theory, vol.T1, ed by J. Awrejcewicz, M. Kazmierczak, P. Olejnik, and J. Mrozowski (Lodz, Polland, 2013), P.461-466.
16. A.V.Glushkov, G. Prepelitsa, A. Svinarenko and P. Zaichko, in: Dynamical Systems Theory, vol.T1, ed by J. Awrejcewicz, M. Kazmierczak, P. Olejnik, and J. Mrozowski (Lodz, Polland, 2013), pp.P.467-487.
17. E. N. Lorenz, Journ. Atm. Sci. 20, 130 (1993).
18. N. Packard, J. Crutchfield, J. Farmer and R. Shaw, Phys.Rev.Lett. 45, 712 (1998).
19. M. Kennel, R. Brown and H. Abarbanel, Phys.Rev.A. 45, 3403 (1992).
20. F. Takens in: Dynamical systems and turbulence, ed by D. Rand and L. Young (Springer, Berlin, 1991), pp.366–381
21. R. Mañé, in: Dynamical systems and turbulence, ed by D. Rand and L. Young (Springer, Berlin, 1999), pp.230–242.
22. M. Paluš, E.Pelikán, K. Eben, P. Krejčíř and P. Juruš, in: Artificial Neural Nets and Genetic Algorithms, ed. V. Kurkova (Springer, Wien, 2001), pp. 473-476.
23. P. Grassberger and I. Procaccia, Physica D. 9, 189 (1993).
24. J. Theiler, S. Eubank, A. Longtin, B. Galdrikian, J. Farmer, Phys.D. 58, 77 (1992).
25. A. Fraser and H. Swinney, Phys Rev A. 33, 1134 (1996).
26. J. Havstad and C. Ehlers, Phys.Rev.A. 39, 845 (1999).
27. M. Sano and Y. Sawada, Phys Rev.Lett., 55, 1082 (1995).
28. T. Schreiber, Phys.Rep. 308, 1 (1999).

29. H. Schuste, Deterministic Chaos: An Introduction (Wiley, N.-Y., 2005), 312 p.
30. A. Glushkov, G. Prepelitsa, S. Dan'kov, V. Polischuk and A. Efimov, Journ. Tech. Phys. 38, 219 (1997).
31. A.G. Vladimirov and E.E. Fradkin, Optics and Spectr. 67, 219 (1999).
32. S.P. Kuznetsov and D.I. Trubetskov, Izv. Vuzov. Ser. Radiophys. 48, 1 (2004).

This article has been received within 2014

UDC 541.13

G. P. Prepelitsa

NONLINEAR DYNAMICS OF QUANTUM AND LASER SYSTEMS WITH ELEMENTS OF A CHAOS

Abstract Nonlinear chaotic dynamics of the quantum and laser systems is studied with using advanced techniques such as a wavelet analysis, multi-fractal formalism, mutual information approach, correlation integral analysis, false nearest neighbour algorithm, the Lyapunov exponent's analysis, and surrogate data method. The detailed analysis of the oscillations in a grid of two autogenerators and single-mode laser with the nonlinear absorption cell shows that the systems exhibit a nonlinear behaviour with elements of a low-dimensional chaos.

Key words: Quantum and laser systems -chaos -non-linear analysis

УДК 541.13

Г. П. Препелица

НЕЛИНЕЙНАЯ ДИНАМИКА КВАНТОВЫХ И ЛАЗЕРНЫХ СИСТЕМ С ЭЛЕМЕНТАМИ ХАОСА

Резюме

Изучается нелинейные хаотическая динамика квантовых и лазерных систем с использованием техники нелинейного анализа, включающей вейвлет-анализ, мульти-фрактальный формализм, метод взаимной информации, метод корреляционного интеграла, алгоритм ложных ближайших соседей, метод показателей Ляпунова, метод суррогатных данных и др. Детальный анализ осцилляций в системе двух автогенераторов и одномодового лазера с нелинейной поглощающей ячейкой показывает, что в динамике указанных систем имеет место нелинейное поведение с элементами низко-размерного хаоса.

Ключевые слова: Квантовые и лазерные систем, хаос, нелинейный анализ

УДК 541.13

Г. П. Препелица

НЕЛІНІЙНА ДИНАМІКА КВАНТОВИХ І ЛАЗЕРНИХ СИСТЕМ З ЕЛЕМЕНТАМИ ХАОСА

Резюме

Вивчається нелінійні хаотична динаміка квантових і лазерних систем з використанням техніки нелінійного аналізу, що включає вейвлет-аналіз, мульті-фрактальний формалізм, метод взаємної інформації, метод кореляційного інтеграла, алгоритм помилкових найближчих сусідів, метод показників Ляпунова, метод сурогатних даних і ін. Докладний аналіз осциляцій в системі двох автогенераторів і одномодового лазеру з нелінійною поглинаючою коміркою показує, що в динаміці вказаних систем має місце нелінійна поведінка з елементами низько-розмірного хаосу.

Ключові слова: Квантові та лазерні систем, хаос, нелінійний аналіз

PACS: 73.20.Hb, 73.25.+I; UDC 621.315.592

O. O. Ptashchenko[1], F. O. Ptashchenko[2], V, R.Gilmutdinova[1]

EFFECT OF DEEP CENTERS ON THE TIME-RESOLVED SURFACE CURRENT INDUCED BY AMMONIA MOLECULES ADSORPTION IN GaAs P-N JUNCTIONS

[1]I. I. Mechnikov National University of Odessa, Dvoryanska St., 2, Odessa, 65026, Ukraine
[2]Odessa National Maritime Academy, Odessa, Didrikhsona St., 8, Odessa, 65029, Ukraine

The time-dependence of the surface current in GaAs p-n structures after placing in concentrated wet ammonia vapors was studied. It is sown that the slope of measured current-time curves is non-monotonous. This effect is explained with taking into account presence of deep surface levels, which are filled, when the quasi-Fermi level is moving to the conduction band. An analysis of time-resolved measurements of surface current in GaAs p-n structures in wet ammonia vapors enabled to estimate depths of some surface levels. The depths of the main revealed surface levels are 0,206 eV, 0,185 eV, and 0,176 eV from c-band. In the interval of depths 0,176 eV – 0,185 eV surface levels are continuously distributed with practically constant density.

1. INTRODUCTION

P-n junctions as gas-sensitive devices [1, 2] have some advantages in comparison with structures, based on oxide polycrystalline films [3, 4] and Shottky diodes [5, 6]. P-n junctions have high potential barriers for current carriers, which results in low background currents. Sensors on p-n junctions [1, 2] have crystal structure, high sensitivity at room temperature. The lowest size of these sensors in a classical variant is limited by the space-charge layer thickness and is of the order of 100 nm.

The mostly interesting for gas sensors on p-n junction are Si and GaAs. The gas sensitivity of GaAs p-n junctions is remarkably higher than that of Si sensors, due to higher electron mobility [1, 2, 7, 8].

GaAs p-n junctions as ammonia vapors sensors have a non-monotonous dependence of the sensitivity to the NH_3 partial pressure due to deep surface centers. This dependence was used for an estimation of corresponding levels depth [9].

The aim of this work is to study the influence of deep surface centers on the time-dependence of the surface current in GaAs p-n structures in ammonia vapors.

2. EXPERIMENT

The measurements were carried out on GaAs p-n structures, described in the previous paper [9]. The junctions were treated by durable exposure in wet ammonia vapors under an NH_3 partial pressure of 12 kPa. *I-V* characteristics of the forward and reverse currents were measured in air with various concentrations of ammonia vapors. The time-dependence of the surface current and the open-circuit voltage was analyzed in ammonia vapors.

Fig.1 represents the time-dependence of the direct current in a p-n structure at V=0,3 Volts after placing in wet ammonia vapors with an NH_3 partial pressure of 12 kPa.

It is seen that the slope of $I(t)$ curve non-monotonously changes with the time. The characteristic changes in the slope occur practically at the same currents in different samples.

The current-dependence of $I(t)$ derivative, obtained from the curve in fig. 1, is presented in fig. 2. Curve $dI/dt(I)$ has distinct minimums at current values of 1,086 μA, 2,386 μA, and 3,353 μA. The values for different samples differ mostly by

5%. The presence of these minimums can be explained by filling of deep surface centers in p-region due to electrical field of adsorbed ammonia molecules, which are donors in GaAs.

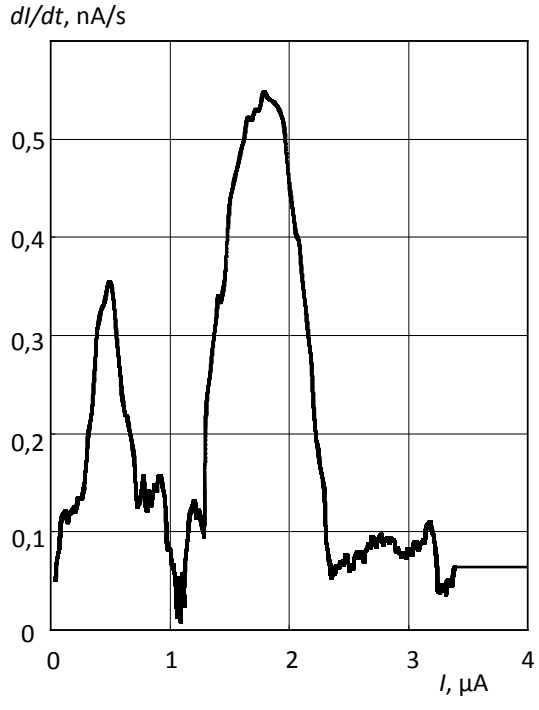

Fig. 1. Current-dependence of dI/dt, obtained from the curve I(t) in fig. 1.

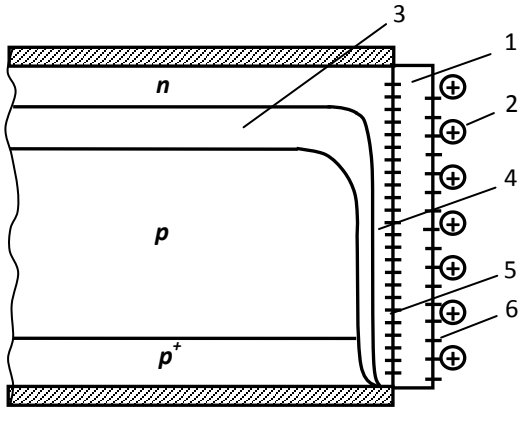

Fig 2. Schematic of a p-n structure, placed in a donor gas: 1 – oxide layer; 2 – ions; 3 – depletion layer; 4 – conducting channel; 5 – surface (fast) centers; 6 – states on the oxide surface (slow centers).

3. DISCUSSION

The experimental results can be explained with the model, depicted in fig. 2. Ionized ammonia molecules 2 are located on the natural oxide surface. Their electric field bend the depletion layer 3 and forms a n- conducting channel 4. After adsorption and ionization of donor molecules the slow centers are filling and after that electrons are captured by fast centers. And only after filling of surface centers the surface depletion layer is widened and the n-channel is forming. During this process the Fermi quasi-level for electrons is moving to the conduction band. In a quasi-stationary approach the electrons surface concentration is defined as

$$n_S = N_c \exp\left[-(E_c - F_n)/(kT)\right], \qquad (1)$$

where N_c is the effective states density in C-band; $E_c - F_n$ is the quasi-Fermi level depth; kT is the Boltzmann factor. And the number of electrons, captured on the surface centers can be calculated as

$$N_S^- = N_S \left\{\exp\left[(E_S - F_n)/(kT)\right] + 1\right\}^{-1}, \qquad (2)$$

where N_s is the density of surface traps; E_s is the corresponding energy level. From (1) and (2) follows that a minimum of dn/dN_S^- corresponds to the equality

$$F_n = E_S . \qquad (3)$$

If , in a limited time, $dN_S^-/dt \approx const$, equality (3) corresponds to minimum dn_s/dt , that corresponds to a minimum dI/dt. Therefore the minimums of curve $dI/dt(I)$ in fig. 2 correspond to crossing the related deep surface levels by the quasi-Fermi level. The minimums of curve $dI/dt(I)$ at current values of 1,086 μA, 2,386 μA, and 3,353 μA yield estimations of surface levels depths 0,206 eV, 0,185 eV and 0,176 eV, respectively.

In the current interval 2,3 – 3,3 μA, that corresponds to

$$0{,}206 \text{ eV} > E_c - F_n > 0{,}176 \text{ eV}, \qquad (4)$$

curve $I(t)$ has a linear section, that corresponds to constant surface states density in the depths interval

$$0{,}206 \text{ eV} > E_c - E_S > 0{,}176 \text{ eV} \cdot \qquad (5)$$

The obtained surface levels depths are in agreement with results of previous work [9], where the corresponding estimations were made by an analysis of the dependence of gas sensitivity of GaAs p-n junctions on the ammonia partial pressure.

The surface level with a depth of 0,18 eV was observed with the method of deep levels transient spectroscopy in the GaAs natural oxide layer [10]. This level is one of the main deep levels in the natural oxide layer on GaAs crystals and its concentration increases at a treatment in oxygen plasma [10]. The electrons capture by this level reduces the gas sensitivity of GsAs p-n junctions [9].

4. CONCLUSIONS

The time-dependence of the surface current in GaAs p-n structures after placing in concentrated wet ammonia vapors has a non-monotonous slope. This effect is explained with taking into account presence of deep surface levels, which are filled, when the quasi-Fermi level is moving to the conduction band.

Time-resolved measurements of surface current in GaAs p-n structures in wet ammonia vapors enable to estimate depths of some surface levels. These estimates are in a good agreement with the results of previous works, obtained with different methods.

The surface level in p-GaAs of a depth of 0,18 eV, which is responsible for the non-monotonous slope of $I(t)$ dependence, corresponds to a point defect in the natural oxide, that includes an oxygen atom.

REFERENCES

1. Ptashchenko O. O., Artemenko O. S., Ptashchenko F. O. Vliyanie gazovoi sredy na poverhnostnyi tok v p-n geterostrukturakh na osnove GaAs-AlGaAs // Fisika i khimiya tverdogo tila. – 2001. – V. 2, № 3. – P. 481 – 485.
2. Ptashchenko O. O., Artemenko O. S., Ptashchenko F. O. Vplyv pariv amiaku na poverkhnevyi strum v p-n perekhodakh na osnovi napivprovidnykiv A^3B^5 // Journal of physical studies. – 2003. – V. 7, №4. – P. 419 – 425.
3. Bugayova M. E., Koval V. M., Lazarenko B. I. et al. Gazovi sensory na osnovi oksydu tsynku (oglyad) // Sensorna electronika i mikrosystemni tehnologii. – 2005. - №3. – P. 34 – 42.
4. Russhikh D.V., Rembeza S. I., Shironkin S. Yu. et al. Vysokochuvstvitel'nyi poluprovodnikovyi datchik gazovych sred // Sensors & Systems. 2008. – № 8. – P. 14 – 16.
5. Bomk O. I., Il'chenko L. G., Il'chenko V. V. et al. Pro pryrodu chutlyvosti do amiaku gazovykh sensoriv na osnovi struktur nadtonka tytanova plivka – kremniy // Ukr. fiz. journ. – 1999. – V. 44, №9. – P. 759 – 763.
6. Baluba V. I., Gritsyk V. Y., Davydova T. A. et al. Sensory ammiaka na osnove diodov Pd-n-Si // Fizika i tekhnika poluprovodnikov. – 2005. – V. 39, № 2. P. 285 – 288.
7. Ptashchenko F. O. Vplyv pariv amiaku na poverkhnevyi strum u kremniyevykh p-n perekhodakh // Ptashchenko F. O. Visnyk ONU, ser. Fizyka.– 2006. – V. 11, №. 7. – P. 116 – 119.
8. Ptashchenko O. O., Ptashchenko F. O., Yemets O. V. Effect of ammonia vapors on the surface current in silicon p-n junctions. // Photoelectronics. – 2006. – No. 16. – P. 89 – 93.
9. Ptashchenko O. O., Ptashchenko F. O., Gilmutdinova V. R. Vplyv poverkhnevogo leguvannya na charakterystyky p-n perekhodiv na osnovi GaAs yak gazovykh sensoriv // Sensorna elektronika i mikrosystemni tekhnologiyi. – 2013 – V. 10, № 1. – P. 114 – 123.
10. Fedorov Yu.Yu., Kharlamova T.S., Chikun V.V. Zavisimost' koncentracii glubokikh urovnei ot sposoba okisleniya poverkhnosti arsenida galliya // Elektronnaya tekhnika. Ser. SVCH-tekhnika. – 1993, No 2 (456). – P. 33-35.

This article has been received within 2014.

O. O. Ptashchenko, F. O. Ptashchenko, V, R.Gilmutdinova

EFFECT OF DEEP CENTERS ON THE TIME-RESOLVED SURFACE CURRENT INDUCED BY AMMONIA MOLECULES ADSORPTION IN GaAs P-N JUNCTIONS

Summary

The time-dependence of the surface current in GaAs p-n structures after placing in concentrated wet ammonia vapors was studied. It is sown that the slope of measured current-time curves is non-monotonous. This effect is explained with taking into account presence of deep surface levels, which are filled, when the quasi-Fermi level is moving to the conduction band. An analysis of time-resolved measurements of surface current in GaAs p-n structures in wet ammonia vapors enabled to estimate depths of some surface levels. The depths of the main revealed surface levels are 0,206 eV, 0,185 eV, and 0,176 eV from c-band. In the interval of depths 0,176 eV – 0,185 eV surface levels are continuously distributed with practically constant density.

Key words: surface current, p – n structure, deep centers.

О. О. Птащенко, Ф. О. Птащенк , В. Р. Гільмутдінова

ВПЛИВ ГЛИБОКИХ ЦЕНТРІВ НА КІНЕТИКУ ПОВЕРХНЕВОГО СТРУМУ, ІНДУКОВАНОГО АДСОРБЦІЄЮ МОЛЕКУЛ АМІАКУ В P-N ПЕРЕХОДАХ НА ОСНОВІ GaAs

Резюме

Досліджено кінетику поверхневого струму в p-n структурах на основі GaAs після їх поміщення у концентровані вологі пари аміаку. Показано, що нахил виміряних часових залежностей струму є немонотонний. Дане явище пояснено за врахуванням наявності глибоких поверхневих рівнів, які заповнюються, коли квазі-рівень Фермі рухається в сторону зони провідності. Аналіз кінетики поверхневого струму в p-n структурах на основі GaAs у вологих парах аміаку дав можливість оцінити глибини деяких поверхневих рівнів. Глибини основних виявлених поверхневих рівнів складають 0,206 еВ, 0,185 еВ і 0,176 еВ від с-зони. В інтервалі глибин 0,185 еВ – 0,176 еВ виявлено додаткові поверхневі рівні, розподілені неперервно з практично постійною щільністю.

Ключові слова: глибокі цунтри, p –n переходи, поверхневы центри.

А. А. Птащенко, Ф. А. Птащенко, В. Р. Гильмутдинова

ВЛИЯНИЕ ГЛУБОКИХ ЦЕНТРОВ НА КИНЕТИКУ ПОВЕРХНОСТНОГО ТОКА, ИНДУЦИРОВАННОГО АДСОРБЦИЕЙ МОЛЕКУЛ АММИАКА В P-N ПЕРЕХОДАХ НА ОСНОВЕ GaAs

Резюме

Исследована кинетика поверхностного тока в p-n структурах на основе GaAs после их помещения в концентрированные влажные пары аммиака. Показано, что наклон измеренных временных зависимостей тока немонотонный. Данное явление объяснено с учетом наличия глубоких поверхностных уровней, которые заполняются, когда квази-уровень Ферми движется в сторону зоны проводимости. Анализ кинетики поверхностного тока в p-n структурах на основе GaAs во влажных парах аммиака позволил оценить глубины некоторых поверхностных уровней. Глубины основных обнаруженных поверхностных уровней составдяют 0,206 эВ, 0,185 эВ и 0,176 эВ от с-зоны. В интервале глубин 0,185 эВ – 0,176 эВ обнаружены дополнительные поверхностные уровни, распределенные непрерывно с практически постоянной плотностью.

Ключевые слова глубокие центры, p – n –гетеропереход, поверхностные центры.

UDC 539.186

V. V. Velikodnaya[1], P. A. Kondratenko[2], Yu. M. Lopatkin[1], A. V. Glushkov[3], T. N. Sakun[2], O. A. Kovalenko[1]

[1]Sumy State University, 2, Rimsky-Korsakov Street, 40007, Sumy, Ukraine
e-mail: yu.lopatkin@gmail.com
[2]National Aviation University, 1, Komarov Ave, 03680 Kiev, Ukraine
[3]Odessa State Environmental University, 15, L'vovskaya str., 65016, Odessa, Ukraine
e-mail: dirac13@mail.ru

QUANTUM CHEMICAL STUDYING THE TRIMETHINE CYANINE DYE STRUCTURE AND RELAXATION DYNAMICS

Quantum-chemical studying polymethine dyes molecular structure and investigation of the relaxation processes of excitation have been carried out. Particularly, in the highly excited triplet state the dissociative surface exists, which corresponds to σ → σ*-excitation of the molecule; relaxation of excitations in the framework of this surface leads to dissociation of the molecule by lengthening the C-C bond of the molecule at the central carbon atom

1. Introduction

Studying polymethine dyes is of a great importance as from fundamental pointview as applied one. Really, they have wide opportunities for application (in dye lasers, in the processes of sensitization of the sensitivity of the silver halide materials, in biology and medicine as complexing agents and fluorescent labels for dyeing etc) due to their unique properties, among which stands out the photo sustainability, intensive fluorescence and absorption in the visible or infrared range of the spectrum, depending on the structure of the dye [1-3]. Moreover, it is of a great actuality development of the new types of polymethine dyes for the needs of the photophysical, chemical and photobiological application.

It is known [4-6], that the molecules of all dyes, without exception, excited by the light of the sufficiently high energy quanta, exhibit instability, as a result tissue lose their color and saturation under the influence of solar irradiation. This work is devoted to quantum-chemical studying polymethine dyes and further investigation of the relaxation processes of excitation in the polymethine dyes.

2. Object of study and research methodology

In this work it is investigated one of the representatives of polymethine dyes − dioksazoltrimetintsianin cation (I):

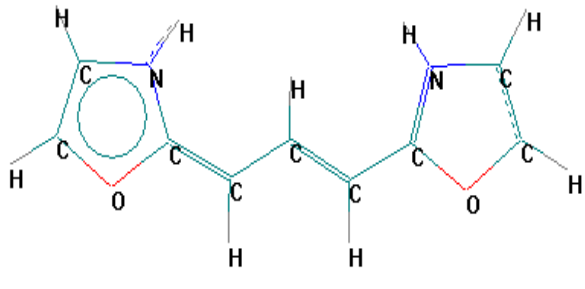

(I)

In the electrically neutral state, this molecule has one unpaired electron which makes it unstable. At the same time, the cationic form of the molecule exhibits stability in solution. As the anion ClO_4^- is often used. Since the molecule is dissociated in solution, we will not consider it in the calculations.

The quantum-chemical calculation methods were used for investigation, in particular AM1 method [7], which has established itself in the study of molecular relaxation of highly excited

states [4-6,8,9]. Since the polymethine dyes established itself resistant to light, we can conclude that the dissociative highly excited states are at sufficiently high energies. In that case, you need to sort several dozen of highly excited states, which is not always possible to make with a semi-empirical calculation methods. Therefore in the work as far as possible the simplest structure of the molecule was chosen to reach the selected target.

The molecule (I) has a symmetrical structure in the ground state, which is described by symmetry group C_{2v}. Its dissociation is possible only with lowering of symmetry. Therefore, we have investigated the dissociation of molecules by lengthening of the bond between the central carbon atom and the neighbouring carbon atom.

3. Results of the study

It is known [4-6] that each molecule has the dissociative energy surface responsible for dissociation of certain chemical bonds in the molecule. Usually the triplet state has a dissociative nature. With increasing of the bond length, which should dissociate, dissociative state becomes the lowest state of the molecule, as a result multiplicity of the molecule is changed from singlet to triplet. This principle underlies the search dissociative state in polymethine dye (I).

Indeed, with stretching of the bond C-C of 1Å (chemical bond between central carbon atom and its neighbor) it appeared that the triplet state has became the ground state of the molecule. So the molecular orbitals (MO) which are responsible for the creation of the dissociative state were found. When the length of the bond C-C is equal to 2,167Å these MO have a view:

As can be seen from these images, MO № 31 has a bonding character in relation to dissociating bond and MO № 33 − antibonding.

If we divide the molecule into two parts, we will see the kind of σ-MO, the interaction between them will lead to creating of the σ-MO which has been shown above :

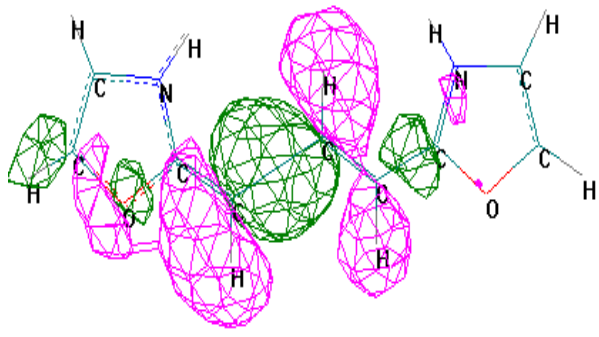

σ-MO № 31

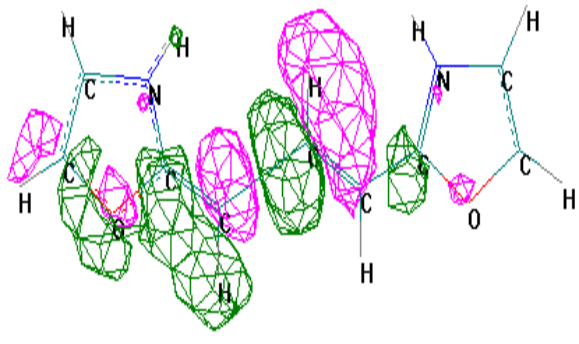

σ*-MO № 33.

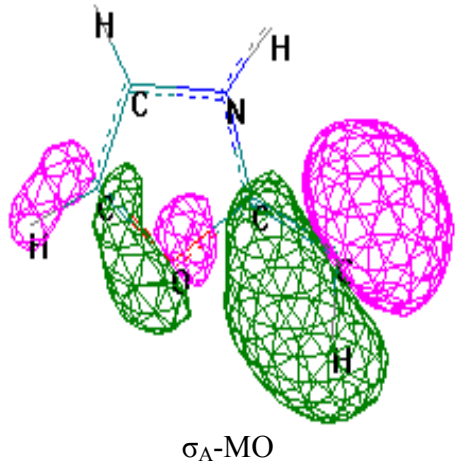

σ_A-MO

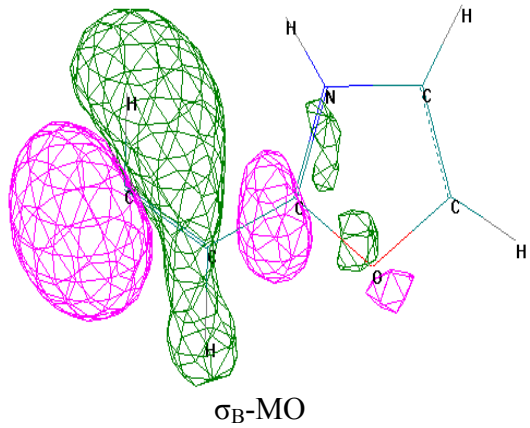

σ_B-MO

It is easy to see that:

$$\sigma = \sigma_A + \sigma_B,$$

$$\sigma^* = \sigma_A - \sigma_B.$$

Further, by reducing the length of the C-C-bond it can be found moving both σ-MO of other orbitals. It was found that at the equilibrium length of the C-C-bond (1,387 Å) σ-MO № 31 became the 29-th, and σ*-MO – № 41. Due to the interaction with other σ-MO their shape is essentially transformed:

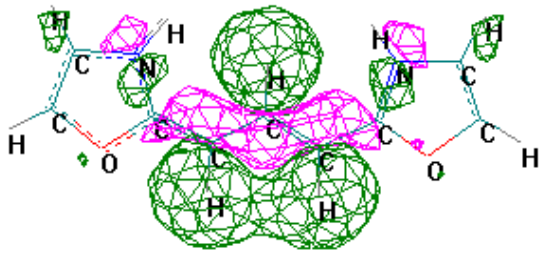

σ*-MO № 41

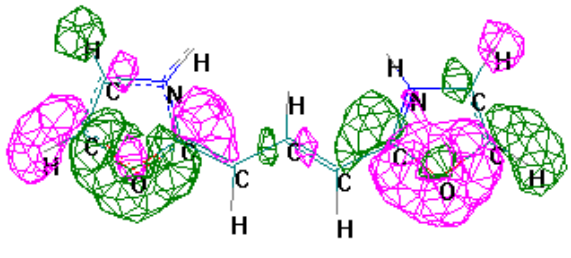

σ-MO № 29

First of these remains was localized at dissociating bonds, and the second was significantly modified.

If we define numbers of the selected MO for all distances, it will be easy to calculate the energy of the electronic system of the molecule in the ground and σ → σ *-excited state.

As for the equilibrium configuration the highest occupied molecular orbitals (HOMO) and lowest unoccupied (LUMO) molecular orbitals are π-MO and π *-MO, Figure 1 shows the position of configuration curves of the singlet and triplet excited states formed by π-MO.

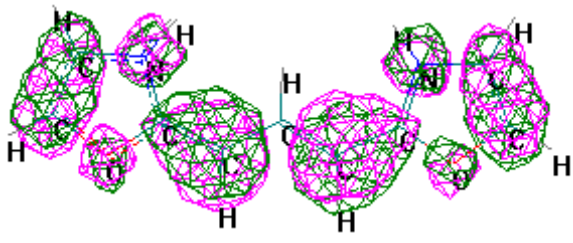

HOMO №33

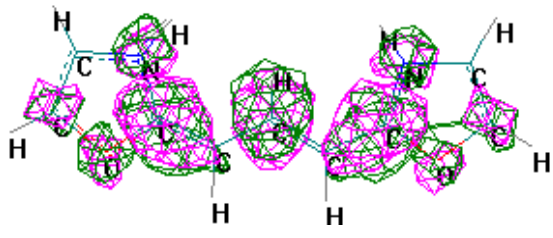

LUMO №34

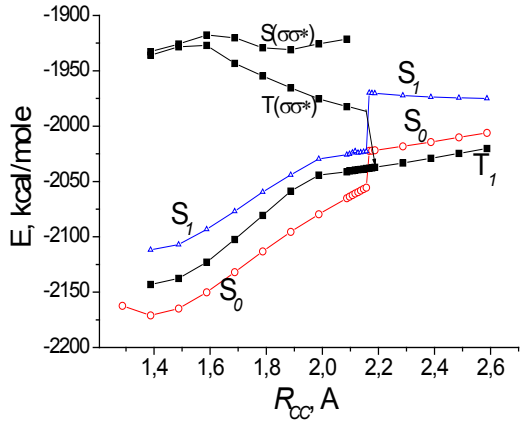

Figure 1. The dependence of the energy of the ground and excited states of molecules (I) of the length of the dissociating bond.

As can be seen from Figure 1, T(σσ*) is really a dissociative state. A new phenomenon is that with stretching of C-C-bond to 2,16Å the phase transition is observed in the electronic system of the molecule (I). As a result, the transition energy of the singlet state significantly increased, while the energy of the triplet state is almost unchanged. However, in the latter case, the nature of the triplet state has changed significantly.

Consider the sequence of occupied MOs after the phase transition. Antibonding σ *-MO took place of № 33, and π-HOMO was transformed and took place № 34. Now this MO was localized on the smaller fragment of the molecule:

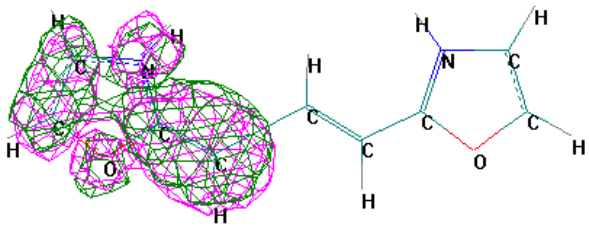

π-MO №34

Since the molecule is in the triplet state now, one electron is localized on σ *-MO, and the second − on π-MO №34. Consequently, we have the basic triplet πσ *-state (electronic configuration $(\pi)^1(\sigma^*)^1$).

The calculation program does not allow to attribute the quantum transitions to certain MO, if the ground state is the triplet one. However, some conclusions can be made. First of all, we can discuss what's happening with the dissociative T (σσ*)-state. It is easy to see that the quantum transition from the σ-MO № 29 to the partially occupied π-MO № 34 will lead to the creation of the desired T (σσ*)-state. Therefore, T (σσ*)-state remains excited state. However, since the ground state is the triplet one, too, the lifetime of this state has declined significantly. This fact does not deny the possibility of the process of dissociation of the molecule (I) to the end. Firstly, in the case of the small heat release immediately after creating T (σσ*)-state at the equilibrium geometry of the molecule it will be broken into fragments without changing of the energy. Secondly, if there are processes of heat release, which take away energy from dissociative T (σσ *)-state by discrete portions, the replacement of T(σσ*)-excitation at the singlet ground state to the singlet S_1-state at the triplet ground state of the molecule (Fig.1) will be possible, which was not only metastable but dissociative one.

It is easy to detect the nature of S_0- and S_1-states in the triplet state by considering the electron transfer inside of the pair σ *-MO № 33 and π-MO № 34 with forming a singlet state. In this case, the electron transfer to the π-MO gives the electron configuration $(\pi)^2(\sigma^*)^0$, which corresponds to the S_0-state. Since π-MO in this case has non-binding nature, increasing the length of the C-C-bond should not significantly affect the magnitude of energy of the electron system in the molecule.

If the electron transfer occurs to σ *-MO, it is formed S_1-state. The corresponding electronic configuration $(\sigma)^2 (\pi)^0(\sigma^*)^2$ resembles the electronic configuration of T (σσ*)-state by the same number of electrons on the σ-MO and σ*-MO. It is clear that this situation will be dissociative, that is consistent with the curve S_1 after the phase transition in Figure 1.

To find out in what state the molecule fragments are formed after the dissociation, in the work carried out calculations of the electronic system energies of both fragments depending on the number of electrons on them. The calculation results are shown in Table 1.

Table 1

The energy of the electronic system (kcal/mol) of fragments depending on the charge state and multiplicity.

№	Smaller fragment: charge, multiplicity and energy of the electronic system	Large fragment: charge, multiplicity and the energy of the elect-ronic system	The total energy of the electron system, E
1	charge 0, doublet, E = -968.258	charge +1, doublet, E = -1054.957	E=-2023.215, triplet
2	charge +1, triplet E = -805.487	charge 0, singlet E = -1187,743	E=-1993.23 triplet
3		charge 0. triplet E = -1193.616	E=-1999.103 singlet
4	charge +1, singlet E = -803.885	charge 0, singlet E = -1187.743	E=-1991.628 singlet
5		charge 0, triplet E = -1193.616	E=-1997.501 triplet

It follows from Table.1 that energetically expedient reaction should be reaction of formation of two radicals from the ground triplet state. Herewith the greater fragment of the molecule (I) must be charged. If the fragments are formed from the singlet state, then the charge will be localized on smaller fragment, and both fragments must be in the triplet state.

Surely, in order to verify the conclusions that follow from Table 1, it is necessary to the study dependence of the magnitude of the charge on the larger fragment at lengthening of dissociating bond in the singlet and triplet state of the molecule.

4. Conclusions

The performed investigation allows to make the following conclusions. We have shown that in the highly excited triplet state the dissociative surface exists, which corresponds to $\sigma \rightarrow \sigma^*$-excitation of the molecule; relaxation of excitations in the framework of this surface leads to dissociation of the molecule by lengthening the C-C bond of the molecule at the central carbon atom. With length increasing of the dissociating bond to 2,16 Å the phase transition of the electronic system of the molecule (I) is observed, as a result the energy of the singlet state is significantly increased, while the energy of the triplet state remained practically unchanged; Besides, at dissociation of molecule from the singlet state the charge will be localized into smaller fragments, and both fragments must be in the triplet state; if dissociation will be occur from the triplet state, then energetically expedient reaction will be the formation of two radicals, and the larger fragment of molecule (I) must be charged;

References

1. Davidenko I.G., Slominsky J.L., Kachkovskii A.D., Tolmachev A.I., Polymethine dyes - derivatives 7,8- dihydrobenzo [cd] furo [2,3-f] indole // Ukr. Journal of Chem.-2008.-Vol.74,N 4.-P.105-113.
2. Kulinich A.V.,Ischenko A.A., Merocyanine dyes: synthesis, structure, properties and application//Uspekhi Khimii (in Russian).- 2009. - Vol.78, N2.-P.151-175.
3. Tarnowski A.H., Razumov T.K., Shchelkin E.P., Veselov T.V., Photophysical, photochemical, and lasing characteristics of symmetric and asymmetric di-and trikarbotsianinovyh dyes// Opt. Spectr.-1993.-Vol.74.-P.107- 115.
4. Kondratenko PA, Lopatkin JM, Sakun T.M .. Relaxation Processes in Highly Excited Molecules of Resazurin // Physics and Chemistry of Solids.-2007. – Vol.,N1.-P.100-108.
5. Kondratenko P.A., Lopatkin S.Yu., Lopatkin Yu.M., Sakun T.N., Photovoltaic properties of polymer layers with dyes // Herald of Sumy State Univ., Ser. Fiz.-mat.- 2007.-N1.-P.145-153
6. Kondratenko P.A., Lopatkin Yu.M, Sakun T.M., Quasi-equilibrium processes in the High Excited Molecules of Resazurin // J. Nano-and Electron Physics.–2012.– Vol.4,N2.–P.1-7.
7. Dewar M.J., Zoebisch E.G., Healy E.F., Stewart J.J., The development and use of quantum-mechanical molecular-models-76.AM1-New general-purpose quantum-mechanical molecular model // Journ. of the American Chem. Soc.-1995.– Vol.107,N13.-P.3902– 3909.
8. Glushkov A.V., Kondratenko P.A., Lepikh Ya.I. , Fedchuk A.P., Svinarenko A.A., Lovett L., Electrodynamical and quantum - chemical approaches to modelling the electrochemical and catalytic processes on metals, metal alloys and semiconductors//Int. Journ. of Quantum Chem.-2009.-Vol.109,N14.-P.3473-3481.
9. Glushkov A.V., Fedchuk A.P., Kondratenko P.A., Lepikh Ya.I., Lopatkin Yu.M., Svinarenko A.A., The Green's functions and density functional approach to vibrational structure in the photoelectron spectra: Molecules of CH, HF// Photoelectronics.-2011.-Vol.20.-P.58-62.

This article has been received within 2014

UDC 539.186

V. V. Velikodnaya, P. A. Kondratenko, Yu. M. Lopatkin, A. V. Glushkov, T. N. Sakun, O. A. Kovalenko

QUANTUM CHEMICAL STUDYING THE TRIMETHINE CYANINE DYE STRUCTURE AND RELAXATION DYNAMICS

Abstract

Quantum-chemical studying polymethine dyes molecular structure and investigation of the relaxation processes of excitation have been carried out. Particularly, in the highly excited triplet state the dissociative surface exists, which corresponds to $\sigma \rightarrow \sigma^*$-excitation of the molecule; relaxation of excitations in the framework of this surface leads to dissociation of the molecule by lengthening the C-C bond of the molecule at the central carbon atom

Key words: polymethine dyes, relaxation processes of excitation, quantum-chemical studying

УДК 539.186

В. В. Великодная, П. А. Кондратенко, Ю. М. Лопаткін, А. В. Глушков, Т. Н. Сакун, О. А. Коваленко

КВАНТОВО-ХИМИЧЕСКОЕ ИЗУЧЕНИЕ СТРУКТУРЫ И ДИНАМИКИ РЕЛАКСАЦИИ ТРИМЕТИН-ЦИАНИНОВОГО КРАСИТЕЛЯ

Резюме

Приведены результаты квантово-химического изучения молекулярной структуры и процессов релаксации возбуждения полиметиновых красителей. В частности, в сильно возбужденном триплетном состоянии существует поверхность диссоциации, отвечающая возбуждению $\sigma \rightarrow \sigma^*$ молекулы; релаксация возбуждения приводит к диссоциации молекулы за счет удлинения СС связи молекулы на центральном атоме углерода.

Ключевые слова: полиметиновые красители, релаксационные процессы возбуждения, квантово-химическое изучение

УДК 539.186

В. В. Великодна, П. О. Кондратенко, Ю. М. Лопаткін, О. В. Глушков, Т. М. Сакун, О. А. Коваленко

КВАНТОВО-ХІМІЧНЕ ВИВЧЕННЯ СТРУКТУРИ І ДИНАМІКИ РЕЛАКСАЦІЇ ТРІМЕТІН-ЦІАНІНОВОГО БАРВНИКА

Резюме

Приведені результати квантово-хімічного вивчення молекулярної структури та процесів релаксаціїв збудження поліметинових барвників. Зокрема, в сильно збудженому триплетному стані існує поверхня дисоціації, що відповідає збудженню σ→σ* молекули; релаксація збудження приводить до дисоціації молекули за рахунок подовження СС зв'язку молекули на центральному атомі вуглецю.

Ключові слова: поліметинові барвники, релаксаційні процеси збудження, квантово-хімічне вивчення

UDK 539.184

S. I. Kosenko, A. A. Kuznetsova, L. A. Vitavetskaya, Yu. G. Chernyakova, S. S. Seredenko

Odessa National Politechnical University, 1, Shevchenko av., Odessa, Ukraine
Odessa National Maritime Academy, Odessa, 4, Didrikhsona str., Odessa, Ukraine
Odessa State Environmental University, 15, Lvovskaya str., Odessa, Ukraine
e-mail: nucvita@mail.ru

CALCULATING THE RADIATIVE VACUUM POLARIZATION CONTRIBUTION TO THE ENERGY SHIFT OF SOME TRANSITIONS IN PIONIC AND KAONIC NITROGEN

Calculating the radiative contribution due to the vacuum polarization effect to energy value for some transitions in pionic and kaonic nitrogen has been carried out using the modified Uehling-Serber potential. The master equation for computing spectrum of the kaonic atoms is the Klein-Gordon-Fock equation. The vacuum polarization contribution to the 8-7 transition energy in kaonic nitrogen is calculated

This paper goes on our work on estimating the vacuum-polarization contributions to the transition energies of the hadronic atoms that is of a great importance especially in the last years (look below) [1-15]. Here we study pionic and kaonic nitrogen. Let us remind [13] that due to the significant progress in the modern experimental technologies now a great interest attracts studying spectra of heavy and super heavy elements atoms, exotic atomic systems, including hadronic and leptonic atoms [1-15]. Especial problem is connected with précised calculating the radiative corrections to the transition energies of the low-Z exotic (pionic, kaonic, muonic) atoms, namely, hydrogen and deuterium. Naturally, it is provided by necessity of further developing the modern as atomic and as nuclear theories. From the other side, detailed information about spectra of the exotic atomic systems (kaonic, pionic, muonic atoms) can be very useful under construction of the new X-ray standards. One could remind a great importance of the muonic chemistry, muonic spectroscopy. Very attractive perspective of the thermonuclear fission through the mechanism of the muonic catalysis is still interesting and widely studied.

The standard Dirac approach is traditionally used as starting basis in calculations of the heavy ions [2]. The problem of accounting the radiative corrections, in particular, self-energy part of the Lamb shift and vacuum polarization contribution is mostly treated with using the expansions on the natural physical parameters $1/Z$, αZ (α is fine structure constant) [5,10]. It permits evaluations of the relative contributions of different expansion energy terms: non-relativistic, relativistic ones, as functions of Z. For high Z (Z is a nuclear charge) it should be necessary to account for the high-order QED corrections and the nuclear finite size correction etc [1-3,10-12,16]. Further improvement of this method in a case of the heavy ions is linked with using gauge invariant procedures of generating relativistic orbital basises and more correct treating nuclear and QED effects [1-3]. In a case of the low-Z exotic atomic systems such as an exotic hydrogen (deuterium) a great interest attracts estimation of the radiative, in particular, vacuum polarization, correction. In refs. [17-19] it has been proposed a precise scheme to calculating spectra of heavy systems with account of nuclear and radiative effects, based on the relativistic many-body perturbation theory (see also

[3]) and advanced effective procedures for accounting the radiative corrections.

In this paper we present the results of calculating the contribution due to the vacuum polarization effect to energy shift for some transitions in pionic and kaonic nitrogen. The obtained result is compared with calculation data by Indelicato [19]. The details of the calculation procedure have been presented earlier, and here we consider only the key topics. The calculation of the radiative vacuum polarization shift in the pionic deuterium should be performed using the Dirac approximation as a zeroth one. Further, the expectation value of the radiative vacuum polarization operator gives the corresponding correction. The total electromagnetic interaction potential:

$$V(r)=V_n(r)+U(r). \qquad (1)$$

includes the electrical V_n and polarization U(r) potentials of a nucleus with accounting the finite size correction. As usually, the Coulomb potential for spherically symmetric density $\rho(r|R)$ can be written as follows:

$$V_n(r|R)=-\left((1/r)\int_0^r dr' r'^2 \rho(r'|R)+\int_r^\infty dr' r' \rho(r'|R)\right). \qquad (2)$$

The details of the determination of this potential can be , for example, found in ref. [21,22]. The vacuum polarization part is usually accounted in the first PT order by using the Uehling potential [1,8,16,17]:

$$U(r)=-\frac{2\alpha}{3\pi r}\int_1^\infty dt \exp(-2rt/\alpha Z)(1+1/2t^2)\frac{\sqrt{t^2-1}}{t^2}\equiv$$

$$=-\frac{2\alpha}{3\pi r}C(g) \qquad (3)$$

$$g=\frac{r}{\alpha Z}. \qquad (4)$$

The corresponding expectation value of this operator gives the corresponding vacuum polarization correction. In the scheme [12] this potential is approximated by quite precise analytical function (see details in refs. [3,16,17]). The most advanced version of the such potential ($C\rightarrow\tilde{\tilde{C}}$) is presented as follows:

$$\tilde{\tilde{C}}(g)=\tilde{C}_1(g)\tilde{\tilde{C}}_2(g)/\left(\tilde{C}_1(g)+\tilde{\tilde{C}}_2(g)\right),$$

$$\tilde{\tilde{C}}_2(g)=\tilde{C}_2(g)\,f(g),$$

$$\tilde{C}_2(g)=-1.8801\exp(-g)/g^{3/2}$$

$$\tilde{C}_1(g)=\mathrm{h}(g/2)+1.410545-1.037837g,$$

$$f(g)=\left((1.1024/g-1.3361)/g+0.8027\right)$$

The using this formula permits one to decrease the calculation errors for this term down to ~0.1%. Error of usual calculation scheme is~10%.

We carried out the calculation of the vacuum polarization contribution to the energy shift for 8k-7 transition in kaonic nitrogen It should be noted that the energy levels of exotic (kaonic) muonic atoms are very sensitive to effects of QED, nuclear structure and recoil since the kaon is heavier than the electron. As usually the fundamental constants from the CODATA 1998 are used in the numerical calculations.

We have evaluated the modified Uehling-Serber potential expectation values and obtained the value for the vacuum-polarization correction: 1.1783 eV. It is interesting to compare this result with the result by Indelicato, namely, the total vacuum polarization contribution: 1.1789 eV and from ref. [23]: 1,1778 eV. Further, let us present the data for the main Coulomb contribution from [8,24] - 2968.4565 eV and from ref. [23] - 2968.4492eV. Our estimate: 2968.4481eV. Further we have evaluated the modified Uehling-Serber potential expectation values and obtained the value for the vacuum-polarization correction into the 5f-4d transition energy in the pionic nitrogen. Our value for the vacuum-polarization correction: 2,9467eV. It is interesting to compare this result with the result by Serga [25] 3,216 eV. It should be noted that the last result is received with account of the Wichman-Kroll and Kallen-Sabry corrections. In any case, the physically reasonable agreement can be easily explained by the fact that pionic and kaonic nitrogen is the low-Z atomic system and in this case the expansion on the parameter αZ works sufficiently well.

References

1. Botham C., Martensson A.M., Sanders P.G. Relativistic effects in atoms and molecules.-Vancouver: Elseiver,2001.-550p.
2. Grant I.P., Relativistic Quantum Theory of Atoms and Molecules.-Oxford, 2008.-650P.
3. Glushkov A.V., Relativistic quantum theory. Quantum mechanics of atomic systems, Odessa: Astroprint, 2008.-700P.
4. Hayano R.S., Hori M., Horvath D., Widman E., Antiprotonic helium and CPT invariance//Rep. Prog. Phys.-2007.-Vol.70.-P.1995-2065.
5. Schlesser S., Le Bigot E.-O., Indelicato P., Pachucki K., Quantum-electrodynamics corrections in pionic hydrogen// Phys.Rev.C.-2011.-Vol.84.-P.015211 (8p.).
6. Gotta D., Amaro F., Anagnostopoulos D., Pionic Hydrogen//Precision Physics of Simple Atoms and Molecules, Ser. Lecture Notes in Physics (Springer, Berlin / Heidelberg).-2008.-Vol.745.-P.165-186.
7. Mitroy J., Quantum defect theory for the study of hadronic atoms/ Mitroy J., Ivallov I.A.// J. Phys. G: Nucl. Part. Phys.-2001.-Vol.**27.-P.**1421–1433
8. Deslattes R., Kessler E., Indelicato P., de Billy L., Lindroth E. , Anton J., Exotic atoms//Rev. Mod. Phys. -2003.-Vol.75.-P.35-70.
9. Borie E., Lamb shift in muonic hydrogen// Phys.Rev. A.-2005.-Vol.71.-P.032508-1-8.
10. Mohr P.J. Quantum Electrodynamics Calculations in few-Electron Systems// Phys. Scripta.-1993.-Vol.46,N1.-P.44-52.
11. Klaft I.,Borneis S., Engel T., Fricke B., Grieser R., Huber G., Kuhl T., Marx D., Neumann R., Schroder S., Seelig P., Volker L. Precision laser spectroscopy of ground state hyperfine splitting of H-like $^{209}Bi^{82+}$// Phys.Rev.Lett.-1994.-Vol.73.-P.2425-2427
12. Khetselius O.Yu., Relativistic perturbation theory calculation of the hyperfine structure parameters for some heavy-element isotopes// Int. Journ. of Quantum Chemistry.-2009.-Vol.109.- N14.-P. 3330-3335.
13. Kuznetsova A.A., Vitavetskaya L.A., Chernyakova Yu.G., Korchevsky D.A., Calculating radiative vacuum polarization contribution to the energy shift of 3p-1s transition in pionic deuterium// Photo-electronics.-2013.-Vol.22.-P.108-111
14. Backenstoss G., Pionic atoms//Ann.Rev. Nucl.Sci.-1990.-Vol.20.-P.467-510.
15. Menshikov L I and Evseev M K, Some questions of physics of exotic atoms// Phys. Uspekhi.2001-Vol. 171.-P.150-184.
16. Ivanova E.P., Ivanov L.N., Aglitsky E.V., Modern trends in spectroscopy of multicharged ions// Phys.Rep.-1991.-Vol.166.-P.315-390.
17. Glushkov A.V., Ambrosov S., Loboda A., Chernyakova Y.G., Khetselius O., Svinarenko A., QED theory of the superheavy elements ions: energy levels, radiative corrections, and hyperfine structure for different nuclear models// Nuclear Phys.A-2004.-Vol. 734.-P.21-28.
18. Glushkov A.V., Khetselius O.Yu., Gurnitskaya E.P., Loboda A.V., Florko T.A., Sukharev D.E., Lovett L., Gauge-invariant QED perturbation theory approach to calculating nuclear electric quadrupole moments, hfs structure constants for heavy atoms and ions// Frontiers in Quantum Systems in Chem. and Phys. (Springer).-2008.-Vol.18.- P.505-522.
19. Vitavetskaya L.A., Malinovskaya S.V., Dubrovskaya Yu., Advanced quantum calculation of beta decay probabilities// Low Energy Antiproton Phys.-2005.-Vol.796.- P.201-205.
20. Gurnitskaya E.P., Khetselius O.Yu., Loboda A.V., Vitavetskaya L.A., Consistent quantum approach to quarkony energy spectrum and semiconductor superatom and in external electric field// Photoelectronics.-2008.-N17.-P.127-130.

21. Kvasikova A.S., Ignatenko A.V., Florko T.A., Sukharev D.E., Chernyakova Yu.G., Photoeffect and spectroscopy of the hydrogen atom in the crossed dc electric and magnetic field// Photoelectronics.-2011.-Vol.20.-P.71-75.
22. Kuznetsova A.A., Kvasikova A.S., Shakhman A.N., Vitavetskaya L.A., Calculating the radiative vacuum polarization contribution to the energy shift of 2p-2s transition in μ-hydrogen// Photoelectronics.-2012.-N21.-P.66-67.
23. Khetselius O.Yu., Turin A.V., Sukharev D.E., Florko T.A., Estimating of X-ray spectra for kaonic atoms as tool for sensing the nuclear structure// Sensor Electr. and Microsyst. Techn.-2009.-N1.-P.30-35..
24. Indelicato P., Pionic nitogen// Private communication.
25. Serga I.N., Relativistic theory of spectra of pionic atoms with account of the radiative and nuclear corrections// Photoelectronics.-2010 - Vol.22.-P.84-92

This article has been received within 2014

UDC 539.184

S. I. Kosenko, A. A. Kuznetsova, L. A. Vitavetskaya, Yu. G. Chernyakova, S. S. Seredenko

CALCULATING THE RADIATIVE VACUUM POLARIZATION CONTRIBUTION TO THE ENERGY SHIFT OF SOME TRANSITIONS IN PIONIC AND KAONIC NITROGEN

Abstract

Calculating the radiative contribution due to the vacuum polarization effect to energy value for some transitions in pionic and kaonic atoms has been carried out using the modified Uehling-Serber potential. The master equation for computing spectrum of the kaonic atoms is the Klein-Gordon-Fock equation. The vacuum polarization contribution to the 8-7 transition energy in kaonic nitrogen is calculated.

Key words: kaonic nitrogen, radiative corrections

УДК 539.184

С. И. Косенко, А. А. Кузнецова, Л. А. Витавецкая, Ю. Г. Чернякова, С. С. Середенко

РАСЧЕТ РАДИАЦИОННОГО ВКЛАДА ЗА СЧЕТ ЭФФЕКТА ПОЛЯРИЗАЦИИ ВАКУУМА В СДВИГ ЭНЕРГИИ РЯДА ПЕРЕХОДАОВ В ПИОННОМ И КАОННОМ АЗОТЕ

Резюме

Проведен расчет радиационного вклада за счет эффекта поляризации вакуума в величину энергии ряда переходов в пионом и каонном атомах с использованием модифицированного потенциала Юлинга-Сербера. Базисным для расчета спектра каонных атомов является уравнение Клейна-Гордона-Фока. Рассчитан вклад за счет поляризации вакуума в энергию 8-7 перехода в каонном азоте.

Ключевые слова: каонный азот, радиационные поправки

УДК 539.184

С. І. Косенко, Г. О. Кузнецова, Л. А. Вітавецька, Ю. Г. Чернякова, С. С. Середенко

РОЗРАХУНОК РАДІАЦІЙНОГО ВНЕСКУ ЗА РАХУНОК ЕФЕКТУ ПОЛЯРИЗАЦІЇ ВАКУУМУ У ЗСУВ ЕНЕРГІЇ ДЕКОТРИХ ПЕРЕХОДІВ У ПІОННОМУ І КАОННОМУ АЗОТЕ

Резюме

Виконано розрахунок радіаційного внеску за рахунок ефекту поляризації вакууму у величину енергії декотрих переходів у піонному і каонному атомах з використанням модифікованого потенціалу Юлінга-Сербера . Базисным для розрахунку спектра каонних атомів є рівняння Клейна-Гордона-Фока. Розраховано внесок за рахунок поляризації вакууму в энергію 8-7 переходу у каонному азоті.

Ключові слова: каонний азот, радіаційні поправки

UDC 621.315.592

A. Yu. Bak, Yu. N. Karakis, A. E. Stupak, M. I. Kutalova, A. P. Chebanenko

Odessa National University, 42, Pasteur St.;
e-mail: wadz@mail.ru

DETERMINATION OF BAND GAP OF SEMICONDUCTOR MATERIAL IN END PRODUCT

The paper puts forward a method for determination of semiconductor activation energy in end product. It is illustrated that band gap can be calculated at cutoffs on both axes of graphs *ln(I)÷U*, measured at different temperatures. Minimum temperature interval is determined depending on measuring accuracy. A new method for determination of value E_g without VAC (volt-ampere characteristics) extrapolation is put forward.

1. INTRODUCTION

Classic method for determination of band gap of semiconductor crystal is a study of temperature dependence of its conductivity [1,2]. Among optical methods the most widely used is determination of excitation light wavelength at maximum photosensitivity and extrapolation of spectral distribution of absorption coefficient [3,4].

However, in some cases, such as identification of semiconductor material, it is required to determine matter activation energy in end product. Simple thermal methods cannot be applied for this purpose, since crystal has already undergone a series of complementary technological operations, such as contact etching, annealing and oxide coating, etc.

Optical methods cannot be used for the same reason. In case of photoconverters measuring results are distorted due to protective coatings, transparent layers of SnO_2 applied as a front window, etc. Frequently photocells are fabricated on a hard opaque surface obstructing the passage of penetrating light. This excludes measurement of absorption coefficient.

In this case temperature variations of volt-ampere characteristics (VAC) are studied. There are two methods [5]. The first one implies study of temperature variations of saturation current I_s in VAC reverse-bias region. However, not to get into junction region, it is necessary to apply fairly large reverse voltages of tens of Volts. For many photocells this is beyond their operating parameters. And in that case rectification of VAC forward biases in semi-log plot is applied to operating region below open circuit voltage – usually a few tenths of a Volt (Fig. 1).

2. RESULTS, DISCUSSION

Photoconverters operate due to potential barrier between p- and n-semiconductors. Effect of relatively insignificant barriers on ohmic contacts in this case is negligible.

Here is the expression for photodiode VAC lines without photo-excited carriers [5]:

$$I = I_s\left[\exp\left(\frac{eU}{kT}\right) - 1\right] \qquad (1)$$

where I_s - reverse saturation current of p-n – junction, created by carriers flowing from the barrier. Its value is in proportion to concentration of minor carriers in p-region

$$n_p = N_c \exp\left(-\frac{E_g}{kT}\right) \qquad (2)$$

and n-region

$$p_n = P_v \exp\left(-\frac{E_g}{kT}\right) \qquad (3)$$

In case of fairly large forward bias, where

$$eU \gg kT \qquad (4)$$

unit (1) can be disregarded. Then, taking into account (2) and (3), the expression (1) can be as follows:

$$I = A\exp\left(-\frac{E_g - eU}{kT}\right) \qquad (5)$$

where A – weakly temperature-dependent coefficient. Taking logarithm (5), we obtain:

$$\ln I = \ln A - \frac{E_g - eU}{kT} \qquad (6)$$

It follows that the set of characteristics lnI(U) at different temperatures is represented by temperature-dependent slope intercept form of a line

$$tg\,\alpha = \frac{\Delta \ln I}{\Delta U} = \frac{e}{kT}. \qquad (7)$$

and meeting at some point with abscissa E_g/e. This enables to calculate band gap of material by measuring diode VAC lines at two different temperatures (Fig. 1).

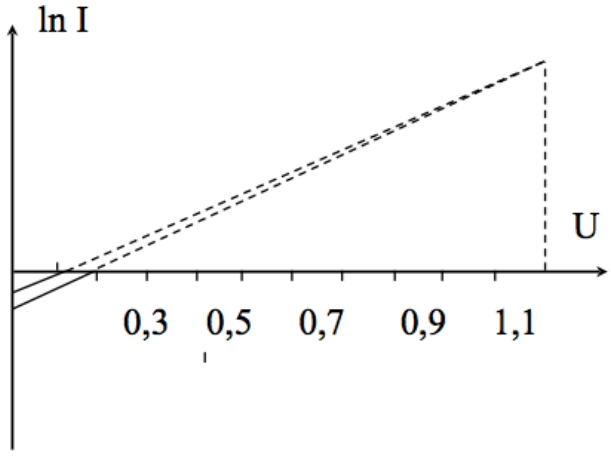

Fig.1. Standard direct current-voltage dependence for silicon diodes in semi-log plot.

However, this method is difficult to apply in practice. Standard potential barrier height at p-n-junction for the most popular silicon diodes is 0.1-0.15 eV. At forward biasing the barrier reduces. That is why beyond the above voltage diode current loses its diode nature and is limited to series resistance only, whereas VA characteristics become linear. This means that experimentally measured points applicable for calculation in the given method, are located as shown in Fig. 1, in the lower quadrant outside voltage ~ 0.2 V (solid graphs).

One should note that ln I = 0 at amperage ~ 1 A. In real low-power diodes direct current is milliampere units or even fractions. Which is equivalent to ln I ~ - 5.0. All points on a graph above this value on current axis can be only extrapolation-based. In other words, a large number of points near both axes disappears, narrowing actual rectification region even more.

Silicon band gap is 1.1 eV. Thus, intersection of graphs should be expected at voltage bias ~ 1.1 V on voltage axis, i.e. extrapolation (dotted lines) is applied to 90-95% of graph length. Clearly, at this arm intersection of lines is extremely sensitive to two factors. Firstly, it is measuring accuracy, i.e. spread of points with confidence interval Δ. And secondly, temperature interval applied at measuring, i.e. difference in slopes of graphs. These values are interconnected. At a large value of confidence interval and insufficient temperature difference graphs may not intersect at all, as shown in Fig. 2 for lines CN and DG.

VAC measuring pattern is the following. Exact applied rectification is specified. Then error current flowing at a given voltage is measured. Value Δ means vertical spread of points on a graph lnI÷U.

Graphs lnI÷U are plotted within a few confidence bands, as shown in Fig. 2. In general, width of these bands differs. It is determined by band slope

$$\Delta_1 = 2\Delta \cdot \cos\alpha \qquad (8)$$

Inclination angle according to (7) depends on measuring temperature.

However, in reality temperature difference is not too large. Lower limit is correlation (4). Naturally, it is assumed that room temperature is the lower. The upper limit is maximum rated temperature of the product (for silicon it is around +60 ^{0}C), when contribution of intrinsic carriers

becomes more obvious due to region-region junction. At this temperature interval for the sake of simplicity we assume that confidence band width in both graphs is the same.

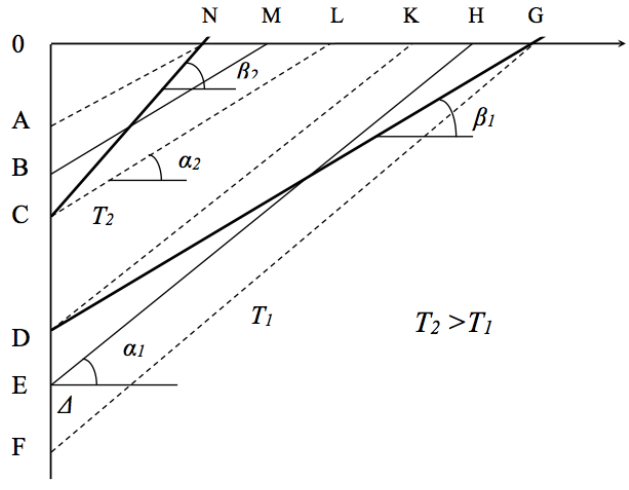

Fig. 2. Operating region for method of VAC intersecting lines.

We can obtain criterion for minimum temperature interval at a given spread of points Δ, subject to parallelism of CN and DG (Fig. 2). Line equation EH $y = a_1x + b_1$, where according to (6)

$$a_1 = \frac{e}{k}\frac{1}{T_1} \qquad b_1 = \ln A - \frac{E_g}{k}\frac{1}{T_1} \tag{9}$$

Value b is negative, since operating region of flowing current is I < 1A. Thus, both summands for a constant term are less than zero.

Then FG line equation is given by $y = a_1x - (/b_1/ + \Delta)$, remembering that values b_1 are negative and F point ordinate increases in comparison with point E. It follows that G point coordinate at $y=0$ is $x_G = \frac{|b_1| + \Delta}{a_1}$. D point coordinate decreases by confidence interval value: $- y_D = - (/b_1/ - \Delta)$. It gives the lowest possible slope for DG graph within confidence band:

$$tg\,\beta_1 = \frac{|b_1| - \Delta}{|b_1| + \Delta} a_1 \tag{10}$$

Note that numerator modulo is less than denominator, so $tg\,\beta_1 < a_1$, i.e. angle β_1 is less than angle α_1.

For similar reasons, at elevated temperature T_2 for BM line $y = a_2x + b_2$, where

$$a_2 = \frac{e}{k}\frac{1}{T_2} \qquad b_2 = \ln A - \frac{E_g}{k}\frac{1}{T_2} \tag{11}$$

we obtain equation for AN $y = a_2x - (/b_2/ - \Delta)$. Thus, N point coordinate will be $x_N = \frac{|b_2| - \Delta}{a_2}$. C point coordinate – $y_c = - (/b_2/ + \Delta)$. Thus, maximum slope within this band for CN is given by equation

$$tg\,\beta_2 = \frac{|b_2| + \Delta}{|b_2| - \Delta} a_2 \tag{12}$$

while $tg\,\beta_2 > tg\,\alpha_2$.

Intersection point will be surely obtained once the condition is met

$$\frac{|b_1| - \Delta}{|b_1| + \Delta} a_1 = \frac{|b_2| + \Delta}{|b_2| - \Delta} a_2$$

or

$$\Delta^2 (a_1 - a_2) - \Delta (a_1 + a_2)(|b_1| + |b_2|) + b_1 b_2 (a_1 - a_2) = 0 \tag{13}$$

Here Δ – confidence interval, and the rest are temperature dependent parameters.

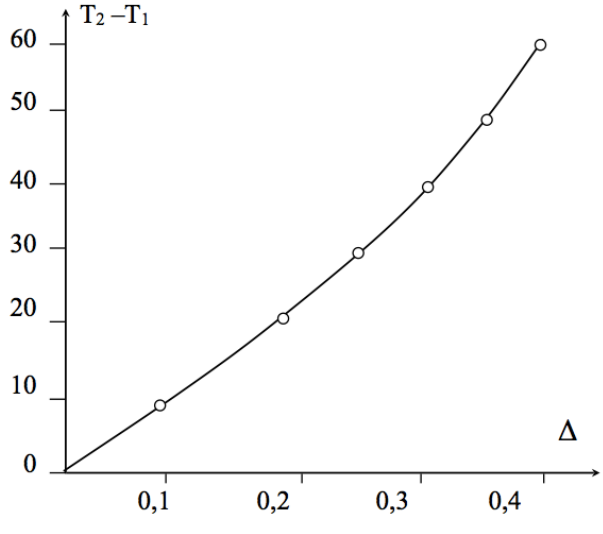

Fig. 3. Lowest possible temperature interval for determination of band gap.

Equation (13) was solved numerically. Parameter value lnA=29.77 is taken from experimental measurement for a sample of one of Si-diodes. a_1 and a_2 slope values were determined from the formulae (9) and (11) at given temperatures. Room temperature was used as reference temperature T_1. Point of graph intersection occurred at $x_0 = \frac{E_g}{e}$ [See dependence (6), silicon band gap 1.1 eV]. Then cutoffs b_i were determined from the equation of the pencil of lines, going through that point

$$\ln A = a_i(T)\left(\frac{E_g}{e}\right) + b_i(T)$$

.

By solving equation (13) two roots were obtained, different by a large ratio – either tenths or hundreds of units. Here b_i values fell in the interval of 12 - 25 units. For the sake of rationality the larger value Δ was discarded as having no physical content. Calculation result is shown in Fig. 3.

The more operating temperatures T_1 and T_2 are different, the more accurate the results are. However, there is a limit for lower temperature. At large errors Δ confidence bands are too wide, and it is necessary to increase minimum temperature interval for graphs to intersect ln I ÷ U.

As shown in Fig. 3, the more spread points are obtained at current measurement, i.e. the larger value Δ is and the wider confidence bands are, the more temperature interval should be applied to measurement of graphs. Here high-temperature band is more sloped, which compensates divergence of lines. However, the problem of determination accuracy of intersection coordinate persists.

To determine diode band gap, there is no need to extrapolate VAC lines at a huge arm till their intersection, as it is recommended in the classic method. This parameter can be obtained with more accuracy at cutoffs on axes.

For current axis those are values $\ln I_1$ and $\ln I_2$, i.e. values b_1 and b_2 from the formulae (9) and (11). As shown in Fig. 4, length of the respective interval is

$$\ln I_1 - \ln I_2 = \frac{E_g}{k}\left(\frac{1}{T_1} - \frac{1}{T_2}\right) \qquad (14)$$

Since temperatures T_1 and T_2 applied for measurement are given, and values on the left are determined directly on the graph, formula (14) enables to calculate value E_g.

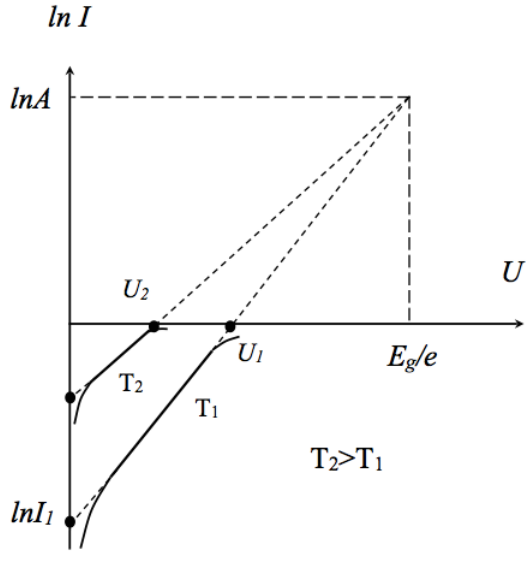

Fig. 4. VAC lines at different temperatures.

Similarly, for voltage axis intersection points (Fig. 4) from equation (6) it is true that

$$-\ln A = -\frac{E_g}{kT_1} + \frac{eU_1}{kT_1} = -\frac{E_g}{kT_2} + \frac{eU_2}{kT_2}$$

from which

$$\frac{E_g}{e}\left(\frac{1}{T_1} - \frac{1}{T_2}\right) = \frac{U_1}{T_1} - \frac{U_2}{T_2} \qquad (15)$$

which also enables to determine parameter E_g, given values U_1 and U_2 from the graph.

Compare accuracy of two offered options with the classic method (Fig. 5). Obviously, for current axis parameter spread is

$$\pm 2\Delta \qquad (16)$$

To determine spread of axis intersection points, it is necessary to determine band width projection from (8) on X-axis:

$$\pm \Delta \cdot (ctg\,\alpha_1 + ctg\,\alpha_2) = \pm \Delta \cdot \left(\frac{1}{a_1} + \frac{1}{a_2}\right) \qquad (17)$$

Formula (17) gives general change of confidence interval when determining coordinates U_1

and U_2 on voltage axis (Fig. 4), i.e. for the right member of dependence (15). However, extension of this interval is not symmetrical, since now it depends on angles α_1 and α_2, which are different for temperatures T_1 and T_2. According to (7), for higher temperature T_2 slope α_2 is lower. Segment U_1 - U_2 spreads more to the right (See Table).

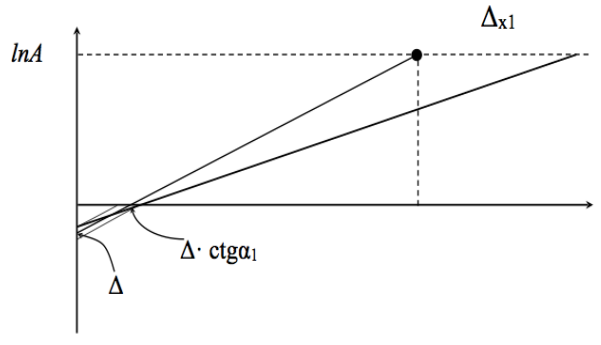

Fig. 5. In the same ratio, as in Fig. 1. Error for axis intersection points and graph convergence point (illustrated by one of dependences in the same ratio as in Fig.1).

It is well to bear in mind that, though absolute error at determining cutoffs U_1 and U_2 on voltage axis is much lower (See Table), absolute magnitude of these values is also an order less than cutoffs b_1 and b_2 for current axis. So it is not possible to say, which method is more accurate.

Define error in the coordinate of VAC graph convergence point. If temperature interval is set correctly based on dependence (13), abscissa of intersection point of lines DM and EH (See Fig. 1-2) shall be $\frac{E_g}{e}$. Then its ordinate from the equation (6) shall be y=lnA (horizontal line in Fig. 5).

Maximum deviation from it to the right can be determined as intersection point of line DG with highest possible slope to the right within confidence interval at temperature T_1 (See Fig. 2). Taking into account (10), we obtain

$$\ln A = \frac{|b_1| - \Delta}{|b_1| + \Delta} a_1 x - \left(|b_1| - \Delta\right).$$

from here

$$\Delta x_1 = \frac{\left[\ln A + \left(|b_1| - \Delta\right)\right] \cdot \left(|b_1| + \Delta\right)}{\left(|b_1| - \Delta\right) \cdot a_1} - \frac{E_g}{e} \qquad (18)$$

Highest possible deviation to the left can be obtained by extending line CN to intersection. According to (12), we obtain

$$\ln A = \frac{|b_2| + \Delta}{|b_2| - \Delta} a_2 x - \left(|b_2| + \Delta\right),$$

from which

$$\Delta x_2 = \frac{E_g}{e} - \frac{\left[\ln A + \left(|b_2| + \Delta\right)\right] \cdot \left(|b_2| - \Delta\right)}{\left(|b_2| + \Delta\right) \cdot a_2} \qquad (19)$$

Numerical values of parameter spread are given in the Table. Values used for calculation: T_1 = 300 K, T_2 = 360 K, Δ = 0.2 (mid segment Fig. 3). Other parameters are the same as for equation calculation (13).

	Inward departure	Outward departure
Determination of E_g at cutoff on Y-axis	0.2	0.2
Determination of E_g at cutoff on X-axis	0.04	0.031
Classic method of graph intersection	0.39	0.96

As shown in Fig. 5, classic method error is a few times higher, which is accounted for by extremely large extrapolation arm.

Suggested methods enable to obtain band gap of material without VAC graph extrapolation. Based on formula (6), distance between VAC lines /ln I_{01} – ln I_{02}/ in operating region at some fixed voltage U_0 will be:

$$-\left|\ln I_{01} - \ln I_{02}\right| = \frac{E_g}{k}\left(\frac{1}{T_2} - \frac{1}{T_1}\right) + \frac{eU_0}{k}\left(\frac{1}{T_1} - \frac{1}{T_2}\right).$$

from here

$$E_g = eU_0 + \frac{k\left|\ln I_{01} - \ln I_{02}\right|}{\left(\frac{1}{T_1} - \frac{1}{T_2}\right)} \qquad (20)$$

By contrast, for a section of horizontal graph system for a certain value ln I_0 in operating region the following is true:

$$\ln I_0 - \ln A = -\frac{E_g}{kT_1} + \frac{eU_{01}}{kT_1} = -\frac{E_g}{kT_2} + \frac{eU_{02}}{kT_2}.$$

from here

$$E_g\left(\frac{1}{T_1} - \frac{1}{T_2}\right) = \frac{eU_{01}}{T_1} - \frac{eU_{02}}{T_2}.$$

or

$$E_g = \frac{\frac{eU_{01}}{T_1} - \frac{eU_{02}}{T_2}}{\frac{1}{T_1} - \frac{1}{T_2}} \qquad (21)$$

where $T_1 < T_2$ – temperatures, at which graphs were measured, and $U_{01} > U_{02}$ are abscissas of section points.

Energy accuracy E_g obtained remains ± 2Δ for a section along voltage axis by the formula (20) and error (17) for the expression (21).

Note that there is no value ln A in the above dependences (20), (21), i.e. it is not required for determination of value E_g by given method.

3. CONCLUSION

Thus, determination of band gap based on volt-ampere characteristics becomes simpler and more accurate, using cutoffs on current and voltage axes or vertical or horizontal sections of VAC graphs instead of extrapolation. It is necessary to bear in mind dependence of required temperature interval on amperage measurement error.

REFERENCES

1. Tereshchenko O.E., Kostyurina A.G. - Opredeleniye shiriny zapreshchennoy zony poluprovodnikov // Novosibirsk, 2004.
2. Pavlov L.P. - Metody izmereniya parametrov poluprovodnikovykh materialov // M., Vysshaya shkola, 1997.
3. Vladimirova L.N., Bormontov Ye.N., Berlo Ye.N. – Vnutrenniy fotoeffekt v poluprovodnikakh // Izdatelsko-poligraficheskiy tsentr Voronezhskogo gosudarstvennogo universiteta, 2009.
4. Andreyev A.N., Gavrilov Ye.V., Ishanin G.G. – Opticheskiye izmereniya // M., Logos, 2012.
5. Lebedev A.I. - Fizika poluprovodnikovykh priborov // M. Fizmatlit., P 2008 .

This article has been received within 2014

UDC 621.315.592

A. Yu. Bak, Yu. N. Karakis A. E. Stupak, M. I. Kutalova, A. P. Chebanenko

DETERMINATION OF BAND GAP OF SEMICONDUCTOR MATERIAL IN END PRODUCT

Abstract

The paper puts forward a method for determination of semiconductor activation energy in end product. It is illustrated that band gap can be calculated at cutoffs on both axes of graphs *ln(I)÷U*, measured at different temperatures. Minimum temperature interval is determined depending on measuring accuracy. A new method for determination of value E_g without VAC extrapolation is put forward.

Key words: determination of band gap, semiconductor material, activation energy.

УДК 621.315.592

А. Ю. Бак., Ю. М. Каракіс.О. Е. Ступак, М. І. Куталова, А. П. Чебаненко

ВИЗНАЧЕННЯ ШИРИНИ ЗАБАРОНЕНОЇ ЗОНИ НАПІВПРОВІДНИКОВОГО МАТЕРІАЛУ В ГОТОВОМУ ВИРОБІ

Резюме

Запропоновано метод визначення енергії активації напівпровідника в готовому виробі. Показано, що ширину забороненої зони можливо розрахувати по відсічкам на обох осях графіків *ln(I)÷U*, виміряних при різних температурах. Визначений мінімальний температурний інтервал в залежності від точності вимірювань. Вказано новий засіб визначення E_g без екстраполяції ВАХ.

Ключові слова: ширина забороненої зони, енергія активації, напівпровідник.

УДК 621.315.592

.

А. Ю.Бак, Ю. М. Каракис, О. Е. Ступак, М. И. Куталова, А. П. Чебаненко

ОПРЕДЕЛЕНИЕ ШИРИНЫ ЗАПРЕЩЁННОЙ ЗОНЫ ПОЛУПРОВОДНИКОВОГО МАТЕРИАЛА В ГОТОВОМ ИЗДЕЛИИ

Резюме

Предложен метод определения энергии активации полупроводника в готовом изделии. Показано, что ширину запрещённой зоны можно рассчитать по отсечкам на обеих осях графиков *ln(I)÷U*, измеренных при разных температурах. Определён минимальный температурный интервал в зависимости от точности измерений. Указан новый способ определения величины E_g без экстраполяции ВАХ.

Ключевые слова: ширина запрещенной зоны, энергия активации, полупроводник.

UDC 539.135

Yu. V. Dubrovskaya, T. A. Florko, D. E. Sukharev

Odessa National Polytechnical University, 1, Shevchenko av., Odessa, Ukraine
Odessa State Environmental University, 15, Lvovskaya str., Odessa, Ukraine
e-mail: nucdubr@mail.ru

ATOMIC CHEMICAL COMPOSITION EFFECT ON THE BETA DECAY PROBABILITIES FOR ^{35}CL, ^{241}PU

Within a new theoretical scheme for sensing the atomic chemical environment effect on the beta decay characteristics there are presented numerical results for chemical environment effect on the beta decay for ^{35}Cl, ^{241}Pu . Despite on the relative smallness of the atomic chemical environment effect on the β

1. Introduction

In this paper we go on studying the atomic chemical environment effect on the beta decay characteristics and consider chemical environment effect on the beta decay for ^{35}Cl, ^{241}Pu. Let us remind [10,11] that though in a modern nuclear physics there is a number of principally new problems, connected with an unprecedented progress in the physical experiment, nevertheless the classical problems, including the beta decay or low energy nucleus-nucleus collision etc. are remained under intensive theoretical and experimental interest (c.f.[1-11]). This paper goes on our investigations on estimating the beta decay characteristics and sensing an influence of the chemical environment on the b decay parameters with using an optimal theoretical schemes (c.f.[11-16]). In last years a calculating the b decay processes and sensing an influence of the chemical environment on the beta b characteristics attracts a great interest especially due to the new experimental studies of the b decay for a number of nuclei [1-10]. A number of experimental and theoretical papers appeared where the different aspects of the b decay theory and accounting for different factors are considered. One of the important topics is problem to get the data about the neutrino mass from the beta decay spectra shape. An exact value of the half-decay period for the whole number of heavy radioactive nuclei is important for standardisation of data about their properties. Disagreement between different experimental data regarding the b-decay in heavy radioactive nuclei is provided by different chemical environment radioactive nucleus. For example, such disagreement in data on the half-decay period for the ^{241}Pu (see, for example, ref. [1,5,8,9]) is explained in some papers by special beta decay channel. The beta particle in this channel does not transit into free state, but it occupies the external free atomic level. According to ref. [1-5], differences in population of these levels are to be a reason of an influence of the chemical environment on the beta decay. So, a sensing the chemical environment effect on the beta decay is very important to be studied as within a consistent, high accurate theoretical calculation scheme as experimental high precise measurement. Under theoretical consideration of the problem, one has to consider the following effects: i.). A changing electron wave functions because of the changing atomic electric field due to the difference in the valence shells occupation numbers in different chemical substances; ii). A changing up limit of integration under calculating the Fermi integral function in different chemical substances [1,6]. As a rule, the beta particle and neutrino bring away the difference between energies of the mother and daughter atoms. This difference energy is equal to sum of values, provided by atomic nucleus reconstruction and atomic electron shell reconstruction. The entire

energy of electron shell of an atom in the different chemical compounds is different. Due to the changing the nuclear charge Z on unite during the beta decay, this entire energy of electron shell of an atom changes in different chemical compounds by different way; iii). Together with beta decay and ejection of the beta particle out atom it is possible additional channel when the beta electron occupies non-occupied place on the bonded external orbitals of atom. As a rule, special tables [9] for the Fermi function and integral Fermi function is used for calculating the beta spectrum shape. In ref. [9] calculation scheme is based on the non-relativistic Hartree-Fock-Slater approach, but the finite size of nucleus is taken into account. In paper [4] the relativistic Dirac-Fock (DF) method was used. Note that the DF approach is the most wide spread method of calculation, but, as a rule, the corresponding orbitals basis's are not optimized. Some problems are connected with correct definition of the nuclear size effects, QED corrections etc. We are applying below the gauge invariant DF (GIDF) type approach [11-17] for estimating the atomic chemical environment effect on the b decay characteristics for ^{35}Cl, ^{241}Pu .

2. Method

The details of our approach have been presented earlier (see, for example, [10,11,17,18]), here we are limited by the key ideas. As it is well known a distribution of the b particles on energy in the permitted transitions is as follows [9]:

$$dW_\beta(E)/dE = \frac{1}{2\pi^3} G^2 \cdot F(E,Z) \cdot E \cdot p \cdot (E_0 - E)^2 \cdot |M|^2 . \quad (1)$$

Here G is the weak interaction constant; E and $p=(E^2-1)^{1/2}$ are an entire energy and pulse of beta particle; $E_0=1+(E_{bn}/m_e c^2)$, E_{bn} is the boundary energy of β-spectrum; |M| is a matrix element, which is not dependent upon an energy in a case of the permitted β- transitions.

As usually for calculation of the b decay shape and decay half period one should use the tables of the Fermi function and integral Fermi function. The Fermi function F and integral Fermi function f are defined as follows:

$$F(E,Z) = \frac{1}{2p^2}(g_{-1}^2 + f_{+1}^2), \quad (2a)$$

$$f(E_0,Z) = \int_1^{E_0} F(E,Z) \cdot E \cdot p \cdot (E_0 - E)^2 dE. \quad (2b)$$

Here f_{+1} and g_{-1} are the relativistic electron radial functions; the indexes $\pm l=c$, where $c=(l-j)/(2j+1)$. Two schemes of calculation are usually used: i). the relativistic electron radial wave functions are calculated on the boundary of the spherical nucleus with radius R_0 (it has done in ref. [4]); ii). the values of these functions in the zero are used (see ref.[9]).

The normalisation of electron radial functions f_i and g_i provides the behaviour of these functions for large values of radial valuable as follows:

$$g_\varkappa(r) \to r^{-1}[(E+1)/E]^{1/2} \sin(pr + \delta_\varkappa), \quad (3a)$$

$$f_\varkappa(r) \to r^{-1}(\varkappa/|\varkappa|)\,[(E-1)/E]^{1/2} \cos(pr + \delta_\varkappa) \quad (3b)$$

An effect of interaction in the final state between beta electron and atomic electrons with an accuracy to $(aZ/v)^2$ is manifested and further accounted for in the first non-vanishing approximation [8]. This contribution changes the energy distribution of the beta electron on value and is derived in Ref. [1].

As method of calculation of the relativistic atomic fields and electron wave functions, we have used the GIDF approach [10,11]. The potential of Dirac equation includes also the electric and polarization potentials of a nucleus (the gaussian form of charge distribution in the nucleus was used).

All correlation corrections of the PT second and high orders (electrons screening, particle-hole interaction etc.) are accounted for [5]. The GIDF equations for N-electron system are written and contain the potential:

$$V(r) = V(r|nlj) + V_{ex} + V(r|R),$$

which includes the electrical and polarization potentials of the nucleus. The part V_{ex} accounts for exchange inter-electron interaction. Note that a procedure of the exchange account in the GIDF scheme is similar to one in the usual DF approach. Regarding the GIDKS scheme, it is

similar to usual DKS scheme. The optimization of the orbital basises is realized by iteration algorithm within gauge invariant QED procedure (look its application in the beta-decay theory [5]). Approach allows calculating the continuum wave functions, taking into account fully an effect of exchange of the continuum electron with electrons of the atom. Note that this is one of the original moments of the paper. Another original moment is connected with using the consistent QED gauge invariant procedure for optimization of the electron functions basis's. Numerical calculation and analysis shows that used methods allow getting the results, which are more precise in comparison with analogous data, obtained with using non-optimized basis's. The details of the numerical procedure are presented in ref. [11-17].

3. Results and conclusions

In Table 1 we present presents our data on the atomic chemical environment effect on the probability of β decay $^{35}Cl \rightarrow ^{35}Ar$. From the physical viewpoint it is understandable that the quantitative effect of the chemical environment of part of the decay is sufficiently small.

The situation (compared with Cl) changes in the transition to the consideration of the decay $^{241}Pu \rightarrow ^{241}Am$. In Table 2 there are presented the corresponding results for the decay $^{241}Pu \rightarrow ^{241}Am$, including the value of $\Delta f/f = -\Delta T_{1/2}/T_{1/2}$.

Table 1

The atomic chemical environment effect on the b decay probability $^{35}Cl \rightarrow ^{35}Ar$; Changing the half-period $T_{1/2}$ (our data)

Decay of neutral atom		
Atom	E_{bn}, eV	$\Delta f/f$. %
$Cl(^0)$	4948000 4948200	0,003
Decay of ionized atom		
Ion	E_{bn} , eV	$\Delta f/f$. %
$Cl(^{-1})$	4947800 4948000	0,003

Table 2

The atomic chemical environment effect on the b decay probability $^{241}Pu \rightarrow ^{241}Am$. Changing the half-period $T_{1/2}$ (our data)

Decay of neutral atom			
Atom	E_{bn}, eV	$f(E_{bn},Z)$	$\Delta f/f$. %
$Pu^{(0}$	20800 20815	1,72248(-3) 1,72615(-3)	0,3
Decay of ionized atom			
Ion	E_{bn} , eV	$f(E_{bn},Z)$	$\Delta f/f$. %
$Pu^{(2+)}$	20785 20800	1,71725(-3) 1,72099(-3)	0,3

Analysis for two versions of data shows that there are obtained give similar results, and, in particular, very similar values for the changing $T_{1/2}$ when the ionic parameter is changed. Regarding the value of the integral Fermi function, the characteristic value for the decay of ionized chlorine is less than in the case of neutral chlorine, respectively chlorine ionized decay is slower. The value of the Fermi function is greater for the neutral Cl and, therefore, β-decay of the neutral Cl is faster. As it can be seen from Table 2, the corresponding difference in the values of $T_{1/2}$ for Pu is about 0,3%.In conclusion let us note that our conclusions fully coincide with analysis and conclusions, presented in [1]. Despite on the relative smallness of the atomic chemical environment effect on the b decay probabilities for corresponding decays, the situation may be significantly changed under consideration of the beta decay for the heavy elements.

References

1. Glushkov A.V., Khetselius O.Yu., Lovett L., Electron-b-nuclear spectroscopy of atoms and molecules and chemical environment effect on the b-decay parameters// Advances in the Theory of Atomic and Molecular Systems Dynamics, Spectroscopy, Clusters, and Nanostructures. Series: Progress in Theoretical Chemistry and Physics, Eds. Piecuch P., Maruani J., Delgado-Barrio G., Wilson S. (Berlin, Springer).-2009.-Vol. 20.-P. 125-172.
2. Tegen R., Beta decay of the free neutron and a (near) degenerate neutrino mass//Nucl.Phys.A.-2002.-Vol.706.-P.193-202.
3. Izosimov I. N., Kazimov A. A., Kalinnikov V. G., Solnyshkin A. A. and Suhonen J., Beta-decay strength measurement, total beta-decay energy determination and decay-scheme completeness testing by total absorption gamma-ray spectroscopy// Phys. Atom. Nucl.-2004.-Vol. 67, N10.-1876-1882.
4. Kopytin I. V., Karelin K. N., and Nekipelov A. A. Exact inclusion of the coulomb field in the photobeta decay of a nucleus and problem of bypassed elements// Phys. Atom. Nucl.-2004.-Vol. 67, N8.-P.1429-1441.
5. Band I.M., Listengarten M.A., Trzhaskovskaya M.B., Possibility of beta decay in model of atom of the Hartree-Fock-Dirac and influence of chemical composition on the beta decay// Izv. AN USSR.-1987.-Vol.51,N11.-P.1998-200
6. Glushkov A.V., Laser- electron-b-nuclear spectroscopy of atomic and molecular systems and chemical environment effect on the b-decay parameters: Review //Photoelectronics.-2010.-N19.-P.28-42.
7. Karpeshin F.,Trzhaskovskaya M.B., Gangrskii Yu.P.,Resonance Internal Conversion in Hydrogen-Like Ions // JETP.-2004.-Vol.99, N2.-P.286-289.
8. Kaplan I., Endpoint energy in the molecular beta spectrum, atomic mass defect and the negative $m^2_{\nu_e}$ puzzle// J.Phys.G.: Nucl.Part.Phys.-1997.-Vol.23.-P.683-692.
9. Drukarev E.G., Strikman M.I., Final state interactions of beta electrons and related phenomena// JETP.-1986. – Vol.64(10).-P.1160-1168.
10. Gelepov B.C., Zyryanova L.N., Suslov Yu.P. Beta processes.-Leningrad: Nauka, 1992.-372p.
11. Malinovskaya S.V., Dubrovskaya Yu.V., Vitavetskaya L.A., Advanced quantum mechanical calculation of the beta decay probabilities// Low Energy Antiproton Phys. (AIP).-2005.-Vol.796.-P.201-205.
12. Malinovskaya S.V., Dubrovskaya Yu.V., Zelentzova T.N., The atomic chemical environment effect on the b decay probabilities: Relativistic calculation// Kiev University Bulletin. Series Phys.-Math.–2004.-№4 .-C.427-432.
13. Glushkov A.V., Malinovskaya S.V., Dubrovskaya Yu.V., Sensing the atomic chemical composition effect on the b decay probabilities // Sensor Electr. & Microsyst. Techn.-2005.-N1.-P.16-20.
14. Dubrovskaya Yu.V., The atomic chemical environment and beta electron final state interaction effect on beta decay probabilities// Photoelectronics.-2005.-N14.-P.86-88.
15. Dubrovskaya Yu.V., The beta electron final state interaction effect on beta decay probabilities// Photoelectronics.-2006 .-N15.-P.92-94.
16. Turin A.V., Khetselius O.Yu.,. Dubrovskaya Yu.V, The beta electron final state interaction effect on beta decay probabilities for ^{42}Se nucleus within relativistic Hartree-Fock approach//Photoelectronics.-2007.-N16.-P.120-122..
17. Dubrovskaya Yu.V., Atomic chemical composition effect on the beta decay probabilities//Photoelectronics.-Vol.22.-P.124-129.
18. Dubrovskaya Yu.V., Sukharev D.E., Vitavetskaya L.A., Relativistic theory of the beta decay: Environment and final state interaction effects// Photoelectronics.-2011.-Vol.20.-P.113-116

This article has been received within 2014

UDC 539.135

Yu. V. Dubrovskaya, T. A. Florko, D. E. Sukharev

ATOMIC CHEMICAL COMPOSITION EFFECT ON THE BETA DECAY PROBABILITIES FOR ^{35}Cl, ^{241}Pu

Abstract

Within a new theoretical scheme for sensing the atomic chemical environment effect on the beta decay characteristics there are presented numerical results for chemical environment effect on the beta decay in the ^{35}Cl, ^{241}Pu . Despite on the relative smallness of the atomic chemical environment effect on the b decay probabilities for corresponding decays, the situation may be significantly changed under consideration of the beta decay for the heavy elements.

Key words: atomic chemical composition effect, beta decay probability

УДК 539.135

Ю. В. Дубровская, Т. А. Флорко, Д. Е. Сухарев

АТОМНЫЙ ЭФФЕКТ ВЛИЯНИЯ ХИМИЧЕСКОГО ОКРУЖЕНИЯ НА ВЕРОЯТНОСТЬ БЕТА РАСПАДА ДЛЯ ^{35}Cl, ^{241}Pu

Резюме

В рамках новой теоретической схемы вычисления эффекта влияния химического окружения на характеристики b распада представлены численные оценки влияния химического окружения на b распад ^{35}Cl, ^{241}Pu. Несмотря на относительную малость эффекта влияния химического окружения на вероятность бета-распада, ситуация существенно изменяется в случае бета-распада тажелых элементов.

Ключевые слова: влияние химического окружения, вероятность бета распада.

УДК 539.135

Ю. В. Дубровська, Т. О. Флорко, Д. Є. Сухарев

АТОМНИЙ ЕФЕКТ ВПЛИВУ ХІМІЧНОГО ОТТОЧЕННЯ НА ІМОВІРНІСТЬ БЕТА РОЗПАДУ ДЛЯ ^{35}Cl, ^{241}Pu

Резюме

На основі нової теоретичної схеми обчислення ефекту впливу хімічного отточення на характеристики b розпаду представлені чисельні оцінки впливу хімічного отточення на b розпад ^{35}Cl, ^{241}Pu . Недивлячись на відносну малість ефекту впливу хімічного отточення на імовірність бета-розпаду, ситуація суттєво змінюється у випадку бета-розпаду важких елементів.

Ключові слова: вплив хімічного отточення, імовірність бета розпаду

UDC 621. 317

I. M. Vikulin, SH. D. Kurmashev. A. V. Veremyova

Odessa national Academy of Telecommunications, Kuznechnaya Street 1, Odessa 65029, Ukraine,
phone/fax: +38-048 -7236118, E-mail: kurmash12@gmail.com

BRIDGE SENSORS BASED ON FIELD-EFFECT TRANSISTORS

Possibility of the use of the field-effect transistors is considered in the bridge sensors of the magnetic field, temperature and light. It is shown that maximum sensitivity is attained in the sensor bridge circuit, where the elements in the four arms of the bridge field effect transistors are used, and one pair of transistors current increases with the growth of measured value, and the other - is decreased.

Keywords: sensor, bridge circuit, field-effect transistor

1. Introduction

The base of measuring systems is represented by the primary sensors. They transform input physical values (temperature, pressure, illumination, magnetic flux, acceleration etc.) into proportional electrical output signal [1]. One of the features of parametric sensors is changing of parameters of electrical, magnetic, optical circuits – resistance, inductance, capacity, light penetration and others. They are passive (i.e. allow to make indirect conclusions about the physical value by connecting the sensor to the electrical circuit) and need a power supply. The effect of active resistance changing frequently is used in such sensors (thermoresistive, photoresistive and magnetic-resistive effects), changing of permittivity, light transmittance and so on.

When connecting resistive sensors bridge circuits in many cases are used. In such measuring circuits eliminates the main drawback of most of measuring circuits with voltage dividers – presence of non-zero output signal with absence of signal on input of the measuring circuit. As is known, bridge measuring scheme has two arms: the measuring arm in which the parametrical sensor is included, and the base one. When the bridge is connected, voltage is given on one of its diagonals, and output signal is read from the other. In non-equilibrium bridge mode in the initial state bridge is balanced, that is, the output signal is set to zero value.

During the further deviation of resistances (impedances) from their initial values a non-zero output signal is formed. Depending on the number of measuring transformers (primary sensors), there are quarter-bridge, half-bridge and full-bridge sensor schemes. To decrease non-linearity of the output characteristic, we apply differential connection to a bridge scheme of measuring transformers, having sensitivities opposite in sign to each other [2]. The weakness of the well-known resistivity (impedance) sensors is their little sensitivity to weak input signals. The purpose of this work is to study the possibilities to increase the sensitivity of parametrical sensors based on bridge schemes by using elements with internal amplification (field-effect transistors -FET).

1. Magnetic field sensors

In a semiconductor placed inside a magnetic field we can observe a magnetic-resistive effect, which shows itself in decreasing charge carriers' mobility and, correspondingly, increase of electric resistance of the material. It completely refers to the channel of the field-effect transistor placed into a transversal magnetic field [3]. In this case, same as in a magnetoresistor, the channel length should be much less than its width. An example that satisfies this condition is FET with *n*-type channel and *p*-*n*-junction as a gate. When the

FET operates as a primary transformer it is usually connected as a dipole (the gate connected to the source, voltage on the gate U_g=0). In this case, saturation current of the FET is defined as

$$I_s = An^2 \mu, \quad (1)$$

where n, μ - concentration and mobility of charge carriers in a channel, A – constant that is defined by geometrical and electrical parameters of channel that depend on voltage [3]. Change of current I_s of such FET in a magnetic field with induction up to 0.5 T is about 1% and, in this case, is of no practical interest as a sensor output parameter.

The most preferable as a sensor is a scheme of two FET, one of them is a magnetosensitive element (MFET), the other one operates as a load. Such scheme is shown on fig. 1. Current-voltage characteristics (CVC) of MFET with such load and the load curve are shown on fig. 2. Here E is the supply voltage. As a result of small angle between voltage axis and CVC in the area of current saturation, a small change of saturation current will lead to significant change of voltage on MFET: from U_0 to U_B. Two FET with similar saturation current are selected for the sensor scheme. When magnetic field is absent (inductance B=0), the supply voltage E is equally divided between two FET, and U_0=E/2. When MFET is placed into a magnetic field that is perpendicular to current direction, the resistance of channel increases, while the saturation current decreases. This leads to increase of voltage on MFET till it reaches the value U_B. Unlike the magnetoresistors' operation, this process is accompanied by internal mechanism of sensitivity increase. This is caused by the fact that resistance of any FET in the area of CVC saturation increases with the increase of voltage, as with increase of voltage U the current I_s slightly increases. Thus, increase of MFET channel resistance leads to increase of voltage drop U_B, and this causes additional increase of channel resistance and increase of U_B.

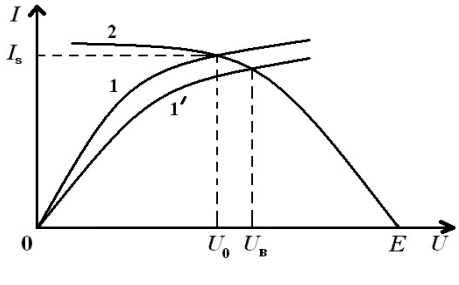

Figure 1. Scheme of the magnetosensitive element with two field-effect transistors: 1 –MFET, 2 – FET.

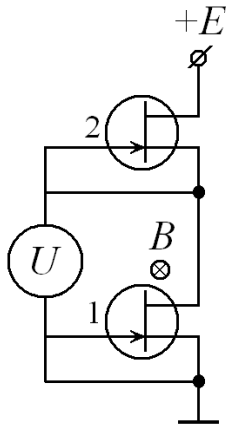

Figure 2. Voltage-current characteristics of MFET: 1 – magnetic field is absent; 1' – with active magnetic field; 2 – load curve.

For the output voltage of sensor to be measured from zero a bridge scheme is used (fig. 3) where another pair of FET (load FET) is connected to a pair of MFET transistors. Two MFET are located in opposite arms of the bridge, load FET – also in the opposite arms. Trimmer alternating resistor R_{tr} serves for precise specification of zero (bridge balancing) when the magnetic field is absent. Besides the obvious doubling of magnetic sensitivity (in comparison to one sensitive element), such half-bridge scheme of four FET (two of them are magnetosensitive) allows to remove the temperature zero drift of zero of the output voltage and to reduce the temperature coefficient of magnetic sensitivity to values less than 0.1 %/^{0}C. Dependence of output voltage U on magnetic inductance B is shown on fig. 4. It is clear that this voltage increases with increase of induction B and increase of supply voltage E. Magnetic sensitivity $\gamma = U/I \cdot B$ for bridge sensors based on FET is ~$5 \cdot 10^3$ V/A·T, which is 50 times greater than for Hall's silicon sensors.

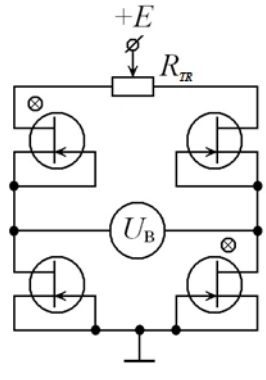

Figure 3. Bridge scheme of the magnetosensitive actuator.

We also notice that in contradiction to magnetoresistors, magnetic sensitivity of FET-based sensors is maximal in the range of weak magnetic fields, while the magnetoresistors have the minimal one.

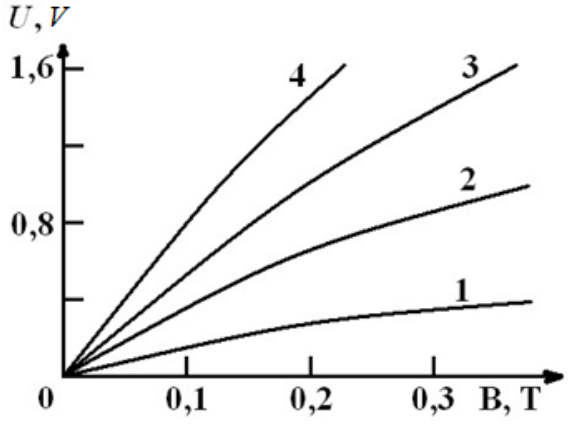

Figure 4. Dependence of output voltage U on magnetic inductance B. Supply voltage E, B: 1 -10, 2 -15, 3 -20, 4 -25.

If we place both MFT (fig. 3) into an inhomogeneous magnetic field, the output signal will be proportional to difference between the inductions of magnetic field in two points of location of FET channels. Such sensor can be used for measuring of gradient of an inhomogeneous magnetic field.

1. **Temperature sensors**

Field-effect transistors can be used as temperature sensors. The maximal sensitivity of the bridge sensor can be obtained in case all the four components are elements sensitive to the measured value and their sensitivities are opposite in sign (fig. 5). The current of the first pair of elements (situated in opposite arms of the bridge) should increase with growth of this value, and the current of the second pair (situated in the other two arms) should increase. For a bridge with such scheme of connection of primary transformers, voltage of the signal on the measuring diagonal is

$$U = \frac{E \Delta R}{R}. \qquad (2)$$

Here E – voltage circuit of the bridge, R – channel resistance of transistor in a circuit "source-drainage", ΔR - change of this resistance with the change of temperature. As the first pair we used FET (T_1) with *p-n*-junction as a gate. Their saturation current I_S decreases with growth of temperature, as a result of recession of charge carriers' mobility in the channel [3]. Metal-oxide-semiconductor (MOS) transistor (T_2) were connected as a second pair. Their current I_s increases with the increase of temperature. This is due to increasing gate voltage cut-off when changing the charge on the surface states under the gate [4].

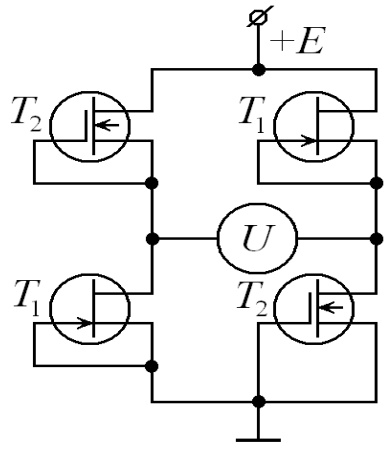

Figure 5. Bridge temperature sensor.

Expansion of linear range U=f(T) can be performed by introducing a resistor R_S into every FET source. Figure 6 shows dependence of output voltage of the bridge that is balanced at a temperature T=0^0 C. Sensitivity of bridge is ~1 V/^{0}C at f supply voltage E=20 V and R_S=0 in the temperature range of (-10…+10) ^{0}C (curve 1). Outside this range sensitivity decreases and nonlinearity of U=f(T) dependence increases.

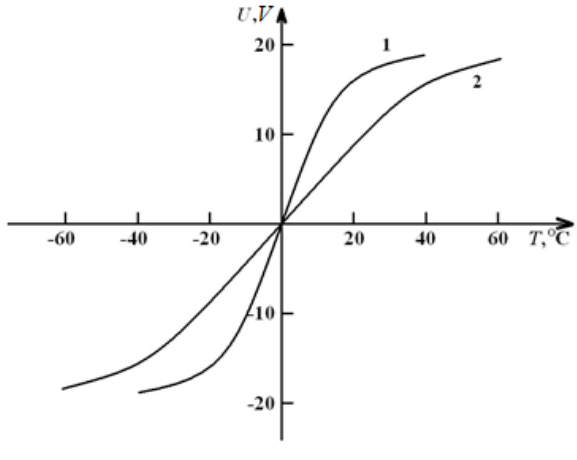

Figure 6. Dependence of output voltage on temperature. Resistance of FET source circuit R_S, kΩ : 1 – 0; 2 – 1.

At R_S=1 kΩ the dependence U=f(T) is linear in the range of (-35…+35) ^{0}C, and sensitivity decreases to the value 0.3 V/ ^{0}C (curve 2). The same resistors can be used to balance the bridge at any given temperature. It is known that the thermosensitivity of a FET-based bridge is 10…100 times higher than the one for bridge sensors based on other elements [5].

2. Photodetecting devices

A full-bridge sensor model, in which the current that flows through one FET pair increases with external influence and decreases when it flows through another pair, can also be used to create a photodetecting device (PhDD). Fig. 7 shows the structures of two types of MOS-FET-phototransistors. Transistor of first type PhT_1 (fig. 7a) is a simple MOS-FET with built-in channel based on semiconductor of n-type conductivity with two contacts (S – source, DR - drainage) with a dielectric (D) and a metallic gate (G), connected to the source. When the structure is lightened from the side of semitransparent metallic gate G, the light is absorbed in the channel, the concentration of charge carriers in it increases, and the current through PhT_1 increases. The transistor PhT_1 can also be lightened from the opposite side of the channel, i.e. from the side of the substrate.

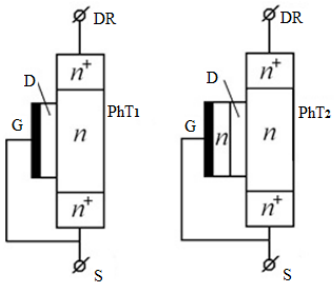

a) b)

b)

Figure 7. MOS-FET with built-in channel (a), with the n-type semiconductor between the gate and the dielectric (b).

The main difference between the transistor PhT_1 and the transistor of the second type PhT_2 (fig. 7b) is the presence of a layer of n-type semiconductor between the metallic layer of the gate and the dielectric. The contact metal-semiconductor (gate) is a Shottky diode (SD). When this structure is lightened from the side of semitransparent metal, a photo-EMF appears in SD with metal as a "plus" and semiconductor as "minus". This photo-EMF stands for the input signal for PhT_2 transistor and reduces concentration of charge carriers in the channel. As a result, the current through PhT_2 decreases with lightning. In this case all the light is absorbed in the n-layer and never reaches the channel.

The sensor operation can be explained with the help of the scheme (fig. 8). When there is no lightning, resistance on all phototransistors in the bridge arms is the same. The applied voltage E is distributed equally to PhT_1 and PhT_2, The potentials U_1 and U_2 in the measuring diagonal of the bridge are equal, and the output signal U_{out} = U_1-U_2=0, that means the bridge is balanced. In real life, phototransistors usually have scattered parameters, that's why the bridge should be balanced with the help of trimmer resistor R_{tr} or the resistors in the circuits of the sources. Lightning of PhDD by a stream Φ causes decrease of PhT_1 resistance and increase of PhT_2 resistance. This leads to misbalancing of the bridge, potential U_1 increases, potential U_2 decreases, i.e. the output signal $U_{out} = U_1$-U_2 increases with increase of light stream Φ.

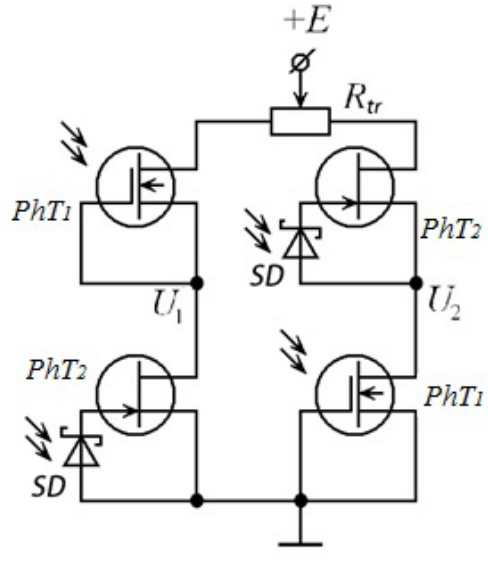

Figure 8. The scheme of a bridge photosensor (PhDD).

Experimental samples of PhDD were made based on serial MOS-FET-transistor (PhT_1) with a structure shown in fig. 7a. With the source-drainage voltage $U_{S\text{-}DR}$ = 10V and a closed gate, channel resistance is ~ 10 kΩ. The main difference between PhT_1 and PhT_2 is the presence of a layer of *n*-type semiconductor between the metallic layer of gate and the dielectric. The thickness of this layer should be such that all the light would be absorbed in it and didn't reach the channel. The lightning of phototransistors was made by a "green" light-emitting diode (maximal light emission at wavelength $\lambda = 0.56\ \mu$m). The maximal lightening power reached 0.6 m*W* with the current through the light-emitting diode 100 mA. Photosensitivity of PhDD experimental samples at E=20 V was 10...100 times greater than the one of photodetectors based on photodiodes and bipolar transistors [5].

Results

To sum up, we shall note that bridge schemes are also applied for construction of pressure sensors. Silicon membranes are widely used as pressure sensors. They are represented by a plate with four diffusion tensoresistors that form a measuring bridge [2]. We have observed that replacing the resistors by field transistors also allows to significantly improve sensitivity of pressure sensors.

Using FET in measuring bridges allows to increase sensitivity of sensors, to reduce energy consumption, and to provide stability of measuring devices.

References

1. Sharapov V. M., Vikulin I. M., Kurmashev Sh. D., Sensors, Cherkassy Brama, - 2008.- pp 430-470 .
2. V. A. Teslenko, Actuators in data and management collecting systems// Journal of Industrial measurements, control, automatics, diagnostics 2004, 2 (1), pp 50-56.
3. Vikulina L. F., Glauberman M.A., Physics of the temperature and magnetic field sensors, Odessa Lighthouse.- 2000-17-123 pp.
4. A. I. Krivonosov, Semiconductor temperature actuators. Moscow, Energy.- 2004 -156 p.
5. Vikulin I.M., Kurmashev Sh.D., Stafeev V.I., Injection-based photodetectors// *J. Semiconductors* 2008, 42 (1), pp 112-127.

This article has been received within 2014

UDC 621. 317

I. M. Vikulin, Sh. D. Kkurmashev. A. V. Veremyova

BRIDGE SENSORS BASED ON FIELD-EFFECT TRANSISTORS

Abstract

Possibility of the use of the field transistors is considered in the bridge sensors of the magnetic field, temperature and light. It is shown that maximum sensitivity is attained in the sensor bridge circuit, where the elements in the four arms of the bridge field effect transistors are used, and one pair of transistors current increases with the growth measured value, and the other - is decreased.

Key words :field transistors, bridge sensors, maximum sensitivity.

УДК 621. 317

И. М. Викулин, Ш. Д. Курмащев, А. В. Веремьева

МОСТОВЫЕ ДАТЧИКИ НА ОСНОВЕ ПОЛЕВЫХ ТРАНЗИСТОРОВ

Резюме

Рассмотрена возможность использования полевых транзисторов в мостовых датчиках магнитного поля, температуры и света. Показано, что максимальная чувствительность достигается в мостовых схемах датчиков, где в качестве всех четырех элементов в плечах моста используются полевые транзисторы, причем у одной пары транзисторов ток увеличивается с ростом измеряемой величины, а у другой – уменьшается.

Ключевые слова: полевые транзисторы, мостовые датчики, максимальная чувствительность.

УДК. 621. 317

І. М. Вікулін, Ш. Д. Курмашев, Г. В. Веремйова

МОСТОВІ ДАТЧИКИ НА БАЗІ ПОЛЬОВИХ ТРАНЗИСТОРОВ

Резюме

Розглянуто можливість використання польових транзисторів в мостових датчиках магнітного поля, температури та світла. Показано, що максимальна чутливість досягається в мостових схемах датчиків, де в якості всіх чотирьох елементів в плечах моста використовуються польові транзистори, причому в однієї пари транзисторів струм збільшується із зростанням вимірюваної величини, а в іншої – зменшується.

Ключові слова: польові транзистори, мостові датчики, максимальна чутливість.

UDC 539.183

A. V. Glushkov, P. A. Kondratenko, Yu. M. Lopatkin, V. V. Buyadzhi, A S. Kvasikova

[1]National Aviation University, 1, Komarov Ave, 03680 Kiev, Ukraine
[2]Odessa National Polytechnical University, 1, Shevchenko av., Odessa, Ukraine
[3]Odessa State Environmental University, 15, Lvovskaya str., Odessa, Ukraine
e-mail: dirac13@mail.ru

SPECTROSCOPY OF COOPERATIVE LASER ELECTRON-γ NUCLEAR PROCESSES IN MULTIATOMIC MOLECULES: OsO_4

The consistent quantum approach to calculating the electron-nuclear γ transition spectra (a set of the vibration-rotational satellites in a spectrum of molecule) of a nucleus in the multiatomic molecules is used to obtain the accurate data on the vibration-nuclear transition probabilities in a case of the emission and absorption spectrum of the nucleus ^{188}Os ($E^{(0)}_{\gamma}$ = 155 ke V) in the molecule of OsO_4. Analysis shows that more sophisticated theoretical approach gives the higher values for the cited probabilities.

1. Introduction

Any alteration of the molecular state must be manifested in the quantum transitions, for example, in a spectrum of the γ-radiation of a nucleus. It is well known that it is possible the transfer of part of a nuclear energy to atom or molecule under radiating (absorption) the γ quanta by a nucleus (c.f.[1-12]). A spectrum contains a set of the electron-vibration-rotation satellites, which are due to an alteration of the state of system interacting with photon. A mechanism of forming satellites in the molecule is connected with a shaking of the electron shell resulting from the interaction between a nucleus and γ quantum. [1,3,13-20]. An appearance of the molecular nuclear lines represents a great interest as it opens a possibility of the changing γ-radiation spectrum by means of changing the vibration-rotational state of a molecule by a laser light [1,12,16]. The well known example is the Szilard-Chalmers effect (molecular dissociation because of the recoil during radiating gamma quantum with large energy; c.f. [1, 2]). This paper is going on our studying the co-operative dynamical phenomena (c.f.[14-19]) due the interaction between atoms, ions, molecule electron shells and nuclei nucleons. We present an advanced approach to description of a new class of dynamical laser-electron-nuclear effects in molecular spectroscopy, in particular, we study the nuclear gamma-emission or absorption spectrum of a molecule. A consistent quantum- mechanical approach to calculation of the electron-nuclear γ transition spectra (set of vibration-rotational satellites in molecule) of a nucleus in the multiatomic molecules has been earlier proposed [14-16]. It generalizes the well known Letokhov-Minogin model [3]. Estimates of the vibration-nuclear transition probabilities in a case of the emission and absorption spectrum of nucleus ^{191}Ir ($E^{(0)}_{\gamma}$ = 82 keV) in the molecule of IrO_4 and other molecules were listed . Here we present the accurate data on the vibration-nuclear transition probabilities in a case of the emission and absorption spectrum of nucleus nucleus ^{188}Os ($E^{(0)}_{\gamma}$ = 155 keV) in the molecule of OsO_4.

2.The electron-nuclear γ transition spectra of nucleus in multi-atomic molecules

As the method of computing is earlier presented in details [14-16], here we consider only by

the key topics The main purpose is calculating a structure of the gamma transitions (a probability of transition) or spectrum of the gamma satellites because of changing the electron-vibration-rotational states of the multi-atomic molecules under gamma quantum radiation (absorption). Here we are limited by a case of the five-atomic molecules (of XY_4 type; T_d). Hamiltonian of interaction of the gamma radiation with a system of nucleons for the first nucleus can be expressed through the co-ordinates of nucleons r_n' in a system of the mass centre of the one nucleus [3,15]:

$$H(r_n) = H(r_n') \exp(-k_\gamma u) \qquad (1)$$

where k_γ is a wave vector of the gamma quantum; u is the shift vector from equality state (coinciding with molecule mass centre) in system of co-ordinates in the space. The matrix element for transition from the initial state "a" to the final state "b" is presented as usually:

$$< \Psi_b^* \mid H \mid \Psi_a > \bullet < \Psi_b^* \mid e^{-ik_\gamma u} \mid \Psi_a > \qquad (2)$$

where a and b is a set of quantum numbers, which define the vibrational and rotational states before and after interaction (with gamma- quantum). The first multiplier in eq. (2) is defined by the gamma transition of nucleus and is not dependent upon the internal structure of molecule in a good approximation. The second multiplier is the matrix element of transition of the molecule from the initial state "a" to the final state "b":

$$M_{ba} = < \Psi_b^*(r_e) \mid \Psi_a(r_e) > \bullet$$
$$\bullet < \Psi_b^*(R_1, R_2) \mid e^{-ik_\gamma R_1} \mid \Psi_a(R_1, R_2) > \qquad (3)$$

The expression (3) gives a general formula for calculating the probability of changing the internal state of molecule during absorption or emitting γ quantum by a nucleus. It determines an intensity of the corresponding γ-satellites. Their positions are fully determined as follows:

$$E_\gamma = E_\gamma^0 \pm R + \hbar k_\gamma v \pm (E_b - E_a) \qquad (4)$$

Here M is the molecule mass, v is a velocity of molecule before interaction of nucleus with γ quantum; E_a and E_b are the energies of the molecule before and after interaction; E_γ is an energy of nuclear transition; R_{om} is an energy of recoil: $R_{om} = [(E_\gamma^{(o)}]^2/2Mc^2$. One can suppose that only single non-generated normal vibration (vibration quantum $\hbar\omega$) is excited and initially a molecule is on the vibrational level $v_a = 0$. If we denote a probability of the corresponding excitation as $P(v_b, v_a)$ and use expression for shift u of the γ-active nucleus through the normal co-ordinates, then an averaged energy for excitation of the single normal vibration is as follows:

$$\overline{E}_{\text{vib}} = \sum_{v=0}^{\infty} \hbar\omega\left(v + \tfrac{1}{2}\right)\overline{P}(v,0) - \hbar\infty/2 =$$
$$= \sum_{v=0}^{\infty} \hbar\omega\left(v + \tfrac{1}{2}\right)P(v,0) - \hbar\omega/2 =$$
$$= \sum_{v=0} \hbar\omega\left(v + \tfrac{1}{2}\right)\frac{z^v}{v!}e^{-z} - \frac{\hbar\omega}{2} = \frac{1}{2}R\left(\frac{M-m}{m}\right), \qquad (5)$$

where $z = (R/\hbar\omega)[M - m/m]\cos^2\vartheta$, and m is the mass of γ-active nucleus, ϑ is an angle between nucleus shift vector and wave vector of γ-quantum and line in $\overline{E}_{\text{vib}}$ means averaging on orientations of molecule (or on angles ϑ).

To estimate an averaged energy for excitation of the molecule rotation, one must not miss the molecule vibrations as they provide non-zeroth momentum $L = k_v u \sin\vartheta$, which is transferred to a molecule by γ-quantum. In supposing that a nucleus is only in the single non-generated normal vibration and vibrational state of a molecule is not changed $v_a = v_b = 0$, one could evaluate an averaged energy for excitation of the molecule rotations as follows:

$$\overline{E}_{\text{rot}} = \left\langle \overline{BL^2} \right\rangle = Bk_\gamma^2 \left\langle u^2 \right\rangle \overline{\sin^2\vartheta} =$$
$$= \tfrac{1}{2} R(B/\hbar\omega)[(M-m)/m] \qquad (6)$$

As for multi-atomic molecules it is typical $B/\hbar\omega \sim 10^{-4}$-$10^{-2}$, so one could miss the molecule rotations and consider γ-spectrum of a nucleus in the molecule mass centre as a spectrum of the vibration-nuclear transitions. A shift u of the γ-active nucleus can be expressed through the normal co-ordinates $Q_{s\sigma}$ of a molecule:

$$u = \frac{1}{\sqrt{m}} \sum_{s\sigma} b_{s\sigma} Q_{s\sigma} \qquad (7)$$

where m is a mass of the γ- active nucleus; components of the vector $b_{s\sigma}$ of nucleus shift due to the σ-component of "s" normal vibration of a molecule are the elements of matrix b [2]; it realizes the orthogonal transformation of the normal co-ordinates matrix Q to matrix of masses of the weighted Cartesian components of the molecule nuclei shifts q. According to eq.(1), the matrix element can be written as multiplying the matrix elements on molecule normal vibration, which takes contribution to a shift of the γ- active nucleus:

$$M(b,a) =$$

$$= \prod_s \left\langle v_s^{\,b} \left| \prod_\sigma \exp(-k_\gamma b_{s\sigma} Q_{s\sigma} / \sqrt{m}) v_s^{\,a} \right| \right\rangle. \qquad (8)$$

It is obvious that missing molecular rotations means missing the rotations which are connected with the degenerated vibrations. Usually wave functions of a molecule can be written for non-degenerated vibration as:

$$| v_s \rangle = \Phi_{v_s}(Q_s), \qquad (9)$$

for double degenerated vibration in the form:

$$|v_s\rangle = (v_s+1)^{-1/2} \sum_{v_{s\sigma_1}, v_{s\sigma_2}, v_{s\sigma_3}} \Phi_{v_{s\sigma_1}}(Q_{s\sigma_1}) \Phi_{v_{s\sigma_2}}(Q_{s\sigma_2}) \qquad (10)$$

(where $v_{s\sigma_1} + v_{s\sigma_2} = v_s$) and for triple degenerated vibration as follows:

$$|v_s\rangle = \left(\frac{2}{(v_s+1)(v_s+2)} \right)^{1/2} \times$$

$$\times \sum_{v_{s\sigma_1}, v_{s\sigma_2}, v_{s\sigma_3}} \Phi_{v_{s\sigma 1}}(Q_{s\sigma_1}) \Phi_{v_{s\sigma_2}}(Q_{s\sigma_2}) \Phi_{v_{s\sigma_3}}(Q_{s\sigma_3}) \qquad (11)$$

where $v_{s\sigma_1} + v_{s\sigma_2} + v_{s\sigma_3} = v_s$.

In the simple approximation function $\Phi_{v_{s\sigma}}(Q_{s\sigma})$ can be chosen in a form of the linear harmonic oscillator one. More exact calculating requires a numerical determination of these functions. Taking directly the wave functions $|v_s^a\rangle$ and $|v_s^b\rangle$, calculating the matrix element (8) is reduced to a definition of the matrix elements on each component γ of the normal vibration.

3. Results and conclusions

Below we present the accurate data on the vibration-nuclear transition probabilities in a case of the emission and absorption spectrum of nucleus ^{188}Os ($E^{(0)}_\gamma$ = 155 keV in the molecule OsO_4. Note that the main difficulty during calculating (8) is connected with definition of the values $b_{s\sigma}$ of the normalized shifts of γ-active decay. It is known that if a molecule has the only normal vibration of the given symmetry type, then the corresponding values of $b_{s\sigma}$ can be found from the well known Eccart conditions, normalization one and data about the molecule symmetry. For several normal vibrations of the one symmetry type, a definition of $b_{s\gamma}$ requires solving the secular equation for molecule $|GF-\lambda E|=0$ [21-24]. We have used the results of advanced theoretical calculating electron structure of the studied system within an advanced relativistic scheme of the X_γ- scattered waves method (see details in Refs.[21,24]). In table 1 we present the results of calculating probabilities of the first several vibration-nuclear transitions in a case of the emission and absorption spectrum of nucleus ^{188}Os ($E^{(0)}_\gamma$ = 155 keV in OsO_4 and compare with available data Ref.[2], where more simple approximation has been used. Analysis shows that more sophisticated calculation gives the higher values for probabilities.

Table 1

Probabilitites of the vibrational-nuclear transitions in spectrum of OsO_4.

Vibration transition $v_3^{\,a}, v_4^{\,a} - v_3^{\,b}, v_4^{\,b}$	$\overline{P}(v_3^{\,a}, v_4^{\,a} - v_3^{\,b}, v_4^{\,b})$ [15]	$\overline{P}(v_3^{\,a}, v_4^{\,a} - v_3^{\,b}, v_4^{\,b})$ This work
0,0 – 0,0	0.795	0.803
1,0 – 0,0	0.018	0.023
0,1 – 0,0	0.074	0.081
1,0 – 1,0	0.750	0.757
0,1 – 0,1	0.673	0.678

References

1. Letokhov V S, 1997 Laser Spectroscopy, Academic Press, N.-Y.
2. Letokhov V S, 1974 *Phys. Lett.A* 46 257.
3. Letokhov V S and Minogin V G, 1995 *JETP.* 69(5) 1568.
4. Ivanov L N, Letokhov V S 1995 *JETP* 68 1748;
5. Glushkov A V, Loboda A, Gurnitskaya E, Svinarenko A 2009 *Phys. Scripta* T135 014022
6. Glushkov A V, 2012 *J. of Phys.: Conf. Ser.*. 397 012011
7. Glushkov A V and Ivanov L N 1992*Phys. Lett.* A 170 33
8. Law J and Campbell J L,1992 *Phys. Rev.C* 25 514.
9. Amudsen P A and Barker P H, 1999 *Phys.Rev.C* 50 2466
10. L Wauters, N Vaeck, M Godefroid, H var der Hart and M Demeur, 1997 *J.Phys.B.* 30 4569.
11. Shahbaz A, Müller C, Staudt A, Bürvenich T J, Keitel C H 2007 *Phys.Rev. Lett.* 98 263901
12. Fedorov M V 1999 *Phys.-Uspekhi* 169 66
13. Ivanov L N and Letokhov V S *Com. Mod. Phys.* D 4 169
14. A V Glushkov, O Yu Khetselius, Malinovskaya S V, 2008 *Europ. Phys. Journ ST* 160 195.
15. A V Glushkov, O Yu Khetselius, Malinovskaya S V, 2008 *Molec.Phys.* 106 1257.
16. Glushkov A V, Khetselius O Yu, Malinovskaya S V, 2008 *Frontiers in Quantum Systems in Chem. and Phys., Ser. Progr. in Theor. Chem. and Phys.*, vol. 18. ed. S Wilson, P J Grout, J Maruani, G; Delgado-Barrio, P Piecuch (Berlin: Springer) p 523
17. Glushkov A V, Malinovskaya S V, Svinarenko A A and Chernyakova Yu G, 2004 *Int. J. Quant. Chem.* 99 889.
18. Glushkov A , Ivanov L, Ivanova E, 1996 *Autoionization Phenomena in Atoms*, Moscow Univ. Press, Moscow, p 58
19. Khetselius OYu, 2012 *J. of Phys.: Conf. Ser.* 397 012012;
20. Khetselius OYu, 2009 *Phys.Scr.* T.135 014023.
21. Glushkov A, 1993 Journ.Struct. Chem. 34(1) 3.
22. Glushkov A.V. and Malinovskaya S.V., 1998 *Russian J.Phys.Chem.* 62(1) 100.
23. G Simons and R G Parr, 2002 Quantum Chemistry, Academic Press, N-Y.
24. V N Gedasimov, A G Zelenkov, V M Kulakov, V A Pchelin, M V Sokolovskaya, A A Soldatov, L V Chistyakov, 1994 *JETP.* 86 1169; A A Soldatov, 1993 Preprint of I.V.Kurchatov Institute for Atomic Energy IAE-3916, Moscow

This article has been received within 2014

UDC 539.183

A. V. Glushkov, P. A. Kondratenko, Yu. M. Lopatkin, V. V. Buyadzhi, A. S. Kvasikova

SPECTROSCOPY OF COOPERATIVE LASER ELECTRON-G-NUCLEAR PROCESSES IN MULTIATOMIC MOLECULES: OsO_4

Abstract

The consistent quantum approach to calculating the electron-nuclear g transition spectra (a set of the vibration-rotational satellites in a spectrum of molecule) of a nucleus in the multiatomic molecules is used to obtain the accurate data on the vibration-nuclear transition probabilities in a case of the emission and absorption spectrum of the nucleus ^{188}Os ($E^{(0)}_g$ = 155 keV) in the molecule of OsO_4. Analysis shows that more sophisticated theoretical approach gives the higher values for the cited probabilities.

Key words: electron-g-nuclear transition spectrum, multiatomic molecules

УДК 539.183

А. В. Глушков, П. А. Кондратенко, Ю. М. Лопаткин, В. В. Буяджи, А. С. Квасикова

СПЕКТРОСКОПИЯ КООПЕРАТИВНЫХ ЛАЗЕРНЫХ ЭЛЕКТРОННО-ГАММА-ЯДЕРНЫХ -ПРОЦЕССОВ В МНОГОАТОМНЫХ МОЛЕКУЛАХ: OsO_4

Резюме

Последовательный квантовый подход к расчету электронно-гамма-ядерного спектра (система колебательно-вращательных спутников в спектре молекуле) в многоатомных молекулах используется, чтобы получить уточненные данные о вероятностях колебательно-ядерных переходов в молекуле OsO_4 в случае испускания и поглощения гамма-кванта ядром ^{188}Os ($E^{(0)}_g$ = 155 кэВ). Анализ показывает, что более последовательный теоретический подход дает более высокие значения искомых вероятностей.

Ключевые слова: спектр электрон- g -ядерных переходов, многоатомные молекулы

УДК 539.183

О. В. Глушков, П. О. Кондратенко, Ю. М. Лопаткін, В. В. Буяджи, Г. С. Квасикова

СПЕКТРОСКОПІЯ КООПЕРАТИВНИХ ЛАЗЕРНИХ ЕЛЕКТРОННО-ГАММА-ЯДЕРНИХ ПРОЦЕСІВ У БАГАТОАТОМНИХ МОЛЕКУЛАХ: OsO_4

Резюме

Послідовний квантовий підхід до розрахунку електронно-гамма-ядерного спектру (система коливально-обертальних супутників у спектрі молекули) в багатоатомних молекулах використовується, щоб отримати уточнені дані по ймовірностям коливально-ядерних переходів в молекулі OsO_4 у випадку випромінювання та поглинання гамма-кванта ядром ^{188}Os ($E^{(0)}_g$ = 155 кеВ). Аналіз показує, що більш послідовний теоретичний підхід дає більш високі значення шуканих ймовірностей.

Ключові слова: спектр електрон- g -ядерних переходів, багатоатомні молекули

UDC 539.182

A. A. Svinarenko, O. Yu. Khetselius, V. V. Buyadzhi, A. S. Kvasikova, P. A. Zaichko

Odessa State Environmental University, L'vovskaya str.15, Odessa-16, 65016, Ukraine
e-mail: quantsvi@mail.ru

SPECTROSCOPY OF RYDBERG ATOMS IN A BLACK-BODY RADIATION FIELD: RELATIVISTIC THEORY OF EXCITATION AND IONIZATION

The combined relativistic energy approach and relativistic many-body perturbation theory with the zeroth model potential approximation are used for computing the thermal Blackbody radiation ionization characteristics of the Rydberg atoms, in particular, the sodium in Rydberg states with n=17,18,40-70. The comparison of the calculated ionization rate values with available theoretical and experimental data is carried out.

1. Introduction

A great progress in experimental laser physics and appearance of the so called tunable lasers allow to get the highly excited Rydberg states of atoms. In fact this is a beginning of a new epoch in the atomic physics with external electromagnetic field. It has stimulated a great number of papers on the ad and dc Stark effect [1-12].

From the other side, the experiments with Rydberg atoms had very soon resulted in the discovery of an important ionization mechanism, provided by unique features of the Rydberg atoms. Relatively new topic of the modern theory is connected with consistent treating the Rydberg atoms in a field of the Blackbody radiation (BBR). It should be noted that the BBR is one of the essential factors affecting the Rydberg states in atoms [1].

The account for the ac Stark shift, fast redistribution of the levels' population and photoionization provided by the environmental BBR became of a great importance for successfully handling atoms in their Rydberg states.

The most popular theoretical approaches to computing ionization parameters of the Rydberg atom in the BBR are based on the different versions of the model potential (MP) method, quasiclassical models. It should be mentioned a simple approximation for the rate of thermal ionization of Rydberg atoms, based on the results of our systematic calculations in the Simons-Fues MP [1].

In fact, using the MP approach is very close to the quantum defect method and other semiempirical methods, which were also widely used in the past few years for calculating atom–field interaction amplitudes in the lowest orders of the perturbation theory.

The significant advantage of the Simons-Fues MP method in comparison with other models is the possibility of presenting analytically (in terms of the hypergeometric functions) the quantitative characteristics for arbitrarily high orders, related to both bound–bound and bound–free transitions. Naturally, the standard methods of the theoretical atomic physics, including the Hartree-Fock and Dirac-Fock approximations should be used in order to determine the thermal ionization characteristics of neutral and Rydberg atoms [2].

One could note that the correct treating of the heavy Rydberg atoms parameters in an external electromagnetic field, including the BBR field, requires using strictly relativistic models. In a case of multielectron atomic systems it is necessary to account for thee exchange-correlation corrections.

Here we apply an energy approach [11-15] and relativistic perturbation theory (PT) with the MP zeroth approximation [16-20] to computing the thermal BBR ionization characteristics of the Ry-

dberg atoms, in particular, the sodium. It is self-understood that the other alkali elements are also of a great actuality and importance.

2. Ionization of the Rydberg atoms in the Blackbody radiation

Qualitative picture of the BBR Rydberg atoms ionization is in principle easily understandable. Even for temperatures of order $T=10^4$ K, the frequency of a greater part of the BBR photons ω does not exceed 0.1 a.u. One could use a single- electron approximation for calculating the ionization cross section $\sigma_{nl}(\omega)$. The latter appears in a product with the Planck's distribution for the thermal photon number density:

$$\rho(w,T)=\frac{\omega^2}{\pi^2 c^3[\exp(\omega/kT)-1]}, \qquad (1)$$

where k=3.1668×10^{-6} a.u., K^{-1} is the Boltzmann constant, c = 137.036 a.u. is the speed of light.

Ionization rate of a bound state *nl* results in the integral over the Blackbody radiation frequencies:

$$P_{nl}(T)=c\int_{|E_{nl}|}^{\infty}\sigma_{nl}(\omega)\rho(\omega,T)d\omega. \qquad (2)$$

The ionization cross-section from a bound state with a principal quantum number n and orbital quantum number l by photons with frequency ω is as follows:

$$\sigma_{nl}(\omega)=\frac{4\pi^2\omega}{3c(2l+1)}[lM^2_{nl\to El-1}+ +(l+1)M^2_{nl\to El+1}], \qquad (3)$$

where the radial matrix element of the ionization transition from the bound state with the radial wavefunction $R_{nl}(r)$ to continuum state ith the wavefunction $R_{El}(r)$ normalized to the delta function of energy. The corresponding radial matrix element looks as:

$$M_{nl\to El'}=\int_0^{\infty}R_{El'}(r)r^3R_{nl}(r)dr. \qquad (4)$$

We apply a generalized energy approach [11-15] and relativistic perturbation theory with the MP zeroth approximation [16-20] to computing the Rydberg atoms ionization parameters. In relativistic theory radiation decay probability (ionization cross-section etc) is connected with the imaginary part of electron energy shift. The total energy shift of the state is usually presented in the form: ΔE = ReΔE + i Γ/2, where Γ is interpreted as the level width, and a decay probability P = Γ. The imaginary part of electron energy shift is defined in the PT lowest order as:

$$\mathrm{Im}\Delta E(B)=-\frac{e^2}{4\pi}\sum_{\substack{\alpha>n>f\\ [\alpha<n\le f]}}V^{|\omega_{\alpha n}|}_{\alpha n\alpha n}, \qquad (6)$$

where (α>n>f) for electron and (α<n<f) for vacancy. The matrix element is determined as follows:

$$V^{|\omega|}_{ijkl}=\iint dr_1dr_2\Psi^*_i(r_1)\Psi^*_j(r_2)\frac{\sin|\omega|r_{12}}{r_{12}}(1- -\alpha_1\alpha_2)\Psi^*_k(r_2)\Psi^*_l(r_1) \qquad (7)$$

Their detailed description of the matrix elements and procedure for their computing is presented in Refs. [12,13,15]. The relativistic wave functions are calculated by solution of the Dirac equation with the potential, which includes the "outer electron- ionic core" potential (in the Miller-Green form [21]) and exchange-polarization potential [20]. All calculations are performed on the basis of the numeral code Superatom-ISAN (version 93).

3. Results

In Table 1 we present results of the ionization rate calculation for the Rydberg sodium atom in the states (17,18D, 18P) at temperatures of 300 K and 500 K: Th5 – our (relativistic MP theory) data, E1 – experimental data by Kleppner etal and Burkhardt etal [4], Th1- theory (nonrelativistic Simons-Fues MP) by Glukhov-Ovsyannikova [9], Th2- theory of Lehman [8], Th3- quasiclassical model by Dyachkov-Pankratov [10] and Th4- theory by Beterov et al. [1].

In whole there is physically reasonable agreement between the theoretical and experimental data. Obviously, the accuracy of the theoretical data is provided by a correctness of the corresponding relativistic wave functions and accounting for the exchange-correlation effects.

In Table 2 we list our results of ionization rate (s^{-1}) for sodium Rydberg states (with n=40-70) induced by BBR radiation (T = 300 K) .

Table 1

Theoretical and experimental values of the ionization rate (10^3 s^{-1}) of sodium Rydberg states: E1- Kleppner et al Burkhardt etal; Th1 – theory by Glukhov-Ovsyannikova; Th2- theory by Lehman, Th3- theory by Dyachkov-Pankratov; Th4- theory by Beterov et al; Th5 – this work.

T	*nL*	E1	Th1	Th2	Th3	Th4	Th5
300	17D	10^3	1.08×10^3	0.95×10^3	0.9×10^3	1.147×10^3	1.02×10^3
500	18P	-	4.18×10^3	-	-	-	5.54×10^3
500	18D	-	4.07×10^3	-	-	-	5.46×10^3

Table 2

Ionization rate (s^{-1}) for the sodium Rydberg states (with n = 40-70), induced by BBR radiation (T = 300 K; our data).

Atom	40	50	60	70
Na S	142	106	61.4	29.5
Na P	804	576	311	141
Na D	707	496	268	122

References

1. Beterov I.I., Tretyakov D.V., Ryabtsev I.I., Entin V.M., Ekers A., Bezuglov N.N. // New J. Phys. – 2009. – Vol. 11. – P. 013052 .
2. Safronova U.I., Safronova M.S. // Phys. Rev. A. – 2009.– Vol. 79. – P. 022512 .
3. Gallagher T.F. // Phys. Rev. Lett. – 1999. – Vol. 42. – P. 835-840.
4. Killian T., Kulin S., Bergeson S., Orozco L., Orzel C., Rolston S. // Phys. Rev. Lett. – 1999. – Vol. 83. – P. 4776-4780.
5. Li W., Noel M.W., Robinson M.P., Tanner P.J., Gallagher T.F. // Phys. Rev. A. – 2004. – Vol. 70. – P. 042713 .
6. Spencer W.P., Vaidyanathan A., Kleppner D., Ducas T. // Phys. Rev. A. – 1992. – Vol. 26. – P. 1490-1498.
7. Burkhardt C., Corey R., Garver W., Leventhal J., Allergini M., Moi L. // Phys. Rev. A.– 1996.– Vol. 34.– P.80-88.
8. Lehman G.W. // J. Phys. B: At. Mol. Phys. – 1993. – Vol. 16.–P.2145-2152.
9. Glukhov I., Ovsiannikov V. // J. Phys. B: At. Mol. Phys. – 2009. – Vol. 42. – P. 075001..
10. D'yachkov L.G., Pankratov P.M. // J. Phys. B: At. Mol. Opt. Phys. – 1994. – Vol. 27. – P. 461-468.
11. Ivanova E.P., Ivanov L.N. // Atom. Data. Nucl. Data. Tabl. – 1999. – Vol. 24. – P. 95-109.
12. Ivanov L.N., Letokhov V.S. // Com. Mod. Phys.–1995.–Vol.D4.–P.169 -192.
13. Ivanov L.N., Ivanova E.P., Aglitsky E.V. // Phys. Rep. – 1988. – Vol. 166. – P. 315-370.
14. Glushkov A.V., Ivanov L.N. // Phys. Lett. A. – 1999. – Vol. 170. – P. 33-38.
15. Glushkov A.V. Advances in the Theory of Quantum Systems in Chemistry and Physics // Ser. Progress in Theoretical Chemistry and Physics (Berlin: Springer), K. Nishikawa, J. Maruani, E. Brandas, G. Delgado-Barrio, P. Piecuch. – 2012. – Vol. 28. – P. 131-172.
16. Glushkov A.V. // J. of Phys.: Conf. Ser. – 2012. – Vol. 397. – P. 012011 .
17. Glushkov A.V., Khetselius O.Yu., Loboda A.V., Svinarenko A.A. Frontiers in Quantum Systems in Chem. and Phys. // Ser. Progress in Theoretical Chemistry and Physics, (Berlin: Springer) ed. S. Wilson, P.J. Grout, J. Maruani, G. Delgado-Barrio, P. Piecuch. – 2008. Vol. 18. – P. 543
18. Glushkov A.V., Khetselius O.Yu., Lo-

boda A.V., Svinarenko A.A. // Phys. Scr.–2009. – Vol. T153 – P.014029 .
19. Khetselius O., // J. of Phys.: Conf. Ser. 2009. – Vol. 397. – P. 012012.
20. Malinovskaya S.V., Glushkov A.V., Khetselius O.Yu., Mischenko E.V., Loboda A.V., Svinarenko A.A. // Int. J. Quant. Chem. – 2009. – Vol. 109. – P. 3031-3036.
21. Miller K.J., Green A.E. // J.Chem.Phys. – 1994. – Vol. 60. – P. 2617-2628.

This article has been received within 2014

UDC 539.182

A. A. Svinarenko, O. Yu. Khetselius, V. V. Buyadzhi, A. S. Kvasikova, P. A. Zaichko

SPECTROSCOPY OF RYDBERG ATOMS IN A BLACK-BODY RADIATION FIELD: RELATIVISTIC THEORY OF EXCITATION AND IONIZATION

Abstract

The combined relativistic energy approach and relativistic many-body perturbation theory with the zeroth model potential approximation are used for computing the thermal Blackbody radiation ionization characteristics of the Rydberg atoms, in particular, the sodium in Rydberg states with n=17,18,40-70. The comparison of the calculated ionization rate values with available theoretical and experimental data is carried out.

Key words: Rydberg atoms, relativistic theory, radiation field.

УДК 539.182

А. А. Свинаренко, О. Ю. Хецелиус, В. В. Буяджи, А. С. Квасикова, П. А. Заичко

СПЕКТРОСКОПИЯ РИДБЕРГОВСКИХ АТОМОВ В ПОЛЕ ИЗЛУЧЕНИЯ ЧЕРНОГО ТЕЛА: РЕЛЯТИВИСТСКАЯ ТЕОРИЯ ВОЗБУЖДЕНИЯ И ИОНИЗАЦИИ

Резюме

Комбинированный релятивистский энергитический подход и релятивистская теория возмущений многих тел с нулевым потенциалом модели приближения используются для вычисления ионизационных характеристик ридберговских атомов в поле теплового излучения черного тела, в частности, натрия в ридберговских состояниях с n=17,18,40-70. Сравнение расчетных значений скорости ионизации с имеющимися теоретическими и экспериментальными данными проводится.

Ключевые слова: ридберговские атомы, релятивистская теория, поля излучения.

УДК 539.182

А. А. Свинаренко, О. Ю. Хецеліус, В. В. Буяджи, А. С. Квасикова, П. О. Заічко

СПЕКТРОСКОПІЯ РІДБЕРГІВСЬКИХ АТОМІВ У ПОЛІ ВИПРОМІНЮВАННЯ ЧОРНОГО ТІЛА: РЕЛЯТИВІСТСЬКА ТЕОРІЯ ЗБУРЕННЯ ТА ІОНІЗАЦІЇ

Резюме

Комбінований релятивістський енергетичний підхід і релятивістська теорія збурень багатьох тіл з нульовим потенціалом моделі наближення використовуються для обчислення іонізаційних характеристик рідбергівських атомів у полі теплового випромінювання чорного тіла, зокрема, натрия в рідбергівських станах з n=17,18,40-70. Порівняння розрахованих значень швидкості іонізації з наявними теоретичними та експериментальними даними проводиться.

Ключові слова: рідбергівські атоми, релятивістська теорія, поля випромінювання.

PACS 73.40.Gk, Lq; 73.61.Ga

V. A. Borschak, V. A. Smyntyna, IE. V. Brytavskyi

MODELLING OF RAPID STAGE DECAY OF SIGNAL OF OPTICAL SENSOR BASED ON HETEROSTRUCTURE CdS-Cu_2S

Odessa I. I. Mechnikov National University,
2, Dvoryanskaya str., Odessa, 65082, Ukraine
Phone: +380(48)7266356, Fax: +380(48)7233461, e-mail: borschak_va@mail.ru

The work is devoted to modeling and calculation of the spatial distribution of the concentration of charge localized in the space charge region (SCR) heterojunction, this distribution changes with time at different initial filling of deep traps centers nonequilibrium holes. Within the framework described model the theoretical calculation of two characteristic stages of relaxation current, compliance with the calculated and experimentally obtained dependencies was demonstrated.

Samples obtaining procedure

Technology of the Cu_2S layer formation is briefly discussed above. The semiconductor grade purity of used CdS powder was checked and controlled by XPS technique (X-ray photoelectron spectroscopy) at respective production facilities. Cartridge with CdS films after cooling to room temperature were transferred to the next vacuum chamber department, where evaporation of CuCl was carried. The graphite mask was used for CuCl film configuration. It was found out technologically that complete evaporation of CuCl powder in an amount of 0.3 g at evaporator temperature 650 º C during 7-10 min leads to creation of CuCl layer of desired thickness ≈ 1 μm. Substrate temperature during evaporation of CuCl changed within 180 - 240 º C.

Then, the cassette with CdS-CuCl layer structure samples was moved into the third section of the vacuum chamber was set to the heater - a flat metallic stove, parallel to the sample surface on 1 cm distance. For 10 - 15 sec sample temperature reached 200 º C and further maintained constant throughout the process of heterojunctions formation. As a result of such heat treatment the substitution reaction proceeded in CdS-CuCl layer system by the scheme: $CdS + 2CuCl \rightarrow Cu_2S + CdCl_2$.

CuCl film thickness and annealing time were chosen experimentally so that all of copper chloride could react with the upper layer of CdS (near 1 μm thickness,_this is the value of CdS layer loss). The best results were obtained with heat treatment time ≈ 3 minutes. Cu_2S thickness directly determined by the initial thickness of the initial layer of CuCl. Thus, the use of different modes , in which time evaporation varied from 4 to 12 min, allowed to receive Cu_2S layer thickness in the range from 200 to 1000 nm. The optimal parameters (temperature and time of formation) to maximize the reaction completeness were obtained experimentally by checking the value of the open circuit voltage and short circuit current through heterojunctions, obtained by using these or other processing parameters. Uniformity of Cu_2S layer was determined by initial CuCl film uniformity and was controlled by using microscopic techniques.

Homogeneous Cu_2S film is formed throughout the sample area, despite local differences in the rate of growth. A prerequisite for this is a complete depletion of copper chloride during the reaction. The formation of a homogeneous film thickness is due to the fact that each part of a copper chloride layer can react only with its adjoining part of the CdS layer.

During the reaction two Cu + ions and one Cd^2 + ion must diffuse in opposite directions through the constantly growing films of copper sulfide and cadmium chloride. Sulfur atoms must stay on one side, and the chlorine atoms - on the other side. As a result of this process, the entire surface is covered with a layer of cadmium chloride, which is easily removed by distilled water. But several phases of Cu_xS, such as $Cu_{1.96}S$ $Cu_{1.92}S$ and other can be formed during the substitution reaction due to different diffusion velocities of the reaction components and lack of Cu + ions in reaction zone as a result. Other observed phases of copper sulphide appear because of sample time degradation (copper atoms diffusion from Cu_xS to CdS layer).

Charge distribution modeling

Consistent with the experimental data model of the processes responsible for the kinetics of decline in short-circuit current CdS-Cu_2S, based on the description of thermal and tunneling mechanisms to release localized charge in the absence of photoexcitation, ie case descending relaxation was developed. Kinetics of non-equilibrium concentration of holes in traps in this case is described by the equation [1-3]:

$$\frac{dp_t}{dt} = -p_t \bar{v} S_{pt} P_V \exp\left(-\frac{E_t}{kT}\right) - p_t \bar{v} S_{pt} P_V D_1(x) - p_t \bar{v} S_{nt} n_0 D_2(x) \quad (1)$$

where $\bar{v}$ – carriers termal velocity, S_{pt} and S_{nt} – capture cross section for electrons and holes, n_0 – free electrons concentration in CdS, $D_1(x)$ and $D_2(x)$ – tunnel transparency coefficients.

Each of the terms describing the devastation traps through a mechanism - thermal emission, tunneling of trapped holes in the valence band electron tunneling Cu2S and CdS conduction band with subsequent recombination in the SCR. Evaluation of the contribution of tunneling in the process of relaxation of the trapped charge is made by calculating the second and third terms of the right side of equation (3), while the probability of tunneling transmission coefficient determined by the values corresponding barriers D1 (x) and D2 (x), which strongly depend on the coordinates [2]. To determine the transmission coefficient for tunnel junctions used equation semiclassical approximation. This takes into account that in the real case the form of the barrier, and with it the transparency coefficients tunnel (respectively the concentration of trapped holes) change over time. That is, the kinetic equation (1) there are values that explicitly depend on time.

The concentration of trapped positive charge $p_t(x,t)$ in the real case depends on the coordinates and the time directly determines the shape of the potential barrier structure. A building in the course is associated with the intensity of tunnel junctions as coefficients tunnel transparency is dependent on the profile $\varphi(x)$ of the barrier [4, 5]. Values are coefficients tunnel transparency, in turn, are present in the expression describing the kinetics of changes in the concentration of trapped holes $\frac{dp_t}{dt}$. Thus, to describe the real situation of $p_t(x,t)$ distribution the self-consistent equations were derived from the scheme:

$$p_t(x,t) \longrightarrow \frac{d^2\varphi}{dx^2} \longrightarrow \varphi(x,t) \longrightarrow D_{1,2}(x,t) \longrightarrow \frac{dp_t}{dt} \quad (2)$$

Described model with thermal release mechanism allows for tunnel release trapped holes in the traps, which prevails in the initial phases of changes in the concentration of space charge. This gained in photoexcited charge is actually the optical information carrier, fixed sensor, so the devastation traps determines the memory effect and re-reading sensor signal.

The results of modeling calculations and nonequilibrium charge distribution localized in the barrier HJ based tunneling charge transport mechanisms. Within The model used in the calculation of two cases of initial concentration distribution of trapped holes at t = 0: the case of complete filling centers traps, exponential distribution and concentration of positive charge (Fig. 1).

For numerical calculation solution program used MathLab and Octave, where computer-implemented Dormand method Prince (Runge-Kutt variation), which is widely used for finding

the solution of ordinary differential equations. The initial set barrier width W of the coordinate x was divided into 100 points, and the value of Δt was set equal to 0.1 sec. These steps were selected partition for reasons of compliance accuracy further building are calculated from recession photocurrent accuracy of the experimental curves.

The simulation results of the process to reduce the concentration of trapped charge-trap centers in the SCR GP presented in Figure 1. Calculated data are presented as a set of normalized ($p_t(x,0) = N_t \equiv 1$) curves of the spatial distribution of concentration p_t^{norm} at certain values of time t, elapsed after photoexcitation termination (at t = 0).

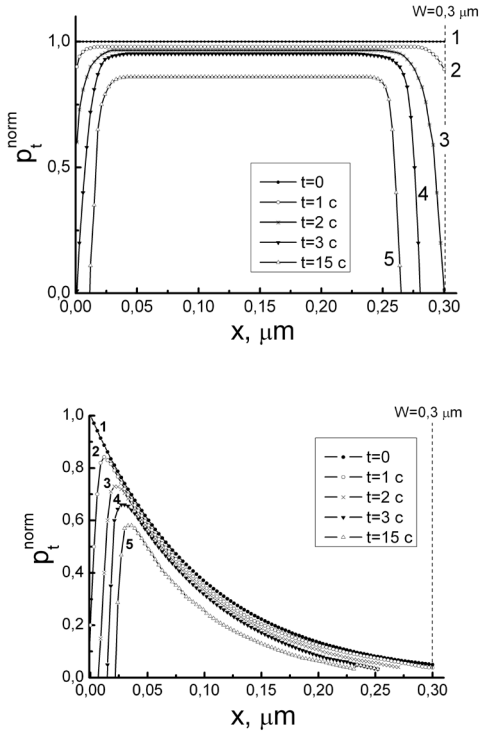

Fig. 1. Calculated dependence of p_t concentration distribution profiles of holes captured in the traps in the initial full (a) and exponential (b) distribution of concentration. Profiles are normalized.

The results of modeling dependencies sensor signal decline after cessation of photoexcitation and comparing them with the experimentally obtained relaxation curves were obtained. The analytical expressions that show the connection of nonequilibrium charge distribution in the SCR, the shape of the potential barrier and heterojunction with a value of short-circuit current through the sample. The principal difference between the proposed and the method used process modeling short circuit photocurrent relaxation (ie, sensor signal) from the previously described are not only taking into account a change in the distribution of quadratic potential barrier near heteroborder on the exponential of the latter CdS, but also quantitatively account tunneling effects [6, 7]. Thus, the model takes into account the demonstrated dramatic change in the transparency of the tunnel barrier and subsequent relaxation effects concentration of trapped non-equilibrium charge and current through GP after termination of photoexcitation [7].

It was found that the best matching relaxation curves calculated short-circuit current of the experimentally obtained values achieved using exponential terms in the modeling of the spatial distribution of the initial concentration of trapped holes in deep traps, which act as carriers of captured optical information in the studied sensor structure.

Within the framework described model the theoretical calculation of two characteristic stages of relaxation of current when first performed this calculation depends on the concentration of trapped deep trap charge with time for a quick relaxation phase, which is caused by the process of tunnel release charge (Fig. 2).

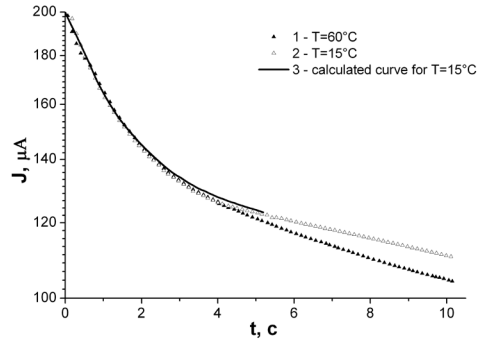

Fig. 2. Experimental (individual points) and calculated (solid curve) short-circuit current dependences in case ofinitial exponential filling of traps by nonequilibrium holes at the stage of fast relaxation.

Conclusion

It is shown that the experimentally obtained dependence is modeled using only one type of traps involved in the accumulation of charge in the SCR. The settlement established by the energy position E_t, capture cross section S_{pt} and concentration N_t trap centers involved in the processes of capture of nonequilibrium holes whose values held to agreement between experimental and theoretical curves of obtained short-circuit current recession: E_t = 0.32 eV, S_{pt} =$3 \cdot 10^{-14}$ cm^2, N_t=$1.4 \cdot 10^{17}$ cm^{-3}. This value is the energy depth of the trap is in accordance with the experimentally obtained changes in research capacity barrier heterojunction.

Reference

[1] K. Moitra, S. Deb. Solar Cells. no. 9, P. 215-228, (1993).

[2] D.L. Vasilevski, M.S. Vinogradov, V.A. Borschak, Appl. Surf. Sci. 103, (1996).

[3] V.A. Smyntyna, V.A. Borschak, M.I. Kutalova, N.P. Zatovskaya, A.P. Balaban, Semiconductor Physics, Quantum Electronics & Optoelectronics. V.7, No 2, (2004).

[4] Manisha Kundu, Tsuyoshi Hasegawa, Kazuya Terabe, Kazuhiro Yamamoto, Masakazu Aono, Sci. Technol. Adv. Mater. No 9. (2008).

[5] H.C. Hsieh, J. Appl. Phys., v. 53, P. 1727-1733, (1992).

[6] E. Castel and J . Vedel, Analysis, V. 3, No 9, P. 487-490, (1995).

[7] V. A. Borschak, V. A. Smyntyna, Ie. V. Brytavskyi, A. A. Karpenko, and N. P. Zatovskaya, Semiconductors, Vol. 47, No. 6, pp. 838–843 (2013).

This article has been received within 2014

PACS 73.40.Gk, Lq; 73.61.Ga

V. A. Borschak, V. A. Smyntyna, Ie. V. Brytavskyi

MODELLING OF RAPID STAGE DECAY OF SIGNAL OF OPTICAL SENSOR BASED ON HETEROSTRUCTURE CdS-Cu2S

Summary. The work is devoted to modeling and calculation of the spatial distribution of the concentration of charge localized in the space charge region (SCR) heterojunction, this distribution changes with time at different initial filling of deep traps centers nonequilibrium holes. Within the framework described model the theoretical calculation of two characteristic stages of relaxation current, compliance with the calculated and experimentally obtained dependencies was demonstrated.

Key words: nonideal heterojunction, image sensor, deep traps, tunneling.

UDC584.96

D. A. Korchevsky, A. V. Malakhov, A. V. Ignatenko, E. L. Ponomarenko, I. M. Shpinareva

[1]Odessa Computing Academy, 3, Osipova str, 65018, Odessa, Ukraine
[2]Odessa National Maritime Universiry, 34, Mechnikova str., 65029, Odessa, Ukraine
Odessa National Polytechnical University, 1, Shevchenko av., 65044, Odessa, Ukraine
Odessa State Environmental University, 15, Lvovskaya str., 65016, Odessa, Ukraine
[3]I. I. Mechnikov Odessa National University, 2, Dvoryanskaya str., 65028, Odessa Ukraine
e-mail: quantign@mail.ru

STOCHASTIC DYNAMICS OF THE LASER FIELD ROTATIONAL EXCITATION FOR MOLECULES

A advanced multi-level optimized stochastic model for definition of the optimal form of laser pulse to reach the maximal effectiveness of laser action in process of selective molecule excitation and ionization is used in calculation the parameters of the optimal excitation for molecule. It is estimated dependence (number of particles) of functional of the quality on the rotational energy and wave length of laser radiation

At present time it is of a great important development of an effective advanced multi-level optimized stochastic models for definition of the optimal form of laser pulse to reach the maximal effectiveness of laser action in process of selective molecule excitation and ionization. The purpose is to calculate the parameters of the optimal excitation for molecule [1-10]. This topic represents a significant theoretical and applied interest for many physical, chemical branches such as an atomic, molecular physics, quantum electronics, physics of elements, devices, sensor technologies, plasmochenistry laser photochemistry and biology. One could remind about physical basis for creation and construction of special devices for sensing physical, chemical properties of the molecular systems and at last their application in the nano-electronics, nano-atomic optics, quantum computing, molecular sensors technologies etc.

As it was indicated in Refs. [1-10], a great perspectives has the studied topic for many problems of laser photochemistry. Letokhov et al [2,3] experimentally studied possibility of cleaning the substance in a gas phase by means of the photoionization or photo dissociation of admixtured molecules in IR laser field on the example of cleaning $AsCl_3$ from admixtures $C_2H_4Cl_2$ and CCl_4.From theoretical and experimental points of view, it is very important theoretical and experimental studying optimal realizations of processes of the multi-step and multi photon excitation and ionization, dissociation. Though many of cited processes are quite satisfactorily described (at least, at qualitative level) by simplified models. A majority of tasks for action of laser radiation and high intensive particles beams on molecular gases are quite acceptably described by multi-level stochastic models, which result in systems of differential equations or differential equation in partial derivatives of the Focker-Plank type [3,7,8,14]. Nowdays a consistent theory of the optimal realizations of these processes is absent. In refs. [12-15] a new multi-level optimized model for definition of the optimal form of laser pulse to reach the maximal effectiveness of laser action in process of selective excitation and ionization of molecules has been proposed. Further within the optimal governing theory a problem of optimization for electron, vibtational and rotational excitation, photo ionization and dissociation in a laser field was studied and As example, the parameters of the optimal excitation and ionization for molecules HCl, $CF_3Br(I)$, SiH_4 etc. have been determined. Here we consider a generalized advanced stochastic model for definition of the optimal form

of laser pulse to reach the maximal effectiveness of laser action in process of selective molecule excitation and ionization, which generalizes earlier formulated approaches [13-15].

As usually, we start from the stochastic differential equation of the Focker-Plank type:

$$\partial f / \partial t = L_{RT} + L_u(f, I) \qquad (1)$$

where f is a density of molecules at a chosen vibrated level with rotational energy x; I is a laser pulse intensity; L_{RT},$L_u(f,I)$ are operators, which describe the RT relaxation and laser radiation action and have the standard form:

$$L_{RT}(f) = \partial^2 f/\partial x^2 + \partial f/\partial x, \ldots, L_u = I(x,t)u(t)(f(x_2,t) - f(x_1,t)) \qquad (2)$$

At initial moment of time there is some initial distribution $f(x,0)$, and for t>0 system is excited by resonance laser field with frequency, which is resonant to rotational transition $x_1 \to x_2$.

Frequency of the exciting field is considered as as governing parameter. To estimate an effectiveness of action one must study a quality functional, which characterises a distribution of molecules on rotational energies to moment t_1:

$$Y(u) = \int_0^R f(x, t_1; u)h(x)dx \qquad (3)$$

where $h(x)$ is some function, which corresponds to required form of the final distribution.

Further we are dealing with real form of the laser pulse. In refs. [12-15] we deal with a multilevel optimized model for definition of the optimal form of laser pulse. In fact it has been used the pulse in a Lorenze form. Here we consider firstly the pulse in the Gaussian form. Further we used the standard procedure of the governing theory The optimal governing task for definition of the optimal laser pulse form to achieve a maximal laser action effectiveness is written as follows [15]:

$$\begin{aligned} &\partial f / \partial t = \partial^2 f/\partial x^2 + \partial f/\partial x + I(x,t)u(t)(f(x_2,t) - f(x_1,t)) \\ &f(x,0) = f_0(x), \ldots\ldots\ldots\ldots 0 < x < R, \\ &\partial f/\partial x + + f|_{x=0,R} = 0, \ldots 0 < t < t_1 \end{aligned} \qquad (4)$$

Following to Ref.[14,15], we use the necessary condition of optimality, i.e. if (x_1^*, x_2^*) is an optimal governing for functional (3) and $f^*(x,t)$ $\Psi^*(x,t)$ are corresponding solutions, then we have the following condition for any x_1, x_2 from interval [0,R]:

$$Y'_{x_1}(x_1^*, x_2^*, f^*, \Psi^*)(x_1 - x_1^*) + Y'_{x_2}(x_1^*, x_2^*, f^*, \Psi^*)(x_2 - x_2^*) \le 0$$

Dependence (number of particles) in the interval of energies $x\hat{I}[x_1, x_2]$ (in units of kT) upon x_1 and wave length of laser radiation, which is corresponding to rotation transition $x_1 \to x_2$, is determined by the functional:

$$I(u) = \int_0^R f(x, t_1; x_1, x_2)h(x)dx \qquad (5)$$

Using the numerical methodics [14,15] we have carried out testing of the advanced model for molecules *HBr* (T=300 K, R=25; the values of parameters are taken from refs.[2-4, 16]). In figure 1 it is presented a dependence (number of particles) of the functional (5) in the interval of energies $x\hat{I}$[13,25] (in units of kT) upon x_1 and wave length of laser radiation, which is corresponding to rotation transition $x_1 \to x_2$. In expression (4) h is a function, which corresponds to required form of the final distribution f(x,t,u), i.e. density of molecules at chosen vibration level, which has a rotational energy x at moment of time t; $x \in [0, R]$). The obtained data are qualitatively similar to results of ref. [14,15] for molecule *HCl, CF_3Br*. The quantitative difference (~5%) is provided by using the real laser pulse form (3) and corrected molecular constants set. Probably, this difference should be in more details analyzed with accounting for the possible photon-correlation stochastic effects.

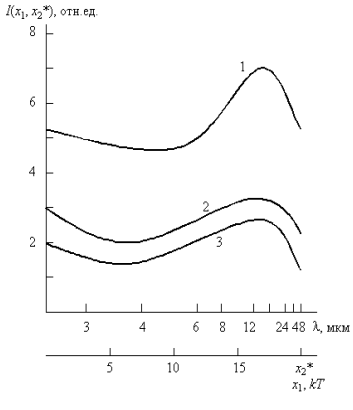

Fig. 1. Dependence of the functional $I(x_1, x_2)$ upon x_1 and wave length of laser radiation for $t_1=2t_R$ (1), $t_1=4t_R$ (2), $t_1=6t_R$ (3) for molecule HBr (see text).

References

1. Lambert J.D.,Vibrational and Rotational Relaxation in Gases (Oxford.-1997).
2. Letokhov V.S., Nonlinear selective photo-processes in atoms and molecules (Moscow.- 2003).
3. Bagratashvili V.N., Letokhov V.S., Makarov A.A., Ryabov E.A., Multi-photon processes in molecules in IR laser field (Moscow.- 1991).
4. Goldansky V.I., Letokhov V.S. Effect of laser radiation on nuclear decay processes// Sov. Phys. JETP.-1994.-Vol.67.-P.513-516.
5. Ivanov L.N., Letokhov V.S. Spectroscopy of autoionization resonances in heavy elements atoms// Com. Mod. Phys.D.:At. Mol.Phys.-1995.-Vol.4.-P.169-184.
6. Glushkov A.V., Ivanov L.N. Radiation Decay of Atomic States: atomic residue and gauge non-invariant contributions // Phys. Lett.A.-1992.-Vol.170,N1.-P.33-37.
7. Panchenko V.Ya., Tolstoshein A.Yu., Optimization of condition of the ritational excitation for molecular gas// Soviet Chem.Phys.-1997.-Vol.6.-P.16-20.
8. Laptev V.B., Ryabov E.A., Isotopically-selective dissociation BCl_3 in a two-colour IR laser field// Soviet Chem. Phys.-1998.-Vol.7,N2.-P.165-170.
9. Glushkov A.V., Malinovskaya S.V., Co-operative laser nuclear processes: border lines effects// In: New projects of research in nuclear physics. Eds. G.Fazio, F.Hanappe, (Singapore, World Sci.- 2003).-P.242-250.
10. Glushkov A.V., Ambrosov S.V., Ignatenko A.V., Korchevsky D.A., DC Strong Field Stark Effect for Non-hydrogenic Atoms//Int.Journ.Quant. Chem.-2004.-Vol.99,N5.-P.936-939.
11. Glushkov A.V., Malinovskaya S.V., Shpinareva I. etal, Diagnostics of collisionally pumped plasma & search of optimal plasma parameters for x-ray lasing//J.Phys.CS.-2005.-Vol.11-P.188-198.
12. Glushkov A.V., Prepelitsa G.P., Svinarenko A.A. Sensing the stochastic laser pulse structure and chaotic and photon-correlation effects in the non-linear multi-photon atomic dynamics in laser and DC electric field// Sensor Electr. & Microsyst. Techn.-2004.-N2.-P.89-95
13. Glushkov A.V., Malinovskaya S.V., Shpinareva I.M., Kozlovskaya V.P., Gura V.I. Quantum stochastic modelling multi-photon excitation and dissociation for CF_3Br molecules: An effect of rotational and V-T relaxation // Int. Journ. Quant. Chem.-2005.-Vol. 104,N4.- P.562-570.
14. Loboda A. , Glushkov A.V., Shpinareva I. et al, Optimization of laser field rotational excitation of molecules and its possible use in the selective photoionization method for cleansing semiconductor surface// Surface and Interface Analysis.-2005.-Vol.16.-P.931-935.
15. Shpinareva I.M., Sensing a dynamics of the laser field rotational excitation for molecules and possible using in laser photoionization cleaning semiconductor surfaces//Sensor Electr and Microsystems Techn.-2005.-N4.-P.22-26.
16. Glushkov A.V., Ambrosov S.V., Shpinareva I.M., etal, Spectroscopy of diatomic van-der-waals molecules: atom of inert gas- atom of galogen// Opt.Spectr.–1998.-Vol.84.-P.567-572.

The articles were received from 1.05 to 30.07.2014

UDC 584.96

D. A. Korchevsky, A. V. Malakhov, A. V. Ignatenko, E. L.Ponomarenko, I. M. Shpinareva

STOCHASTIC DYNAMICS OF THE LASER FIELD ROTATIONAL EXCITATION FOR MOLECULES

Abstract. An advanced multi-level optimized stochastic model for definition of the optimal form of laser pulse to reach the maximal effectiveness of laser action in process of selective molecule excitation and ionization is used in calculation the parameters of the optimal excitation for molecule. It is calculated dependence (number of particles) of functional of the quality on the rotational energy and wave length of laser radiation.

Key words: rotational excitation, molecules in a laser field, stochastic modelling

УДК 584.96

Д. А. Корчевский, А. В. Малахов, А. В. Игнатенко, Е. Л. Пономаренко, И. М. Шпинарева

СТОХАСТИЧЕСКАЯ ДИНАМИКА ВРАЩАТЕЛЬНОГО ВОЗБУЖДЕНИЯ МОЛЕКУЛ В ПОЛЕ ЛАЗЕРНОГО ИЗЛУЧЕНИЯ

Резюме. Обобшенная многоуровневая оптимизационная стохастическая модель определения оптимальной формы лазерного импульса для достижения максимальной эффективности лазерного воздействия в процессе селективного возбуждения и ионизации молекул использована в оценке параметров оптимального вращательного возбуждения молекул. Рассчитана зависимость функционала качества (число частиц) от величины вращательной энергии и длины волны лазерного излучения.

Ключевые слова: вращательного возбуждения, молекулы в поле лазерного излучения, стохастическая модель

УДК 584.96

Д. О. Корчевський, О. В. Малахов, Г. В. Ігнатенко, О. Л. Пономаренко, І. М. Шпінарева

СТОХАСТИЧНА ДИНАМІКА РОТАЦІЙНОГО ЗБУДЖЕННЯ МОЛЕКУЛ У ПОЛІ ЛАЗЕРНОГО ВИПРОМІНЮВАННЯ:

Резюме. Узагальнена багаторівнева оптимізаційна стохастична модель визначення оптимальної форми лазерного імпульсу для досягнення максимальної ефективності лазерної дії у процесі селективного збудження та іонізації молекул використана у розрахунку параметрів оптимального збудження молекул. Оцінена залежність функціоналу якості (число частинок) від величини ротаційної енергії та довжини хвилі лазерного випромінювання.

Ключові слова: ротаційне збудження, молекули у лазерному полі, стохастична модель

UDC 539.182

P. A. Kondratenko, O. Yu. Khetselius, V. B. Ternovsky, P. A. Zaichko, A. V. Duborez

[1]National Aviation University, 1, Komarov Ave, 03680 Kiev, Ukraine
[2]Odessa National Polytechnical University, 1, Shevchenko av., Odessa, Ukraine
[3]Odessa State Environmental University, 15, Lvovskaya str., Odessa, Ukraine
e-mail: nuckhet@mail.ru

SIMULATION CHAOTIC DYNAMICS OF COMPLEX SYSTEMS AND DEVICES WITH USING CHAOS THEORY, GEOMETRIC ATTRACTORS, AND QUANTUM NEURAL NETWORKS

Nonlinear simulation and forecasting chaotic evolutionary dynamics of complex systems can be effectively performed using the concept of compact geometric attractors. We are developing a new approach to analyze and forecasting complex systems evolutionary dynamics based on the concept of geometric attractors, chaos theory methods and algorithms for quantum neural network simulation.

In recent years a considerable number of works, including an analysis from the perspective of the theory of dynamical systems and chaos, fractal sets, is devoted to time series analysis of dynamical characteristics of physics and other systems [1-11]. In a series of papers [10-20] the authors have attempted to apply some of these methods in a variety of the physical, geophysical, hydrodynamic problems. In connection with this, there is an extremely important task on development of new, more effective approaches to the nonlinear modelling and prediction of chaotic processes in different complex systems.

In this work nonlinear simulation and forecasting chaotic evolutionary dynamics of complex systems are carried out using the concept of compact geometric attractors [17-20]. We are developing a new approach to analyze complex system dynamics based on the concept of geometric attractors, chaos theory methods and algorithms for quantum neural network simulation

The basic idea of the construction of our approach to prediction of chaotic processes in complex systems is in the use of the traditional concept of a compact geometric attractor in which evolves the measurement data, plus the implementation of neural network algorithms. The existing so far in the theory of chaos prediction models are based on the concept of an attractor, and are described in a number of papers (e.g. [1-8]).

From a mathematical point of view, it is a fact that in the phase space of the system an orbit continuously rolled on itself due to the action of dissipative forces and the nonlinear part of the dynamics, so it is possible to stay in the neighborhood of any point of the orbit $y(n)$ other points of the orbit $y^r(n)$, $r = 1, 2, ..., N_B$, which come in the neighborhood $y(n)$ in a completely different times than n. Of course, then one could try to build different types of interpolation functions that take into account all the neighborhoods of the phase space and at the same time explain how the neighborhood evolve from $y(n)$ to a whole family of points about $y(n+1)$. Use of the information about the phase space in the simulation of the evolution of some physical (geophysical etc.) process in time can be regarded as a fundamental element in the simulation of random processes.

In terms of the modern theory of neural systems, and neuro-informatics (e.g. [11]), the process of modelling the evolution of the system can be generalized to describe some evolutionary dynamic neuro-equations (miemo-dynamic equations). Imitating the further evolution of a com-

plex system as the evolution of a neural network with the corresponding elements of the self-study, self- adaptation, etc., it becomes possible to significantly improve the prediction of evolutionary dynamics of a chaotic system. Considering the neural network with a certain number of neurons, as usual, we can introduce the operators S_{ij} synaptic neuron to neuron u_i u_j, while the corresponding synaptic matrix is reduced to a numerical matrix strength of synaptic connections: $W = | | w_{ij} | |$. The operator is described by the standard activation neuro-equation determining the evolution of a neural network in time:

$$s_i^{'} = sign(\sum_{j=1}^{N} w_j s_j - \theta_i) \qquad (1)$$

where 1<i<N.

From the point of view of the theory of chaotic dynamical systems, the state of the neuron (the chaos-geometric interpretation of the forces of synaptic interactions, etc.) can be represented by currents in the phase space of the system and its the topological structure is obviously determined by the number and position of attractors. To determine the asymptotic behavior of the system it becomes crucial a information aspect of the problem, namely, the fact of being the initial state to the basin of attraction of a particular attractor.

Modelling each physical attractor by a record in memory, the process of the evolution of neural network, transition from the initial state to the (following) the final state is a model for the reconstruction of the full record of distorted information, or an associative model of pattern recognition is implemented. The domain of attraction of attractors are separated by separatrices or certain surfaces in the phase space. Their structure, of course, is quite complex, but mimics the chaotic properties of the studied object. Then, as usual, the next step is a natural construction parameterized nonlinear function ***F*** *(x,* ***a)***, which transforms:

$$\mathbf{y}(n) \rightarrow \quad \mathbf{y}(n+1) = \mathbf{F}(\mathbf{y}(n), \mathbf{a}),$$

and then to use the different (including neural network) criteria for determining the parameters a (see below). The easiest way to implement this program is in considering the original local neighborhood, enter the model(s) of the process occurring in the neighborhood, at the neighborhood and by combining together these local models, designing on a global nonlinear model. The latter describes most of the structure of the attractor.

Although, according to a classical theorem by Kolmogorov-Arnold -Moser, the dynamics evolves in a multidimensional space, the size and the structure of which is predetermined by the initial conditions, this, however, does not indicate a functional choice of model elements in full compliance with the source of random data. One of the most common forms of the local model is the model of the Schreiber type [3] (see also [17-20]).

Nonlinear modelling of chaotic processes can be based on the concept of a compact geometric attractor, which evolve with measurements. Since the orbit is continually folded back on itself by the dissipative forces and the non-linear part of the dynamics, some orbit points $\mathbf{y}^r(k)$, $r = 1, 2, \ldots, N_B$ can be found in the neighbourhood of any orbit point $\mathbf{y}(k)$, at that the points $\mathbf{y}^r(k)$ arrive in the neighbourhood of $\mathbf{y}(k)$ at quite different times than k. Then one could build the different types of interpolation functions that take into account all the neighborhoods of the phase space, and explain how these neighborhoods evolve from y (n) to a whole family of points about y (n + 1). Use of the information about the phase space in modelling the evolution of the physical process in time can be regarded as a major innovation in the modelling of chaotic processes.

This concept can be achieved by constructing a parameterized nonlinear function F(x, a), which transform y(n) to y(n+1)=F(y(n), a), and then using different criteria for determining the parameters a. Further, since there is the notion of local neighborhoods, one could create a model of the process occurring in the neighborhood, at the neighborhood and by combining together these local models to construct a global nonlinear model that describes most of the structure of the attractor.

As shown Schreiber [3], the most common form of the local model is very simple:

$$s(n+\Delta n) = a_0^{(n)} + \sum_{j=1}^{d_A} a_j^{(n)} s(n-(j-1)\tau) \qquad (2)$$

where Δ n - the time period for which a forecast .

The coefficients $a_j^{(k)}$, may be determined by a least-squares procedure, involving only

points $s(k)$ within a small neighbourhood around the reference point. Thus, the coefficients will vary throughout phase space. The fit procedure amounts to solving $(d_A + 1)$ linear equations for the $(d_A + 1)$ unknowns. When fitting the parameters a, several problems are encountered that seem purely technical in the first place but are related to the nonlinear properties of the system. If the system is low-dimensional, the data that can be used for fitting will locally not span all the available dimensions but only a subspace, typically. Therefore, the linear system of equations to be solved for the fit will be ill conditioned. However, in the presence of noise the equations are not formally ill-conditioned but still the part of the solution that relates the noise directions to the future point is meaningless .Other modelling techniques are described, for example, in [3,10, 17-20].

Assume the functional form of the display is selected, wherein the polynomials used or other basic functions. Now, we define a characteristic which is a measure of the quality of the curve fit to the data and determines how accurately match y (k + 1) with F (y (k), a), calling it by a local deterministic error:

$$\varepsilon_D(k) = \mathbf{y}(k + 1) - \mathbf{F}(\mathbf{y}(k), \mathbf{a}). \qquad (3)$$

The cost function for this error is called W (ε). If the mapping F (y, a), constructed by us, is local, then one has for each adjacent to y (k) point, $y^{(r)}(k)$ $(r = 1, 2, ..., N_B)$,

$$\varepsilon_D^{(r)}(k) = \mathbf{y}(r, k + 1) - \mathbf{F}(\mathbf{y}^{(r)}(k), \mathbf{a}), \quad (4)$$

where y (r, k + 1) - a point in the phase space which evolves y (r, k). To measure the quality of the curve fit to the data, the local cost function is given by

$$W(\varepsilon, k) = \frac{\sum_{r=1}^{N_B} \left|\varepsilon_D^{(r)}(k)\right|^2}{\sum_{r=1}^{N_B} \left[\mathbf{y}(k) - \langle \mathbf{y}(r, k) \rangle\right]^2} \qquad (5)$$

and the parameters identified by minimizing W (ε, k), will depend on a.

Furthermore, formally the neural network algorithm is launched, in particular, in order to make training the neural network system equivalent to the reconstruction and interim forecast the state of the neural network (respectively, adjusting the values of the coefficients). The starting point is a formal knowledge of the time series of the main dynamic parameters of a chaotic system, and then to identify the state vector of the matrix of the synaptic interactions $||w_{ij}||$ etc. Of course, the main difficulty here lies in the implementation of the process of learning neural network to simulate the complete process of change in the topological structure of the phase space of the system and use the output results of the neural network to adjust the coefficients of the function display.

Further we consider implemetatiom of the quantum neural networks algorithm into general scheme of studying chaotic dynamics. The basic aspects of theory of the photon echo based neural networks are stated previously (see, for example, [10,11, 18,21,22]). So here we mention only the essential elements. Photon echo is a nonlinear optical effect, in fact this is the phenomenon of the four wave interaction in a nonlinear medium with a time delay between the laser pulses. One promising approach to the realization of an quantum neural network is proposed in refs. [11,18]. We have used a software package for numerical modeling of the dynamics of the photon echo neural network, which imitates evolutionary dynamics of the complex system. It has the following key features: multi-layering, possibility of introducing training, feedback and controlled noise. There are possible the different variants of the connections matrix determination and binary or continuous sigmoid response (and so on) of the model neurons. In order to imitate a tuition process we have carried out numerical simulation of the neural networks for recognizing a series of patterns (number of layers N=5, number of images p=640; the error function:

$$SSE = \sum_{p=1}^{p_{max}} \{.. \sum_{k=}^{k_{max}} [t(p,k) - O(p,k)]^2\}, \qquad (6)$$

where $O(p,k)$ – neural networks output k for image p and $t(p,k)$ is the trained image p for output κ; SSE is determined from a procedure of minimization; the output error is $RMS=sqrt(SSE/P_{max})$; As neuronal function there is used function of the form: $f(x) = 1[1 + \exp(-\delta x]$. In our calculation there is tested the function $f(x,T)=\exp[(xT)^4]$ too.

The result of the PC simulation (with using our neural networks package NNW-13-2003 [11]) of

dynamics of the quantum multilayer neural networks with the input sinusoidal pulses is listed in fig.1. Fig. 2 demonstrates the results of modeling the dynamics of multilayer neural network for the case of noisy input sequence. The input signal was the Gaussian-like pulse with adding a noise with intensity D. At a certain value of the parameter D (the variation interval .0001-0.0040) the network training process and signal playback is optimal. The optimal value of D is 0.0017 . A coherency of input and output is optimal for the indicated optimal noise level. Thus, a stochastic resonance effect is in fact discovered in our PC experiment. In our view, this phenomenon is apparently typical for the neural network system. Obviously, one should search for the same effect for human tuition process. Analysis of the PC experiment results allows to make conclusion about sufficiently high-quality processing the input signals of very different shapes and complexity by a photon echo based neural network.

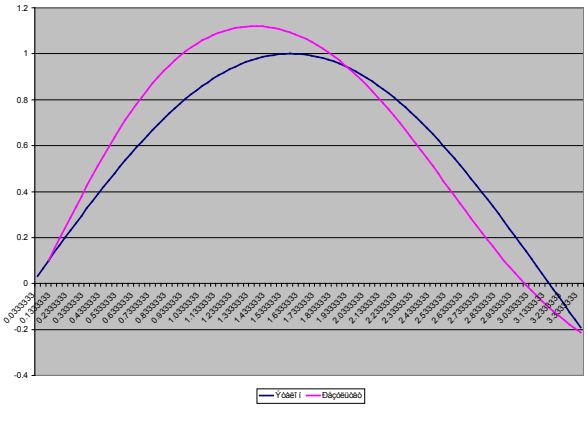

Fig. 1. The results of modeling the dynamics of multilayer neural networks with sinusoidal input pulse.

The most fundamental feature of the approach in development is combined using elements of of a chaos theory, concept of a compact geometric attractor, and one of the neural network algorithms, or, in a more general definition of a model of artificial intelligence. The meaning of the latter is precisely the application of neural network to simulate the evolution of the attractor in phase space, and training most neural network to predict (or rather, correct) the necessary coefficients of the parametric form of functional display. Using phase space information on the evolution in time and results of the of quantum neural network modelling techniques can be considered as one of the fundamentally approaches in forecasting chaotic dynamics of the really very complex systems.

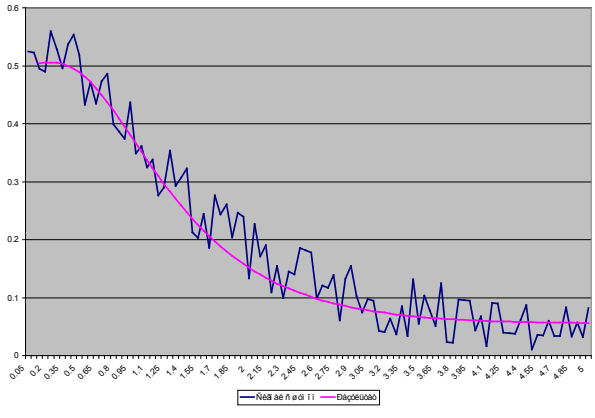

Fig. 2. The results of modeling the dynamics of multilayer neural for the case of noisy input sequence.

References

1. Lichtenberg, A., Liebermann, A.: Regular and chaotic dynamics // Springer, N.-Y. – 1992.
2. Abarbanel H.: Analysis of observed chaotic data // Springer, N.-Y. – 1996.
3. Schreiber T.: Interdisciplinary application of nonlinear time series methods // Phys. Rep. – 1999. – Vol. 308. – P. 1-64.
4. Sivakumar B.: Chaos theory in geophysics: past, present and future // Chaos, Solitons & Fractals. – 2004. – Vol. 19. – P. 441-462
5. Kennel, M., Brown, R., Abarbanel, H. Determining embedding dimension for phase-space reconstruction using a geometrical construction // Phys.Rev.A. – 1992. – Vol. 45. – P. 3403-3411.
6. Turcotte, D.L. Fractals and chaos in geology and geophysics // Cambridge University Press, Cambridge. – 1997.
7. Hastings, A.M., Hom, C., Ellner, S, Turchin, P., Godfray, Y. Chaos in ecology: is Mother Nature a strange attractor // Ann.Rev.Ecol.Syst. – 1993. – Vol. 24. – P. 1-33.
8. May, R.M.: Necessity and chance: deterministic chaos in ecology and evolu-

tion // Bull. Amer. Math. Soc. – 1995. – Vol. 32. – P. 291-308.
9. Grassberger, P., Procaccia, I.: Measuring the strangeness of strange attractors // Physica. – 1993. – Vol. D.9. – P. 189–208.
10. Glushkov A.V.: Methods of a chaos theory // Ecology, Odessa. – 2012.
11. Glushkov, A.V., Svinarenko, A.A., Loboda, A.V. Theory of neural networks on basis of photon echo and its program realization // TEC, Odessa. – 2004.
12. Glushkov, A.V., Loboda, N.S., Khokhlov, V.N.: Using meteorological data for reconstruction of annual runoff series: Orthogonal functions approach // Atmospheric Research (Elsevier). – 2005. – Vol. 77. – P. 100-113.
13. Glushkov, A.V., Khokhlov, V.N., Tsenenko, I.A.: Atmospheric teleconnection patterns: wavelet analysis // Nonlinear Processes in Geophysics. – 2004. – Vol. 11(3). – P. 285-293.
14. Khokhlov, V.N., Glushkov, A.V., Loboda, N.S, Bunyakova, Yu.Ya., Short-range forecast of atmospheric pollutants using non-linear prediction method // Atmospheric Environment (Elsevier). – 2008. – Vol. 42. – P. 1213-1220.
15. Glushkov, A.V., Kuzakon', V.M., Khetselius, O.Yu., Prepelitsa, G.P., Svinarenko, A.A., Zaichko, P.A.: Geometry of Chaos: Theoretical basis's of a consistent combined approach to treating chaotic dynamical systems and their parameters determination // Proceedings of International Geometry Center. – 2013. – Vol. 6(1). – P. 43-48.
16. Khetselius, O.Yu., Forecasting evolutionary dynamics of chaotic systems using advanced non-linear prediction method // Dynamical Systems - Theory and Applications. – 2013. – Vol. LIF142. – P.1-11.
17. Glushkov A.V., Khetselius O.Y., Brusentseva S.V., Zaichko P.A., Ternovsky V.B., Studying interaction dynamics of chaotic systems within a nonlinear prediction method: application to neurophysiology// Advances in Neural Networks, Fuzzy Systems and Artificial Intelligence, Series: Recent Advances in Computer Engineering, Ed. J.Balicki. (Gdansk, WSEAS Pub.).-2014.-Vol.21.-P.69-75.
18. Glushkov A.V., Svinarenko A.A., Buyadzhi V.V., Zaichko P.A., Ternovsky V.B., Chaos-geometric attractor and quantum neural networks approach to simulation chaotic evolutionary dynamics during perception process// Advances in Neural Networks, Fuzzy Systems and Artificial Intelligence, Series: Recent Advances in Computer Engineering, Ed. J.Balicki.(Gdansk, WSEAS Pub.).-2014.-Vol.21.-P.143-150.
19. Khetselius O.Yu., Forecasting evolutionary dynamics of chaotic systems using advanced non-linear prediction method// Dynamical Systems Applications, Eds. J. Awrejcewicz, M. Kazmierczak, P. Olejnik, J, Mrozowski (Lodz, Polland).-2013.-Vol.T2.-P.145-152
20. Khetselius O.Yu., Brusentseva S.V., Tkach T.B. Studying interaction dynamics of chaotic systems within nonlinear prediction method: Application to neurophysiology// Dynamical Systems Applications, Eds. J. Awrejcewicz, M. Kazmierczak, P. Olejnik, J, Mrozowski (Lodz, Polland).-2013.-Vol. T2.-P.251-259.
21. Neural Computers, Eds. Eckmiller, R., Malsburg, C. // Springer, Berlin. – 1998.
22. Neural Networks for Computing, Ed. Denker J. // AIP Publ.,N.-Y. – 2000.

This article has been received within 2014

UDC 539.182

P. A. Kondratenko, O. Yu. Khetselius, V. B. Ternovsky, P. A. Zaichko, A. V. Duborez

SIMULATION CHAOTIC DYNAMICS OF COMPLEX SYSTEMS AND DEVICES WITH USING CHAOS THEORY, GEOMETRIC ATTRACTORS, AND QUANTUM NEURAL NETWORKS

Abstract

Nonlinear simulation and forecasting chaotic evolutionary dynamics of complex systems can be effectively performed using the concept of compact geometric attractors. We are developing a new approach to analyze and forecasting complex systems evolutionary dynamics based on the concept of geometric attractors, chaos theory methods and algorithms for quantum neural network simulation

Key words: geometric attractor conception, quantum neural networks, chaotic dynamics

УДК 539.182

П. А, Кондратенко, О. Ю. Хецелиус, В. Б. Терновский, П. А. Заичко, А. В. Дуборез

МОДЕЛИРОВАНИЕ ХАОТИЧНОЙ ДИНАМИКИ СЛОЖНЫХ СИСТЕМ И ПРИБОРОВ С ИСПОЛЬЗОВАНИЕМ ТЕОРИИ ХАОСА, ГЕОМЕТРИЧЕСКИХ АТТРАКТОРОВ И КВАНТОВЫХ НЕЙРОСЕТЕЙ

Резюме

Нелинейное моделирование и прогнозирование хаотических эволюционных динамик сложных систем может быть эффективно выполнено с использованием концепции компактных геометрических аттракторов. Мы развиваем эффективный подход для анализа и прогнозирования нелинейной эволюционной динамики сложных систем, основанный на концепции геометрических аттракторов, методов теории хаоса и алгоритмов для моделирования квантовой нейронной сети.

Ключевые слова: концепция геометрического аттрактора, квантовые нейронные сети, хаотическая динамика

УДК 539.182

П. О. Кондратенко, О. Ю. Хецеліус, В. Б. Терновський, П. А. Заичко, А. В. Дуборез

МОДЕЛЮВАННЯ ХАОТИЧНОЇ ДИНАМІКИ СКЛАДНИХ СИСТЕМ І ПРИЛАДІВ З ВИКОРИСТАННЯМ ТЕОРІЇ ХАОСУ, ГЕОМЕТРИЧНИХ АТТРАКТОРІВ І КВАНТОВИХ НЕЙРОМЕРЕЖ

Резюме

Нелінійне моделювання і прогнозування хаотичних еволюційних динамік складних систем може бути ефективно виконане з використанням концепції компактних геометричних аттракторів. Ми розвиваємо ефективний підхід для аналізу й прогнозування нелінійної еволюційної динаміки складних систем, оснований на концепції геометричних аттракторів, методів теорії хаосу і алгоритмів для моделювання квантової нейронної мережі.

Ключевые слова: концепція геометричного аттрактора, квантові нейронні мережі, хаотична динаміка

UDC 539.27

L. V. Nikola, S. S. Seredenko, P. G. Bashkaryov

I. Mechnikov Odessa National University, 2, Dvoryanskaya str., Odessa, Ukraine
e-mail: quantnik@mail.ru

CALCULATION OF AUGER-ELECTRON ENERGIES FOR SOME SOLIDS

Within a new relativistic approach there are presented the calculation data on the Auger electron transition energies for solids of As and Ag. New data on the Auger-electron energies for atoms and solids of the As and Ag are analyzed and compared with alternative theoretical semiempirical equivalent core approximation results, obtained by Larkins as well as experimental data. There is physically reasonable agreement between theory and experiment.

1. Introduction

This work goes on our investigation in a field of theoretical Auger spectroscopy of atoms and solids [1,2]. In Refs. [1-7] there were presented the calculation data on the Auger electron transition energies for a whole number of atomic systems and solids, in particular, alkali and transient metals and inert gases. Here we present the Auger electron energy data for As and Ag.

In eRefs. [1,2] it has been indicated that the Auger electron spectroscopy remains an effective method to study the solids electron structure, chemical composition of solid surfaces and near-surface layers [8-12]. Sensing the Auger spectra in atomic systems and solids gives the important data for the whole number of scientific and technological applications. So called two-step model is used most widely when calculating the Auger decay characteristics [8-14]. Since the vacancy lifetime in an inner atomic shell is rather long (about 10^{-17} to 10^{-14}s), the atom ionization and the Auger emission are considered to be two independent processes. In the more correct dynamic theory of the Auger effect [9] the processes are not believed to be independent from one another. The fact is taken into account that the relaxation processes due to Coulomb interaction between electrons and resulting in the electron distribution in the vacancy field have no time to be over prior to the transition. In fact, a consistent Auger decay theory has to take into account correctly a number of correlation effects, including the energy dependence of the vacancy mass operator, the continuum pressure, spreading of the initial state over a set of configurations etc. Now it is clear that an account of the relativistic and exchange-correlation effects is very important for the adequate description of the Auger spectra of atoms and solids. This problem is partly solved in this paper. As basic approach to calculating the Auger spectra of solids we use a new approach [1-7], basing on the S-matrix formalism by Gell-Mann and Low and relativistic perturbation theory (PT) formalism [13]. Earlier the method has been applied to calculation of the Auger-electron spectra (transitions), the ionization cross-sections of inner shells in various atomic systems and solids [1-7]. Here we are limited only by the key topics. Other details can be, for example, found in Refs. [1-5].

2. Method

Within the frame of the relativistic many-body theory , the Auger transition probability and the Auger line intensity are defined by the square of an electron interaction matrix element having the form:

$$V^{\omega}_{1234} = [(j_1)(j_2)(j_3)(j_4)]^{1/2} \sum_{\lambda\mu} (-1)^{\mu} \begin{pmatrix} j_1 j_3 & \lambda \\ m_1 - m_3 & \mu \end{pmatrix} \times \mathrm{Re}\, Q_{\lambda}(1234).$$

$$Q_{\lambda} = Q_{\lambda}^{\mathrm{Qul}} + Q_{\lambda}^{\mathrm{Br}}. \qquad (1)$$

The terms $Q_{\lambda}^{\mathrm{Qul}}$ and Q_{λ}^{B} correspond to subdivision of the potential into Coulomb part $cos|\omega|r_{12}/r_{12}$ and Breat one, $cos|\omega|r_{12}\alpha_1\alpha_2/r_{12}$. The

real part of the electron interaction matrix element is determined using expansion in terms of Bessel functions:

$$\frac{\cos|\omega|r_{12}}{r_{12}} = \frac{\pi}{2\sqrt{r_1 r_2}} \sum_{\lambda=0} (\lambda) J_{\lambda+1/2}(|\omega| r_<) J_{-\lambda-1/2}(|\omega| r_>) P_\lambda(\cos \mathbf{r}_1 \mathbf{r}_2) \quad (2)$$

where J is the 1st order Bessel function, $(\lambda)=2\lambda+1$.

The Coulomb part Q_λ^{Qul} is expressed in terms of the radial integrals R_λ and the angular coefficients S_λ [13]:

$$\mathrm{Re}\, Q_\lambda^{\mathrm{Qul}} = \frac{1}{Z} \mathrm{Re}\{R_l(1243) S_\lambda(1243) + R_\lambda(\tilde{1}\,24\tilde{3}) S_\lambda(\tilde{1}\,24\tilde{3}) + \quad (3)$$
$$+ R_\lambda(1\tilde{2}4\tilde{3}) S_\lambda(1\tilde{2}4\tilde{3}) + R_\lambda(\tilde{1}\,\tilde{2}4\tilde{3}) S_\lambda(\tilde{1}\,\tilde{2}4\tilde{3})\}$$

As a result, the Auger decay probability is expressed in terms of $\mathrm{Re}Q_\lambda(1243)$ matrix elements:

$$\mathrm{Re}\, R_\lambda(1243) = \iint dr_1 r_1^2 r_2^2 f_1(r_1) f_3(r_1) f_2(r_2) f_4(r_2) Z_\lambda^{(1)}(r_<) Z_\lambda^{(1)} \quad (4)$$

where f is the large component of radial part of single electron state Dirac function; function Z and angular coefficient are defined in refs. [2-4,13]. The other items in (3) include small components of the Dirac functions; the sign «~» means that in (3) the large radial component f_i is to be changed by the small g_i one and the moment l_i is to be changed by $\tilde{l}_i = l_i - 1$ for Dirac number æ$_1$> 0 and l_i+1 for æ$_i$<0.

The Breit interaction is known to change considerably the Auger decay dynamics in some cases. The Breit part of Q is defined in [7,13]. The Auger width is obtained from the adiabatic Gell-Mann and Low formula for the energy shift [7]. Namely, according to [1,7], the Auger level width with a vacancy $n_\alpha l_\alpha j_\alpha m_\alpha$ can be represented as:

$$\sum_\lambda \frac{2}{(\lambda)(j_\alpha)} \sum_{\beta\gamma \le f} \sum_{k>f} Q_\lambda(\alpha k \gamma \beta) Q_\lambda(\beta \gamma k \alpha), \quad (5)$$

$$\frac{2}{(j_\alpha)} \sum_{\lambda_1 \lambda_2} \sum_{\beta\gamma \le f} \sum_{k>f} Q_{\lambda_1}(\alpha k \gamma \beta) Q_{\lambda_2}(\beta \gamma k \alpha) \begin{Bmatrix} j_\alpha & j_\gamma & \lambda_2 \\ j_k & j_\beta & \lambda_1 \end{Bmatrix} \quad (6)$$

The partial items of the $\sum_{\beta\gamma} \sum_k$ sum answer to contributions of $\alpha^{-1} \to (\beta\gamma)^{-1} K$ channels resulting in formation of two new vacancies $\beta\gamma$ and one free electron k: $\omega_k = \omega_\alpha + \omega_\beta - \omega_\alpha$. The final expression for the width in the representation of jj-coupling scheme of single-electron moments is given by the corresponding sum on over all possible decay channels.

The basis of the electron state functions was determined by the solution of Dirac equation (integrated numerically using the Runge-Cutt method). The contribution of the lower order PT corrections to the energies of the auger transitions is carried out according to the methodology [11,12,14]. The calculation of radial integrals $\mathbf{Re}R_\lambda(1243)$ is reduced to the solution of a system of differential equations [13]:

$$y_1' = f_1 f_3 Z_\lambda^{(1)}(\alpha|\omega|r) r^{2+\lambda}$$
$$y_2' = f_2 f_4 Z_\lambda^{(1)}(\alpha|\omega|r) r^{2+\lambda} \quad (7)$$
$$y_3' = [y_1 f_2 f_4 + y_2 f_1 f_3] Z_\lambda^{(2)}(\alpha|\omega|r) r^{1-\lambda}$$

In addition,
$y_3(\infty) = \mathbf{Re}R_\lambda(1243)$,
$y_1(\infty) = X_\lambda(13)$.

The formulas for the Auger decay probability include the radial integrals $R_\alpha(\alpha k \gamma \beta)$, where one of the functions describes electron in the continuum state. The energy of an electron formed due to a transition jkl is defined by the difference between energies of atom with a hole at j level and double-ionized atom at kl levels in final state:

$$E_A(jkl, {}^{2S+1}L_J) = E_A^+(j) - E_A^{2+}(kl, {}^{2S+1}L_J) \quad (8)$$

In order to take into account the dynamic correlation effects, the equation (8) can be rewritten as:

$$E_A(jkl, {}^{2S+1}L_J) = E(j) - E(k) - E(l) - \Delta(k,l; {}^{2S+1}L_J) \quad (9)$$

where the item Δ takes into account the dynamic correlation effects (relaxation due to hole screening with electrons etc.) To take these effects into account, the set of procedures elaborated in the atomic theory [2,3] is used. For solid phase, the more precise form of equation (9) is as follows:

$$E^s{}_A(jkl, {}^{2S+1}L_J) = E_A(jkl, {}^{2S+1}L_J) + \Delta E^s + R_{rel} + e\Phi \quad (10)$$

where ΔE^s is a correction for the binding energy change in the solid; R_{rel}, the same for out-of-atom

relaxation; $e\Phi$ takes into account the work of output. Other details can be found in Refs. [1-7].

3. Some results

In table 1 we present our calculation data on Auger-electron energies for As and Ag (column B) and also the semi-empirical method under Larkins' equivalent core approximation (from [8,9] (column A) as well as experimental data [2]. The calculation accuracy using the Larkins' method is within about 2a few V as an average. As earlier calculation show, our approach provides more accurate results that is due to a considerable extent to more correct accounting for the exchange-correlation effects. Especially physically reasonable accuracy has reached for alkali and alkali-earth elements. At the same time atoms of the transient metals are related to significantly more complex systems and a role of different exchange-correlation effects is of a critical importance. However, we believe that an approach used can be improved at this case too.

Table 1. Experimental and theoretical data for Auger electron energy: Exp-experiment;

A, semi-empirical method - [8,9]; B- present paper;

Solid	Auger line	Exp	Theory: A	Theory: D
As	$L_3M_{4,5}M_{4,5}$ $^1G_4$	1226,4	1227,1	1226,6
Ag	$M_5N_{4,5}N_{4,5}$ $^1G_4$	353.4	358.8	354.8

References

1. Nikola L.V., Ignatenko A.V., Shakhman A.N., Relativistic theory of Auger (auto-ionization) decay of excited states in spectrum of multicharged ion// Photoelectronics.- 2010.-N19.-P.61-64.
2. Nikola L.V., Resonant Auger spectroscopy of the atoms of inert gases //Photo-electronics.-2011.-Vol.20.-P.104-108.
3. Svinarenko A.A., Nikola L.V., Prepelitsa G.P., Tkach T., Mischenko E., The Auger (autoionization) decay of excited states in spectra of multicharged ions: Relativistic theory//Spectral Lines Shape (AIP, USA).-2010.-Vol.16.-P.94-98.
4. Ambrosov S.V., Glushkov A.V., Nikola L.V., Sensing the Auger spectra for solids: New quantum approach// Sensor Electr. and Microsyst. Techn.-2006.-N3.-P.46-50.
5. Nikola L.V., Quantum calculation of Auger spectra for Na, Si atoms and solids//Photoelectronics.-2007.-N16.-P.102-105.
6. Khetselius O.Yu., Nikola L.V., Turin A.V., Sukharev D.E., Sensing the finite size nuclear effect in calculation of the Auger spectra for atoms and solids// Sensor Electr. and Microsyst. Techn.-2007.-N1.-P.18-21..
7. Glushkov A.V., Khetselius O.Yu., Nikola L.V., Dubrovskaya Yu.V., Quantum calculation of Auger spectra for atoms and semiconductors: New approach// Photoelectronics.-2008.-N17.-P.12-16.
8. Nikola L.V., Auger-electron spectroscopy of transient metals// "Photoelectronics" -2013.-Vol.22.-P.135-138
9. Aberg T., Hewat G. Theory of Auger effect. Springer-Verlag: Berlin, 1999.
10. Amusia M.Ya. Atomic photoeffect. Acad.Press: N.-Y., 1998.
11. Letokhov V. Nonlinear Selective Photoprocesses in Atoms and Molecules.-Moscow, 1997.
12. Aglitsky E.V., Safronova U.I. Spectroscopy of Autoionization states of atomic systems. Energoatomizd.: Moscow, 1992.
13. Glushkov A.V., Relativistic Quantum Theory. Quantum Mechanics of Atomic Systems.-Odessa: Astroprint, 2008.-704p.
14. Kulekshov V.F., Kukharenko Yu.A., Fridrikhov S.A. et al. Spectroscopy and Electron Diffraction in Solid Surfaces Studies. Nauka: Moscow, 1995.

This article has been received within 2014

UDC 539.27

L. V. Nikola, S. S. Seredenko, P. G. Bashkaryov

CALCULATION OF AUGER-ELECTRON ENERGIES FOR SOME SOLIDS

Abstract

Within a new relativistic approach there are presented the calculation data on the Auger electron transition energies for solids of As and Ag. New data on the Auger-electron energies for atoms and solids of the As and Ag are analyzed and compared with alternative theoretical semiempirical equivalent core approximation results , obtained by Larkins as well as experimental data. There is physically reasonable agreement between theory and experiment.

Key words: Auger-spectroscopy, atoms, solids

УДК 539.27

Л. В. Никола, С. С. Середенко, П. Г. Башкарьов

РАСЧЕТ ЭНЕРГИЙ ОЖЕ-ЭЛЕКТРОНОВ ДЛЯ ТВЕРДЫХ ТЕЛ

Резюме

В рамках нового релятивистского подхода выполнен расчет энергий Оже переходов для ряда твердых тел. Новые данные по Оже-электронным энергиям для As и Ag анализируются и сравниваются с альтернативными теоретическими полуэмпирическими данными, полученными в приближении эквивалентного остова Larkins, а также экспериментальными результатами.. Получено достаточно хорошее согласие теории и эксперимента.

Ключевые слова: Оже-спектроскопия, атомы, твердые тела

УДК 539.27

Л. В. Нікола, С. С. Середенко, П. Г. Башкарьов

РОЗРАХУНОК ЕНЕРГІЙ ОЖЕ ЕЛЕКТРОНІВ ДЛЯ ТВЕРДИХ ТІЛ

Резюме

В межах нового релятивістського підходу виконано розрахунок енергій Оже переходів для ряду твердих тіл. Нові дані по Оже-електронним енергіям для As і Ag аналізуються і порівнюються з альтернативними теоретичними напівемпіричними даними, отриманими у наближенні еквівалентного остову Larkins а також експериментальними результатами. Получено достатньо добре узгодження теорії та експерименту..

Ключові слова: Оже-спектроскопія, атоми, тверді тела

UDC 539.184

I. N. Serga

Odessa State Environmental University, 15, Lvovskaya str., Odessa, Ukraine
e-mail: nucserga@mail.ru

RELATIVISTIC THEORY OF SPECTRA OF PIONIC ATOMS WITH ACCOUNT OF THE RADIATIVE CORRECTIONS: HYPERFINE STRUCTURE

A new theoretical approach to the description of spectral parameters pionic atoms in the excited states with precise accounting relativistic, radiation and nuclear effects is applied to studying spectral structure for pionic nitrogen. Energies and probabilities of radiation transitions between hyperfine structure lines components, such as 5f-4d, in the spectrum of the pion nitrogen are calculated and analyzed.

Our work is devoted to the application of earlier developed new theoretical approach to the description of spectral parameters pionic atoms in the excited states with precise accouting relativistic, radiation to studying energy parameters of the hyperfine structure of pionic atoms. As introduction let us remind that at present time studying the exotic hadronic atomic systems such as pionic atoms is of a great interest for further development of atomic and nuclear theories as well as new tools for sensing the nuclear structure and fundamental pion-nucleus strong interactions. In the last few years transition energies in pionic atoms [1] have been measured with an unprecedented precision. Besides, light pionic atoms can additionally be used as a new low-energy X-ray standards [1]. More over, their spectra studying allows to determine the pion mass using the highest accuracy in comparison with other methods. TO nowadays, new advanced experiments are been preparing in order to make sensing the electromagnetic and strong interaction effects in different pionic atoms.

The most popular theoretical models are naturally (pion is the Boson with spin 0, mass m_{π^-} =139.57018 МэВ, r_{π^-}=0.672±0.08 fm) based on the using the Klein-Gordon-Fock equation, but there are many important problems connected with accurate accounting for as pion-nuclear strong interaction effects as QED radiative corrections (firstly, the vacuum polarization effect etc.). This topic has been a subject of intensive theoretical and experimental interest (see [1-14]). The perturbation theory expansion on the physical; parameter αZ is usually used to take into account the radiative QED corrections, first of all, effect of the polarization of electron-positron vacuum etc. This approximation is sufficiently correct and comprehensive in a case of the light pionic atoms, however it becomes incorrect in a case of the heavy atoms with large charge of a nucleus Z.

So, there is a high necessity to develop non-perturbative methods in order to account the QED effects. Besides, let us underline that more correct accounting of the finite nuclear size and electron-screening effects for heavy pionic atoms is also very serious and actual problem. At last, a development of the comprehensive theory of hyperfine structure is of a great interest and importance in a modern theory of the pionic atom spectra.

As usually, the relativistic dynamic of a spinless boson particle should be described on the basis of the Klein-Gordon-Fock (KGF) equation. The electromagnetic interaction between a negatively charged pion and the atomic nucleus can be taken into account introducing the nuclear potential A_ν in the KG equation via the minimal coupling $p_\nu \rightarrow p_\nu - qA_\nu$.

The wave functions of the zeroth approximation for pionic atoms are determined from the KGF equation [1]:

$$m^2c^2\Psi(x) = \{\frac{1}{c^2}[i\hbar\partial_t + eV_0(r)]^2 + \hbar^2\nabla^2\}\Psi(x) \quad (1)$$

where *h* is the Planck constant, c the velocity of the light and the scalar wavefunction Ψ_0(x) depends on the space-time coordinate x = (ct,r). Here it is considered a case of a central Coulomb potential (V_0(r), 0). The corresponding stationary equation looks as:

$$\{\frac{1}{c^2}[E + eV_0(r)]^2 + \hbar^2\nabla^2 - m^2c^2\}\varphi(x) = 0 \quad (2)$$

where E is the total energy of the system (sum of the mass energy mc^2 and binding energy ε_0). In principle, the central potential V_0 should include the central Coulomb potential, the radiative (in particular, vacuum-polarization) potential as well as the electron-screening potential in the atomic-optical (electromagnetic) sector. Surely, the full solution of the pionic atom energy especially for the low-excited state requires an inclusion the pion-nuclear strong interaction potential. However, if a pion is on the high orbit of the atom, the strong interaction effects can not be accounted because of the negligible value.

The important nuclear effect is the finite size one (the Breit-Rosenthal-Crawford-Schawlow effect). We will use the widespread Gaussian model for nuclear charge distribution. This is the smooth function, and as result it has a advantage in comparison with usually used model of a uniformly charged sphere [2-5]. It is obvious that it simplifies the calculation procedure and permits to perform a flexible simulation of the real distribution of the charge in a nucleus. The Gauss model is determined as follows:

$$\rho(r|R) = \left(4\gamma^{3/2}/\sqrt{\pi}\right)\exp\left(-\gamma r^2\right), \quad (3)$$

where $\gamma = 4\pi/R^2$, R is an effective radius of a nucleus.

The next important topic is connected with a correct accounting the radiation QED corrections and, first of all, the vacuum polarization correction. We firstly introduce into the theory the Flambaum-Ginges radiative potential. In includes the standard Ueling-Serber potential and electric and magnetic form-factors plus potentials for accounting of the high order QED corrections such as [15]:

$$\Phi_{rad}(r) = \Phi_U(r) + \Phi_g(r) + \Phi_f(r) + \Phi_l(r) + \frac{2}{3}\Phi_U^{high-order}(r) \quad (4)$$

where

$$\Phi_U^{high-order}(r) = -\frac{2\alpha}{3\pi}\Phi(r)\frac{0.092Z^2\alpha^2}{1+(1.\beta\ r/r_C)^4} \quad (5)$$

$$\Phi_l(r) = -\frac{B(Z)}{e}Z^4\alpha^5 m^{\ 2}e^{-r/a_B} \quad (6)$$

Here *e* – a proton charge and universal function *B*(*Z*) is defined by expression: $B(Z)=0.074+0.35Z\alpha$.

The next step is an account of the electron screening effect. It should be noted that the electron shells are not survived in the light pionic atoms during the cascade processes accompanying the formation of a pionic atom. However, in a case of the heave systems, the internal electron shells survive and this fact should be reflected in a precise theory. Our procedure for accounting this effect is a standard one and includes addition to the total interaction potential SCF potential of the electrons, which can be determined within the Dirac-Fock method by solution of the standard relativistic Dirac equations. To realize this step, we have used the QED perturbation theory formalism for relativistic many-electron atom. Further in order to calculate probabilities of the Radiative transitions between energy level of the pionic atoms we have used the relativistic energy approach [16].

The final topic of the theory is calculation of the hyperfine structure parameters. Here one could use the standard theory of hyperfine structure of the usual multi-electron atom. As usually, the hyperfine structure is arisen because of the interaction of the orbital pion with a magnetic dipole moment μ and quadruple electric moment Q of a nucleus. Hitherto, only magnetic contribution has been studied. The quadruple interaction is not treated hitherto. One could consider energy of the hyperfine interaction, which looks as:

$$W = W_\mu + W_Q = -\mu\cdot H(0) + \frac{1}{6}e\sum_{\alpha\beta}Q_{\alpha\beta}\frac{\partial^2\varphi}{\partial x_\alpha\partial x_\beta} \quad (7)$$

Here H and φ are defined as, respectively, the magnetic field and electrostatic potential produced by an electron (pion) in the position of the nucleus. Following to the standard procedure, after multiple transformations the final expression for the energy of the hyperfine splitting (magnetic part of) the energy levels of the atom in the pion:

$$E_1^{nlF} = \frac{\mu_l \mu_N e \mu_0 \hbar c^2}{4\pi\left(E_0^{nl} - \langle nl|V_0(r)|nl\rangle\right)} \times \left[\frac{F(F+1) - I(I+1) - l(l+1)}{2I}\right] \langle nl|r^{-3}|nl\rangle \quad (8)$$

Here $\mu_N = e\hbar / 2m_p c$; other notations are standard. In a consistent precise theory it is important allowance for the contribution to the energy of the hyperfine splitting of the levels in the spectrum of the pion atom due to the interaction of the orbital momentum of the pion with the quadrupole moment of the atomic nucleus. The corresponding part looks as follows:

$$< LIFM|W_Q|LIFM >= \Delta + BC(C+1) \quad (9)$$

where

$$C=F(F+1)-L(L+1)-I(I+1), \quad (10)$$

$$B = -\frac{3}{4}\frac{e^2 Q}{I(2I-1)} \frac{(\gamma \cdot L \| \eta_2 \| \gamma \cdot L)}{\sqrt{L(L+1)(2L-1)(2L+1)(2L+3)}} \quad (11)$$

$$\Delta = \frac{e^2 Q(I+1)}{(2I-1)} \frac{(\gamma \cdot L \| \mu_2 \| \gamma \cdot L) L(L+1)}{\sqrt{L(L+1)(2L-1)(2L+1)(2L+3)}} \quad (13)$$

Here L – is orbital moment of pion, F is a total moment of an atom.

As example of application of the presented approach, in table 1 we present our data on the energies (in eV) of transitions between hyperfine structure components 5f-4d in the spectrum of the pion nitrogen (our data)

The analogous computing energies of transitions between hyperfine structure components 5f-4d in the spectrum of the pion neon has demonstrated physically reasonable agreement with other theoretical data by Indelicato et al and measured results. So, the received data can be considered as sufficiently accurate ones and used in the corresponding applications.

Table 1

Energy (in eV) transitions between hyperfine structure components 5f-4d in the spectrum of the pion nitrogen (our data)

F-F'	ΔE, Our data	P, Our data.
4-3	4057.6819	4.57×10^{13}
3-2	4057.6915	3.16×10^{13}
3-3	4057.6799	2.98×10^{13}
2-1	4057.6978	2.13×10^{13}
2-2	4057.6905	2.25×10^{13}
2-3	4057.6789	0.01×10^{13}

References

1. Deloff A., Fundamentals in Hadronic Atom Theory, Singapore: World Scientific, 2003.-352P.
2. Serga I.N., Electromagnetic and strong interactions effects in X-ray spectroscopy of pionic atoms// Photoelectronics.-2011.-Vol.20.-P.109-112.
3. Deslattes R., Kessler E., Indelicato P., de Billy L., Lindroth E. , Anton J., Exotic atoms//Rev. Mod. Phys. -2003.-Vol.75.-P.35-70.
4. Backenstoss G., Pionic atoms//Ann. Rev.Nucl.Sci.-1990.-Vol.20-P.467-510.
5. Menshikov L I and Evseev M K, Some questions of physics of exotic atoms// Phys. Uspekhi.2001-Vol. 171.-P.150-184.
6. Indelicato P., Trassinelli M., From heavy ions to exotic atoms// arXiv:physics.-2005.-V1-0510126v1.-P 16..
7. Mitroy J., Ivallov I.A., Quantum defect theory for the study of hadronic atoms// J. Phys. G: Nucl. Part. Phys.-2001.-Vol.**27.-P.**1421–1433
8. Lyubovitskij V., Rusetsky A., πp atom in ChPT: Strong energy-level shift// Phys. Lett.B.-2000.-Vol.494.-P.9-13.

9. Schlesser S., Le Bigot E.-O., Indelicato P., Pachucki K., Quantum-electro-dynamics corrections in pionic hydrogen // Phys.Rev.C.-2011.-Vol.84.-P.015211 ..
10. Sigg D., Badertscher A., Bogdan M. et al, The strong interaction shift and width of the ground state of pionic hydrogen// Nucl. Phys. A.-1996.-Vol.609.-P.269-309.
11. Gotta D., Amaro F., Anagnostopoulos D., Conclusions from recent pionic–atom experiments//Cold Antimatter Plasmas and Application to Fundamental Physics, ed. Y.Kania and Y.Yamazaki (AIP).-2008.-Vol.CP1037.-P.162-177.
12. Gotta D., Amaro F., Anagnostopoulos D., Pionic Hydrogen//Precision Physics of Simple Atoms and Molecules, Ser. Lecture Notes in Physics (Springer, Berlin / Heidelberg).-2008.-Vol.745.-P.165-186
13. Serga I.N., Dubrovskaya Yu.V., Kvasikova A.S., Shakhman A.N., Sukharev D.E., Spectroscopy of hadronic atoms: Energy shifts// Journal of Physics: C Ser.-2012.- Vol.397.-P.012013.
14. Pavlovich V.N., Serga I.N., Zelentsova T.N., Tarasov V.A., Mudraya N.V., Interplay of the hyperfine, electroweak and strong interactions in heavy hadron-atomic systems and x-ray standards status// Sensor Electronics and Microsyst. Techn.-2010.-N2.-P.20-26.
15. Flambaum V.V., Ginges J.S.M., Radiative potential and calculation of QED radiative corrections to energy levels and electromagnetic amplitudes in many-electron atoms //Phys.Rev.-2005.-Vol.72.-P.052115 .
16. Serga I.N., Relativistic theory of spectra of pionic atoms with account of the radiative and nuclear corrections// Photoelectronics.2013.-Vol.22.-P.84-92.
17. Glushkov A.V., Relativistic quantum theory. Quantum mechanics of atomic systems, Odessa: Astroprint, 2008- P 700.

This article has been received within 2014

UDC 539.184

I. N. Serga

RELATIVISTIC THEORY OF SPECTRA OF PIONIC ATOMS WITH ACCOUNT OF THE RADIATIVE CORRECTIONS: HYPERFINE STRUCTURE

Abstract

A new theoretical approach to the description of spectral parameters pionic atoms in the excited states with precise accounting relativistic, radiation and nuclear effects is applied to studying spectral structure for pionic nitrogen. Energies and probabilities of radiation transitions between hyperfine structure lines components, such as 5f-4d, in the spectrum of the pion nitrogen are calculated and analyzed.

Key words: relativistic theory, hyperfine structure, pionic atom

УДК 539.184

И. Н. Серга

РЕЛЯТИВИСТСКАЯ ТЕОРИЯ СПЕКТРОВ ПИОННЫХ АТОМОВ С УЧЕТОМ РАДИАЦИОННЫХ ПОПРАВОК: СВЕРТОНКАЯ СТРУКТУРА

Резюме

Новый теоретический подход к описанию спектральных параметров пионных атомов в возбужденном состоянии с учетом релятивистских, радиационных эффектов применен к изучению спектральной структуры пионного азота. Рассчитаны и проанализированы значения энергий и вероятностей радиационных переходов между компонентами линий сверхтонкой структуры (типа 5f-4d) в спектре пионного азота.

Ключевые слова: релятивистская теория, сверхтонкая структура, пионный атом

УДК 539.184

І. М. Сєрга

РЕЛЯТИВІСТСЬКА ТЕОРІЯ СПЕКТРІВ ПІОННИХ АТОМІВ З УРАХУВАННЯМ РАДІАЦІЙНИХ ПОПРАВОК: НАДТОНКА СТРУКТУРА

Резюме

Новий теоретичний підхід до опису спектральних параметрів піонних атомів у збудженому стані з урахуванням релятивістських, радіаційних ефектів застосовано до вивчення спектральної структури піонного азоту. Розраховані і проаналізовані значення енергій і ймовірностей радіаційних переходів між компонентами ліній надтонкої структури (типу 5f-4d) в спектрі піонного азоту.

Ключові слова: релятивістська теорія, надтонка структура, піонний атом

UDC 539.185

A. P. Fedchuk, A. V. Glushkov, Ya. I. Lepikh, A. V. Ignatenko, A. S. Kvasikova

[1]I. Mechnikov Odessa National University, 2, Dvoryanskaya str., Odessa, Ukraine
[2]Odessa National Polytechnical University, 1, Shevchenko av., Odessa, Ukraine
[3]Odessa State Environmental University, 15, Lvovskaya str., Odessa, Ukraine
e-mail: dirac13@mail.ru

ATOM OF HYDROGEN AND WANNIER-MOTT EXCITON IN CROSSED ELECTRIC AND MAGNETIC FIELDS

Spectroscopy of atoms in the crossed external electric and magnetic fields is investigated on the basis of the operator perturbation theory. The data for ground state energies of the hydrogen atom in sufficiently weak crossed external electric and magnetic fields are calculated. Generalization of the method on a case of the Wannier-Mott excitons in the bulk semiconductors in a case of the crossed fields is given.

1. This work goes on our investigations of the multi-electron atomic systems and excitons in semiconductrs in an external electric field (the Stark effect) [1-17]. The remarkable Stark effect has a long history and until recently it was believed that the Stark effect is fully understood and fundamental problems remained (look [1-16]). However, an observation of the Stark effect in a constant (DC) electric field near threshold in hydrogen and alkali atoms led to the discovery of resonances extending into the ionization continuum by Glab et al and Freeman et al (c.f.[1]). Calculation of the characteristics of these resonances as well as the Stark resonances in the strong electric field and crossed electric and magnetic fields remains very important problem of as modern atomic physics as physics of semiconductors (speech is about excitons in bulk semiconductors, quantum dots , wires etc.).

It should be noted that the same class of problems has been arisen in a physics of semiconductors (c.f.[14-17]). It is well known that the availability of excitons in semiconductors resulted experimentally in the special form of the main absorption band edge and appearance of discrete levels structure (f.e. hydrogen-like spectrum in Cu_2O). Beginning from known papers of Gross-Zaharchenya, Thomas and Hopfield et al (c.f.[13-17]), a calculation procedure of the Stark effect for exciton spectrum attracts a deep interest permanently. Very interesting physics occurs in a case of the excitons in quantum dots, wires etc, where the other geometry and energetics in comparison with the bulk semiconductor makes the field effect more intrigues. The exciton states in the quantum dots have been studied in a number of papers and have been observed by photoluminescence experiments (c.f. [14-17]). Naturally, the electronic states in quantum dots (wires) depends on either the confining potential and the interacting force between the particles. Now the electric field effect on the electron-hole states and on the confined excitonic states is often referred to the quantum confined Stark effect. In this paper we are interested by spectroscopy of atoms in the crossed external electric and magnetic fields. Method studying is based on the operator perturbation theory and analysis of the level statistics in spectra. Generalization of method on a case of the Wannier-Mott excitons in the bulk semiconductors is given.

2. As our approach to strong field DC Stark effect was presented in a series of papers (see, for example, [1-6]), here we are limited only by the

key aspects. According to [1,2], the essence of operator perturbation theory approach is the inclusion of the well known method of "distorted waves approximation" in the frame of the formally exact perturbation theory. According to [2,3], the Schrödinger equation for the electronic eigenfunction taking into account the uniform DC electric field (the field strength is F)and the field of the nucleus (Coulomb units are used: a unit is $h^2/Ze^2 m$ and a unit of $mZ^2 e^4/h^2$ for energy) looks like:

$$[-(1 - N/Z) / r + F z - 0{,}5\Delta - E\,]\,\psi = 0 \quad (1)$$

where E is the electronic energy, Z — charge of nucleus, N — the number of electrons in atomic core. Our approach allow to use more adequate forms for the core potential (c.f.[25-27]). According to standard quantum defect theory (c.f.[3]), relation between quantum defect value μ_l, electron energy E and principal quantum number n is: $\mu_l = n - z^*(-2E)^{-1/2}$. As it is known, in an electric field all the electron states can be classified due to quantum numbers: n, n_1, n_2, m (principal, parabolic, azimuthal: $n = n_1 + n_2 + m + 1$). Then the quantum defect in the parabolic co-ordinates $n(n_1 n_2 m)$ is connected with the quantum defect value of the free ($F=0$) atom by the following relation [3]:

$$\delta(n_1 n_2 m) = (1/n) \sum_{l=m}^{n-1} (2l+1)(C^{JM}_{J,M-m;lm})^2 \mu_l$$
$$J = (n-1)/2, \quad M = (n_1 - n_2 + m)/2;$$

After separation of variables, equation (1) in parabolic co-ordinates could be transformed to the system of two equations for the functions f and g:

$$f'' + \frac{|m|+1}{t} f' + [0{,}5E + (\beta_1 - N/Z) / t - 0{,}25\, F(t)\ t\,]\, f = 0 \quad (2)$$

$$g'' + \frac{|m|+1}{t} g' + [0{,}5E + \beta_2 / t + 0{,}25\, F(t)\ t\,]\, g = 0 \quad (3)$$

coupled through the constraint on the separation constants: $\beta_1 + \beta_2 = 1$.

For the uniform electric field $F(t) = F$. In ref. [11], the uniform electric field ε in (3) and (4) was substituted by model function $F(t)$ with parameter τ ($\tau = 1.5\, t_2$) . Here we use similar function, which satisfies to necessary asymptotic conditions (c.f.[11,12]) :

$$F(t) = \frac{1}{t} F\left[(t-\tau)\frac{\tau^2}{\tau^2 + t^2} + \tau\right] \quad (4)$$

Potential energy in equation (4) has the barrier. Two turning points for the classical motion along the η axis, t_1 and t_2 , at a given energy E are the solutions of the quadratic equation ($\beta = \beta_1$, $E = E_0$). It is necessary to know two zeroth order EF of the H_0: bound state function Ψ_{Eb} (ε, ν, φ) and scattering state function Ψ_{Es} (ε, η, φ) with the same EE in order to calculate the width G of the concrete quasi-stationary state in the lowest PT order. Firstly, one would have to define the EE of the expected bound state. It is the well known problem of states quantification in the case of the penetrable barrier. We solve the (2, 3) system here with the total Hamiltonian H using the conditions [11]:

$$f(t) \to 0 \text{ at } t \Rightarrow \infty$$
$$\partial x(\beta, E) / \partial E = 0 \quad (5)$$

with

$$x(\beta, E) = \lim_{t \Rightarrow \infty} [\, g^2(t) + \{g'(t) / k\}^2\,]\, t^{|m|+1}.$$

These two conditions quantify the bounding energy E, with separation constant β_1 . The further procedure for this two-dimensional eigenvalue problem results in solving of the system of the ordinary differential equations(2, 3) with probe pairs of E, β_1. The bound state EE, eigenvalue β_1 and EF for the zero order Hamiltonian H_0 coincide with those for the total Hamiltonian H at $\varepsilon \Rightarrow 0$, where all the states can be classified due to quantum numbers: n, n_1, l, m (principal, parabolic, azimuthal) that are connected with E, β_1, m by the well known expressions.. The scattering states' functions must be orthogonal to the above defined bound state functions and to each other. According to the OPT ideology [11,12], the following form of $g_{E's}$:is possible:

$$g_{E's}(t) = g_1(t) - z_2' g_2(t) \qquad (6)$$

with $f_{E's}$, and $g_1(t)$ satisfying the differential equations (2) and (3). The function $g_2(t)$ satisfies the non-homogeneous differential equation, which differs from (3) only by the right hand term, disappearing at $t \Rightarrow \infty$.

3. In Ref, [7] it has been presented approach, based on solution of the 2-dimensional Schrödinger equation [20,21] for an atomic system in crossed fields and operator perturbation theory [10]. For definiteness, we consider a dynamics of the complex non-coulomb atomic systems in a static magnetic and electric fields. The hamiltonian of the multi-electron atom in a static magnetic and electric fields is (in atomic units) as follows:

$$H = 1/2(p_\rho^2 + l_z^2/\rho^2) + B_z/2 + (1/8)B^2\rho^2 + \\ + (1/2)p_z^2 + F + V(r) \qquad (7)$$

where the electric field F and magnetic field B are taken along the z-axis in a cylindrical system; In atomic units: 1 a.u.B=2.35×10^{5}T, 1a.u.F=5,144×10^6 kV/cm. If one consider only the m=0 state, thus l_z=0; $V(r)$ is a one-electron model potential, which can be in principle choosed in the standard form for multielectron atom; naturally, it results in the usual Coulomb potential for hydrogen one. For solution of the Schrödinger equation with hamiltonian equations (7) we constructed the finite differences scheme which is in some aspects similar to method [7]. An infinite region is exchanged by a rectangular region: $0<\rho< L_\rho$, $0<z< L_Z$. It has sufficiently large size; inside it a rectangular uniform grid with steps h_ρ, h_Z was constructed. The external boundary condition, as usually, is: $(\partial\Psi/\partial n)_r = 0$. The knowledge of the asymptotic behaviour of wave function in the infinity allows to get numeral estimates for L_ρ, L_Z. A wave function has an asymptotic of the kind as: $exp[-(-2E)^{1/2}r]$, where $(-E)$ is the ionization energy from stationary state to lowest Landau level. Then L can be estimated as $L\sim9(-2E)^{-1/2}$. The more exact estimate is found empirically. The difference scheme is constructed as follows. The three-point symmetric differences scheme is used for second derivative on z. The derivatives on ρ are approximated by (2m+1)-point symmetric differences scheme with the use of the Lagrange interpolation formula differentiation. The eigenvalues of hamiltonian are calculated by means of the inverse iterations method. The corresponding system of inhomogeneous equations is solved by the Thomas method. To calculate the values of the width G for resonances in spectra of atomic system in crossed electric and magnetic field one can use the modified operator perturbation theory method (see details in ref.[10,20]). Note that the imaginary part of the state energy in the lowest PT order is defined as follows:

$$\mathrm{Im}E = G/2 = \pi < \Psi_{Eb} \mid H \mid \Psi_{Es} >^2 \qquad (10)$$

with the total Hamiltonian of system in an electric and magnetic field. The state functions Ψ_{Eb} and Ψ_{Es} are assumed to be normalized to unity and by the δ(k -k')-condition, accordingly. Other calculation details can be found in ref. [7].

The above presented method can be naturally generalized for description of the Stark effect for the Wannier-Mott excitons in the bulk semiconductors [4]. Really, the Schrödinger equation for the Wannier-Mott exciton looks as follows:

$$[-\hbar^2\nabla_e^2/2m_e^* - \hbar^2\nabla_h^2/2m_h^* - e^2/\varepsilon r_{eh} + \\ + eFr_e - eFr_h]\Psi = E\Psi \qquad (11)$$

where m^*_e (m^*_h) are the effective-mass for the electron (hole), ε is the background dielectric constant. Introducing the relative coordinates: $r = r_e - r_h$ and the momentum p with reduced mass p= $m^*_e m^*_h/M$ (the momenta P with the total-mass M= m^*_e + m^*_h ,) and center-of-mass coordinate $\rho = (m_e^* r_e + m_h^* r_h)(m_e^* + m_h^*)$, one could rewrite (15) as:

$$[-\hbar^2\nabla^2/2\mu - e^2/\varepsilon r - \hbar/2\cdot(1/m_h^* - 1/m_e^*)K\cdot p - \\ - eFr]\Psi F = [E - \hbar^2K^2/8\mu]\Psi \qquad (12)$$

This equation then could be solved by the method, described above. The other details can be found in Refs. [1,4]. A problem of the combined Stark and

Zeemane effects for quantum dots requires more detailed consideration.

4. As an illustration,, we make computing the energy of the ground state of the hydrogen atom in crossed fields and compare results with data obtained within analytical perturbation theory by TurbinerV (see. [8]) for the case of sufficiently weak fields. According TurbinerV, the expansion for the energy of the hydrogen atom in crossed fields is as follows:

$$E = E_{SZ} + E^{(\|,\perp)} \qquad (13)$$

where E_{SZ} - the total energy of the fields F and B separately:

$$E_{SZ} = -1 - \frac{9}{2}F^2 + \frac{B^2}{2} - \frac{3555}{32}F^4 - \frac{53}{96}B^4 + \ldots \qquad (14)$$

a $E^{\|,\perp}$ contains a previously unknown cross members for mutually parallel ($E^{\|}$) and perpendicular ($E^{\perp}$) directions of fields F и B:

$$E^{\|} = \frac{159}{16}F^2B^2 - \frac{1742009}{26880}F^2B^4 + \ldots \qquad (15a)$$

$$E^{\perp} = \frac{93}{4}F^2B^2 - \frac{22770991}{107520}F^2B^4 + \ldots \qquad (15b)$$

Table 1 shows the values of the energy of the ground state of the hydrogen atom (the following designations: $E+E^{\|}$ - energy for the case of the electric and magnetic fields are parallel;$E+E^{\perp}$corresponds to the case of the electric and magnetic fields are perpendicular). Since the examined fields are sufficiently weak, between the results of both calculations there is a very good agreement. At the same time it is clear that the perturbation theory in the version by Turbiner V is correct only for weak fields, while for strong fields it can lead to substantially inaccurate data. Numerical finite-difference method can be used to calculate the characteristics of the atom in crossed electric and magnetic fields of arbitrary strength.

Table 1

Energy values (Ry) of the H ground state in electric F (1au=5.14·10^9 V/cm) and magnetic B (1 au.B=2.35·10^5 T) fields

F,B 10^{-2}	$E+E^{\|}$ Turbiner theory [8]	$E+E^{\perp}$ Turbiner heory [8]	$E+E^{\|}$ This work	$E+E^{\perp}$ This work
0,0	-1,000000	1,000000	-1,000000	-1,000000
0,1	-1,000004	1,000004	-1,000004	-1,000004
0,5	-1,000099	1,000099	-1,000099	-1,000099
1,0	-1,000402	1,000401	-1,000401	-1,000401
1,5	-1,000906	1,000905	-1,000905	-1,000904
2,0	-1,001617	1,001615	-1,001616	-1,001614
2,5	-1,002542	1,002537	-1,002540	-1,002535
3,0	-1,003685	1,003674	-1,003682	-1,003671
3,5	-1,005054	1,005037	-1,005053	-1,005033
4,0	-1,0066619	1,006628	-1,006659	-1,006626
4,5	-1,008520	1,008465	-1,008517	-1,008463
5,0	-1,010642	1,010558	-1,010636	-1,010553

References

1. Glushkov A.V., Atom in electromagnetic field.-Kiev: KNT, 2005.-400P.
2. Glushkov A.V.,Ivanov L.N. DC Strong-Field Stark-Effect: Consistent Quantum-mechanical Approach // J. Phys. B: At. Mol. Opt. Phys.-1993.-Vol.26,N16.-P.L379-L386.
3. Glushkov A.V., Ambrosov S.V., Ignatenko A.V., Korchevsky D.A., DC Strong Field Stark effect for non-hydrogenic atoms: consistent quantum mechanical approach // Int.Journ.Quant. Chem.-2004.-Vol.99,N5.-P.936-949.
4. Glushkov A.V.,Lepikh Ya.I.,Khetselius O.Yu.,Fedchuk A.P., Ambrosov S.V , Ignatenko A.V.,Wannier-mott excitons and atoms in a DC elecric field: photoionization, Stark effect, resonances in the ionization continuum// Sensor Electr. and Microsyst. Techn.-2008.-N4.-P.5-11.
5. Ambrosov S.V., Khetselius O.Yu., Ignatenko A.V., Wannier-mott exciton and H, Rb atom in a dc elecric field: Stark effect// Photoelectronics.-2008.-N17.-P.82-85.

6. Ambrosov S.V., Ignatenko V.M., Korchevsky D.A., Kozlovskaya V.P., Sensing stochasticity of atomic systems in crossed electric and magnetic fields by analysis of level statistics for continuous energy spectra//Sensor Electronics and Microsystems Technologies-2005.-N2.-P.19-23.;
7. Superintense Laser Atoms Physics.Eds. C.A Ullrich., S Erhard., E.K.Gross.-N-Y: Kluwer,2005.
8. Lisitsa V.S. New in Stark and Zeemane effects for Hydrogen Atom// Usp.Fiz. Nauk.- 1997.-Vol.153,N3.- P.379-422.
9. Harmin D.A. Theory of the Non hydrogenic Stark Effect// Phys.Rev. Lett.-1992.-Vol.49,N2.-P.128-131.
10. Krajewska K, Kaminski J.Z., Potvliege R.M., Stabilization of Resonance States in Crossed Magnetic and Laser Fields in a Parabolic Quantum Well// Laser Physics.-2005.-Vol.15,N2.-P.238-244.
11. Glushkov A.V.,Malinovskaya S.V., Chernyakova Yu.G., Svinarenko A.A., Cooperative Laser-Electron-Nuclear Processes: QED Calculation of Electron Satellites Spectra for Multi-Charged Ion in Laser Field// Int.Journ.Quant.Chem.-2004.-Vol.99, №5.-P.889-894.
12. Popov V.S., Mur V.D., Sergeev A.V., Weinberg V.M., Strong field Stark effect: perturbation theory and 1/n expansion / //Phys.Lett.A.-1990.-V.149.-P.418-424.
13. Zimmerman M., Littman M., Kash M., Kleppner D., Stark and Zeemane structure of Rydberg states of alkali-metal atoms/ // Phys.Rev.A.-1999.-V.20,N6.-P.2251-2275.
14. Electron-Hole Drops in Semiconductors. Eds. Jeffriss K.D., Keldysh L.V. (Moscow, 1998).
15. Singh S. Physics of Semiconductors and Heterostructures.-Singapore: McGraw-Hill Book Co., 1993.
16. Nguyen Ba A., Hartmut Haug, Theory of the excitonic optical Stark effect in quasi-one-dimensional semiconductor quantum weires//Phys.Rev.A..-1999.-Vol.46(15).-P.9569-9576.
17. Jaziri S., Bastard G., Bennaceur R., Stark effect in parabolic quantum dot// J. de Physique.IV. Colloque C.5.-1993.-Vol.11(3).-P.367-374

This article has been received within 2014.

UDC 539.185

O. P. Fedchuk, A. V. Glushkov , Ya. I. Lepikh, A. V. Ignatenko, A. S. Kvasikova

ATOM OF HYDROGEN AND WANNIER-MOTT EXCITON IN CROSSED ELECTRIC AND MAGNETIC FIELDS

Abstract

Spectroscopy of atoms in the crossed external electric and magnetic fields is investigated on the basis of the operator perturbation theory. The data for ground state energies of the hydrogen atom in sufficiently weak crossed external electric and magnetic fields are calculated. Generalization of the method on a case of the Wannier-Mott excitons in the bulk semiconductors in a case of the crossed fields is given. .

Key words: atom, exciton, crossed electric and magnetic fields

УДК 539.185

О. П. Федчук, О. В. Глушков, Я. І. Лепіх, Г. В. Ігнатенко, Г. С. Квасікова

АТОМ ВОДНЮ І ЕКСІТОН ВАНЬЄ-МОТТА В СХРЕЩЕНИХ ЕЛЕКТРИЧНОМУ І МАГНІТНОМУ ПОЛЯХ

Резюме

Вивчається спектроскопія атомів в схрещених зовнішніх електричних і магнітних полях на основі операторної теорії збурень. Наведено результати розрахунку енергії основного стану атому водню в достатньо слабких схрещених електричному та магнітному полях. Надано узагальнення методу на випадок екситонів Ваньє-Мотта в напівпровідниках у випадку наявності схрещених зовнішніх полів.

Ключові слова: атом, екситон, схрещені електричне і магнітне поля

УДК 539.185

А. П. Федчук, А. В. Глушков, Я. И. Лепих, А. В. Ігнатенко, А. С. Квасикова

АТОМ ВОДОРОДА И ЭКСИТОН ВАНЬЕ-МОТТА В СКРЕЩЕННЫХ ЭЛЕКТРИЧЕСКОМ И МАГНИТНОМ ПОЛЯХ

Резюме

Изучается спектроскопия атомов в скрещенных внешних электрических и магнитных полях на основе операторной теории возмущений. Приведены результаты расчета энергии основного состояния атому водорода в достаточно слабых скрещенных электрическом и магнитном полях. Дано обобщение метода на случай экситонов Ванье-Мотта в полупроводниках в случае наличия скрещенных внешних полей.

Ключевые слова: атом, экситон, скрещенные электрическое и магнитное поля

UDC 539.182

A. N. Shakhman

Odessa National Polytechnical University, 1, Shevchenko pr., Ukraine
e-mail: quantsha@mail.ru

RELATIVISTIC THEORY OF SPECTRA OF HEAVY PIONIC ATOMS WITH ACCOUNT OF STRONG PION-NUCLEAT INTERACTION EFFECTS: NEW DATA FOR ^{175}Lu, ^{205}Tl, ^{202}Pb,

New relativistic method of the Klein-Gordon-Fock equation with an generalized pion-nuclear potential is used to determine the transition energies with accounting for the strong pion-nuclear interactions effects in spectroscopy of some heavy pionic atoms. As example, there is carried out studying the Coulomb, nuclear and strong interaction contributions into the 4f-3d, 5g-4f transitions energies for the ^{175}Lu, ^{205}Tl, ^{202}Pb pionic atoms.

1. Introduction

In papers [1-3] we have developed a new relativistic method of the Klein-Gordon-Fock equation with an generalized pion-nuclear potential to determine transition energies in spectroscopy of light, middle and heavy pionic atoms with accounting for the strong interaction effects. In this paper, which goes on our studying on spectroscopy of pionic atoms, we firstly applied method [1-3] to calculating transition energies in a set of the heavy pionic atoms, in particular, atoms of ^{175}Lu, ^{205}Tl, ^{202}Pb, with accounting for the strong pion-nuclear interaction effects.

Following [1-3], let us remind that spectroscopy of hadron atoms has been used as a tool for the study of particles and fundamental properties for a long time. Exotic atoms are also interesting objects as they enable to probe aspects of atomic and nuclear structure that are quantitatively different from what can be studied in electronic or "normal" atoms. At present time one of the most sensitive tests for the chiral symmetry breaking scenario in the modern hadron's physics is provided by studying the exotic hadron-atomic systems. Nowadays the transition energies in pionic (kaonic, muonic etc.) atoms are measured with an unprecedented precision and from studying spectra of the hadronic atoms it is possible to investigate the strong interaction at low energies measuring the energy and natural width of the ground level with a precision of few meV [1-10].

The strong interaction is the reason for a shift in the energies of the low-lying levels from the purely electromagnetic values and the finite lifetime of the state corresponds to an increase in the observed level width. The possible energy shifts caused by the pion-induced fluorescence X-rays were checked in the measurement of the pion beams at PSI in Switzerland. For a long time the similar experimental investigations have been carried out in the laboratories of Berkley, Virginia (USA), CERN (Switzerland).

The most known theoretical models to treating the hadronic (pionic, kaonic, muonic, antiprotonic etc.) atomic systems are presented in refs. [1-5,7,8]. The most difficult aspects of the theoretical modeling are reduced to the correct description of pion-nuclear strong interaction [1-3] as the electromagnetic part of the problem is reasonably accounted for. Besides, quite new aspect is linked with the possible, obviously, very tiny electroweak and hyperfine interactions.

2. Relativistic approach to pionic atoms spectra

As the basis's of a new method has been published, here we present only the key topics of an approach [1-3]. All available theoretical models to treating the hadronic (kaonic, pionic) atoms are naturally based on the using the Klein-Gordon-Fock equation [2,5], which can be written as follows :

(1)

where c is a speed of the light, *h* is the Planck constant, and $\Psi_0(x)$ is the scalar wave function of the space-temporal coordinates. Usually one considers the central potential [$V_0(r)$, 0] approximation with the stationary solution:

$$\Psi(x) = \exp(-iEt/\hbar)\,\varphi(x), \qquad (2)$$

where $\varphi(x)$ is the solution of the stationary equation:

$$\{\frac{1}{c^2}[E + eV_0(r)]^2 + \hbar^2\nabla^2 - m^2c^2\}\varphi(x) = 0 \qquad (3)$$

Here E is the total energy of the system (sum of the mass energy mc^2 and binding energy ε_0). In principle, the central potential V_0 naturally includes the central Coulomb potential, the vacuum-polarization potential, the strong interaction potential.

The most direct approach to treating the strong interaction is provided by the well known optical potential model (c.g. [2]). Practically in all papers the central potential V_0 is the sum of the following potentials. The nuclear potential for the spherically symmetric density $\rho(r|R)$ is [6,13]:

$$V_{nucl}(r|R) = -\left((1/r)\int_0^r dr'r'^2\rho\left(r'\middle|R\right) + \int_r^\infty dr'r'\rho\left(r'\middle|R\right)\right) \qquad (4)$$

The most popular Fermi-model approximation the charge distribution in the nucleus $\rho(r)$ (c.f.[11]) is as follows:

$$\rho(r) = \rho_0 / \{1 + \exp[(r-c)/a)]\}, \qquad (5)$$

where the parameter *a=0.*523 fm, the parameter *c* is chosen by such a way that it is true the following condition for average-squared radius:

$$<r^2>^{1/2} = (0.836\cdot A^{1/3} + 0.5700)\text{fm}.$$

The effective algorithm for its definition is used in refs. [12] and reduced to solution of the following system of the differential equations:

$$V'nucl(r,R) = \left(1/r^2\right)\int_0^r dr'r'^2\rho\left(r',R\right) \equiv \left(1/r^2\right)y(r,R) \qquad (6)$$

,

$$y'(r,R) = r^2\rho(r,R), \qquad (7)$$

$$\rho'(r) = (\rho_0/a)\exp[(r-c)/a]\{1+\exp[(r-c)/a)]\}^2 \qquad (8)$$

with the corresponding boundary conditions. Another, probably, more consistent approach is in using the relativistic mean-field (RMF) model, which been designed as a renormalizable meson-field theory for nuclear matter and finite nuclei [13].To take into account the radiation corrections, namely, the effect of the vacuum polarization we have used the generalized Ueling-Serber potential with modification to take into account the high-order radiative corrections [5,12].

The most difficult aspect is an adequate account for the strong interaction. In the pion-nucleon state interaction one should use the following pulse approximation expression for scattering amplitude of a pion on the "i" nucleon [2,3]:

$$f_i(r) = \left\{b_0' + b_1'(t\tau) + \left[c_0' + c_1'(t\tau)\right]kk'\right\}\delta(r - r_i); \qquad (9)$$

where t and τ are the isospines of pion and nucleon. The nucleon spin proportional terms of the kind $\sigma[kk']$ are omitted. The constants in (9) can be expressed through usual s-wave (α_{2T}) and p-wave $(\alpha_{2T,2J})$ scattering length (T and J -isospin and spin of he system πN. The corresponding parameters in the Compton wave length $\lambda\!\!\!^{-}_{\pi}$ terms are as follows:

$$b_0' = (\alpha_1 + 2\alpha_3)/3 = -0.0017\,\lambda_\pi.$$
$$b_0' = (\alpha_3 - \alpha_1)/3 = -0.086\,\lambda_\pi.$$
$$c_0' = (4\alpha_{33} + 2\alpha_{13} + 2\alpha_{31} + \alpha_{11})/3 = -0.208(\lambda_\pi)^3.$$
$$c_1' = (2\alpha_{33} - 2\alpha_{13} + \alpha_{31} - \alpha_{11})/3 = -0.184(\lambda_\pi)^3.$$

(10)

The scattering amplitude for pion on a nucleus can be further received as a coherent sum of the πN-scattering lengths. рассеяния. In approximation of the only s-wave interaction the corresponding potential can be written in the Dezer form:

$$V_N(r) = -2\pi\hbar^2\mu_\pi^{-1}\left[ZA^{-1}a_p + (A-Z)A^{-1}a_n\right]\rho(r). \quad (11)$$

The s-wave lengths of the $\pi^{-1}p$-scattering $a_p = (2\alpha_1 + \alpha_3)/3$ и $\pi^{-1}n$- scattering $a_n = \alpha_3$; scattering are introduced to Eq. (11). Because of the equality between $a_n = b_0' + b_1'$ and $a_p = b_0' - b_1'$ (with an opposite sign) the theoretical shift of the s-level with $T = 0$ $(A = 2Z)$ from Eq. (12) is much less than the observed shift. So, the more correct approximation must take into account the effects of the higher orders.

In whole the energy of the hadronic atom is represented as the sum:

$$E \approx E_{KG} + E_{FS} + E_{VP} + E_N; \quad (12)$$

Here E_{KG}-is the energy of a pion in a nucleus (Z, A) with the point-like charge (dominative contribution in (12)), E_{FS} is the contribution due to the nucleus finite size effect, E_{VP} is the radiation correction due to the vacuum-polarization effect, E_N is the energy shift due to the strong interaction V_N.

The strong pion-nucleus interaction contribution can be found from the solution of the Klein-Gordon equation with the corresponding pion-nucleon potential.

3. Results and conclusions

In table 1 the data on the transition energies in some pionic atoms of ^{175}Lu, ^{205}Tl, ^{202}Pb (from. Refs. [4-7]): the measured values form the Berkley, CERN and Virginia laboratories, the theoretical values for the *4f-3d, 5g-4f* pionic transitions (E_{th1}^N - values from the Klein-Gordon-Fock equation with the pion-nucleus potential [2]; E_{KGF}- values from the Klein-Gordon-Fock equation with account of radiative corrections (our data); E_{KS} – the RMF finite nuclear size contribution (our data), E_{th2}^N - values from the Klein-Gordon-Fock equation with the generalized pion-nuclear potential [5] (our data).

The analysis of the presented data indicate on the necessity of the further more exact experimental investigations and further improvement of the pion-nuclear potential modelling.

Table 1

Transition energies (keV) in the spectra of some heavy pionic atoms (see text)

Atom	E_{EXP} Berkley	E_{EXP} CERN	E_{KGF}	E_{FS}	E_{th1}^N	E_{th2}^N
Transition *4f-3d*						
^{133}Cs	$560{,}5 \pm 1{,}1$	$562{,}0 \pm 1{,}5$	556,80	-0,33	561,47	560.88
^{205}Tl	-	-	-	963.920	-	968.25
Transition 5g-4f						
^{175}Lu	-	-	-	427.313	-	428.80
^{205}Tl	-	561.67 ± 0.25	559.65	559.681	560.93	561.63

One can see that the contributions provided by the finite size effect should be accounted in a precise theory. Really, under availability of the ”exact” values of the transitions energies one can perform the comparison of the theoretically and experimentally defined transition energies in the X-ray spectra in order to make a redefinition of the pion-nucleon model potential parameters using Eqs. (9)-(11). Taking into account the increasing accuracy of the X-ray pionic atom spectroscopy experiments, one can conclude that the such a way will make more clear the true values for parameters of the pion-nuclear potentials and correct the disadvantage of widely used parameterization of the potentials (9)-(11).

References

1. Shakhman A.N., Strong π-nucleat interaction effects in spectroscopy of hadronic atoms //Photoelectronics.-2013.-Vol.22.-P.93-97
2. Serga I.N., Dubrovskaya Yu.V., Kvasikova A.S., Shakhman A.N., Sukharev D.E., Spectroscopy of hadronic atoms: Energy shifts// Journal of Physics: C Ser. (IOP).-2012.- Vol.397.-P.012013 (5p.).
3. Kuznetsova A.A., Kvasikova A.S., Shakhman A.N., Vitavetskaya L.A., Calculating the radiative vacuum polarization contribution to the energy shift of 2p-2s transition in μ-hydrogen// Photoelectronics.-2012.-N21.-P.66-67.
4. Deslattes R., Kessler E., Indelicato P., de Billy L., Lindroth E. , Anton J., Exotic atoms// Rev. Mod. Phys. -2003.-Vol.75.-P.35-70.
5. Backenstoss G., Pionic atoms//Ann.Rev. Nucl.Sci.-1990.-Vol.20.-P.467-510.
6. Menshikov L I and Evseev M K, Some questions of physics of exotic atoms// Phys. Uspekhi.2001-Vol. 171.-P.150-184.
7. Scherer S, Introduction to chiral perturbation theory//Advances in Nuclear Physics, Eds. J.W. Negele and E.W. Vogt (Berlin, Springer).-2003.-Vol.27.-P.5-50.
8. Schroder H., Badertscher A., Goudsmit P., Janousch M., Leisi H., Matsinos E., Sigg D., Zhao Z., Chatellard D., Egger J., Gabathuler K., Hauser P., Simons L., Rusi El Hassani A., The pion-nucleon scattering lengths from pionic hydrogen and deuterium//Eur.Phys.J.-2001.-Vol. C21.-P.473
9. Lyubovitskij V., Rusetsky A., πp atom in ChPT: Strong energy-level shift/ // Phys. Lett.B.-2000.-Vol.494.-P.9-13.
10. Anagnostopoulos D., Biri S., Boisbourdain V., Demeter M., Borchert G. et al-PSI, Low-energy X-ray standards from pionic atoms/ //Nucl. Inst. Meth.B.-2003.-Vol.205.-P.9-18.
11. Batty C.J., Eckhause M., Gall K.P., et al, Strong interaction effects in high Z-K^- atoms//Phys. Rev. C.-1999.-Vol.40.-P.2154-2160.
12. Glushkov A.V., Gauge-invariant QED perturbation theory approach to calculating nuclear electric quadrupole moments, hyperfine structure constants for heavy atoms and ions/ Glushkov A.V., Khetselius O.Yu., Sukharev D.E., Gurnitskaya E.P., Loboda A.V., Florko T.A., Lovett L.// Frontiers in Quantum Systems in Chemistry and Physics (Berlin, Springer).-2008.-Vol.18.- P.505-522.
13. Serot B. D., Advances in Nuclear Physics Vol. 16: The Relativistic Nuclear Many Body Problem/ Serot B. D., Walecka J. D.-Plenum Press, New York, 1996.

This article has been received within 2014

UDC 539.182

A. N. Shakhman

RELATIVISTIC THEORY OF SPECTRA OF HEAVY PIONIC ATOMS WITH ACCOUNT OF STRONG PION-NUCLEAT INTERACTION EFFECTS: NEW DATA FOR ^{175}Lu, ^{205}Tl, ^{202}Pb

Abstract

New relativistic method of the Klein-Gordon-Fock equation with an generalized pion-nuclear potential is used to determine the transition energies with accounting for the strong pion-nuclear interactions effects in spectroscopy of some heavy pionic atoms. As example, there is carried out studying the Coulomb, nuclear and strong interaction contributions into the 4f-3d, 5g-4f transitions energies for the ^{175}Lu, ^{205}Tl, ^{202}Pb pionic atoms.

Key words: strong interaction, pionic atom, relativistic theory

УДК 539.182

А. Н. Шахман

РЕЛЯТИВИСТСКАЯ ТЕОРИЯ СПЕКТРОВ ТЯЖЕЛЫХ ПИОННЫХ АТОМОВ С УЧЕТОМ ЭФФЕКТОВ СИЛЬНОГО ПИОН-ЯДЕРНОГО ВЗАИМОДЕЙСТВИЯ: НОВЫЕ ДАННЫЕ ДЛЯ ^{175}Lu, ^{205}Tl, ^{202}Pb

Резюме

Новый релятивистский метод на основе уравнения Клейна-Гордона-Фока с обобщенным пион-ядерным потенциалом применен к вычислению энергий переходов с учетом эффектов сильного пион-ядерного взаимодействия в спектроскопии некоторых тяжелых пионных атомов. В качестве примера проведено детальное изучение кулоновского, ядерного вкладов, вклада за счет сильного взаимодействия в энергии переходов 4f-3d, 5g-4f для ^{175}Lu, ^{205}Tl, ^{202}Pb пионных атомов.

Ключевые слова: сильное взаимодействие, пионный атом, релятивистская теория

УДК 539.182

А. М. Шахман

РЕЛЯТИВІСТСЬКА ТЕОРІЯ СПЕКТРІВ ВАЖКИХ ПІОННИХ АТОМІВ З УРАХУВАННЯМ ЕФЕКТІВ СИЛЬНОЇ ПІОН-ЯДЕРНОЇ ВЗАЄМОДІЇ: НОВІ ДАННІ ДЛЯ ^{175}Lu, ^{205}Tl, ^{202}Pb

Резюме

Новий релятивістський метод на основі рівняння Клейна-Гордона-Фока із узагальненим піон-ядерним потенціалом застосовано до розрахунку енергій переходів з урахуванням ефектів сильної піон-ядерної взаємодії в спектроскопії декотрих важких піонних атомів. В якості приклада проведено докладне вивчення кулонівського, ядерного внесків, внеску за рахунок сильної взаємодії в енергії переходів 4f-3d, 5g-4f для ^{175}Lu, ^{205}Tl, ^{202}Pb піонних атомів.

Ключові слова: сильна взаємодія, піонний атом, релятивістська теорія

UDC 539.175

V. N. Pavlovich, T. N. Zelentsova, D. E. Sukharev

Institute for Nuclear Researches, National Academy of Sciences of Ukraine, Kiev
Odessa National Polytechnical University, 1, Shevchenko av., 65028, Odessa, Ukraine
Odessa State Environmental University, 15, Lvovskaya str., Odessa, Ukraine
e-mail: quantmis@mail.ru

ELECTROMAGNETIC AND STRONG INTERACTIONS EFFECTS IN NUCLEAR SPECTROSCOPY OF HADRONIC ATOMS

Theoretical studying transition energies and widths from X-ray spectroscopy of hadronic atoms is carried out. The electromagnetic and strong interaction effects in nuclear spectroscopy of hadronic (kaonic) atoms are analyzed from the pointview of a new tool for studying nuclear structure.

1. Introduction

Theoretical and experimental studying exotic hadronic atomic systems such as kaonic or pionic or hyperonic atoms represents a great fundamental and applied interest as for further development of atomic and nuclear theories as for search of a new tools for investigation a nuclear structure and strong pion-hyperon-kaon- nuclear interaction etc. Surely, studying these complex systems gives a new low-energy key to understanding and even further check of the Standard Model [1-16]. In the last few years transition energies in the kaonic atoms [1-7] have been measured with an unprecedented precision. The spectroscopy of kaonic hydrogen allows to study the strong interaction at low energies by measuring the energy and natural width of the ground level with a precision of few meV [6,7]. Let us remind about well-known application of the light kaonic atoms as the new low-energy X-ray standards and unique possibility to evaluate the kaon (pion) masses using methods of theoretical and experimental high accuracy X-ray spectroscopy. The known example of the experimental studying is the E570 collaboration experiment [6,7] on measurement of the X-ray energies in the kaonic helium atom, which is an atom consisting of a kaon (a negatively charged heavy particle) and a helium nucleus. Another impressive experiment is with DEAR allowed to perform an improved measurement of kaonic hydrogen [4] (look fig.1). It has been received significantly higher precision and smaller shift and width values than the KpX experiment [11], still for the given precision the results are compatible. The similar experiments are performed or in a status of preparing for the pionic systems (look c.g. [1,2,9,10]). It is important to note that because of the tiny strong interaction effect the study of pionic hydrogen and other elements calls for an X-ray spectrometer system with ultimate precision - provided by a crystal spectrometer which is feasible due to the huge pion beam intensity provided at PSI - whereas kaonic hydrogen can be studied with X-ray detectors like CCDs or SDDs directly. Batty et al [5] had carried out performed theoretical and experimental studying the strong-interaction effects in spectra of high Z kaonic atoms. Now new exciting experiments are been preparing in order to make sensing the strong interaction effects in other hadronic atoms.

Studying the low-energy kaon-nuclear strong interaction with strangeness have been performed by measurements of the kaonic atom X-rays with atomic numbers Z=1-92 [1]. It is known that the shifts and widths due to the strong interaction can be systematically understood using phenomenological optical potential models. Nevertheless, one could mention a large discrepancy between the theories and experiments on the kaonic heli-

um 2p state. A large repulsive shift (about -40 eV) has been measured by three experimental groups in the 1970's and 80's, while a very small shift (< 1 eV) was obtained by the optical models calculated from the kaonic atom X-ray data with Z>2 [1-6]. This significant disagreement (a difference of over 5 standard deviations) between the experimental results and the theoretical calculations is known as the "kaonic helium puzzle". A possible large shift has been predicted using the model assuming the existence of the deeply bound kaonic nuclear states. However, even using this model, the large shift of 40 eV measured in the experiments cannot be explained. A re-measurement of the shift of the kaonic helium X-rays is one of the top priorities in the experimental research activities. In the theory of the kaonic and pionic atoms there is an important task, connected with a direct calculation of the X-ray transition energies. The standard way to solution the hadronic atom problem is using the Klein-Gordon-Fock equation. Here one deal with important problem of the accurate accounting for as kaon-nuclear strong interaction effects as QED radiative corrections (firstly, the vacuum polarization effect etc.) [1-13].

In the present paper awe present the results of theoretical studying transition energies and widths from X-ray spectroscopy of hadronic atoms. The electromagnetic and strong interaction effects in nuclear spectroscopy of hadronic (kaonic) atoms are analyzed from the pointview of a new tool for studying nuclear structure

2. Electromagnetic and strong effects in spectroscopy of kaonic atoms

Earlier we presented the detailed description of approach to kaonic atom spectra problem, so here we are stopping only at the key fundamental topics [11-15]. All available theoretical models to treating the hadronic (kaonic, pionic) atoms are naturally based on the using the Klein-Gordon-Fock equation. Its stationary version is as follows (in atomic units!):

$$\{\alpha^2[E+eV_0(r)]^2+\hbar^2\nabla^2-m^2c^2\}\varphi(x)=0 \quad (1)$$

Here α is the fine structure constant, E is the total energy of the system, V_0 is a central potential, which contents the nuclear electric potential (due to the charge distribution in a nucleus), potential, provided by the radiative (QED) effect of vacuum polarization and, at last, the strong kaon-nuclear interaction potential (for example, the optical model potential). Earlier we computed spectral characteristics of some hadronic systems using the nuclear charge distribution in the Gaussian form (c.f. [12]). The advantage of the Gaussian form nuclear charge distribution is provided by using the smooth function instead of the discontinuous one as in the model of a uniformly charged sphere [16]. It is obvious that it simplifies the calculation procedure and permits to perform a flexible simulation of the real distribution of the charge in a nucleus.

The new important topic is connected with a correct accounting the radiation QED corrections and, first of all, the vacuum polarization correction. Procedure for an account of the radiative QED corrections in a theory of the multi-electron atoms is given in detail in refs. [11,12]. Regarding the vacuum polarization effect let us note that this effect is usually taken into account in the first PT order by means of the Uehling-Serber potential:

$$U(r)=-\frac{2\alpha}{3\pi r}\int_1^\infty dt\exp(-2rt/\alpha Z)(1+1/2t^2)\frac{\sqrt{t^2-1}}{t^2}\equiv$$
$$=-\frac{2\alpha}{3\pi}C(g) \quad (2)$$

where $g=\frac{r}{\alpha Z}$.

In our calculation we usually use more exact approach [16]. The Uehling-Serber potential, is usually derived determined as a quadrature (2.). Nevertheless, [10, 17], it can be approximated with high precision by a definite analytical function. The use of new approximation of the cited potential [17] permits one to decrease the computing error for this term down to 0.5 – 1%. Besides, using such a simple analytical function form for approximating the Uehling-Serber potential allows its easy inclusion into the general system of differential equations [12,14,15].

.

3. Some results for heavy systems and conclusions

In ref. [11-15] we have presented some results of calculation for a selection of kaonic atom transitions. The kaon mass was assumed to be 493.677±0.013MeV [1]. In table 1 we present the calculated electro-magnetic (EM) X-ray energies of kaonic atoms for transitions between circular levels.

Table 1

Calculated electromagnetic (E_c) and measured (E_m) energies (keV) of the X-ray transitions in the KA: the Batty et al theory EM1,2 [5] with using simple cascade Fermi-Teller model (Leon-Seki code), data by Indelicato et al (theory EM3) [3,4] and theory [11] (theory EM4) and our work (EM5).

KA	Transition	E_c, our theory EM4	E_c, [5] theory EM1	E_c, [5] theory EM2
W	8-7	346.586	346.54	-
Pb	8-7	426.175	426.15	426.201
U	8-7	538.520	538.72	538.013
KA	Transition	E_c, [3,4] theory EM3	This work EM5	E_m, [1,12]
W	8-7	346.571	346.603	346.624(25)
Pb	8-7	426.180	426.198	426.221(57)
U	8-7	537.44	538.945	538.315(100)

The transitions are identified by the initial (n_i) and final (n_f) quantum numbers. The calculated values of transition energies are compared with available measured (E_m) and other calculated (E_c) values [1-7].

It is easily to understand that when there is the close agreement between theoretical and experimental shifts, the corresponding energy levels are not significantly sensitive to strong nuclear interaction, i.e the electromagnetic contribution is dominative. In the opposite situation the strong-interaction effect is very significant.

The detailed analysis of theoretical and separated experimental data shows that indeed there is a physically reasonable agreement between the cited data. But, obviously, there may take a place the exception too as it is shown on example of the kaonic uranium. Further one can perform the comparison of the theoretically and experimentally determined transition energies in the X-ray spectra and further to find the strong interaction contribution into transition energy. From the other side, solution of the Klein-Gordon-Fock equation with directly implemented kaon-nucleon (say, from optical model) potential with a set of parameters allows to estimate the correctness of their definition. parameters using Eqs. (8)-(11). Moreover, such a way will make more clear the true values for parameters of the kaon -nuclear potentials and correct the disadvantage of widely used parameterization of the cited potential. Let us also in conclusion to note that the known perspective can be opened on the way of sensing the parity non-conservation in the heavy hadron atomic systems, in particular, kaonic atoms. Obviously, this effect will be small in the light hadronic systems as K^-- H, K^-- N, but its contribution is increasing as Z^3, so one could wait for the increased contribution in the high-Z atoms (as K^-- Pb, K^-- W , K^- -U etc.).

References

1. Pavlovich V.N., Zelentsova T.N., Tarasov V.A., Serga I.N., Mudraya N.V., Interplay of the hyperfine, electroweak and strong interactions in heavy hadron-atomic systems and x-ray standards status// Sensor Electronics and Microsystem Technologies.-2010.-N2.-P.20-26.
2. Hayano R.S., Hori M., Horvath D., Widman E., Antiprotonic helium and CPT invariance//Rep. Prog. Phys.-2007.-Vol.70.-P.1995-2065.
3. Deslattes R., Kessler E., Indelicato P., de Billy L., Lindroth E. , Anton J., Exotic atoms//Rev. Mod. Phys. -2003.-Vol.75.-P.35-70.

4. Santos J.P., Parente F., Boucard S., Indelicato P., Desclaux J.P., X-ray energies of the circular transitions and an electron scattering in kaonic atoms// Phys.Rev.A.-2005.-Vol.71.-P.032501.
5. Batty C.J., Eckhause M., Gall K.P., et al. Strong interaction effects in high-Z kaonic atoms // Phys. Rev. C.-1989.-Vol.40.-P.2154-2160.
6. Ito T.M., Hayano R.S., Nakamura S.N., Terada T.P., Observation of kaonic hydrogen atom x rays// Phys. Rev. C.-1998.-Vol.58.-P.2366 – 2382
7. Ishiwatari T. on behalf of the SIDDHARTA Collaboration, Silicon drift detectors for the kaonic atom X-ray measurements in the SIDDHARTA experiment// Nucl.Instr. and Methods in Physics. Research Sec.A. Accelerators, Spectrometers, Detectors and Associated Equipment.-2007.-Vol.581,N1-2.-P.326-329.
8. Okada S., Beer G., Bhang H., et al, Precision measurement of the 3d→2p x-ray energy in kaonic ^{4}He//Phys.Lett.B.-2007.-Vol.653, N 5-6.-P. 387-391.
9. Glushkov A.V., Makarov I.T., Nikiforova E.S., Pravdin M.I., Sleptsov I.Ye., Muon component of EAS with energies above 10^{17}eV // Astroparticle Phys.-1995.-Vol. 4. -P. 15-22
10. Glushkov A.V., Relativistic quantum theory. Quantum mechanics of atomic systems, Odessa: Astroprint, 2008-P. 700.
11. Pavlovich V.N., Zelentsova T.N., Serga I.N., Analysis of the electromagnetic and strong interactions effects in x-ray spectroscopy of hadronic atoms and “kaonic helium puzzle”//Photoelectronics - 2010.-N19.-P.65-69.
12. Sukharev D.E., Sensing the electromagnetic and strong interactions effects in spectroscopy of the kaonic atoms// Photoelectronics.-2011.-Vol.20.-P.124-127.
13. Sukharev D.E., Khetselius O.Yu., Dubrovskaya Yu.V., Sensing strong interaction effects in spectroscopy of hadronic atoms//Sensor Electronics and Microsystem Technologies.- 2009.-N3.-P.16-21.
14. Glushkov A.V., Khetselius O.Yu., Gurnitskaya E.P., Loboda A.V., Sukharev D.E., Relativistic Quantum Chemistry of Heavy Ions and Hadronic Atomic Systems: Spectra and Energy Shifts// Theory and Applications of Computational Chemistry (AIP).-2009.-Vol.1290.-P.131-134.
15. Turin A.V., Khetselius O.Yu., Sukharev D.E., Florko T.A., Estimating of X-ray spectra for kaonic atoms as tool for sensing the nuclear structure//Sensor Electr. and Microsyst. Techn.-2009.-N1.-P.30-35.
16. Glushkov A.V., Rusov V.D., Ambrosov S.V., Loboda A.V., Resonance states of compound super-heavy nucleus and EPPP in heavy nucleus collisions // New Projects and New Lines of research in Nuclear physics.Eds. Fazio G. and Hanappe F.: Singapore, World Sci.-2003.-P. 142-154.
17. Khetselius O.Yu., Relativistic many-body perturbation theory calculation of the hyperfine structure parameters for some heavy-element isotopes //Int. Journ. of Quantum Chemistry.-2009.-Vol.109.-P. 3330-3335.

This article has been received within 2014

UDC 539.175

V. N. Pavlovich, T. N. Zelentsova, D. E. Sukharev

ELECTROMAGNETIC AND STRONG INTERACTIONS EFFECTS IN NUCLEAR SPECTROSCOPY OF HADRONIC ATOMS

Abstract

Theoretical studying transition energies and widths from X-ray spectroscopy of hadronic atoms is carried out. The electromagnetic and strong interaction effects in nuclear spectroscopy of hadronic (kaonic) atoms are analyzed from the pointview of a new tool for studying nuclear structure

Key words: X-ray spectroscopy, hadronic systems, kaon-nuclear interaction

УДК 539.175

В. Н. Павлович, Т. Н. Зеленцова, Д. Е. Сухарев

ЭФФЕКТЫ ЭЛЕКТРОМАГНИТНОГО И СИЛЬНОГО ВЗАИМОДЕЙСТВИЙ В ЯДЕРНОЙ СПЕКТРОСКОПИИ АДРОННЫХ АТОМОВ

Резюме

Проведено теоретическое изучение энергий переходов и ширин в рентгеновской спектроскопии адронных атомов. С точки зрения выявления новых инструментов изучения структуры ядра проведен анализ эффектов электромагнитного и сильного взаимодействия в ядерной спектроскопии адронных (каонных) атомов.

Ключевые слова: Рентгеновская спектроскопия, адронные системы, каон-ядерное взаимодействие

УДК 539.175

В. М. Павлович, Т. М. Зеленцова, Д. Є. Сухарев

ЕФЕКТИ ЕЛЕКТРОМАГНІТНОЇ ТА СИЛЬНОЇ ВЗАЄМОДІЇ В ЯДЕРНОЇ СПЕКТРОСКОПІЇ АДРОННИХ АТОМІВ

Резюме

Проведено теоретичне вивчення енергій переходів і ширин в рентгенівської спектроскопії адронних атомів. З точки зору виявлення нових інструментів вивчення структури ядра проведено аналіз ефектів електромагнітної та сильної взаємодії в ядерній спектроскопії адронних (каонних) атомів.

Ключові слова: Рентгенівська спектроскопія, адронні системи, каон-ядерна взаємодія

UDC 541.27, 584.96

V. I. Mikhailenko, V. N. Vaschenko, S. V. Ambrosov, A. V. Loboda, E. L. Ponomarenko

[1]State Environmental Academy, Kiev, Ukraine
[2]Odessa National Polytechnical University, 1, Shevchenko av., 65028, Odessa, Ukraine
[3]Odessa State Environmental University, L'vovskaya str.15, Odessa-16, 65016, Ukraine
e-mail: andmolec@mail.ru

NON-LINEAR CHAOTIC TREATING VIBRATIONAL MOTION FOR MOLECULES IN THE MULTI-PHOTON PHOTOEXCITATION REGIME

It has been studied a stochastization of vibrational motion for molecules in the multi-photon photo-excitation regime on example of the CF_3I, SF_5 molecules within quantum-stochastic kinetic approach and given more accurate data for stochastization threshold energies.

At present time the topics of laser –molecular interactions has a great interest as for molecular spectroscopy , laser physics, photochemistry as for different applied applications in construction of optical devices and optical [1-13]. It is known that while the dynamical aspects of ionization of molecules in a strong laser field are considered to be well understood at least within quantitative simplified models, the multi-photon dissociation and excitation of molecules in real laser field is a topic of actuality and importance. Many experiments of studying the multi-photon processes were fulfilled in the conditions, when the collisional factor may be missed. A question about chaotic elements of the vibrational motion of molecules in a laser field, when the vibrational energy is randomly distributed among the vibrational modes during interaction with laser pulse is to be very actual and complicated task.

In Refs. [12,13] it has been presented new theoretical scheme to sensing dynamics of the zone type multi-level system in a laser field, which is based on the quantum stochastic kinetic approach, developed in refs. [11]. Dependencies of the multi-photon dissociation yield, selectivity coefficient and absorbed energy upon the laser pulse energy density for BCl_3 molecules in the oxygen O_2 buffer gas are calculated. It has been studied a phenomenon of stochastization of the vibrational motion for molecules in the multi-photon photo-excitation regime on example of the CF_3I, $SF_6$and BCl_3 molecules with using the non-linear inter-mode resonances interaction model and stochastic Focker-Plank equation.

Here we study stochastization of vibrational motion for molecules in the multi-photon photo-excitation regime on example of a set of molecules within quantum- stochastic model [13] and obtain more accurate estimates for the stochastization energy. The obtained data are compared with earlier obtained theoretical and experimental results [2,10,13].

Taking into account the possible manifestations of a chaos phenomenon on molecular dynamics one should use molecular hamiltonian (in variables "action *I*-angle *q*")of influence on the mode 1 from the side of other modes as a sum of resonant contributions, which are lying inside non-linear width Dw_1 (look full details look in Refs. [12,15]):

$$H_1^{\text{int}} = I_1^{1/2} \sum_n F_n \cos(\theta_1 - \theta_n) \quad (1)$$

Condition of periodicity on q results in the quantization of action and energy, i.e. $I_n=n\hbar$ and $E_n=H_0(n\hbar)$. Resonances are arisen for such values of the action that it is right:

$$kw(I_0)=lW\ ,\ w(I)=dH_0/dI$$

for whole numbers k,l. The interaction (1) changes quasi-energy of the mode 1as follows:

$$dE_1 / dt = I_1^{1/2}[\Omega-\omega(I_1)]\times$$
$$\times\sum_n F_n \sin(\theta_1-\theta_n)-(e\bar{x}_1 E/2\hbar^{1/2})\sum_n F_n \sin\theta_n \quad (2)$$

The first term in eq.(2) describes the inter mode relaxation; second term –the interaction with an external field. The whole process of the energy acceptance is in fact stochastic. Speech is about the diffusion with coefficient $D(E)$ (see below). Its calculation gives the following result:

$$D(E)=(\pi/4\hbar)(e\bar{x}_1 E)^2 J(\Omega)$$

$$J(\Omega)=|F(\Omega)|^2/\Delta_0 \quad (3)$$

Here a variable $J(W)$ has an essence of spectral intensity of the perturbation $H_1^{(int)}$ on the field frequency. In ref. [12-15] it has been formulated an effective Focker-Plank equation approach to process of the multi-photon molecular excitation. Till its application, the the vibrational spectrum is usually divided into two parts: a). the low-lying discrete states and b). high-excited levels of the quasicontinuum. At the definite energy threshold the vibrational energy can be randomly distributed among the vibrational modes during the interaction with the laser pulse. The excitation process into continuum is described by system of the kinetic equations [13-15]:

$$\partial Z_n / \partial t\ t=(W_{n-1,n}+k^{VT}_{n-1,n}p)Z_{n-1}+(W_{n+1,n}+$$
$$+k^{VT}_{n+1,n}p)Z_{n+1}-$$
$$(W_{n-1,n}+k^{VT}_{n,n-1}pW_{n+1,n}+k^{VT}_{n,n+1}p)Z_n-$$
$$-d_n Z_n+\partial/\partial n\ [\Theta(n-N_{min})D(R)n^3\ \partial Z/\partial n\ ] \quad (4)$$

where z_n are the populations of the laser-excited states with energy E_n ; $W_{n,n\pm1}$ is the rate of the radiative transitions; $W_{n,n\pm1}=s_{n',n\pm1}I(t)$, where $s_{n',n\pm1}$ are the cross-sections of the radiative transitions up and down, $I(t)$ is the laser radiation intensity (photon×cm^{-2}×s^{-1}) ; $k^{VT}_{n,n\pm1}$ are the constants of rate of the V-T relaxation; d_n is the mono-molecular decay rate; $Q(n-N_{min})$ is the Heaviside function as an additional multiplier in the diffusion coefficient $D(R)n^3$, which "freezes" the stochastic processes in the area of the low-lying states according to the well known Chirikov's criterion [10].

The model presented explicitly accounts for effect of stochastic diffusion into quasi-continuum. The constants of relaxation rate $k^{VT}_{n,n-\pm1}$ are defined by the physical parameters of molecule. According to ref. [2,15] the collisional redistribution of populations is determined by the probability function of transition due to the collision $k(E\to E')$. The physically significant variable is an energy, transmitted during collision:

$$\Delta E(E)=\int_0^\infty dE'(E-E')k(E\to E') \quad (5)$$

The similar parameter in eqs. (6) is defined as follows:

$$\Delta E_n=(k^{VT}_{n,n-1}-k^{VT}_{n,n+1})h\nu/Z \quad (6)$$

Here Z is a frequency of the gas-kinetic collisions. The condition $DE(E_n)=DE_n$ determines the relationship between phenomenological relaxation constants in eqs.(1) and microscopical variable $DE(E)$.

To describe an influence of the collisions on excitation of the molecule at the lowest discrete levels, we suppose that q-factor in the uncollisional case is created due to the heterogeneity of interaction of the different initially populated states with a field.

System of the low levels is characterized by two rates: the radiative rate of excitation of the states W_0 and rate of the rotational relaxation k_{Rp}, which is proportional to the pressure. According to [14,15], the equations defining the molecule involvement into quasi-continuum during the laser pulse are as follows:

$$dN_0/dt=-W_0 z_0,$$

$$dz_0/dt=-W_0 z_0+k_{Vp}\,(fN_0-z_0),$$

$$dq/dt=-dN_0/dt, \qquad (7)$$

$$N_0(0)=l, \quad z_0(0)=f,$$

Here *f* is the part of molecules interacting resonantly with a laser field. In difference of the previous works [14,15] we have a real model for the shape of laser pulse [2,10]. This is related to more accurate data for dependence D*E(E)* in the quasicontinuum. The following estimate has been taken for. $D_n=k_{diss}r(E_n-D)r(E_n)$ [2], where r is the density of vibrational states.

From physical point if view, a chaotic c feature of vibrational motion is arisen during process of interaction with the IR laser field because of the non-linear inter-mode resonance interaction. In fact speech is about a strong non-linear interaction of resonances with possible

We carried out more accurate estimates of the stochastization threshold using more real input parameters of the quantum-stochastic modeling. Minimal density of energy of the CO_2 laser pulse was taken as 0,06J/cm^2 [2]. From known values of q and e_q (F) one can calculate an average absorbed energy. With accounting for initial average vibrational energy (T= 293 K) we obtained the following estimates for stochastization threshold energy E_b=4080 cm^{-1} that is in agreement with experiment [2,3,8,9]: E_b»(3900±500) cm^{-1} for SF_6. The theoretical value obtained in Ref. [13] is 3970 cm^{-1}. Data for other molecules are as: E_b= 3620 cm^{-1} for BCl_3, E_b=5760cm^{-1} for CF_3Br.

References

1. Lambert J.D. Vibrational and Rotational Relaxation in Gases // Oxford. – 1997.
2. Letokhov V.S., Nonlinear selective photo-processes in atoms and molecules // Moscow. – 2003.
3. Bagratashvili V.N., Letokhov V.S., Makarov A.A., Ryabov E.A., Multiphoton processes in molecules in IR laser field // Moscow. – 1991.
4. Gutzwiller M.,Chaos in Classical and Quantum Mechanics // N.-Y.,Springer-Verlag. – 2003.
5. Zaslavsky G.M., Chirikov B.V. Studied on theory of non-linear resonance and stochasticity// Usp.Phys.Nauk.-1991.-Vol.105.-P.3.
6. Shuryak E.V. Non-linear resonance in quantum systems// JETP.-1996.-Vol.71.-P.2039-2050.
7. Bagratashvili V.,Vayner Y.,Dolzhikov V. etal, Inter and intra-molecular distribution of vibration energy for multiphoton excitation by IR laser field// JETP. – 1990. – Vol.80. – P. 1008-1018.
8. Makarov A., Platonenko V., Tyakht V., Interaction of quantum system level-zone with quasi-resonant monochromatic field// JETP.-1978.-Vol.85.-P.2075-2086.
9. Laptev V.B., Ryabov E.A., Isotopically-selective dissociation BCl_3 in a two-colour IR laser field// Soviet Chem. Phys.-1998.-Vol.7,N2.-P.165-170.
10. Glushkov A., Malinovskaya S., Shpinareva I., Kozlovskaya V., Gura V., Quantum stochastic modelling multiphoton excitation and dissociation for CF_3Br molecules: An effect of rotational and V-T relaxation // Int. Journ. Quant. Chem.-2005.-Vol. 104,N3.- P.541-546.
11. Glushkov A.V., Zelentsova T.N., Shpinareva I., Svinarenko A., Kinetics of energy transfer in molecules of CF_3Br in the buffer gas medium in an intense laser radiation field// Phys. Aerodisp. Syst.-2002.-Vol.39.-P.129-136.
12. Shpinareva I., Gura V., Kozlovskaya V., Kinetics of energy transfer in molecules of SF_6 in an intense laser field; Stochastic effects// Phys. Aerodisp. Systems.-2004.-Vol.41.-P.133-138.
13. Loboda A., Shpinareva I., Polischuk V. and Gura V., Sensing dynamics of zone type multi-level system in a laser field: stochastization of vibrational motion for molecules in multi-photon photo-excitation regime//Sensor Electr. & Microsyst.Techn.-2005.-N2.-P. 13-18.

The articles were received from 1.05 up to 29.07.2014

UDC 541.27, 584.96

V. I. Mikhailenko, V. N. Vaschenko, S. V. Ambrosov, A. V. Loboda, E. L. Ponomarenko

NON-LINEAR CHAOTIC TREATING VIBRATIONAL MOTION FOR MOLECULES IN THE MULTI-PHOTON PHOTOEXCITATION REGIME

Abstract

It has been studied a stochastization of vibrational motion for molecules in the multi-photon photo-excitation regime on example of the CF_3I, SF_5 molecules within quantum-stochastic kinetic approach and given more accurate data for stochastization threshold energies..

Key words: molecule in laser field, vibrational stochastization

УДК 541.27, 584.96

В. И. Михайленко, В. Н. Ващенко, С. В. Амбросов, А. В. Лобода, Е. Л. Пономаренко

НЕЛИНЕЙНОЕ ХАОТИЧЕСКОЕ РАССМОТРЕНИЕ КОЛЕБАТЕЛЬНОГО ДВИЖЕНИЯ В МОЛЕКУЛАХ В УСЛОВИЯХ МНОГОФОТОННОГО ВОЗБУЖДЕНИЯ

Резюме

Изучается стохастизация колебательного движения в молекулах у условиях многофотонного возбуждения для молекул CF_3I, SF_6 в рамках квантово-стохастического кинетического подхода и приведены уточненные данные энергий порога стохастизации.

Ключевые слова: молекула в поле лазерного излучения, колебательная стохастизация

УДК 541.27, 584.96

В. І. Михайленко, В. М. Ващенко, С. В. Амбросов, А. В. Лобода, Е. Л. Пономаренко

НЕЛІЙНИЙ ХАОТИЧНИЙ РОЗГЛЯД КОЛИВАЛЬНОГО РУХУ У МОЛЕКУЛАХ В УМОВАХ БАГАТОФОТОННОГО ЗБУДЖЕННЯ

Резюме

Вивчається стохастизація коливального руху у молекулах в умовах багатофотонного збудження для молекул CF_3I, SF_6 в межах вантово-стохастичного кінетичного підходу і наведені уточнені данні по енергіям порога стохастизації.

Ключові слова: молекула у лазерному полі, коливальна стохастизація

INFORMATION FOR CONTRIBUTORS OF "PHOTOELECTRONICS" ARTICLES

"Photoelectronics" Articles publishes the papers which contain the results of scientific research and technical designing in the following areas:

- **Physics of semiconductors, hetero- and low-dimensional structures;**
- **Physics of microelectronic devices;**
- **Quantum optics and spectroscopy of nuclei, atoms, molecules and solids;**
- **Optoelectronics, quantum electronics and sensorics;**
- **Photophysics of nucleus, atoms and molecules;**
- **Interaction of intense laser radiation with nuclei, atomic systems, substance.**

"Photoelectronics" Articles is defined by the decision of the Highest Certifying Commission as the specialized edition for physical-mathematical and technical sciences and published and printed at the expense of budget items of Odessa I. I. Mechnikov National University.

"Photoelectronics" Articles is published in English. Authors send two copies of papers in English. The texts are accompanied by 3.5″ diskette with text file, tables and figures. Electronic copy of a material can be sent by e-mail to the Editorial Board and should meet the following requirements:

1. The following formats are applicable for texts — MS Word (rtf, doc).

2. Figures should be made in formats — EPS, TIFF, BMP, PCX, JPG, GIF, WMF, MS Word I MS Giaf, Micro Calc Origin (opj). Figures made by packets of mathematical and statistic processing should be converted into the foregoing graphic formats.

The papers should be sent to the address:

Kutalova M. I., Physical Faculty of Odessa I. I. Mechnikov National University, 42 Pastera str, 65026 Odessa, Ukraine, e-mail: wadz@mail.ru, tel. +38-0482-7266356.

Information is on the site:

http://www.photoelectronics.onu.edu.ua

The title page should contain:

1. Codes of PACS.
2. Surnames and initials of authors.
3. TITLE OF PAPER.
4. Name of institution, full postal address, number of telephone and fax, electronic address.

Equations are printed in MS Equation Editor.

References should be printed in double space and should be numbered in square brackets consecutively throughout the text. References for literature published in 1999—2011 years are preferential.

Illustrations will be scanned for digital reproduction. Only high-quality illustrations will be taken for publication. Legends and symbols should be printed inside. Neither negatives, nor slides will be taken for publication. All figures (illustrations) should be numbered in the sequence of their record in text.

An abstract of paper should be not more than 200 words. Before a text of summary a title of paper, surnames and initials of authors should be placed.

For additional information please contact with the Editorial Board.

ИНФОРМАЦИЯ ДЛЯ АВТОРОВ НАУЧНОГО СБОРНИКА «PHOTOELECTRONICS»

В сборнике «Photoelectronics» печатаются статьи, которые содержат результаты научных исследований и технических разработок в следующих направлениях:

- **Физика полупроводников, гетеро- и низкоразмерные структуры;**
- **Физика микроэлектронных приборов;**
- **Квантовая оптика и спектроскопия ядер, атомов, молекул и твердых тел;**
- **Оптоэлектроника, квантовая электроника и сенсорика;**
- **Фотофизика ядра, атомов, молекул;**
- **Взаимодействие интенсивного лазерного излучения с ядрами, атомными системами, веществом.**

Сборник «Photoelectronics» издаётся на английском языке. Рукопись подается автором в двух экземплярах на английском и русском языках. К рукописи прилагаются дискета с текстовым файлом и рисунками. Электронная копия материала может быть прислана в редакцию по электронной почте.

Электронная копия статьи должна отвечать следующим требованиям:

1. Электронная копия (или дискета) материала присылается одновременно с твердой копией текста и рисунков.

2. Для текста допустимые следующие форматы — MS Word (rtf, doc).

3. Рисунки принимаются в форматах — EPS, TIFF, BMP, PCX, JPG, GIF, CDR, WMF, MS Word И MS Giaf, Micro Calc Origin (opj). Рисунки, выполненные пакетами математической и статистической обработки должны быть конвертируемые в вышеуказанные графические форматы.

Рукописи присылаются в адрес:

Отв. секр. Куталовой М. И., ул. Пастера, 42, физ. факультет ОНУ им. И. И. Мечникова, г. Одесса, 65026. E-mail: wadz@mail.ru, тел. (0482) 726-63-56.

Аннотации статей сб. «Photoelectronics» находятся на сайте: **http://photoelectronics.onu.edu.ua**

К рукописи прилагается

Титульная страница:

1. Коды PAC и УДК.
2. Фамилия и инициалы автора(ов).
3. Учреждение, полный почтовый адрес, номер телефона, номер факса, адреса электронной почты для каждого из авторов.
4. Название статьи

Текст должен печататься шрифтом 14 пунктов через два интервала на белой бумаге формата А4.

Уравнения необходимо печатать в редакторе формул MS Equation Editor. Необходимо давать определение величин, которые появляются в тексте впервые.

Таблицы подаются на отдельных страницах. Должны быть выполнены в соответствующих табличных редакторах или представленные в текстовом виде с использованием разделителей (точка, запятая, запятая с точкой, знак табуляции).

Ссылки на литературу должны печататься через два интервала, нумероваться в квадратных дужках последовательно в порядке их появления в тексте статьи. Ссылаться необходимо на литературу, которая издана позднее 2000 года. Для ссылок используются следующие форматы:

Книги. Автор(ы) (инициалы, потом фамилии), название книги курсивом, издательство, город и год издания. (При ссылке на главу книги, указывается название главы, название книги курсивом, номера страниц). *Журналы*. Автор(ы) (инициалы, потом фамилии), название статьи, название журнала (используются аббревиатуры только для известных журналов), год издания, номер выпуска, номер страниц. *Иллюстрации* будут сканироваться цифровым сканером. Принимаются в печать только высококачественные иллюстрации. Подписи и символы должны быть впечатаны. Не принимаются в печать негативы, слайды, транспаранты.

Рисунки должны иметь соответствующий к формату журнала размер не больше 160×200 мм. Текст на рисунках должен выполняться шрифтом 12 пунктов. На графиках единицы измерения указываются через запятую. Все рисунки (иллюстрации) нумеруются и размещаются в тексте статьи.

Резюме объемом до 200 слов пишется на английском, русском языках и на украинском (для авторов из Украины). Перед текстом резюме соответствующим языком указываются УДК, фамилии и инициалы всех авторов, название статьи.

ІНФОРМАЦІЯ ДЛЯ АВТОРІВ НАУКОВОГО ЗБІРНИКА «PHOTOELECTRONICS»

У науковому збірнику «Photoelectronics» друкуються статті, які містять результати наукових досліджень та технічних розробок у таких напрямках:

- **Фізика напівпровідників, гетеро- і низькорозмірні структури;**
- **Фізика мікроелектронних приладів;**
- **Квантова оптика і спектроскопія ядер, атомів, молекул та твердих тіл;**
- **Оптоелектроніка, квантова електроніка і сенсоріка;**
- **Фотофізика ядра, атомів, молекул;**
- **Взаємодія інтенсивного лазерного випромінювання з ядрами, атомними системами, речовиною.**

Збірник «Photoelectronics» видається англійською мовою. Рукопис подається автором у двох примірниках англійською мовою. До рукопису додається дискета з текстовим файлом і малюнками. Електронна копія матеріалу може бути надіслана до редакції електронною поштою.

Електронна копія статті повинна відповідати наступним вимогам:

1. Електронна копія (або дискета) матеріалу надсилається одночасно з твердою копією тексту та малюнків.
2. Для тексту припустимі наступні формати — MS Word (rtf, doc).
3. Малюнки приймаються у форматах — EPS, TIFF, BMP, PCX, JPG, GIF, CDR, WMF, MS Word і MS Graf, Micro Calc Origin (opj). Малюнки, виконані пакетами математичної та статистичної обробки, повинні бути конвертовані у вищевказані графічні формати.

Рукописи надсилаються на адресу:

Відп. секр. Куталовій М. І., вул. Пастера, 42, фіз. факультет ОНУ ім. І. І. Мечникова, м. Одеса, 65026. E-mail: wadz@mail.ru 6, тел. (0482) 726-63-56.

Всі довідки на нашому сайті:

http://www.photoelectronics.onu.edu.ua

До рукопису додається:

Титульна сторінка:

1. Коди PAC та УДК. Допускається використання декількох шифрів, що розділяються комою. У випадку, коли автором (авторами) не буде вказано жоден шифр, редакція збірника встановлює шифр статті за своїм вибором.
2. Прізвище (-а) та ініціали автора (-ів).
3. Установа, повна поштова адреса, номер телефону, номер факсу, адреса електронної пошти для кожного з авторів
4. Назва статті

Текст повинен друкуватися шрифтом 14 пунктів через два інтервали на білому папері формату А4. Назва статті, а також заголовки підрозділів друкуються прописними літерами і відзначаються напівжирним шрифтом.

Рівняння необхідно друкувати у редакторі формул MS Equation Editor. Необхідно давати визначення величин, що з'являються в тексті вперше.

Таблиці повинні бути виконані у відповідних табличних редакторах або представлені у текстовому вигляді з використанням роздільників (крапка, кома, кома з крапкою, знак табуляції).

Посилання на літературу повинні друкуватися через два інтервали, нумеруватись в квадратних дужках, послідовно у порядку їх появи в тексті статті. Необхідно посилатись на літературу, яка вийшла з друку пізніше 2000 року. Для посилань використовуються наступні формати:

Книги. Автор(и) (ініціали, потім прізвища), назва книги курсивом, видавництво, місто і рік видання. *Журнали*. Автор(и) (ініціали, потім прізвища), назва статті, назва журналу курсивом (використовуються абревіатури тільки для відомих журналів), номер тому і випуску, номер сторінок і рік видання

Ілюстрації будуть скануватися цифровим сканером. Приймаються до друку тільки високоякісні ілюстрації. Підписи і символи повинні бути вдруковані. Не приймаються до друку негативи, слайди, транспаранти.

Рисунки повинні мати відповідний до формату журналу розмір не більше 160×200 мм. Текст на рисунках повинен виконуватись шрифтом 10 пунктів. На графіках одиниці виміру вказуються через кому. Усі рисунки (ілюстрації) нумеруються і розміщуються у тексті статті.

Резюме друкується англійською, російською і українською мовами (для авторів з України). Перед текстом резюме відповідною мовою вказуються УДК, прізвища та ініціали всіх авторів, та назва статті.

Комп'ютерне верстання – О. І. Карлічук

Підп.до друку 04.08.2014. Формат 60×84/8.
Ум.-друк. арк. 23,02. Тираж 300 пр.
Зам. № 1039.

Видавець і виготовлювач
Одеський національний університет імені І. І. Мечникова

Свідоцтво суб'єкта видавничої справи ДК № 4215 від 22.11.2011 р.

Україна, 65082, м. Одеса, вул. Єлісаветинська, 12
Тел.: (048) 723 28 39